Radiation Response and Tolerance in Planarian Stem Cells

Thesis submitted for the degree of Doctor of Philosophy in Biology

By
Zhong Cheng Yap

Department of Biology
Linacre College
University of Oxford

Acknowledgements

First and foremost, my deepest gratitude goes towards my parents and family for their unconditional love and support, which has been the bedrock of my journey thus far. Their sacrifices have laid the foundation enabling me to stand where I am today.

I extend heartfelt gratitude to my supervisor, Aziz Aboobaker, for accepting me and providing me with an opportunity to engage in graduate research within his group. Under his patient mentorship, I progressed from an inexperienced undergraduate to someone capable of tackling scientific challenges with greater confidence and maturity.

I would like to express my gratitude to both present and past members of the Aboobaker group for their invaluable contributions, particularly through intellectual discussions and constructive feedback. I wish to offer special recognition to my colleague, Yian Hang, who embarked on this journey of graduate study alongside me, for the fruitful exchange of knowledge and techniques. Additionally, I am grateful to Simon Kershenbaum, Dr. Manuel Jara-Espejo, and Jakke Neiro for generously sharing their expertise in bioinformatics and assisting me in troubleshooting computational problems.

I would also like to thank both Prof. Mark Hill and Prof. Stephen Kearsey for assessing my progress during key milestones of the project, and for providing valuable external feedback. Further gratitude extends to Prof. Mark Hill for his guidance in operating the gamma irradiator and dosimetry calibrations. I am thankful to Dr. Estelle Kilias for her advice and assistance on flow cytometry. Furthermore, I would like to thank Prof. Jordi Solana, Helena Garcia-Castro, and Elena Emili, for our intellectual discussions as well as for sharing their expertise in planarian cell dissociation and single-cell RNA-sequencing.

I would like to give special mentions to members and staff of the Biology Department and Linacre College at the University of Oxford for assisting me in administrative matters and welfare, especially during the height of the Covid-19 pandemic.

Abstract

Ionizing radiation threatens cellular survival, a property strategically exploited in radiotherapy to eradicate cancer cells. However, the efficacy of radiotherapy is impeded by two co-existing challenges: the presence of radiotolerant cancer stem cells capable of withstanding treatment and subsequently driving cancer recurrence; coupled with collateral damage to normal stem cells, which are typically radiosensitive. Despite the pressing demand for radiotherapy, the underlying mechanisms governing radiosensitivity in normal stem cells and radiotolerance in cancer stem cells remain enigmatic, particularly within an in vivo setting. Here, we leverage the planarian *Schmidtea mediterranea*, which harbours abundant populations of experimentally tractable adult stem cells, as an in vivo model system to investigate stem cell radiation response and recovery. Employing a functional genomics approach, we aim to assess the transcriptional response of planarian stem cells to gamma radiation at both bulk and single-cell levels, as well as to uncover novel genes crucial for planarian radiotolerance.

We generated SPLiT-Seq libraries from irradiated planarians to explore their response to acute gamma radiation at the single-cell level. Our single-cell atlas delineates distinct stem cell clusters exhibiting varying sensitivity to gamma radiation. RNA velocity analyses further reveal dose and time-dependent changes in cell fate trajectories following irradiation. By integrating marker patterns and cell fate trajectories, we proposed a model linking radiosensitivity to cell cycle phase, with stem cells in S/G2/M phases exhibiting heightened sensitivity to gamma radiation.

Guided by insights from our single-cell and previous bulk RNA-sequencing data, we conducted an RNAi screen to identify novel regulators of planarian radiotolerance. We silenced the expression of 105 candidate genes and exposed animals to a sub-lethal dose of gamma radiation. Our screen unveiled six genes, namely Slmap, Kin-17, Dkc, Rab32, Rasl-12, and DMXL-1, as essential regulators of planarian radiotolerance in vivo. An additional 20 single-gene knockdowns were observed to significantly delay the post-irradiation stem cell recovery process, although these knockdowns alone were insufficient to cause animal mortality. Multiple members of the FHL gene family were amongst the single knockdowns

causing this delay phenotype. To account for potential redundancies, we knocked down the FHL family members in all possible combinatorial pairs, revealing distinct RNAi pairs that rendered planarians sensitive to gamma radiation.

We then examined the in vivo functions of Slmap, Kin-17, Dkc, Rab32, Rasl-12, and DMXL-1 in the regulation of planarian radiotolerance. We determined that following sub-lethal irradiation, the residual surviving stem cells in Slmap, Kin-17, and Dkc RNAi-treated animals were proliferation incompetent. In contrast, RNAi of Rab32, Rasl-12, and DMXL-1 led to an abnormally prolonged state of cell-cycle arrest in the remaining stem cells. Whether it was complete abolition of stem cell recovery in the former set of gene knockdowns or partial recovery in the latter, the knockdown-induced impairments prevented animal survival following exposure to sub-lethal irradiation. Among these six genes, we identified Dkc as a key player for DNA strand break repair in planarians.

In the wider framework, the genes demonstrated in this study to be vital for planarian radiotolerance could be tested in other model organisms, potentially uncovering novel and conserved mechanisms employed by adult stem cells to counteract the deleterious effects of ionizing radiation. The potential conservation of these mechanisms in mammals may also hold biomedical relevance, as targeting these genes could be explored for imparting radioprotection to normal stem cells, or to sensitize cancer stem cells to radiotherapy.

Table of Contents

List of Figures

Chapter 5: Characterization of Slmap, Kin-17, Dkc, Rab32, Rasl-12 and DMXL-1 functions in Planarian Radiotolerance

Chapter 1: Introduction

1.1 DNA Damage and The DNA Damage Response

In the late 1920s, a series of pioneering studies demonstrated the deleterious effects of X-ray-induced DNA damage (Muller, 1927; Muller, 1928; Gager and Blakeslee, 1927). These observations preceded the set of landmark experiments which unveiled DNA as the blueprint of life (Avery et al., 1944; Hershey and Chase, 1952). Currently, it is widely acknowledged that the preservation of genomic integrity is crucial for cellular function, and the faithful transmission of genetic material to the next generation. The accomplishment of this task, however, is complicated by the constant attack on a cell's DNA by a myriad of both endogenous and exogenous factors. For instance, reactive oxygen species (ROS) generated from biochemical reactions such as oxidative respiration; transposition of repetitive elements; replication errors; and even spontaneous hydrolysis of nucleotides are amongst the recognized causes of mutagenesis from endogenous sources (Hakem, 2008; Marnett and Plastaras, 2001). Exogenous threats to genomic integrity primarily include solar ultraviolet radiation, and increasingly from various human-made compounds (Chatterjee and Walker, 2017). Due to the deleterious consequences of these mutagens, cells have evolved a plethora of countermeasures that act as a barrier to protect their genomes against damage. To name a few, pigments such as melanin protect cells against ultraviolet radiation (Brenner and Hearing, 2008), ROS scavenging systems protect cells against oxidative damage (Pizzino et al., 2017), proofreading polymerases check for replication errors (Preston et al., 2010), and transposable element silencing mechanisms (Aravin et al., 2017) may all work in concert to ensure genome fidelity.

Despite the presence of these primary defence mechanisms, damage to a cell's genome remains highly pervasive. In humans, it is predicted that each of our cells receive an average of 10^5 genotoxic insults per day (Lindahl and Barnes, 2000). If the damage to a cell's genome is left unchecked or repaired incorrectly, mutations ranging from single base-pair alterations up to large-scale chromosomal aberrations may result, compromising cell function and viability, which in turn may cause defects on a tissue or even an organismal scale. Moreover, failure to correctly repair DNA damage may lead to genomic instability, predisposing cells to oncogenic transformation (O'Driscoll and Jeggo, 2006).

To counteract the threats posed by DNA damage, cells have evolved multiple, largely distinct but interconnected pathways, which are collectively referred to as the DNA damage response [DDR] (Harper and Elledge, 2007). These pathways detect, flag the presence of, and mediate the repair of the diverse types of DNA lesions that can arise. The major DNA repair pathways within the DDR network include mismatch repair, base-excision repair, nucleotide excision repair, homologous recombination, and non-homologous end-joining (Harper and Elledge, 2007; Chatterjee and Walker, 2017). Most components within this network exhibit strong conservation throughout eukaryotes (Polo and Jackson, 2011), reflecting the importance of genomic stability on cellular fitness. The existence of multiple repair pathways also reflects the heterogeneity of DNA-damaging agents and the corresponding range of genetic lesions.

The nature of the DDR is influenced by the type of DNA damage incurred. For instance, mismatch repair efficiently corrects mis-paired bases arising from replication errors; the base-excision repair pathway removes erroneous chemical alterations to DNA bases; while nucleotide-excision repair specializes in resolving bulky, helix-distorting lesions (Chatterjee and Walker, 2017). Most genetic lesions that occur will typically be cleared by one of these three pathways. These pathways, however, are incapable of repairing DNA double-stranded breaks, a form of damage that is considered the most toxic and difficult-to-repair (Cannan and Pederson, 2015). One cause of DNA double-stranded break formation is exposure of cells to ionizing radiation, to which cells may call upon the homologous recombination pathway or the non-homologous end-joining pathway for repair (Khanna and Jackson, 2001). It is important to acknowledge that double-stranded break generation is an intermediary step required to facilitate normal, physiological processes such as recombination during meiosis, V(D)J recombination during lymphocyte maturation, and class-switch recombination in activated B-cells. In these processes, double-stranded breaks occur in well-defined regions of the genome in a controlled manner (Petes, 2001; Dudley et al., 2005). In comparison, double-stranded breaks amongst other deleterious lesions caused by ionizing radiation exposure are typically clustered, uncontrolled, and stochastic in nature (Nikjoo et al., 1997; Nikjoo et al., 2001; Nikjoo et al., 2002; Watanabe et al., 2015; Hill, 2018; Mavragani et al., 2019).

1.2 Cellular responses to the damaging effects of ionizing radiation

Ionizing radiation is defined as radiation that has sufficient energy to liberate electrons from atoms as it passes through a medium (National Research Council, 2006). Gamma rays and X-rays, which reside on the high frequency end of the electromagnetic spectrum, are forms of radiation that fall into this category. Both these forms of radiation are highly penetrating and highly energetic, with gamma rays to a greater degree than X-rays. Unlike solar ultraviolet radiation, a form of non-ionizing radiation, X-rays and more so gamma rays are capable of inducing double-stranded breaks to a cell's DNA, either directly or indirectly (Morgan and Sowa, 2005; Rastogi et al., 2010; Reisz et al., 2014; Singh and Singh, 1982).

In the direct route, high-energy radioactive particles directly collide with DNA, displacing electrons and disrupting bonds, which ultimately alters the molecular structure of DNA (Reisz et al., 2014). In the indirect route, DNA damage is induced by toxic by-products from the radiolysis of water. This phenomenon involves the radiation-induced excitation of water molecules, leading to the formation of a multitude of unstable intermediates, which are collectively known as reactive oxygen species [ROS] (Cadet and Wagner, 2013). Such molecules include hydroxyl radicals ($^{\bullet}OH$), ionized water ($H2O^{+}$), superoxides ($O_2^{\bullet -}$), and the more stable hydrogen peroxide (H_2O_2). Acute exposure to ionizing radiation can cause an abrupt spike in intracellular ROS levels, overwhelming the cell's primary ROS scavenging mechanisms, and wreaking havoc on biological molecules by virtue of their potent oxidative effects (Desouky et al., 2015; Cadet and Wagner, 2013). Overall, it is estimated that most cell types in G0/G1 phase suffer between 25-40 double-stranded breaks per Gray (Gy) of ionizing radiation absorbed (Olive, 1998; Mori et al., 2018)

In response to the damage caused by ionizing radiation exposure, cells commonly exhibit three cellular outcomes – repair, death, or senescence (Maier et al., 2016). When cells deem the damage reparable, they may temporarily arrest the cell-cycle, allowing for repair. The cell may then re-enter the cell cycle once repair is completed and DDR signalling is attenuated. In the cases of irreparable damage, cells may undergo senescence or be eliminated via apoptosis to prevent genomic instability and to avoid the spread of mutations

to their progeny (Maier et al., 2016). In mammals, the tumour suppressor p53 plays a central role in a cell's decision process, with low or high levels of p53 preferentially inducing cell-cycle arrest or apoptosis respectively (Aylon and Oren, 2007).

Repair

Immediately following the induction of a double-stranded break, sensor proteins such as the MRE11-RAD50-NBS1 (MRN) complex assemble at the break site. These sensors then recruit and activate transducers in the DDR network such as Ataxia Telangiectasia Mutated (ATM), Ataxia Telangiectasia and Rad3-related (ATR) and DNA-dependent Protein Kinase (DNA-PK). Once activated, these three apical kinases co-ordinately phosphorylate a wide array of targets to modulate the DDR. In the case of reparable damage, typically when the frequency and complexity of double-stranded breaks are low, ATM activation is relatively mild. Mild ATM activity translates to relatively low levels of p53 activity, as ATM acts as an upstream activator of p53 (Saito et al., 2002; Lakin and Jackson, 1999). In this state, p53 activates the cyclin-dependent kinase (CDK) inhibitor, p21. p21-mediated inhibition of CDK4 and CDK6 leads to G1 arrest (Weinberg and Denning, 2002). For cells that receive damage in S or G2 phase, p21 can also target the CDK1-CyclinB complex, resulting in G2 arrest (Smits et al., 2000). During this period when the cell cycle is paused, repair takes place. The two canonical double-strand break repair pathways in eukaryotes are non-homologous end-joining (Lieber, 2010), and homologous recombination (San Filippo et al., 2008). In the non-homologous end-joining pathway, DNA ends at the break sites are tightly bound by Ku70/80 heterodimers, which act as a docking site for core components of the pathway. End-processing exonucleases such as Artemis are then recruited to trim away damaged bases or secondary structures that may prevent ligation (Ma et al., 2002). Subsequently, polymerases such as those from the pol X family may be recruited to fill the gaps left by the nucleases (Ramsden, 2011). The nuclease and polymerase activities generate compatible ends for blunt-ended ligation, to which the XRCC4-DNA Ligase IV-XLF ligation complex completes the process. Non-homologous end-joining is known to be error prone, as the nuclease and polymerase activities in the process may lead to indel mutations (Lieber, 2010).

In comparison, double-stranded break repair via homologous recombination is precise and error-free. However, repair by homologous recombination is restricted to S/G2 phases of the cell cycle, after DNA replication has taken place. This is because homologous recombination requires an undamaged repair template in the form of a sister chromatid (San Filippo et al., 2008). In this pathway, the MRN complex in combination with CtIP initiates strand resection from the 5' to 3' direction, leading to the formation of single-stranded 3' overhangs on both sides of the break (Chen et al., 2008). The overhangs will first be coated and protected by replication protein A (RPA), but RPA will eventually be replaced by Rad51 with the help of BRCA2 (Shivji et al., 2006). The RAD51-coated overhangs can invade homologous duplex DNA, where DNA polymerases can begin synthesis to replace the missing bases in a template-dependent manner (San Filippo et al., 2008). Once synthesis is complete, the heteroduplex structures known as Holliday junctions are uncoupled in a process mediated by resolvase enzymes such as Gen1 in humans (Chan and West, 2015).

Death

When the frequency and complexity of double-stranded breaks are high, ATM activation is strong and prolonged. This in turn leads to a strong and prolonged activation of p53. In this state, p53 can activate an array of pro-apoptotic genes such as BAX (BCL-2 associated X protein), PUMA (p53-upregulated modulator of apoptosis), and the protein NOXA, triggering apoptosis of the cell via the intrinsic apoptosis pathway (Kuribayashi et al., 2011; Oda et al., 2000). Hence, p53 has dual functions dependent on its activation level. The underlying mechanism driving this dynamic is thought to be caused by p53 having high promoter-binding affinities for pro-arrest genes including p21, but lower affinities for pro-apoptotic genes (Horvath et al., 2007).

Other modes of radiation-induced apoptosis have also been documented. Cell death may occur via the extrinsic apoptotic pathway, which is also dependent on p53 activity (Sheard, 2001). Furthermore, cells exposed to ionizing radiation may die via the membrane stress apoptotic pathway, which is independent of DNA damage and does not depend on p53 activity (Maier et al., 2016). It is important to acknowledge that ionizing radiation can also inflict direct or indirect damage to other key biological molecules. Lipid peroxidation

may occur in response to radiation-induced ROS (Reisz et al., 2014), disrupting the structure and function of cell membranes, eventually leading to cell death via the aforementioned membrane stress pathway. Exposure to higher doses of ionizing radiation may even lead to immediate cell death by necrosis, due to acute and widespread damage to membranes and proteins (Reisz et al., 2014).

Another route leading to radiation-induced cell death is through mitotic catastrophe. Mitotic catastrophe is characterized by the abnormal arrest of cells in metaphase due to defects in spindle formation, which in turn signals apoptosis via the intrinsic pathway (Castedo et al., 2004). Mitotic catastrophe can occur when DNA damage takes place during M phase, or when cells prematurely attempt mitosis despite the presence of unrepaired damage (Vakifahmetoglu et al., 2008).

Senescence

In a similar fashion to the previously described repair pathway, cellular senescence initially begins with a p53-p21-mediated reversible cell cycle arrest. During this transient arrest period, the CDK inhibitor, p16, is activated (Maier et al., 2016). p16 inhibits CDK4/6, thus preventing the phosphorylation and activation of Retinoblastoma-1 (Serrano et al., 1993), a key driver of progression into S phase. Senescence, which is characterized as a permanent and irreversible withdrawal from the cell cycle, may be induced because of prolonged p21 signalling. Prolonged p21 signalling can lead to the accumulation p16, which unlike the former, is capable of constitutive activation and hence the maintenance of cell-cycle arrest, despite the attenuation of DDR signalling (Beausejour, 2003; Rayess et al., 2011). In many cases, senescent cells remain metabolically active, and are still able to contribute some if not all of their normal biological functions. Similar to apoptosis, undergoing senescence following radiation exposure may be a programmed response to protect individuals from carcinogenesis.

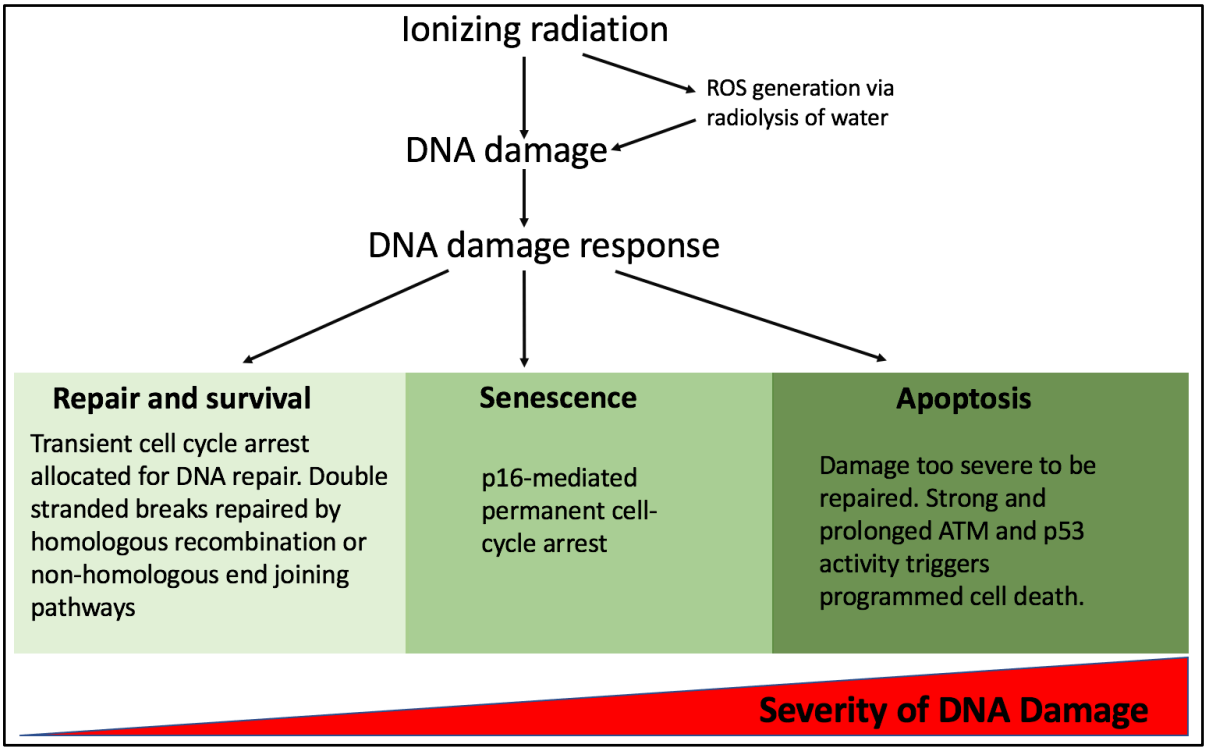

Figure 1. Cellular outcomes of ionizing radiation exposure.

What factors influence the cell's decision to repair, senesce, or undergo apoptosis in response to ionizing radiation? A simplistic perspective would be that the cellular outcome is primarily dependent on the dose received, and correspondingly the level of DNA damage sustained (Figure 1). In this scenario, cells are predicted to survive and repair at low doses, undergo senescence at intermediate doses due to prolonged p21 signalling, and die at high doses due to strong p53 activity. However, the reality is much more complex and multi-dimensional, evident by the observation that the degree of radiotolerance can vary significantly between different cell types. For instance, most human haematopoietic stem cells were found to undergo apoptosis after treatment with only 0.8 Gy of ionizing radiation (Heylmann et al., 2014). In comparison, the vast majority of human astrocytes in vitro were capable of repair and subsequent re-entry into the cell cycle after 10 Gy of acute ionizing radiation exposure, with no incidence of apoptosis (Bylicky et al., 2018). The thresholds of damage that permit repair or force a cell into senescence or apoptosis are cell-type specific and may vary significantly between cell types. The factors that establish these thresholds remain poorly understood. Predicting the aftermath of ionizing radiation exposure is further complicated by the incidence of alternative outcomes beyond the three canonical fates described. This is underscored by observations of radiation-induced premature neural stem cell differentiation in both vertebrate and invertebrate systems (Monje et al., 2002; Schneider et al., 2013; Konířová et al., 2019; Wagle and Song, 2020).

1.3 Radiation response in mammalian stem cells

Bona fide stem cells are characterized by the ability for long-term self-renewal and the capacity to differentiate into one or multiple specialized cell types (Weissman, 2000). Hierarchical models have been established for various tissues, with adult stem cells, typically multipotent, self-renewing and giving rise to all other cell-types within the hierarchy (Derényi and Szöllősi, 2017; Dingli et al., 2007; Tumbar et al., 2004; Potten et al., 2009). Even within the same tissue lineage, varying levels of tolerance to ionizing radiation exist. In mammals, stem cells are typically more sensitive to ionizing radiation in comparison to their post-mitotic progeny, although exceptions to this rule exist (Fabbrizi et al., 2018a). Studies on various mammalian stem cell types suggest that stem cells exposed to ionizing radiation are highly prone to favour apoptosis over repair and survival (Katoh et al., 1995; Jacobs et al., 2016; Meyer et al., 2016; Sokolov and Neumann, 2012; Acharya et al., 2010; Becker et al., 2009).

This phenomenon may initially seem paradoxical, considering the reported mechanisms of enhanced DNA damage surveillance and repair in human embryonic stem cells (Maynard et al., 2008), as well as adult stem cells of hematopoietic (Bracker et al., 2006), muscle (Narciso et al., 2007), and mesenchymal lineages (Chen et al., 2006), in relation to their respective differentiated progeny. The presence of robust genome-protective mechanisms in stem cells are reasonable, given that adult stem cells are typically rare in number yet are responsible for the critical role of replenishing cells lost due to homeostatic turnover (Reya et al., 2001). Robust genome protective mechanisms would promote long-term stem cell survival, which in turn would be imperative for tissue maintenance and organismal function. Furthermore, the maintenance of genomic integrity in stem cells would be especially important to prevent oncogenic transformation, as the typical long lifespans of stem cells render them susceptible to accumulate cancer-causing mutations over time. In the case of germline stem cells, genome-protective mechanisms would be favourable to prevent the transmission of mutations to the next generation, which may carry an evolutionary significance.

Despite evidence of effective mechanisms promoting genomic stability in stem cells, stem cells on the contrary display significantly higher levels of sensitivity to ionizing radiation when compared to their differentiated progeny (Katoh et al., 1995; Jacobs et al., 2016; Meyer et al., 2016; Sokolov and Neumann, 2012; Acharya et al., 2010; Becker et al., 2009). This paradox may be explained by the fact that while stem cells have evolved countermeasures against naturally occurring genotoxic stressors, acute exposure to high levels of ionizing radiation is unnatural and only achieved via artificial means. Hence, cells are not naturally equipped with tools to negate the sudden onset of complex and widespread damage as a consequence of acute ionizing radiation exposure. Nevertheless, understanding how stem cells respond to acute ionizing radiation is currently of high biomedical significance, as many diagnostic and treatment procedures result in cells exposed to such levels of radiation (Bhargavan, 2008).

One of the most radio-hypersensitive cell types in mammals are pluripotent embryonic stem cells, with acute exposure to 1 Gy gamma radiation being sufficient to trigger robust apoptotic responses in cultured human embryonic stem cells [hESCs] (Sokolov and Neumann, 2012). The sensitivity of hESCs to radiation is not limited to ionizing forms, as they were also shown to exhibit hypersensitivity to non-ionizing UV radiation (Qin et al., 2007). Transcriptional profiling of irradiated hESCs revealed a significant upregulation of pro-apoptotic genes 2 hours after 1 Gy irradiation relative to unirradiated controls, corroborating the observed apoptotic response to ionizing radiation (Sokolov et al., 2011). In a separate study, Wilson and colleagues also demonstrated an apoptotic gene expression profile in hESCs after varying doses of ionizing radiation, although the core set of pluripotency factors remained unchanged post-treatment with up to a 4 Gy dose (Wilson et al., 2010). Interestingly, the surviving cell fractions at all doses tested were found to retain pluripotency and proliferative competency, as teratomas, tumours containing cells derivative from all three germ layers, could be formed when the surviving hESCs were transplanted into immunocompromised mice (Wilson et al., 2010). It is postulated that hESCs may be primed to undergo apoptosis by sequestering high levels of the pro-apoptotic protein BAX in its active conformation at the Golgi, which can then be rapidly released in response to genotoxic insult amongst other stresses (Dumitru et al., 2012). This harbouring

of active BAX at the Golgi was no longer observed upon embryonic stem cell differentiation (Dumitru et al., 2012)

Unlike rapidly dividing embryonic stem cells, tissue-resident adult stem cells in mammals are predominantly quiescent (Cheung and Rando, 2013). Adult stem cells typically reside in specialized niches, dividing asymmetrically on occasion to self-renew, and to give rise to a fast-dividing daughter cell that is commonly termed a transit-amplifying cell. Both adult stem cells and their transit-amplifying progeny generally exhibit markedly heightened levels of sensitivity to ionizing radiation relative to the differentiated cells further along their respective tissue hierarchies. This phenomenon has been observed in hematopoietic (Katoh et al., 1995; Becker et al., 2009), neural (Acharya et al., 2010), intestine (Jacobs et al., 2016), testes (Jacobs et al., 2016), and skin (Martin et al., 2016) cell lineages studied in the context of ionizing radiation exposure.

The genetic factors that influence stem cell radiosensitivity beyond the conserved DNA damage response network remain poorly understood, partly due to the lack of omics-based approaches specifically focused on radiation response in stem cells. However, one gene that is well-characterized to confer radiosensitivity across multiple mouse and human stem cell-types is the gene Phosphoprotein Phosphatase 2A (PP2A). PP2A was identified to be selectively expressed in stem cells but not differentiated cells via DNA microarray (Fabbrizi et al., 2018b). Mechanistically, PP2A was proposed to inhibit repair signalling whilst promoting apoptosis in irradiated stem cells, and the transient suppression of PP2A was found to impart a radioprotective effect on stem cells in vitro (Fabbrizi et al., 2018b).

Most of the known factors underlying the differences in radiotolerance between stem and non-stem cells were attributed to be at the epigenetic level, which is comprehensible given the known distinctions in epigenetic landscapes between stem and non-stem cells. One important histone modification that aids in double-stranded break repair is phosphorylation on serine-139 of the histone variant H2AX (Burma et al., 2001). This modification is termed yH2AX, which binds chromatin around the double-stranded break, and functions as a docking site for downstream repair factors (Paull et al., 2000). In a study by Jacobs and colleagues, stem cells in the mouse brain, intestine, and testis were

found to possess heavily diminished yH2AX signals relative to non-stem cells after irradiation in vivo (Jacobs et al., 2016). Underlying this phenomenon may be the failure of stem cells, but not differentiated cells, to dephosphorylate tyrosine-142 on the same histone H2AX (H2AX-pY142) upon the induction of DNA damage (Jacobs et al., 2016). This may have negative implications on the outcome of irradiated stem cells, as H2AX-pY142 is a modification that is proposed to simultaneously impair double-stranded break repair by sterically hindering the formation of yH2AX, and may directly promote apoptosis by stimulating the activation of various pro-apoptotic factors (Cook et al., 2009).

Other stem-cell-specific epigenetic modifications that were shown to confer sensitivity to ionizing radiation in mammals are Histone-3-lysine-56 acetylation (H3K56ac), and Histone-3-lysine-9 acetylation (H3K9ac). Both these marks were found to be enriched in embryonic stem cells, and their footprints decreased sharply upon differentiation (Jacobs et al., 2016; Meyer et al., 2016). Both modifications were found to be refractory for DNA repair in vitro (Jacobs et al., 2016; Meyer et al., 2016). The former is believed to impair the repair process by hindering the induction of yH2AX at the break-sites (Jacobs et al., 2016). The latter is believed to obstruct the establishment of Histone-3-lysine-9 trimethylation (H3K9me3) at sites of damage (Meyer et al., 2016), which impairs repair, as H3K9me3 was previously found to accumulate at break sites of differentiated cells to facilitate repair (Ayrapetov et al., 2014). Validating their roles, transient depletion of H3K56ac and H3K9ac via siRNA knockdowns of their writers, the acetyltransferase p300, and the acetyltransferase Monocytic Leukemia Zinc Finger protein (MOZ), respectively, were both found to impart radioprotective effects onto mouse embryonic stem cells in vitro (Jacobs et al., 2016; Meyer et al., 2016).

While most mammalian stem cell-types were observed to display radiosensitivity, one exception is the radiotolerant mesenchymal stem cell. Human mesenchymal stem cells were observed to tolerate acute exposures of up to 20 Gy of ionizing radiation, with minimal evidence of apoptotic death in vitro (Cmielova et al., 2012; Sokolov and Neumann, 2010). Nevertheless, the function of these stem cells would be ablated since majority of the irradiated cells underwent radiation-induced senescence. Although double-stranded breaks were found to be efficiently repaired in mesenchymal stem cells, even to a better degree

than its differentiated progeny (Oliver et al., 2013), DNA damage response signalling was persistent. p53 activity remained elevated even after 6 days post-treatment, driving the execution of the senescence programme (Cmielova et al., 2012).

1.4 Radiation tolerance in cancer stem cells

Unlike normal stem cells, cancer stem cells commonly exhibit resistance to ionizing radiation. The cancer stem cell theory postulates that tumours, heterogenous in nature, are initiated and sustained by a rare population of cancer stem cells, which possess the capacity for long-term self-renewal and multi-lineage differentiation (Reya et al., 2001). A common trait that confers radiotolerance in cancer stem cells is the heightened ability to protect their genomes from radiation-induced ROS. This is achieved through the constitutive upregulation of ROS scavengers observed in cancer stem cells from various origins (Diehn et al., 2009; Skvortsov et al., 2011; Skvortsov et al., 2014; Zhang and Martin, 2014; Chang et al., 2014). Consequently, the number of double-stranded breaks that occur in irradiated cancer stem cells may be reduced due to the diminished contributions of indirect effects. This may in turn prompt cells to elect pro-repair pathways over senescence or apoptosis.

Protection against ROS is often coupled with enhanced DNA repair capacities in cancer stem cells. Overexpression of NBS-1, a component of the double-stranded break-sensing MRN complex, is reported in various cancer stem cell types (Yang et al., 2006; Yang et al., 2007; Chen et al., 2005; Cheng et al., 2011; Skvortsov et al., 2015), and may contribute to their increased radiotolerance. Furthermore, elevated activity of DNA damage response transducers such as ATM, ATR, and their two downstream checkpoint kinases, Chk1 and Chk2, are also believed to contribute to improved DNA repair in cancer stem cells (Vitale et al., 2017; Bao et al., 2006; Bartucci et al., 2014; Carruthers et al., 2014; Ahmed et al., 2015; Schulz et al., 2019). While enhanced DNA repair is commonly observed in various cancer stem cell types, it is important to acknowledge that exceptions exist as contradictory observations have been reported (Lundholm et al., 2013; McCord et al., 2009).

Akin to normal stem cells, cancer stem cells are also believed to be quiescent in nature (Moore and Lyle, 2011). In radiotherapy, most fast-dividing cancer cells can be killed by ionizing radiation, as they often lack functional DNA damage checkpoints and hence die in M-phase via mitotic catastrophe when they attempt mitosis despite the presence of unrepaired DNA damage (Vakifahmetoglu et al., 2008). However, the quiescent nature of cancer stem cells increases the likelihood that DNA repair is completed before the eventual entry into M phase, avoiding mitotic catastrophe and enabling them to persist after treatment.

Contrary to normal stem cells, cancer stem cells possess multiple mechanisms to circumvent apoptosis despite sustaining genetic lesions due to ionizing radiation. A dysregulated bias towards pro-survival signalling is commonly associated with cancer stem cell resistance to radiation amongst other therapeutic agents (Chang et al., 2016). Attenuated p53 signalling has also been reported in some cancer stem cell types which impairs the induction of apoptosis (Chen et al., 2012; Schulz et al., 2019). Upregulated expression of anti-apoptotic proteins, such as those from the inhibitor of apoptosis (IAP) family, has also been found in various cancer stem cell types (Schimmer, 2004; Ji et al., 2018; Vellanki et al., 2009). Overall, these mechanisms may collectively promote cancer stem cell survival upon treatment with ionizing radiation, often allowing cells to persist despite the accumulation of genetic lesions. Over time, this promotes intra-tumoral heterogeneity, contributing to cancer evolution and typically resulting in poor prognoses.

Taken together, many parallels can be drawn between tissue-resident adult stem cells and cancer stem cells in their properties as well as their roles in their respective hierarchies. However, a stark difference between normal stem cells and their malignant counterparts that is currently of major clinical significance is their differential responses to ionizing radiation. Efficacious use of radiotherapy in cancer eradication is hampered by the presence of radiotolerant cancer stem cells that can withstand treatment and expand via self-renewal to cause recurrence. In extreme cases, the recurrence rates of mid-staged ovarian cancer (Corrado et al., 2017) and glioblastoma (Nabors et al.,2013) approaches 100%. At the same time, radiotherapy may result in debilitating side-effects such as cognitive impairment (Duffner, 2014), epithelial erosion (Smith and DeCosse, 1986; Wei et

al., 2019), and infertility (Ash, 1980; Biedka et al., 2016) due the ablation of radiosensitive adult stem cells. Therefore, an improved understanding of how normal and cancer stem cells differentially respond to ionizing radiation would be imperative for the development of therapeutic strategies aimed to impart radioprotection to normal tissues and to sensitize cancer stem cells to radiotherapy, reducing the likelihood of recurrence.

1.5 Radiation tolerance across the animal kingdom

Mice and humans have been the primary subjects of research on the topic of cellular responses to ionizing radiation. In recent years, high throughput genetic screens have been employed to investigate the factors that influence cellular radiotolerance in various normal as well as cancerous mammalian cell lines (Wang et al., 2019; Herr et al., 2015; Zhu et al., 2021; Zhou et al., 2023; Hayman et al., 2021; Yu et al., 2021; Han et al., 2020; reviewed in Tamaddondoust et al., 2022). Several studies have identified novel factors important for cellular radiotolerance in vitro, but only a handful of these regulators were functionally examined in vivo (Wang et al., 2019; Hayman et al., 2021). Conducting in vivo experiments in mammalian systems remains challenging due to a multitude of pragmatic and ethical constraints, particularly when studying adult stem cells, which are extremely rare in number and are often elusive in vivo. These limitations restrict most studies on mammalian radiation response to cell lines in vitro. However, observations of radiation response made in vitro may not be a full representation of events in vivo, as cells in vitro experience an artificial cellular environment and are subjected to passage number effects. Hence, research using alternative model organisms, especially those with radiotolerant properties, may hold significant biomedical value. Understanding what makes these organisms radiotolerant may potentially allow us to uncover conserved regulators of radiation response, which in turn may translate to novel therapeutic targets aimed to safeguard normal stem cells, or to sensitize cancer stem cells to radiotherapy.

Organisms across the animal kingdom exhibit significant variations in their levels of radiotolerance. Humans, along with other mammals, represent one of the most radiosensitive classes of organisms. Across various mammalian species, the 30-day median lethal dose ($LD50/30_{days}$) from acute whole-body ionizing radiation exposure ranges between 2.4 Gy to 10 Gy (DiCarlo et al., 2013). The hematopoietic syndrome, resulting from the selective ablation of radiosensitive hematopoietic stem and precursor cells, is a common cause of death at these doses (Macia i Garau et al., 2011). On the opposite side of the spectrum, animals such as tardigrades and some nematodes exhibit remarkable tolerance to ionizing radiation, as they have been observed to survive acute whole-body ionizing radiation exposures exceeding 1000 Gy without the incidence of morbidity or mortality. Table 1 provides a summary of the observed tolerance to acute ionizing radiation in adult-stage organisms across different animal phyla. For chordates and arthropods, only selected organisms are listed here as representatives, as the tolerance to acute ionizing radiation in mammals (DiCarlo et al., 2013), amphibians (Conger and Clinton, 1973; Fuma et al., 2012), birds (Mellinger et al., 1975), insects (Paithankar et al., 2021), and crustaceans (Dallas et al., 2012; Fuller et al., 2015) have been reviewed previously. Table 1 also incorporates studies that investigated the transcriptional response of adults exposed to acute ionizing radiation, where available, as omics-based approaches may serve as an invaluable tool to uncover novel and conserved mechanisms that different animals employ to counteract the detrimental effects of ionizing radiation.

Table 1. Summary of mortality and transcriptomic studies across metazoans in the context of acute ionizing radiation exposure.

Phylum	Availability of IR-related studies	Species	Maximum tolerable dose or median lethal dose where applicable	Availability of post-irradiation transcriptome profile	Reference(s)
Ctenophora	No	N/A	N/A	N/A	
Porifera	Yes	*Tethya wilhelma*	>600 Gy X-rays, maximum tolerable dose unknown. 17/21 animals remained alive one year post 600 Gy X-ray treatment.	Yes (RNA-seq 24 hours, 7 days, and 21 days after 600 Gy X-ray exposure)	Fortunato et al., 2021a
Placozoa	Yes	*Trichoplax adhaerens*	5% survival 8 days post 218.6 Gy X-ray treatment. Surviving individuals capable of culture repopulation.	Yes (2 hours post 218.6 Gy X-ray exposure)	Fortunato et al., 2021b
Cnidaria	Yes	*Hydractinia echinata*	Between 300 to 500 Gy gamma radiation. Surviving and functional stem cells detected after 300 Gy gamma radiation, but not after exposure to 500 Gy gamma radiation.	No* (Data unpublished)	Bradshaw et al., 2015
Xenoturbellida	No	N/A	N/A	N/A	
Acoela	Yes	*Isodiametra pulchra*	<60 Gy X-rays. Rare surviving and proliferation-competent stem cells were observed after 60 Gy X-ray irradiation but failed to sustain the animal.	No	De Mulder et al., 2009
Hemichordata	No	N/A	N/A	N/A	
Echinodermata	Yes	*Arbacia punctulata*	$LD_{50/30days}$ = 389 Gy gamma radiation	No	White and Angelovic, 1966
Chordata	Yes	*Uromastyx hardwickii*	$LD_{50/30days}$ ≈ 40 Gy gamma radiation	No	Ahmed and Taqawi, 1978
		Mus musculus	$LD_{50/30days}$ across 10 different female lab-mouse strains range from 5.85 Gy to 7.74 Gy X-rays	Yes. Studies referenced involve total RNA extraction from specific tissues after irradiation of adults in vivo.	Storer, 1966; Jafer et al., 2020 (various tissues); Leduc et al., 2021 (skin); Yin et al., 2003 (brain)
		Danio rerio	$LD_{50/30days}$ ≈ 25 to 30 Gy gamma radiation	Yes – Microarray analyses of adults 4 hours after 0.1 and 1 Gy gamma radiation	Traver et al., 2004; Jaafar et al., 2013

Chordata (continued)		*Bufo fowleri*	$LD_{50/30days} \approx$ 23 Gy gamma radiation $LD_{50/50days} \approx$ 18 Gy gamma radiaiton	No	Landreth et al., 1974
		Gallus gallus domesticus	$LD_{50/30days}$ = 7-11 Gy gamma radiation (juveniles). No data on adults found.	No	Stearner and Christian, 1972
Chaetognatha	No	N/A	N/A	N/A	
Rotifera	Yes	*Adineta vaga*	>1120 Gy gamma radiation (100% survival at two weeks after 1120 Gy gamma ray exposure, maximum tolerable dose unknown)	Yes (0,4,24,48,72 hours post 1000 Gy X-ray irradiation)	Gladyshev and Meselson, 2008 Nicolas et al., 2023 (transcriptome)
		Philodina roseola	>1120 Gy gamma radiation (100% survival after two weeks, maximum tolerable dose unknown)	No	Gladyshev and Meselson, 2008
		Brachionus koreanus	LD_{50} = 2900 Gy gamma radiation (24-hour survival) LD_{50} = 2300 Gy gamma radiation (96-hour survival)	No	Won et al., 2016
Gnathostomulida	No	N/A	N/A	N/A	
Gastrotricha	No	N/A	N/A	N/A	
Platyhelminthes	Yes	*Macrostomum lignano*	10% of subjects survived long-term after 105 Gy fractionated gamma radiation. Zero long-term survivors post 150 Gy fractionated dose despite observations of stem cell recovery. Elimination of stem cell function and 100% mortality after 210 Gy fractionated dose.	Yes (12,24,72 hours post 210 Gy fractionated* gamma radiation) *three pulses of 70 Gy gamma radiation administered within 1 day.	De Mulder et al., 2010; Grudniewska et al., 2016 (transcriptome)
		Dugesia ryukyuensis	Range of 4.4–8.8 Gy X-rays (strain-specific)	No	Kobayashi et al., 2008
		Dugesia japonica	15 Gy X-ray irradiation led to 70% mortality after 4 weeks, some long-term survivors developed tumours. 30 Gy irradiation led to 100% mortality after 4 weeks post-exposure.	Yes (Microarray analyses 1 to 7 days after 5 Gy and 30 Gy X-ray irradiation)	Salvetti et al., 2009; Rossi et al., 2007 (microarray)
		Schmidtea mediterranea	100% survival post 15 Gy acute gamma radiation. 100% mortality by 40 days after 20 Gy acute gamma radiation.	Present study. Previous studies referenced in-text.	Sahu et al., 2021

Bryozoa	No	N/A	N/A	N/A	
Entoprocta	No	N/A	N/A	N/A	
Nemertea	No	N/A	N/A	N/A	
Brachiopoda	No	N/A	N/A	N/A	
Phoronida	No	N/A	N/A	N/A	
Annelida	Yes	*Lumbricus terrestris*	$LD_{50/30days}$ = 680 Gy gamma radiation	No	Reichle et al., 1972
		Eisenia fetida	$LD_{50/30days}$ = 650 Gy gamma radiation	No	Suzuki and Egami, 1983
		Neanthes arenacoedenta	No death up to 60 days post 500 Gy acute gamma radiation. Steep decline in survival between day 60 to day 100 post irradiation. For animals irradiated at 1000 Gy, death occurred between day 20-50.	No	Anderson et al., 1990
Mollusca	Yes	*Biomphalaria glabrata*	No adult lethality observed after 20 Gy gamma irradiation. Maximum tolerable dose unknown.	No	De Freitas Tallarico et al., 2004
		Crassostrea gigas	$LD_{50/30days}$ = 1000 Gy gamma radiation	No	Mix and Sparks, 1970
		Lymnaea japonica	$LD_{50/7days}$ = 200 Gy X-rays	No	Bonham and Palumbo, 1951
		Nassarius obsoletus	$LD_{50/30days}$ = 375 Gy gamma radiation	No	White and Angelovic, 1966
		Nucella lamellosa	$LD_{50/7days}$ = 200 Gy X-rays	No	Bonham and Palumbo, 1951
		Physa acuta	$LD_{50/30days}$ = 400 Gy gamma radiation	No	Fujita and Egami, 1984
		Urosalpinx cinerea	$LD_{50/30days}$ = 380 Gy gamma radiation	No	White and Angelovic, 1966
Kinorhyncha	No	N/A	N/A	N/A	
Priapulida	No	N/A	N/A	N/A	
Nematomorpha	No	N/A	N/A	N/A	
Nematoda	Yes	*Caenorhabditis elegans*	>1000 Gy gamma radiation. Maximum tolerable dose unknown	Yes (1 hour after 200 Gy and 400 Gy X-ray exposure. Post-irradiation proteome is also available.	Johnson and Hartman, 1988; Xu et al., 2019; Dubois et al., 2019 (proteome)

Nematoda (continued)		*Neoaplectana carpocapsae*	$LD_{50/30days}$ ≈ 6000 Gy gamma radiation	No	Gaugler and Boush, 1979
		Bursaphelenchus xylophilus	Lethal dose between 6000 to 8000 Gy gamma radiation	No	Eichholz et al., 1991
Arthropoda	Yes	*Drosophila melanogaster*	$LD_{50/30days}$ ≈ 400 Gy gamma radiation	Yes (2,10 and 20 days after 0.1, 10, 50, 100, 200 Gy gamma radiation)	Antosh et al., 2014
		Tigriopus japonicus	$LD_{50/7days}$ = Between 400 and 600 Gy gamma radiation	No	Han et al., 2014
		Calliopius laeviusculus	$LD_{50/21days}$ = 160 Gy X-rays $LD_{50/35days}$ = 90 Gy X-rays	No	Bonham and Palumbo, 1951
		Allorchestes Augustus	$LD_{50/21days}$ = 160 Gy X-rays $LD_{50/35days}$ = 90 Gy X-rays	No	Bonham and Palumbo, 1951
		Tetranychus urticae	$LD_{50/10days}$ = 1000 Gy gamma radiation	No	Nelson and Stafford, 1972
		Callinectes sapidus	$LD_{50/30days}$ = 510 Gy gamma radiation	No	Engel, 1967
		Artemia salina	$LD_{50/5days}$ = 910 Gy X-rays	No	Bonham and Palumbo, 1951
		Palaemonetes pugio	$LD_{50/30days}$ = 15 Gy gamma radiation	No	Rees, 1962
Onychophora	No	N/A	N/A	N/A	
Tardigrada	Yes	*Milnesium tardigradum*	$LD_{50/48hours}$ = 5000 Gy gamma radiation	No	Horikawa et al., 2006
		Richtersius coronifer	$LD_{50/18hours}$ = 4700 Gy gamma radiation $LD_{50/30days}$ = 2500 Gy gamma radiation No observable difference in survival and lifecycle of animals irradiated at 1000 Gy or below relative to unirradiated controls.	No	Jönsson et al., 2005
		Hypsibius dujardini	$LD_{50/48hours}$ = 4180 Gy gamma radiation	No	Beltrán-Pardo et al., 2015
		Ramazzottius varieornatus	$LD_{50/48hours}$ > 4000 Gy gamma radiation. Maximum tolerable dose unknown.	Yes (RNA-seq at 0, 4, 6, 9, 12, 15, 18, 21, and 24 hours post 500 Gy gamma radiation)	Horikawa, 2008 Yoshida et al., 2021 (transcriptome)
		Echiniscoides sigismundi	$LD_{50/7days}$ = 1449 Gy gamma radiation	No	Jönsson et al., 2016

Although many studies have provided invaluable mortality data in animals across diverse phyla, experimental characterization of the effects of ionizing radiation exposure remains challenging and hence limited to only a few organisms. Among them is the nematode *Caenorhabditis elegans*, which was used as a model organism to investigate radiation-induced bystander effects in vivo (Guo et al., 2013). This phenomenon is currently of clinical significance due to undesired effects on unirradiated cells around the zone targeted for radiotherapy. Additionally, *Drosophila melanogaster* was used to demonstrate the occurrence of radiation-induced premature differentiation of neural stem cells and its developmental consequences (Wagle and Song, 2020). These two well-established model organisms were also used as in vivo models to understand the role of conserved radiation-response genes, such as spindle assembly checkpoint regulators, Bub-3 and Mad-3, in *C. elegans* (Bertolini et al., 2017); and the H4K16-acetyltransferase, Males absent on the First (MOF), in *Drosophila* (Bhadra et al., 2011). High throughput genetic screens have also been employed in both *C. elegans* (van Haaften et al., 2004; van Haaften et al., 2006) and *Drosophila* (Vaisnav et al., 2014), revealing genes that influence radiation response on a global scale. Recently, perturbing the DREAM complex was reported to promote DNA repair in *C. elegans* somatic cells, conferring DNA damage resistance in the animals (Bujarrabal-Dueso et al., 2023).

In addition, rotifers and tardigrades have been used as models to understand how some animals withstand acute treatment with extreme levels of ionizing radiation. A major component conferring radiotolerance in the bdelloid rotifer, *Adineta vaga*, is a highly efficient antioxidant system shown to have a significant proteome-protective role when challenged with ionizing radiation. Interestingly, the genome-protective role of the same antioxidant system was found to be negligible (Krisko et al., 2012).

In various tardigrade species, which are extremophiles by nature, a contributing factor to their extreme radiotolerance is a low rate of adult cell proliferation, due to low rates of cell turnover under homeostatic conditions (Gross et al., 2018; Poprawa et al., 2014; Czernekova and Jonsson, 2016). Additionally, genome analysis of the tardigrade *Ramazzottius varieornatus* revealed a copy number expansion of stress-related genes that putatively function in the mitigation of oxidative damage (Hashimoto et al., 2016). In the

same study, a loss of multiple regulators linking genotoxic and oxidative damage to the induction of autophagy were reported. This is hypothesized to benefit the organism under extreme conditions by allowing partially damaged biomolecules to persist (Hashimoto et al., 2016).

Studies involving rotifers and tardigrades have highlighted the potential of non-classical model systems in uncovering novel radiation-related genes with biomedical relevance. This was first exemplified by the discovery of Dsup, a tardigrade-specific DNA-binding protein, whose ectopic expression successfully imparted radiotolerance to human cells in vitro (Hashimoto et al., 2016). Ectopic Dsup is proposed to act by directly binding and shielding the human genome from radiation-induced damage (Chavez et al., 2019). More recently, the ectopic expression of another tardigrade-specific DNA-binding protein, Tardigrade DNA damage Response 1 (TDR1), was observed to protect human U2OS cells against double-stranded breaks (Anoud et al., 2024). A rotifer DNA ligase E, AvLigE, was also capable of imparting X-ray tolerance to human HEK-293T cells upon its ectopic expression (Nicolas et al., 2023).

The use of both classical and non-classical model organisms has advanced our molecular understanding of radiotolerance at the organismal level. Despite this, the in vivo mechanisms governing adult stem cell radiosensitivity remain enigmatic. Interpretation of survival curves associated with radiation-induced mortality studies, as presented in Table 1, indicate a consistent theme of enhanced stem cell sensitivity to ionizing radiation across metazoans. This is because most animals exposed to lethal doses of ionizing radiation typically exhibit initial survival without significant reports of changes in morphology or behaviour. A steep decline in survival then occurs typically days or weeks after exposure, symbolic of death by progressive tissue degradation due to compromised stem cell function. While many of the organisms described are powerful model systems in their own right, investigating stem-cell-specific responses to gamma radiation in an in vivo setting remains extremely challenging. This is because adult stem cells remain elusive in many organisms, and may even be completely non-existent in some lineages. Here, we leverage the unique characteristics of the flatworm *Schmidtea mediterranea* to circumvent certain limitations associated with traditional model organisms. By employing *Schmidtea mediterranea* as our

model system, we aim to shed novel insight into how adult stem cells respond to and potentially withstand exposure to gamma radiation in vivo.

1.6 *Schmidtea mediterranea* – an attractive in vivo model system for the study of stem cell radiation response and tolerance

The planarian *Schmidtea mediterranea* is a freshwater flatworm assigned to the phylum Platyhelminthes. Planarians possess a triploblastic body plan exhibiting bilateral symmetry, and are best known for their remarkable regenerative capacities (Reddien and Sanchez-Alvarado, 2004; Salo, 2006; Agata, 2003). This includes the ability to regenerate the whole body, inclusive of all cell-types in the correct proportions, from fragments as small as $1/279^{th}$ of the original size (Morgan, 1901); and the ability to regenerate a fully functional central nervous system de-novo within 7 days upon head amputation (Cebria et al., 2002). Planarian regeneration is powered by a large pool of mitotically-active adult stem cells that are known as neoblasts (Reddien and Sanchez-Alvarado, 2004; Salo, 2006; Agata, 2003; Aboobaker, 2011). A small subset of adult stem cells in planarians are believed to possess pluripotency, as single-cell transplantation of a rare number of neoblasts was successful in rescuing host animals that had been purged of all stem cells using lethal irradiation (Wagner et al., 2011; Zeng et al., 2018). Furthermore, neoblasts represent the sole proliferative cell-type within the body of adult planarians (Newmark and Sanchez-Alvarado, 2000), and their mitotic activity serves the continuous replenishment of all differentiated cell types lost during normal turnover processes (Pellettieri and Sanchez-Alvarado, 2007; Pellettieri et al., 2010). Stringent control mechanisms regulate the rates of neoblast proliferation and differentiation, and the intricate balance between these two processes can be modulated by environmental signals such as nutrient availability and response to injury (Baguna and Romero, 1981; Oviedo et al., 2003; Takeda et al., 2009; González-Estévez et al., 2012; Forsthoefel et al., 2011; Reddien, 2018).

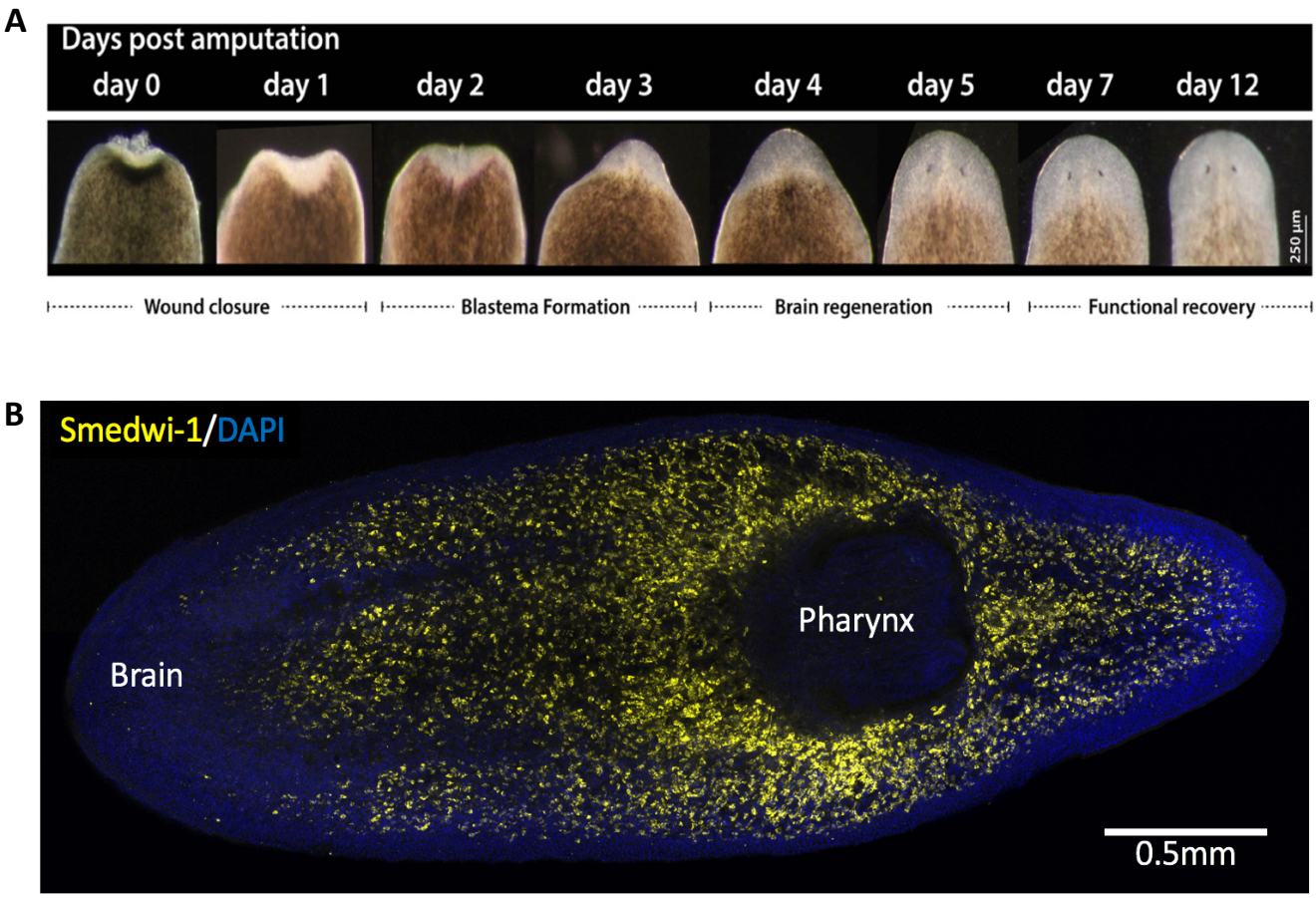

Figure 2. Regenerative capacity of the planarian *S. mediterranea*. (A) Stages of regeneration after anterior decapitation. **(B)** Regenerative capacity is driven by an abundant population of adult stem cells, labelled by the stem cell marker, Smedwi-1, using whole-mount in situ hybridization.

S. mediterranea possesses several compelling features making it an attractive model for in vivo studies on stem cell biology. Most notably, while adult stem cells are typically scarce in many animals employed as experimental models, each planarian possesses abundant numbers of adult stem cells that are experimentally tractable in vivo. Testament to the fact, adult stem cells can make up to 20-30% of all cells within the body of an adult planarian (Baguna et al., 1989). These stem cells are spatially distributed throughout the planarian mesenchyme, absent only in the pharynx, brain, and the anterior tip of the animal [Figure 2] (Reddien and Sanchez-Alvarado, 2004). Akin to other organisms across the animal kingdom, planarian stem cells also exhibit enhanced sensitivity to ionizing radiation in comparison to their differentiated progeny. The radiosensitivity of stem and non-stem cells in planarians differ by a significant margin, to the extent that neoblasts can be selectively ablated by doses of ionizing radiation that do not cause any direct lethality to their differentiated progeny (Hayashi et al., 2006; Peiris et al., 2016a). Exploiting this property, ionizing radiation is routinely incorporated in experimental designs within the planarian research community, yielding novel insights into planarian stem cell function, which in turn may have broader implications for human stem cell biology. For instance, ionizing radiation has been used in various studies to deplete stem cells within host animals in preparation for cell transplantation from donors (Wagner et al., 2011; Zeng et al., 2018, Raz et al., 2021; Wang et al., 2018). Lethal doses of gamma radiation have also been employed to identify genes that are enriched in stem cells or their progeny (Eisenhoffer et al., 2008), with the rationale that neoblast genes would be downregulated at the earliest instance as a direct result of their depletion following radiation exposure. Genes enriched in stem cell progeny were also identified in the same study, as progeny cells differentiate without replenishment, causing their numbers to decline shortly after the depletion of stem cells (Eisenhoffer et al., 2008). Sub-lethal doses of radiation, which permit a small number of stem cells to evade lethality, have also been used in studies investigating the stem cell repopulation process (Wagner et al., 2012; Lei at al., 2016; Zhu et al., 2015; Rossi et al., 2014; Raz et al., 2021; Wang et al., 2018).

Moreover, diligent and collaborative efforts have led to the generation of numerous genomic and transcriptomic resources that facilitate molecular-scale studies of planarian biology. Firstly, the genome of *S. mediterranea* had been sequenced and deposited in a

readily accessible format through the SmedGD platform (Robb et al., 2008). Recent advances have further improved the *S. mediterranea* genome assembly (Grohme et al., 2018), alongside with improvements in genome annotation (Dattani et al., 2018; Neiro et al., 2022).

In addition to the sequenced genome, multiple *S. mediterranea* transcriptome assemblies have also been generated and are curated in readily accessible formats (Brandl et al., 2016; Rozanski et al., 2019). Furthermore, the generation of ChIP-seq (Dattani et al., 2018; Mihaylova et al., 2018; Duncan et al., 2015; Zeng et al., 2013) and ATAC-seq (Neiro et al., 2022; Pascual-Carreras et al., 2023) datasets, which investigate DNA-protein interactions and chromatin accessibility respectively, provides further insights into the complex regulation of planarian gene expression. Last but not least, an expansion in single-cell RNA-sequencing studies in the past decade has facilitated the generation of organism-wide and tissue-specific single-cell atlases of planarians (Fincher et al., 2018; Plass et al., 2018; van Wolfswinkel et al., 2014; Wurtzel et al., 2015; Zeng et al., 2018; Benham-Pyle et al., 2021; Garcia-Castro et al., 2021). By examining gene expression at the single-cell level, these studies reveal novel cell-types, enable lineage reconstruction in silico, and further unveil the heterogeneity that exists within the planarian stem cell compartment. Single-cell studies in planarians are further explored in Chapter 3.

Single-cell approaches, combined with an array of molecular studies, have provided evidence of functional heterogeneity within the planarian stem cell compartment. For instance, a single-cell multiplexed qPCR approach identified three prominent neoblast expression classes termed the sigma, zeta, and gamma states (van Wolfswinkel et al., 2014). Sigma neoblasts were inferred to be multipotent (van Wolfswinkel et al., 2014) and capable of long-term self-renewal (Lai et al., 2018). These sigma neoblasts were hypothesized to give rise to the epidermal-committed zeta neoblasts and the intestinal-committed gamma neoblasts (van Wolfswinkel et al, 2014). Each of these subclasses are characterized by the expression of unique transcription factors that are reproducible in vivo (van Wolfswinkel et al., 2014; Zhu et al., 2015; Lai et al., 2018; Mihaylova et al., 2018). Such transcription factors include Soxp1/2 which mark the sigma state, Zfp-1 and Soxp3 which mark the zeta state; as well as Gata4/5/6 and Hnf4 which mark the gamma state.

Molecular studies have uncovered additional lineage-specified neoblast states poised to differentiate into mature cells of various tissues. These include the eye (Lapan and Reddien, 2011; Lapan and Reddien, 2012), pharynx (Adler et al., 2014), nervous system (Currie and Pearson, 2013; Cowles et al., 2013; Scimone et al., 2014; Roberts-Galbraith et al., 2016; Molinaro and Pearson, 2016), excretory system (Scimone et al., 2011), pigment cells (Wang et al., 2016; He et al., 2017) and muscle (Scimone et al., 2017; Scimone et al., 2018). These investigations have also unveiled distinct fate-specifying transcription factors (FSTFs) associated with different neoblast classes. The expression of distinct FSTFs instructs stem cell differentiation into specific cell lineages. Examples of FSTFs include Zfp-1, required for epidermal specification (van Wolfswinkel et al., 2014; Tu et al., 2015), ovo, required for eye specification (Lapan and Reddien, 2012), albino, required for pigment cell formation (Wang et al., 2016), and foxA, required for differentiation into pharyngeal cells (Adler et al., 2014).

Overall, the studies described have contributed to the establishment of the neoblast fate restriction model (term coined in Reddien, 2022). According to this model, neoblasts are organized into a hierarchy based on their differentiation potential. The model suggests that at the top of the hierarchy reside the naïve stem cells, which potentially include the putatively pluripotent cNeoblast (Wagner et al., 2011), or the more recently proposed pluripotent state marked by high Tetraspanin-1 protein expression (Zeng et al., 2018). The model also posits a progressive restriction in differentiation potency along the hierarchy, where naïve stem cells give rise to fate-specialized neoblasts, which in-turn go on to differentiate into various mature cell-types (Figure 3A).

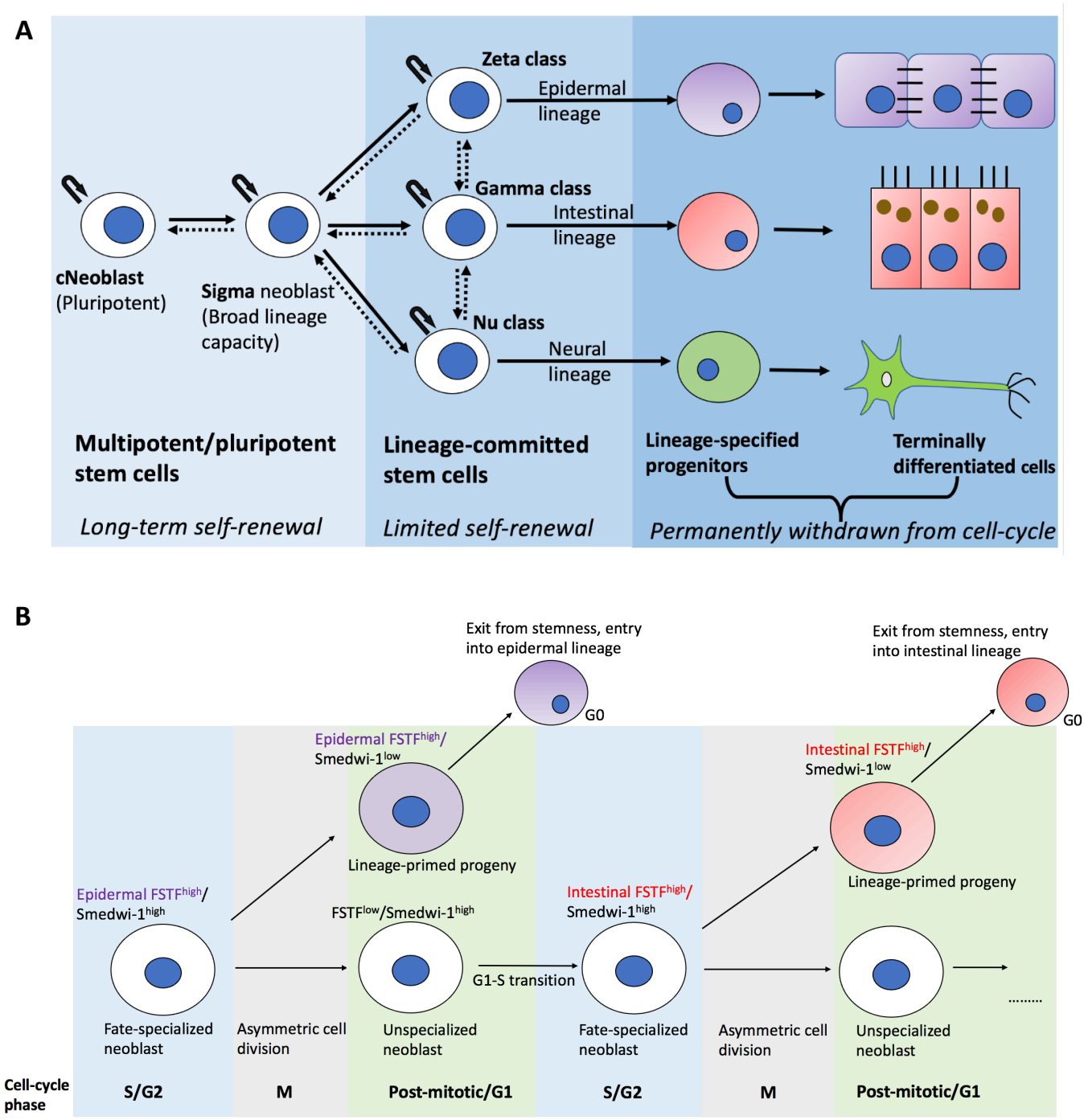

Figure 3. Suggested models of fate specification and potency in planarian stem cells.

(A) Hierarchical fate-restriction model of neoblast specialization and potency.

(B) Non-hierarchical single-step fate model of neoblast specialization and potency. The illustrations have been simplified to feature selected lineages as representatives.

An emerging view that challenges the conventional fate restriction model is the single-step fate model (Figure 3B) proposed by Raz and colleagues (Raz et al., 2021). The authors first demonstrated a close association between FSTF expression and cell-cycle stage. FSTF expression was notably enriched in S/G2 phase neoblasts, with limited expression in G1 phase. During asymmetric cell division, markers of stemness and FSTFs are disproportionally inherited, yielding an $FSTF^{high}$/Smedwi-1^{low} daughter that withdraws from stemness and undergoes differentiation; and an $FSTF^{low}$/Smedwi-1^{high} daughter that retains stemness and reverts to a naïve state. This model proposes that pluripotency is not restricted to any specific neoblast subclass; rather, plasticity exists, allowing neoblast fates to be reversed after asymmetric cell division. Support for this model comes from single-cell transplantation assays into lethally irradiated hosts, showing that distinct lineage-specified stem cells could give rise to stem cells of different classes, ultimately rescuing the irradiated hosts (Raz et al., 2021). Despite these findings, it is crucial to acknowledge that the observed phenomenon of fate-switching has only been documented under stressful conditions, where stem cells are required to rapidly proliferate to rescue irradiated hosts. Whether fate-switching occurs under homeostatic conditions requires further investigation. Further efforts to investigate the influence of epigenetic fate memory on this model would also be important for understanding planarian pluripotency, which in turn may provide broader insights into pluripotency across metazoans.

Nevertheless, coupling the unique properties of planarians with the recent advances in sequencing and molecular biology, the mechanistic basis behind many biological processes can be readily investigated in vivo. Robust protocols had been developed for gene-specific knockdown in planarians using RNA-interference (RNAi) [Sanchez-Alvarado and Newmark, 1999). RNAi has been employed in many systematic screens to delineate the key players in biological processes such as gut development (Forsthoefel et al., 2012), germ cell development (Wang et al., 2010) and central nervous system regeneration (Roberts-Galbraith et al., 2016) amongst many others. In addition, protocols for tissue fixation, in situ hybridization and immunostaining in planarians have been established (King and Newmark, 2013; Forsthoefel et al., 2018). This, coupled with the ever-growing list of cell-type specific markers, allows researchers to quantitatively assess changes to specific cell types or tissues at the molecular level. Moreover, whole animals can be dissociated into single-cells, and

neoblasts can subsequently be enriched from a heterogeneous cell population using fluorescence activated cell-sorting (Hayashi et al., 2006). Without the need for cell-type specific markers, cells in planarians can be categorically sorted into three subgroups: X1, X2 and Xins, based on their nuclear-to-cytoplasmic ratios. The X1 cell population, characterized by high (>2C) DNA content, small cell size, and sensitivity to ionizing radiation, is comprised of cycling stem cells in S/G2/M phases; the X2 fraction is comprised of non-cycling stem cells (in G0/G1) and immediate stem cell progenies; while the Xins compartment is comprised almost entirely of radiation insensitive differentiated cell-types (Eisenhoffer et al., 2008). Cohorts of genes enriched in each of the sorted cell fractions have also been identified (Eisenhoffer et al., 2008).

Despite the array of tools described, it is crucial to acknowledge the current experimental limitations of the planarian model system. For instance, tools for genome editing and transgenesis are currently unavailable in *S. mediterranea*. Besides, while loss-of-function experiments using RNAi can be reliably conducted in vivo, tools for ectopic expression or overexpression of genes are currently unavailable. This is because the delivery of exogenous mRNAs and DNA cassettes into planarian cells remains a major challenge. Although recent efforts have demonstrated successful delivery of exogenous mRNA into planarian cells via transfection (Hall et al., 2022), robust and reproducible transfection protocols have yet to be established. Hence informative studies involving gain-of-function experiments remain inaccessible in planaria. While the advances in omics-based techniques and the availability of RNAi makes planarians a powerful system for reverse genetics, low fecundity in sexual strains and the complete absence of fecundity in obligate asexual strains limit the application of forward genetics in planarians. Furthermore, the development of culture systems for the in vitro maintenance of neoblasts is still in its infancy phase (Lei et al., 2023), as the methodologies for long-term culture and clonal expansion of neoblasts in vitro have yet to be robustly established. By leveraging the strengths of the planarian model system while being mindful of its shortcomings (Table 2), planarians remain an exciting tool that can be used to broaden our understanding on how adult stem cells respond to, and potentially withstand exposures to ionizing radiation.

Table 2. Current strengths and limitations of the planarian model system in research.

Strengths	Limitations
Easy of husbandry	Ectopic gene expression unavailable
Cost efficient to maintain	Overexpression of genes unavailable
Genome has been sequenced	No established stem cell culture system
Transcriptome datasets readily accessible	Tools for transgenesis unavailable
Possess a large number of adult stem cells (20%-30% of adult body comprised of stem cells)	Asexual strains have zero fecundity, sexual strains have relatively low fecundity
Stem cells can be purified by FACS	
Many cell-type specific markers identified	
Robust protocols for gene-specific knockdown using RNA-interference	
Stem cells experimentally tractable in vivo	
Possess elevated radiotolerance in contrast to humans	

1.7 The DNA damage response and outcomes of ionizing radiation exposure in *S. mediterranea*

To dissect the dose of acute gamma radiation that is lethal to *S. mediterranea*, previous work in our group examined the survival of individuals exposed to varying gamma radiation doses (Sahu et al., 2021). We observed that *S. mediterranea* can withstand whole-body treatments with up to a 15 Gy dose of acute gamma radiation without the occurrence of any long-term physiological defect (100% survival). However, acute gamma radiation doses equal to or exceeding 20 Gy led to 100% mortality among the irradiated individuals [Figure 4A]. While no morphological defect was observed in sub-lethally irradiated animals, individuals exposed to lethal doses exhibited morphological changes stereotypical of a loss-in-stem-cell-function phenotype, attributed by anterior regression that usually starts between 20 – 30 days post-exposure (dose-dependent), followed by ventral curling and eventual tissue lysis [Figure 4B] (Bardeen and Baetjer, 1904; Reddien et al., 2005a).

In the same study, we also investigated the temporal changes in neoblast numbers in vivo after planarians were subjected to various doses of acute gamma radiation [Figure 4E] (Sahu et al., 2021). Initially, we observed that across all doses, neoblast numbers remain at wild-type levels as of 3 hours post-irradiation. This is ensued by a dose-dependent decline in the number of neoblasts, finally reaching a minima at 3 days post irradiation. When planarians were exposed to sub-lethal doses of up to 15 Gy, some, if not all of the surviving stem cells were capable of retaining proliferative competency. The surviving stem cells were able to re-enter the cell cycle, proliferate, and repopulate the stem cell compartment of the animal. Ultimately, sub-lethally irradiated animals were able to restore full physiological function, as they could persist long-term and are able to continuously produce offspring without an observable defect. Subsequently, we investigated the recovery kinetics of mitotic cells over a time course after various doses of gamma radiation [Figure 4F]. Since neoblasts are the only cell-type within planarians capable of proliferation, immunostaining against the mitotic marker, Phospho-Histone H3 (H3P), would be a direct proxy for stem cell activity. In animals exposed to sublethal doses of up to 15 Gy, we observed that surviving neoblasts initially deploy a proliferative block, likely allocated for DNA repair, with the duration of this mitotic arrest being dose-dependent. Mitotic cells then gradually reappeared in sub-lethally irradiated animals, eventually returning to wild-type levels (Figure 4F). This phenomenon of dose-dependency in the rates of mitotic cell recovery and stem cell repopulation is relatable to observations in the more radiotolerant flatworm, *Macrostomum lignano* (Pfister et al., 2007; De Mulder et al., 2010).

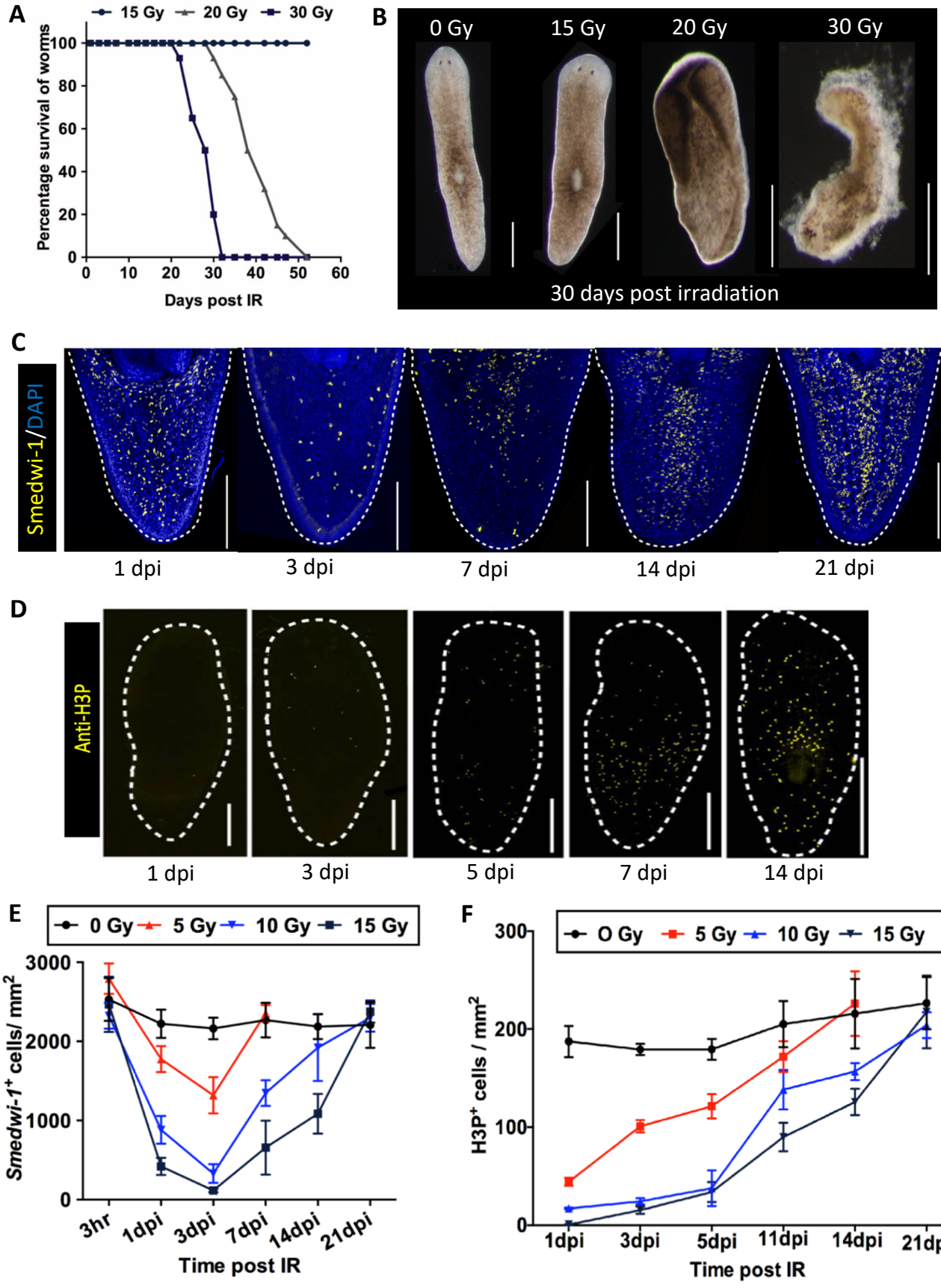
A
15 Gy
20 Gy
30 Gy
Percentage survival of worms
Days post IR
B
0 Gy
15 Gy
20 Gy
30 Gy
30 days post irradiation
C
Smedwi-1/DAPI
1 dpi
3 dpi
7 dpi
14 dpi
21 dpi
D
Anti-H3P
1 dpi
3 dpi
5 dpi
7 dpi
14 dpi
E
0 Gy
5 Gy
10 Gy
15 Gy
Smedwi-1+ cells/ mm2
3hr
1dpi
3dpi
7dpi
14dpi
21dpi
Time post IR
F
O Gy
5 Gy
10 Gy
15 Gy
H3P+ cells / mm2
1dpi
3dpi
5dpi
11dpi
14dpi
21dpi
Time post IR

Figure 4. Outcomes of sublethal and lethal irradiation in planarians. (A) Survival curve of planarians exposed to a sublethal (15 Gy) dose or lethal (20 Gy and 30 Gy) doses of acute gamma radiation. **(B)** Brightfield images of planarians 30 days post-exposure to varying doses of acute gamma radiation. **(C)** In situ hybridization for stem cell marker Smedwi-1 over time post-exposure to sublethal 15 Gy acute gamma radiation. **(D)** Anti-H3P immunofluorescence for mitotic marker H3P over time post-exposure to sublethal 15 Gy acute gamma radiation. **(E)** Recovery kinetics of Smedwi-1^{+} cells in planarians exposed to varying doses of acute gamma radiation. **(F)** Recovery kinetics of mitotic cells in planarians exposed to varying doses of acute gamma radiation. Figure adapted from Sahu et al., 2021.

When planarians were exposed to lethal doses such as 20 Gy and 30 Gy, residual surviving stem cells could still be detected between 3 to 7 days after radiation exposure. However, these stem cells were rendered proliferation incompetent, thus failing to rescue the animal, as evidenced by the absence of detectable mitotic cell recovery in individuals irradiated with such doses (Sahu et al., 2021).

The molecular mechanisms enabling planarians to survive radiation doses as high as 15 Gy remain poorly understood. It is unlikely that tolerance to acute gamma radiation has evolved in planarians due to direct selection pressure from the environment. This is because planarians naturally inhabit the base of freshwater streams or ponds, with many biotic and abiotic components associated with the habitat that provide protection against all forms of radiation. On the contrary, we hypothesize that radiotolerance in planarians may exist as a by-product of adaptation against other genotoxic stressors naturally encountered in the planarian life history, or it may be an emergent characteristic resulting from their highly regenerative life history.

Highly regenerative planarians can bypass the phenomenon of biological aging (Pearson and Sanchez-Alvarado, 2008; Tan et al., 2012; Sahu et al. 2017). Given this property, asexual strains of planarians have been termed somatically immortal (Sahu et al., 2017). Unlike mammalian stem cells, which are typically quiescent (Cheung and Rando, 2013), a quiescent stem cell state has yet to be characterized in planarians. Rather,

planarian stem cells cycle actively under homeostatic conditions to balance the high rates of cell turnover (Pellettieri and Sanchez-Alvarado, 2007; Pellettieri et al., 2010; Rink, 2013). These studies investigating cell turnover in planarians report that all cells within their bodies may be completely renewed in just a matter of weeks. Even the central nervous system, which is commonly subjected to age-related pathologies in mammals due to poor renewal and repair (Huebner and Strittmatter, 2009), is fully renewed in planarians in just 28 days (Brown and Pearson, 2017; Currie et al., 2016). Given the high levels of activity, planarian stem cells may have evolved efficient DNA damage surveillance and repair mechanisms to counteract the various forms of replication-induced DNA damage. Besides, even though planarians possess theoretically immortal lifespans, naturally occurring planarian cancers are believed to be extremely rare (Pearson and Sanchez-Alvarado, 2009; Sahu et al., 2017; Oviedo and Beane, 2017; Barghouth et al., 2019). This may also imply that mechanisms to maintain genomic fidelity actively function in planarians to limit tumorigenesis over extensive periods of time. Correspondingly, the same machinery driving the properties of anti-aging and tumour suppression may be called upon when the animals are challenged with ionizing radiation.

To better understand the planarian response to ionizing radiation, our group investigated the conservation of core DNA damage response genes in *S. mediterranea*. Through in silico analysis of the planarian genome, it was found that most genes within the canonical DNA damage response network are also conserved in planarians, although some notable exceptions exist. For instance, the crucial regulator of eukaryotic cell senescence, p21; the pro-apoptotic protein, BAX; and multiple XRCC family genes involved in DNA strand break repair, are absent from the planarian genome. Our findings corroborated a prior study by Barghouth and colleagues investigating the conservation of DNA damage response genes in planarians (Barghouth et al., 2019). The loss of these genes could potentially be a causation or consequence of the planarian's supposed immortal life history, prompting stem cells to favour survival over p21-mediated senescence or BAX-mediated apoptosis for instance. While these genes play key roles in radiation-induced cellular outcomes observed in mammals (Maier et al., 2016), how the loss of these genes in planarians influence the neoblast response to ionizing radiation remains unclear.

Next, our group investigated the function of various DNA damage response genes in the context of planarian radiotolerance. We observed that RNAi-mediated silencing of various components within this network rendered planarians sensitive to gamma radiation (Figure 5). This illustrates that many of these genes, known to be essential for DNA repair across diverse phyla, may also have conserved roles in planarians. However, an exception is the canonical non-homologous end-joining pathway, which appears to be dispensable for planarian survival after radiation exposure. This is because single knockdowns of canonical end-joining components – Ku70, Ku80, Artemis, and Lig4 failed to sensitize planarians to sublethal irradiation (Peiris et al., 2016c; Shiroor et al., 2023).

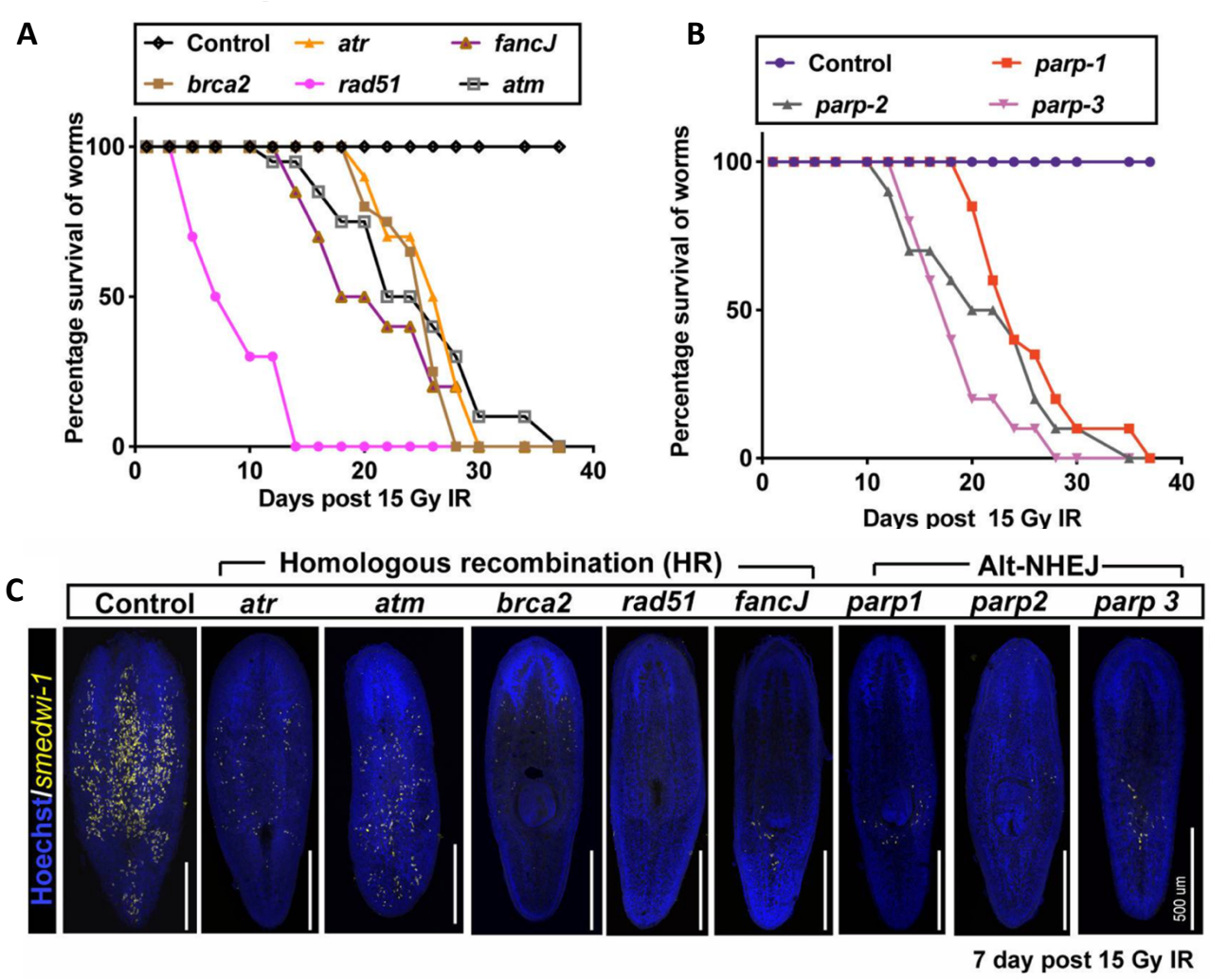

Figure 5. RNAi of evolutionarily conserved DNA repair genes sensitizes planarians to sublethal irradiation. **(A)** and **(B)** Survival curves of various RNAi-treated planarians exposed to sublethal irradiation. **(C)** Assessment of neoblast recovery after irradiation in various RNAi backgrounds by in situ hybridization targeting the stem cell marker, Smedwi-1, at 7 days post 15 Gy irradiation. Figure adapted from Sahu et al., 2021.

At present, one gene within the conserved DNA damage response network that is of functional ambiguity in planarians is the apical kinase ATM. In our group, we observed that RNAi-mediated knockdown of ATM caused animals to succumb to a normally sublethal 15 Gy dose of acute gamma radiation, despite some degree of stem cell recovery being observed after knockdown and irradiation (Figure 5C). This observation contradicts two findings in the literature, where ATM RNAi appeared to confer radioprotection to planarian stem cells instead. Namely, Peiris and colleagues observed that ATM RNAi accelerated the stem cell recovery process in animals irradiated with a sublethal 12 Gy dose of acute gamma radiation (Peiris et al., 2016c); while Shiroor and colleagues reported that ATM RNAi increased the overall radiotolerance of individuals, enabling them to survive a 20 Gy acute dose of gamma radiation (Shiroor et al., 2023), a dose that is normally lethal to untreated planarians. Shiroor and colleagues theorized that this radioprotective role may be due to divergence of ATM function in planarians, with the loss of the N-terminal solenoid in the planarian ATM orthologue potentially causing the protein to lose its pro-repair functions, whilst retaining its pro-apoptotic roles. However, due to the lack of assays measuring DNA repair in ATM knockdown animals, the function of planarian ATM in the context of DNA repair remains inconclusive and cannot be ruled out. It remains plausible that ATM possesses dual functionalities in planarians dependent on its activation level, as it is in mammals, with low levels of ATM activity facilitating repair, and high levels of ATM activity driving p53-induced apoptosis (Khanna et al., 2001; Jeggo and Lobrich, 2006; Zhang et al., 2011; Enoch and Norbury, 1995; Banin et al., 1998; Canman et al., 1998). The disparities between our observations and those reported in the literature may be attributed to differences in dosimetry, and pragmatic limitations of RNAi, namely the incompleteness and variability in the extent of gene silencing. Variances in the extent of gene silencing between our study and the study by Shiroor and colleagues may have arisen due to the different methods of double-stranded RNA (dsRNA) delivery employed, with the use of microinjection in the former and feeding in the latter. The higher precision and payload of microinjection may have allowed us to abrogate both ATM's apoptotic and repair roles. In contrast, the feeding method opted by Shiroor and colleagues may have yielded sufficient gene silencing to disable the apoptotic functions of ATM, but residual activity of the gene may permit sufficient pro-repair effects to aid in the radiation recovery process. Further investigations

involving assays measuring DNA repair would be imperative to better understand the function of ATM in planarians both under homeostatic and irradiated conditions.

While several genes within the DNA damage response network were found to be important for planarian radiotolerance, our knowledge of factors beyond this network that influence the planarian radiation response remains in its infancy phase. Recently, animals wounded before or immediately after exposure to gamma radiation were found to be more resilient against radiation-induced lethality (Shiroor et al., 2020). The act of wounding may prime the animals to better withstand ionizing radiation, as the same pro-survival pathways activated upon wounding may be re-allocated to combat the damaging effects of radiation exposure. Furthermore, conserved tumour suppressors such as PTEN, Akt, Rb, and p53, have all been shown to possess important roles in regulating planarian tissue homeostasis and regeneration (Oviedo et al., 2008; Pearson and Sanchez-Alvarado, 2010; Peiris et al., 2016b; Zhu and Pearson, 2013). However, their contribution to the planarian radiation response remains unexplored.

In summary, *S. mediterranea* can tolerate acute whole-body exposures of up to a 15 Gy dose of gamma radiation. This dose permits a small number of stem cells to evade the initial phase of radiation-induced lethality. Some, if not all of the surviving stem cells, are capable of DNA repair, cell-cycle re-entry, and subsequent clonal expansion to rescue the irradiated animal. In contrast to humans, planarians display a five-fold greater tolerance to acute gamma radiation, as a 3 Gy dose is sufficient to cause lethality in adult humans without medical intervention (Shao et al., 2014; Waselenko et al., 2004). The relatively higher radiotolerance of planarian stem cells compared to humans, combined with their abundance and tractability in vivo, makes planarians a promising model system to identify novel and conserved regulators influencing radiation response and tolerance in stem cells. While progress has been made in our understanding of conserved DNA repair genes and their contributions to planarian radiotolerance, many intriguing questions remain unanswered. For instance, do the neoblasts that survive treatment with gamma radiation occur at random, or are there inherent properties unique to the survivors that render them more resilient towards radiation-induced apoptosis, such as seen in a rare number of cancer stem cells after radiotherapy? What are the factors outside of the DNA damage response

network that contribute to planarian radiotolerance? In this study, we adopt a functional genomics approach with the overarching goal of increasing our mechanistic understanding of planarian stem cell radiation response and tolerance, which may in turn be broadly informative for our understanding of radiation response in human stem cells.

1.8 Research objectives and overview of results chapters

The two main research objectives are to investigate the transcriptional response of planarian stem cells following exposure to gamma radiation at both bulk and single-cell levels, and subsequently to uncover novel genes crucial for driving planarian radiotolerance.

In Chapter 3, we constructed single-cell gene expression atlases of irradiated planarians. By assessing changes in the single-cell atlases, we identified distinct stem cell populations exhibiting differential sensitivities to gamma radiation. Utilizing RNA velocity, we discerned dose and time-dependent shifts in cell fate trajectories post-irradiation. By investigating the markers enriched in each neoblast cluster and integrating these findings with the inferred cell fate transitions, we proposed a model linking stem cell radiosensitivity to cell-cycle phase.

In Chapter 4, we investigated genes exhibiting differential expression in the bulk X1 cell fraction in response to acute gamma radiation exposure. Coupling insights from both our single-cell and bulk RNA-sequencing efforts, we selected candidate genes for a primary RNAi screen aimed to uncover important regulators of planarian radiotolerance. Our screen encompassed the silencing of 105 single genes, revealing six pivotal genes conferring radiotolerance to planarians in vivo. We identified an additional 20 single-gene knockdowns that significantly delayed the post-irradiation stem cell recovery process, although these knockdowns alone were insufficient to cause animal mortality.

In Chapter 5, the six hits from our primary RNAi screen were functionally characterized in vivo. We evaluated DNA strand break repair capacity, neoblast cell-cycle re-entry kinetics, as well as the kinetics of stem cell proliferation and differentiation in animals subjected to targeted gene RNAi in tandem with sublethal irradiation. Our objective was to pinpoint the specific stage(s) of recovery impacted by each gene knockdown. Our findings indicate significantly impaired post-irradiation stem cell recovery upon target gene knockdown. We also identified one gene, Dkc, as a novel contributor to post-irradiation DNA strand break repair in planarians.

Chapter 2: Materials and Methods

1. Planarian culture

Asexual freshwater *Schmidtea mediterranea* were used throughout this study. Planarians were housed in food-grade containers with 0.5 g/L of Instant Ocean (Aquarium Systems) and cultured in the dark at 20°C. The animals were fed organic calf liver twice a week, with water replaced after each feed. Planarians were starved 7 days prior to each experiment.

2. Gamma irradiation

Animals received acute whole-body gamma radiation from a 137 Cs source using a GSR D1 GsM gamma irradiator (Gamma-service Medical GmbH) at a dose rate of 1.75 Gy/min. During irradiation, animals were kept in 30 mm diameter plastic petri dishes with a thin layer of Instant Ocean solution, enough to cover their bodies and prevent desiccation. Irradiated planarians were subsequently housed in 100 mm diameter plastic petri dishes throughout the course of each experiment, with water changes performed every 48 hours.

3. Gene cloning

3.1 Total RNA isolation

To enrich for radiation-responsive transcripts, total RNA was extracted from animals 24 hours post-exposure to 5 Gy gamma radiation. In each reaction, 2 irradiated worms (~5 mm in length) were placed in a microcentrifuge tube, treated with 500 μl of TRIzol (Invitrogen) and snap frozen in dry ice for 1 hour. The tissue was homogenized and incubated at -20°C for 15 minutes. 100 μl of chloroform was added, and samples were vortexed vigorously for 15 seconds before incubation at room temperature for 5 minutes. The sample was then centrifuged at 12000 rcf for 15 minutes at 4°C and the aqueous fraction was carefully harvested. The sample was then treated with 250 μl of 100% isopropanol for 15 minutes at -20°C. Samples were centrifuged again at 12000 rcf for 15 minutes at 4°C, followed by the addition of pre-chilled 70% ethanol and centrifuged at 7500 rcf for 7 minutes at 4°C. The supernatant was discarded, and the pellet was air-dried to remove residual ethanol before resuspension in nuclease-free water. The quality and quantity of RNA were assessed using a nanodrop and by agarose gel electrophoresis before long-term storage at -80°C.

3.2 cDNA synthesis

1 μg of total RNA was used for each cDNA synthesis reaction using Oligo(dT)$_{18}$ primers (Invitrogen) and the SuperScript Reverse Transcriptase III kit (Invitrogen). 1 μg of total RNA, 1 μl of 50 μM Oligo(dT)$_{18}$ primers, 1 μl of dNTP mix (containing 10 mM of each dNTP), and nuclease-free water to a total volume of 13 μl, were first incubated at 65°C to help denature RNA secondary structures and to pre-anneal the dT primers to polyA tails. A mixture containing 4 μl 5X first-strand buffer mix (Invitrogen), 1 μl 0.1 M DTT and 2 μl of 200 U/μl SuperScript Reverse Transcriptase III (Invitrogen) was then added to the reaction mix and incubated at 50°C for 90 minutes. Enzymes were heat-inactivated at 80°C for 20 minutes. RNAse H (NEB) was then added at a working concentration of 1 U/μl and the reaction mix was incubated at 37°C for 20 minutes. The resulting cDNA was kept at -20°C for long-term storage.

3.3 Amplification of target genes from cDNA

Transcript sequences of target genes were retrieved from the PlanMine 3.0 database (Rozanski et al., 2019). Gene-specific primers were designed using Primer3Plus (Untergasser et al., 2012) with the following specifications: product size range 500-800 bp, GC content 50-55%, Tm: 57-60°C, and conserved regions were avoided to prevent non-specific amplification. Primer sequences for the cloned genes can be found in Appendix Table 7. For each primer set, the following adapter sequences, complementary to the bases flanking the vector insertion site, were incorporated:

Forward primer adapter: $^{5'}$CATTACCATCCCG$^{3'}$
Reverse primer adapter: $^{5'}$CCAATTCTACCCG$^{3'}$

Target gene fragments were amplified from cDNA using a PCR-reaction mix containing 1-3 μl of cDNA (to be optimized on a gene-by-gene basis), 25 μl OneTaq 2X Master Mix (NEB), 0.5 μM of each forward and reverse primer, and water to a total volume of 50 μl. PCR cycling parameters used were as follows: initial denaturation at 95°C for 3 minutes, 35 cycles of denaturation at 95°C for 45 seconds, annealing at 58°C for 30 seconds, extension at 72°C for 1 minute, and a final extension at 72°C for 5 minutes. PCR products were evaluated by

electrophoresis on a 1% agarose gel, followed by gel extraction using the MinElute Gel Extraction Kit (Qiagen) as per manufacturer's instructions.

3.4 Cloning into PPR-T4P Vector

The purified PCR products, containing the target insert flanked by specific adapters, were cloned into PPR-T4P vectors (kind gift from Dr. Jochen Rink, Max Planck Institute). 1 μg of PPR-T4P plasmid was first linearized using the SmaI restriction enzyme kit (NEB) as per manufacturer's instructions. The digested plasmids were gel extracted using the MinElute Gel Extraction Kit (Qiagen). Both the linearized vector and purified inserts (refer to section 3.3) were individually diluted with nuclease-free water to achieve 300 ng of product in a volume of 8 μl in preparation for digestion using T4 DNA polymerase. To the inserts, 0.5 μl 50 mM dCTP was added, and to the vector, 0.5 μl of 50 mM dGTP was added. Subsequently, 1 μl 10X NEBuffer r2.1 (NEB) and 0.5 μl of 3 U/μl T4 DNA polymerase (NEB) were added to both reactions. The mixtures were incubated at 22°C for 30 minutes followed by heat inactivation at 75°C for 20 minutes. The T4 DNA polymerase-treated inserts and vectors were combined at an insert-to-vector molar ratio of 5:1 at room temperature for 1 hour to facilitate ligation. The ligation products were then transformed into competent DH5α cells (ThermoFisher) by adding 5 μl of the ligation mix to 50 μl aliquots of competent cells for 2 minutes on ice, followed by heat-shock at 42°C for 30 seconds. The cells were incubated on ice for 2 minutes for recovery before 250 μl of Luria-Bertani (LB) medium was added. The culture was incubated at 37°C for 1 hour in a shaking incubator. The culture was then spread on LB-agar plates containing kanamycin at a working concentration of 50 μg/ml and incubated at 37°C overnight. Colonies were screened using colony PCR and positive colonies were validated by Sanger Sequencing (service by Source Bioscience). The final plasmid product contains the target insert flanked by opposing T7 promoter sites, facilitating the PCR-synthesis of DNA templates using specific primer sets to either include both promoters (to generate dsRNA for RNAi), or only the promoter on the anti-sense strand (to generate riboprobes for in situ hybridization).

4. Synthesis of dsRNA and riboprobes

100 ng of cloned plasmids (refer to section 3.4) were used as templates for PCR to generate the DNA templates for in vitro transcription. For dsRNA synthesis, M13 forward and reverse primers were used, while AA18 and PPR244 primer sets were used for riboprobe synthesis. Primer sequences are as follows:

M13 Forward: $^{5'}$TGTAAAACGACGGCCAGT$^{3'}$
M13 Reverse: $^{5'}$CAGGAAACAGCTATGACC$^{3'}$
PPR244: $^{5'}$GGCCCCAAGGGGTTATGTGG$^{3'}$
AA18: $^{5'}$CCACCGGTTCCATGGCTAGC$^{3'}$

The PCR reaction mix comprised 100 ng plasmid, 0.5 μM of each appropriate forward and reverse primer, 25 μl OneTaq 2X Master Mix (NEB), and water to a total volume of 50 μl. PCR cycling parameters were as follows: initial denaturation at 95°C for 3 minutes, 40 cycles of denaturation at 95°C for 45 seconds, annealing at 58°C for 30 seconds, extension at 72°C for 1 minute, and a final extension at 72°C for 5 minutes. PCR products were evaluated by electrophoresis on a 1% agarose gel to ensure the absence of non-specific amplicons and substantial primer dimers, and were purified using the QIAquick PCR Purification Kit (Qiagen) as per manufacturer's instructions.

For dsRNA synthesis, in vitro transcription was performed using 500 ng of the purified PCR products as templates. The reaction mixture included 3 μl of 50 U/μl T7 RNA polymerase (NEB), 4 μl 10X RNAPol buffer (NEB), 4 μl rNTP mix (containing 20 mM of each rNTP) and nuclease-free water to a total volume of 40 μl. The mixture was incubated for 6 hours at 37°C, then treated with 2 μl of 2 U/μl TURBO DNAse (Invitrogen) for 30 minutes at 37°C to remove residual DNA. The products were precipitated using sodium acetate (0.3 M final concentration, pH 5.2) dissolved in 500 μl pre-chilled 100% ethanol for 16 hours at -20°C. The samples were then centrifuged at 13000 rcf for 20 minutes at 4°C. Resulting pellets were washed with pre-chilled 70% ethanol and centrifuged at 13000 rcf for 20 minutes at 4°C. Final pellets were air-dried, and RNA was eluted in nuclease-free water. The eluted RNA was incubated at 68°C for 15 minutes, followed by incubation at 37°C for 30 minutes to anneal dsRNA. dsRNA quality and yield were assessed by electrophoresis on a 1% agarose gel, and dsRNA was kept at -80°C for long-term storage.

Riboprobes were synthesized via in vitro transcription in a reaction containing 500 ng of the purified PCR products as templates, 2 μl of 50 U/μl T7 RNA polymerase (NEB), 2 μl 10X RNAPol reaction buffer (NEB), 2 μl of either 10X DIG RNA-labelling mix (Roche) or 10X FITC RNA-labelling mix (Roche) and nuclease-free water to a total volume of 20 μl. The mixture was incubated for 3 hours at 37°C, then treated with 2 μl of 2 U/μl TURBO DNAse (Ambion) for 30 minutes at 37°C to remove residual DNA. The products were precipitated by using lithium chloride (0.5 M final concentration) dissolved in 500 μl of 100% ethanol for 16 hours at -20°C. Riboprobes were pelleted and eluted following the same procedure described for dsRNA synthesis. The eluted riboprobes were incubated at 68°C for 15 minutes, followed by quality assessment and storage, as outlined in the dsRNA synthesis process.

5. RNAi for gene knockdown in planarians

dsRNA was administered directly into the planarian gut via microinjection using a Nanoject II (Drummond Scientific) with 3.5" glass capillaries (Harvard Apparatus) pulled into fine needles using a PC-100 micropipette puller (Narishige). Each worm received 96 nl of dsRNA, calibrated to a concentration of 1 μg/μl, on each injection day. The injection schedule involved six days of injections over a period of ten days, with injections on three consecutive days, followed by a four-day rest-period, and injections on another three consecutive days. Irradiations were conducted 24 hours after the last injection where required.

The morphology and behaviour of RNAi-treated animals were assessed daily until day 50 post-irradiation (or equivalent for unirradiated animals) using a Zeiss SteREO Discovery V8 microscope. Bright-field images of the animals were taken with a Canon EOS1200D digital camera attached to the same microscope. Scale bars were allocated using Fiji software (Schindelin et al., 2013).

6. Validation of knockdown efficacy by RT-qPCR

RNAi-treated animals received 5 Gy acute whole-body gamma radiation 24 hours after the final injection dose. Total RNA was extracted from these animals 24 hours post-irradiation following the protocol outlined in section 3.1. For each RNAi condition, RNA was extracted from three biological replicates, each consisting of two RNAi-treated animals. 1 μg of RNA

was reverse transcribed into cDNA as described in section 3.2. Each qPCR reaction mix contained 1 μl cDNA, 25 μl 2X One-Taq master mix, forward and reverse primers at a final concentration of 300 nM, 2.5 μl 20X EvaGreen dye (Biotium) and nuclease-free water to a total volume of 50 μl. Primers used were as follows:

Forward – Slmap: $^{5'}$ATCGACAAAGTGAAATGTCC$^{3'}$
Kin-17: $^{5'}$CTGGCGTTTAAATCAGAAAC$^{3'}$
Dkc: $^{5'}$TCCTCCTATTGATGGATCTG$^{3'}$
Rab32: $^{5'}$TTGGGAATCAAAAGTCTACG$^{3'}$
Rasl-12: $^{5'}$CATCAGAGCTCGGAATTTAC$^{3'}$
DMXL-1: $^{5'}$GTTGATATCGTGCAACAATG$^{3'}$

Reverse – Slmap: $^{5'}$TGTCATTTCCAATCCTTCTC$^{3'}$
Kin-17: $^{5'}$GTTCCAGTTTCATTTGTTCC$^{3'}$
Dkc: $^{5'}$CTACGACTTCATGGGAAGAG$^{3'}$
Rab32: $^{5'}$AACGTTTACATAGGGCAGAG$^{3'}$
Rasl-12: $^{5'}$CAACCGGCTTATTGTTAGTC$^{3'}$
DMXL-1: $^{5'}$ATCTTATGCCACAATCATCC$^{3'}$

qPCR cycling parameters were as follows: initial denaturation at 95°C for 3 minutes, 35 cycles of denaturation at 95°C for 30 seconds, annealing at 58°C for 20 seconds, extension at 72°C for 20 seconds. To normalize gene expression levels, GAPDH was used as the reference gene using primer sequences that were previously designed (Eisenhoffer et al., 2008). A no-template control for each RNAi condition was run to validate the absence of primer-dimer formation.

7. Fluorescence in situ hybridization

Whole mount fluorescence in situ hybridization was conducted following the established protocol by King and Newmark (King and Newmark, 2013), with minor adaptations. Animals were treated with freshly prepared 5% N-acetyl cysteine solution for 5 minutes to remove mucus, then fixed using freshly prepared 4% formaldehyde solution for 25 minutes. Animals were rinsed twice in PBSTx (1X PBS with 0.3% Triton-X), then dehydrated using methanol of increasing concentrations (25%, 50%, 75%, 100%). Samples can be safely stored in 100% methanol for up to 3 months. To resume with staining, samples were rehydrated with the same iterative concentrations of methanol in descending order, rinsed 3 times with PBSTx, and bleached in freshly prepared bleaching solution (5% non-deionized formamide, 1.2%

H_2O_2, 0.5X SSC) for 2-3 hours under bright light until satisfactory pigment removal was achieved. After 3 rinses in PBSTx, the samples were treated with freshly prepared proteinase K solution (0.1% SDS, 10 μg/mL proteinase K, in PBSTx) for 10 minutes, followed by fixation using 4% formaldehyde solution for 20 minutes. Samples were washed 3 times with PBSTx, then incubated in pre-hybridization solution for 2 hours at 56°C. Subsequently, animals were incubated in hybridization solution (containing the desired DIG/FITC labelled riboprobes and 5% dextran sulphate) at 56°C for 18-20 hours. Riboprobes targeting Smedwi-1, Prog-1 and Agat-1 were calibrated to and stored at a concentration of 100 ng/μl. For planarians up to 10 days post-irradiation, where fewer stem and progeny cells are present, riboprobes were diluted 1:500 in hybridization solution, while a dilution factor of 1:300 was applied for wild-type planarians to achieve optimal signal-to-noise ratios.

As the hybridization solution tends to be viscous due to the addition of dextran sulphate, an equal part of 2X saline sodium citrate (SSC) solution was added to dilute the hybridization solution, preventing mechanical damage to the tissue during solution removal. After this, samples underwent a series of washes at 56°C first using 2X SSC (3 times), then 0.2X SSC (4 times), each lasting 20 minutes. Samples were then rinsed twice in TNTx solution for 5 minutes each at room temperature, followed by a 2-hour incubation in blocking solution (5% Horse serum and 0.5% Roche western blocking reagent diluted in TNTx) at room temperature. Samples were then incubated at 4°C overnight in an antibody solution containing Anti-Dig-POD or Anti-FITC-POD (Anti-Dig or Anti-Fitc antibodies conjugated with peroxidase) [Roche] diluted 1:2000 in blocking solution. To remove excess antibodies, 6 washes with TNTx at 20-minute intervals were performed, and the samples were developed using tyramide signal amplification with a fluorophore of choice (TAMRA or Alexa-488, 1:500 dilution).

For single-FISH, samples were rinsed in PBSTx 3 times and post-fixed using 4% formaldehyde solution for 20 minutes. Animals were then stained with 0.1 μg/mL of DAPI (Thermo) dissolved in 1X PBS overnight at 4°C. After nuclear staining, samples were rinsed twice with PBSTx, kept in 80% glycerol overnight, and mounted on glass slides for imaging. For double FISH, after incubation with the first fluorophore, samples were rinsed 3 times with PBSTx and incubated in azide solution (100 mM sodium azide in PBSTx) for 1 hour to eliminate

peroxidase activity. Samples were then washed four times with PBSTx, twice with TNTx, incubated with blocking solution for 1 hour, and subsequently incubated overnight at 4°C with the second antibody of choice, diluted 1:2000 in blocking solution. The samples were washed and developed with a different fluorophore of choice, then processed for nuclear staining and mounting as described for single-FISH. The detailed composition of each reagent, together with the comprehensive staining protocol, can be referenced in the source publication (King and Newmark, 2013).

8. Immunofluorescence

The procedure for whole mount immunofluorescence was adapted from the protocol established by Forsthoefel and colleagues (Forsthoefel et al., 2018). Animal fixation was performed as described in section 7, involving treatment with 5% N-acetyl cysteine, 4% formaldehyde, and dehydration with methanol. After rehydration, samples underwent 3 rinses with PBSTx and were bleached using 6% H_2O_2 in PBSTx. Bleaching was performed for 16 hours at room temperature, without the need for bright light. Bleached animals were washed 6 times with PBSTx, 20 minutes each wash. Samples were then blocked in PBSTxS (PBSTx with 10% horse serum) for 4 hours at room temperature. Subsequently, samples were incubated in primary antibody solution, containing Anti-H3P antibodies (Rabbit polyclonal, Sigma-Aldrich) diluted 1:1000 in PBSTxS for 20 hours at 4°C. Samples were then washed for 8 times with PBSTx for 20 minutes each wash, and blocked for an additional 2 hours in PBSTxS. Following this, samples were incubated in a secondary antibody solution containing Anti-Rabbit-488 (Invitrogen) diluted 1:1000 in PBSTxS for 20 hours at 4°C. Samples were then washed 8 times with PBSTx, 20 minutes each wash. Finally, samples were stained with DAPI and mounted on glass slides as described in section 7.

9. Fluorescence image processing and analysis

Fluorescence images of whole animals were captured using an Axiocam 202 monochromatic camera (Zeiss) attached to an Axioskop 2 Plus compound microscope (Zeiss) at objective magnifications of either 4X or 10X. ZenCore v3.5 software (Zeiss) was used for image acquisition. Subsequent image processing, including background adjustment, channel colour assignment, and incorporation of scale bars, was performed using Fiji software. An Olympus

FluoView FV1000 confocal microscope was used to image specimens at higher objective magnifications of 40X or 63X. Confocal images were acquired as Z-stacks with a thickness of 4 μm along the dorsoventral axis, and stitched as maximum projections using Fiji software. Quantification of Smedwi-1/Prog-1 and Smedwi-1/Agat-1 co-expression was performed in Fiji using the JaCoP v2.1.4 plugin (Bolte and Cordeliers, 2006). Costes' automatic threshold (Costes et al., 2004) was selected as the input parameter for each measurement to serve as the method for background subtraction and signal threshold establishment. The other input parameters applied were as defaulted. Output images of JaCoP were manually validated to ensure that any positive colocalization signals did not arise from overlapping cytoplasm of adjacent cells. Measurements of co-expression were made on Smedwi-1$^+$ cells located at the dorsal periphery of the stem cell compartment, which borders the more superficial cell layer housing Prog-1$^+$ cells, across all conditions to ensure consistency. This strategy aimed to minimize variations in signal intensity at different tissue depths due to differences in riboprobe and antibody penetration, as well as to account for confocal laser power attenuation across tissues.

10. Single-cell RNA-sequencing library preparation

We generated SPLiT-Seq libraries for four post-irradiation conditions and a non-irradiated sample as the control. Thirty planarians (asexual *S. mediterranea*) of approximately 8 mm in length were used in each condition. The animals from different conditions were dissociated into single cells using the Acetic acid-Methanol (ACME) method as previously described (Garcia-Castro et al., 2021). The dissociated cells were stored overnight at -80°C in the presence of 10% DMSO as a cryoprotectant. All centrifugation steps in this workflow to pellet cells were performed at 1000 rcf for 5 minutes at 4°C. After storage, samples were thawed on ice and centrifuged to remove DMSO. Cell pellets were resuspended in 1 mL washing buffer (1X PBS with 1% BSA) and centrifuged again to pellet cells. The cells were then resuspended in 1 mL 1X PBS. From this stock, a 100 μl aliquot from each sample was stained using 0.05 mM Draq5 (Invitrogen) and 5 μg/mL Concanavalin-A conjugated with Alexa-Fluor-488 (Invitrogen) dissolved in washing buffer. Stained cells were washed using 1 mL washing buffer, pelleted, and then resuspended in 100 μl 1X PBS. The stained cells were analysed using a CytoFlex S Flow Cytometer (Beckman Coulter) to assess the quality of

dissociation and measure cell concentrations. Draq5 signals were detected using a red laser (Wavelength of 640 nm, with a 780/60 nm filter), while Concanavalin-A-488 signals were detected using a yellow-green laser (Wavelength of 561 nm, with a 525/40 nm filter). The stock cells were pelleted and resuspended in an appropriate volume of 1X PBS to achieve 5000 singlet cells per 8 μl, which were then loaded into each well for the first round of SPLiT-Seq barcoding.

The first round of barcoding took place on a 48-well plate, with each well featuring a unique barcode. All barcodes and linker constructs for the sequential SPLiT-seq barcoding rounds were supplied lyophilized by Integrated DNA Technologies (IDT) and were reconstituted to working concentrations as described in Garcia-Castro et al., 2021. For the first round of barcoding, each well of the plate was pre-loaded with 8 μl of 12 μM well-specific barcodes, 0.35 μl of 20 U/μl SUPERase-In RNAse Inhibitor (Invitrogen), 1 μl dNTP mix (containing 10 mM of each dNTP), 2 μl of 200 U/μl Maxima-H Minus Reverse Transcriptase (ThermoFisher), 0.65 μl of nuclease-free water, and 5 μl of 5X RT buffer (Thermo). 8 μl of cells from various conditions were then loaded into pre-defined wells and incubated in a thermocycler at 50°C for 40 minutes to facilitate in-cell reverse transcription. After incubation, individual reactions were pooled into a 15 mL Falcon tube on ice. To this pooled mixture, 12 μL of 10% Triton X-100 (0.1% working concentration) was added, and the cells were pelleted. The supernatant was discarded, and the pellet was resuspended in 2 mL of 1X NEBuffer 3.1 (NEB).

Subsequently, the cells were evenly distributed across a 96-well plate pre-loaded with Round 2 barcodes and linkers for the second round of barcoding, which involves a ligation reaction. Rounds 2 and 3 of SPLiT-seq barcoding were conducted following the protocol outlined in Garcia-Castro et al., 2021. After the third round of barcoding, cells were pooled into a 15 mL Falcon tube and pelleted. The cells were stained in 1 mL staining solution, which contained 0.05 mM Draq5 (Invitrogen) and 5 μg/mL Concanavalin-A-488 (Invitrogen) diluted in washing buffer. After staining, the cells were washed using 1 mL washing buffer, pelleted, and resuspended in 2 mL 1X PBS. BD FACS Aria III (BD Biosciences) was employed to isolate intact singlet cells that endured the relatively harsh barcoding process. Draq5 and Concanavalin-A-488 signals were detected as previously described. Singlets were sorted

directly into a collection tube containing 50 μl of lysis buffer (20 mM Tris pH 8.0, 400 mM NaCl, 100 mM EDTA pH 8.0, 4.4% SDS). After sorting, the tube's volume was topped up to 100 μl with additional lysis buffer, and 10 μl of 20 mg/mL proteinase K (Invitrogen) was added. Cell lysis was carried out at 55°C for 2 hours with mild agitation, and the lysates were stored at -80°C. Subsequent steps, encompassing the purification of barcoded cDNA from lysate using streptavidin-coated Dynabeads (Invitrogen), template switching, and the first round of low-cycle PCR amplification, were performed as described in Garcia-Castro et al., 2021. The PCR products underwent two rounds of SPRI size selection using KAPA pure beads (Roche) at a ratio of 0.8X, according to manufacturer's instructions, to remove fragments smaller than 300 bp. The library was then tagmented using the Nextera XT DNA Library Preparation Kit (Illumina) per the manufacturer's instructions. A final low-cycle PCR was conducted as described in Garcia-Castro et al., 2021 to achieve sufficient DNA for sequencing and to ligate sequencing adaptors. The resulting PCR products were size-selected using the same SPRI kit at a ratio of 0.7X to eliminate primer and adapter dimers. For library quality control, yield measurement was conducted in a Qubit 4 fluorometer (Thermo) using the Qubit dsDNA High Sensitivity Kit (Thermo). The library was also assessed on an Agilent 2100 bioanalyzer following the Agilent High Sensitivity DNA Kit guide to check for fragment size distribution. The library was sequenced on an Illumina NovaSeq 6000 (service provided by Novogene) to obtain 150 bp paired-end reads, with a depth of 400 million read pairs.

11. Single-cell RNA-sequencing data analysis

11.1 Quality control and processing of sequencing reads

Sequencing read quality was assessed using FastQC (Andrews, 2010). CutAdapt v2.8 (Martin, 2011) was then used to remove low-quality bases and short reads, as well as trim residual adaptor sequences. Read 1 (containing transcript sequence) and Read 2 (containing UMI and barcode sequences) were trimmed separately with different clean-up strategies. For Read 1, *cutadapt -j 4 -m 60 -q 10 -b AGATCGGAAGAG* was run, removing residual sequencing adapters and reads with lengths shorter than 60 bp. For read 2, *cutadapt -j 4 -m 94 --trim-n -q 10 -b CTGTCTCTTATA* was run, removing reads shorter than 94 bp (the minimum length to span all cell barcodes), terminal Ns, and residual Nextera adapter

sequences. Accounting for potential indels during library making, Read 2 sequences were also assessed for phase by using grep to compare the sequenced reads with a fixed reference. Only reads with UMI and cell barcodes in the expected positions were retained for further analyses. As quality control and adapter trimming desynchronises Read 1 and Read 2 sequences, the Pairfq v0.16 (Staton, 2013) 'Makepairs' command was employed to re-pair the reads, and to remove singleton reads without a corresponding pair. A secondary round of FastQC analysis was performed to validate the effective removal of adaptors and low-quality sequences. BBMap (Bushnell, 2014) was then used to merge the paired reads and reformat them into a unified bam file. Next, Picard SortSam (Broad Institute, 2018) was applied to sort the bam file, arranging querynames (header of each read pair) in ascending order, a prerequisite before input into the SPLiT-seq pipeline (Zhang, 2020).

11.2 Barcode demultiplexing, read mapping, and matrix production

The SPLiT-seq pipeline first extracts UMIs and cell barcodes from Read 2 sequences and tags these constructs to their corresponding Read 1 pairs. Drop-seq tools (Saunders et al., 2018) TrimStartingSequence and polyAtrimmer were then used to remove template switching oligo sequences and polyA tails from the 5' and 3' ends of Read 1, respectively. Next, demultiplexing was carried out by comparing the extracted barcode tags to a reference tag list using the custom python script provided in Drop-seq_tools v2.1.0 (Saunders et al., 2018). One mismatch in the cell barcode region was permitted, while reads with more than one unexpected base in the barcode region were discarded. The tagged bam file was converted into fastq format using Picard SamToFastq (Broad Institute, 2018), and reads were aligned to the reference *S. mediterranea* S2F2 genome (Grohme et al., 2018) using STAR v2.7.10b (Dobin et al., 2013), employing the *–quantMode GeneCounts* option in default settings. The reference gene annotation file used for mapping was generated in-house (Neiro et al., 2022). The mapping step causes the loss of UMIs and cell barcodes, which were recovered and re-tagged to the mapped reads using Picard MergeBamAlignment (Broad Institute, 2018). This involved combining the mapped but untagged bam file (output of STAR), with the tagged bam file prior to mapping. Drop-seq_tools v2.1.0 TagReadWithInterval and TagReadWithGeneFunction commands were then sequentially run, providing each read with information on its genomic location and putative functions respectively. The output

produced a genome-aligned bam file containing reads tagged with UMI, cell barcode, and gene information. This file was then used to build digital expression matrices for each of the five experimental conditions using the Drop-seq_tools v2.1.0 DigitalExpression function with the settings: *READ_MQ=0, EDIT_DISTANCE=1, MIN_NUM_GENES_PER_CELL=100,* and we applied the parameter *LOCUS_FUNCTION_LIST=INTRONIC* to retain read counts mapping to intronic regions. The evaluation of sequencing saturation at 10%, 25%, 50%, 75%, and 100% of total read depth was conducted as described in Garcia-Castro et al., 2021.

11.3 Feature identification, clustering, dataset integration, and pseudo-bulk differential gene expression analyses in Seurat

The digital expression matrices for each experimental condition were imported into Seurat v4.3.0 (Hao et al., 2021) within the R environment v4.2.0 (R core team, 2021). A Seurat object was created for each condition with the parameter of *min.cells = 1* to eliminate genes with zero counts across all cells. To visualize the distribution of genes and UMIs per cell, *VlnPlot [features = c(nFeature_RNA and nCount_RNA)]* was run in Seurat. Cells with fewer than 125 detected genes and cells with UMI counts exceeding 5000 were excluded by applying the criteria *nFeature_RNA >125* and *nCount_RNA < 5000*, respectively.

Subsequently, an 'Integrated data assay' was created by combining the five distinct Seurat objects. This was achieved by first normalizing the counts for each dataset with respect to total library size using the *NormalizeData* feature with default settings. Next, the variable features for each dataset were independently found using the *FindVariableFeatures* command with parameters: *selection.method = "vst", nfeatures = 10000*. These variable features were then used to identify integration anchors using the *FindIntegrationAnchors* function. Using this set of anchors, the five Seurat objects were integrated using the *IntegrateData* function with default settings. Linear transformation and scaling were then applied to each dataset using the *ScaleData* function, before running principal component analyses on the scaled data using the *RunPCA* function. The *ElbowPlot* function was used to understand the dimensionality of the data, which aids in determining the number of principal components to be retained for further analysis.

Next, cells were clustered by first using the *FindNeighbours* function and *FindClusters* function at a resolution of 1.5, before performing non-linear dimensional reduction with the *RunUMAP* function. UMAP embeddings of the data were created with the settings: *dims= 1:30, reduction = "pca"*. The *DimPlot* function was used to colour and visualize the clustering of the data. Next, differentially expressed features for each cluster were identified using the *FindAllMarkers* function with default parameters. The top 30 differentially expressed genes in each cluster were used as markers for cluster identity assignment. The *FeaturePlot* function was used to highlight the expression of the stem cell marker, Smedwi-1, in the UMAP. The *FindAllMarkers* function was also used for pseudo-bulk differential gene expression analyses between two specific cell clusters by inputting the desired *ident.1* and *ident.2* subsetting parameters. In addition, the default "wilcox" parameter was used, specifying the application of the non-parametric Wilcoxon rank sum test as the statistical method for pseudo-bulk differential gene expression testing. Comprehensive details regarding all analyses performed in this section can be referenced in the Seurat tutorial (https://satijalab.org/seurat/v3.0/pbmc3k_tutorial.html).

11.4 RNA velocity analyses

The .bam file containing the aligned reads (refer to section 11.2) was imported into the Python implementation of Velocyto v0.17.15 (La Manno et al., 2018), generating two separate matrices of unspliced and spliced mRNA counts. The resulting unspliced/spliced count matrices were contained within a .loom file, which in turn was imported into the Python package scVelo v0.2.5 (Bergen et al., 2020).

Concurrently, the five Seurat objects (as outlined in section 11.3) were each converted into the .h5ad file format using the R package SeuratDisk (Hoffman, 2020). These .h5ad files were then imported into scVelo to merge clustering information such as cell IDs, UMAP coordinates, and cluster identity with the unspliced/spliced mRNA counts. The data was then filtered and normalized by using the *scv.pp.filter_and_normalize(adata)* command. The dynamical model of RNA velocity was elected for trajectory inference, which required the two following commands to be run sequentially: *scv.tl.recover_dynamics(adata)* and *scl.tl.velocity(adata, mode='dynamical')*. The computed RNA velocities were projected onto

the UMAP embeddings using the *scv.pl.velocity_embedding(adata, basis='UMAP')* function. Comprehensive details regarding RNA velocity analyses can be referenced in the scVelo tutorial (http://scvelo.readthedocs.io/en/stable/VelocityBasics/).

12. Phylogenetic analyses

Protein sequences of target planarian genes were retrieved from the PlanMine3.0 database (Rozanski et al., 2019). Orthology predictions were conducted using OrthoFinder v2.4.0 (Emms and Kelly, 2019) by querying target gene peptide sequences against reference proteomes retrieved from the Ensembl (Martin et al., 2023) repository. The orthology predictions made by OrthoFinder were further evaluated by cross-referencing them with predictions made by EggNOG v6.0 (Hernandez-Plaza et al., 2023) and OrthoDB v11 (Zdobnov et al., 2021) web interfaces. To validate orthology predictions, a reciprocal best blast hit approach was employed through a series of BlastP searches against the UniProtKB/Swiss-Prot database (Boutet et al., 2007) with an e-value cutoff of $< 1x10^{-5}$. MEGA v11 software (Tamura et al., 2021) was used to align protein sequences and to build maximum likelihood phylogenetic trees. The MUSCLE v5 (Edgar, 2022) plugin within the MEGA suite was used to align multiple protein sequences. Maximum likelihood trees were constructed using whole protein sequences, assuming a Whelan and Goldman model for amino acid substitution (Whelan and Goldman, 2001), and incorporating a discrete gamma distribution model (Yang, 1994) with k = 5 to consider evolutionary rate variation among individual sites, for computing tree topology and branch lengths. Protein domain identification and predictions of domain conservation were conducted by querying target gene protein sequences against the Pfam database (Finn et al., 2014) through the InterProScan v5 (Jones et al., 2014) web interface. These predictions were further cross-referenced with predictions from the Prosite Database (Hulo et al., 2006) accessed via the Expasy web interface (Duvaud et al., 2021). Domain Graph v1.0 (Ren et al., 2009) was used to illustrate protein domain architecture.

13. Alkaline Comet assay

Alkaline Comet assays were conducted following the protocol previously optimized in our group (Sahu et al., 2021), with minor adaptations. Animals underwent gene knockdown and irradiation as detailed in section 5. For each post-irradiation timepoint, two biological

replicates, each consisting of three RNAi-treated animals, were dissociated into single cells using papain, diluted to a fixed concentration, mixed with an equal amount of 1.5% low-melting agarose, and embedded on pre-coated glass microscope slides as previously described (Sahu et al., 2021). The slides were then immersed in a coplin jar containing lysing solution (2.5M NaCl, 100 mM EDTA, 10 mM Trizma base, pH 10, pre-chilled to 4°C) and incubated for 16 hours at 4°C. After incubation, the slides were transferred to another coplin jar containing neutralisation buffer (0.4 M Tris in dH_2O, pH 7.5) for 20 minutes at 4°C. Concurrently, an electrophoresis chamber was filled with freshly prepared electrophoresis buffer (300 mM NaOH and 1 mM EDTA in dH_2O, pH 13) and allowed to cool to 4°C in a temperature-controlled dark room. The slides were then transferred to a new coplin jar containing dH_2O to rinse off excess neutralisation buffer, before being placed flat into the electrophoresis chamber and submerged in electrophoresis buffer. The cells were allowed to equilibrate for 20 minutes at 4°C in the dark within the electrophoresis buffer without the application of any current. Following the equilibration period, electrophoresis was performed at 20 V (1 V/cm distance between electrodes) for 20 minutes at 4°C in the dark. Post-electrophoresis, the slides were transferred back into a coplin jar with neutralisation buffer for 5 minutes. Slides were rinsed with TE buffer (10mM Tris-HCl, 1 mM EDTA, pH 7.5) and then stained with DAPI (0.1 μg/mL dissolved in TE buffer) for 20 minutes at room temperature in the dark. After staining, slides were rinsed with TE buffer twice, and then submerged in 100% ethanol for 5 minutes at room temperature. Slides were air-dried at room temperature for 15 minutes before storage.

Images were acquired using an Axiocam 202 monochromatic camera (Zeiss) attached to an Axioskop 2 Plus compound microscope (Zeiss) at an objective magnification of 20X. The images were analysed in Fiji using the OpenComet v1.3 plugin (Gyori et al., 2014), which performs comet finding and measures comet head/tail DNA content ratios. OpenComet's 'Auto' setting, which is the default, was employed for comet analysis. The output images and computed statistics were reviewed, and only comets defined as 'Normal' were retained for further analyses. Comprehensive details regarding the comet assay protocol can be referred to Sahu et al., 2021, and detailed information on the image analysis pipeline can be found in the OpenComet documentation (http://cometbio.org/documentation.html).

14. Bulk RNA sequencing data analysis

Sequencing read quality was assessed using FastQC (Andrews, 2010). CutAdapt v2.8 (Martin, 2011) was used to trim residual adaptor sequences, and to discard short reads (< 30 bases) as well as low-quality bases (phred score < 25) with the parameters *-m 30 -q 25*. Another round of FastQC was performed for quality control after trimming. Read mapping was performed as described in section 11.2. The average mapping rate for the non-irradiated X1 libraries was 68.91%, while the 24-hour post 5 Gy irradiation X1 libraries had an average mapping rate of 70.04%. FeatureCounts v1.6.1 (Liao et al., 2014) was then used to quantify the number of reads mapping to each gene and to generate a count matrix. The default parameter of *Feature type = Exon* was applied to retain only reads mapping to exonic regions. Data normalization and subsequent differential gene expression analyses were performed using DESeq2 v1.38.3 (Love et al., 2014) using default parameters as outlined in the DESeq2 tutorial:
https://bioconductor.org/packages/devel/bioc/vignettes/DESeq2/inst/doc/DESeq2.html

Chapter 3: Single-cell RNA-sequencing of Irradiated Planarians

Chapter 3 – Introduction

The recent advancements in single-cell transcriptome profiling technologies, coupled with their increased accessibility, have accelerated our understanding of mammalian tissues both under homeostatic as well as diseased states (Jovic et al., 2022; Jagadeesh et al., 2022). Through single-cell sequencing, complex, heterogenous systems can be simplified into their constituent parts, enabling the characterization of cellular diversity (Regev et al., 2017, Karlsson et al., 2021), facilitating the discovery of novel cell states (Villani et al, 2017; Shekhar et al., 2016), whilst also providing the opportunity to reconstruct developmental trajectories in silico (Trapnell et al., 2014; Welch et al., 2016; La Manno et al., 2018). For instance, single-cell RNA sequencing has enabled the discovery of novel progenitor states and improved our understanding of key cell fate transitions during developmental processes such as limb development in mice (Cao et al., 2019), as well as haematopoiesis (Pellin et al., 2019) and brain development (Eze et al., 2021) in humans. Alterations in cell-type compositions when comparing single-cell atlases of tissues in a healthy versus diseased state have also emerged as a promising prognostic tool for understanding disease progression. This is exemplified through the recent use of single-cell RNA sequencing to identify aberrant changes in cellular landscapes associated with conditions such as Alzheimer's disease (Xu and Jia, 2021), rheumatoid arthritis (X. Wu et al., 2021), as well as cancers of the breast, (S. Wu et al., 2021) lung (Yang et al, 2021; Kim et al., 2020; Xing et al., 2021), ovary (Zhao et al., 2021), and colon (Joanito et al., 2022).

In planarians, single-cell sequencing studies have been instrumental in advancing our understanding of the model organism across various biological contexts. For instance, the generation of organism-wide single-cell gene expression atlases has enabled the detection of novel cell types, including rare or transient cell states that may have been eluded from conventional bulk sequencing methods (Fincher et al., 2018; Benham-Pyle et al., 2021). Rare cell types such as notum-expressing cells in the anterior pole and brain, photoreceptor progenitors, and photoreceptor neurons (Fincher et al., 2018), as well as transient wound-induced muscle cell-types (Benham-Pyle et al., 2021) have been resolved through single-cell sequencing experiments. This enables the selective profiling of their gene expression patterns, which may have been previously obscured in population-level averages obtained

through bulk analyses due to their rarity. Additionally, single-cell studies have unravelled unprecedented heterogeneity within the planarian stem cell compartment, and have contributed to the characterization of putative, functionally distinct neoblast subclasses (van Wolfswinkel et al., 2014; Zeng et al., 2018). These include sigma, zeta, and gamma class neoblasts elucidated in the study by van Wolfswinkel and colleagues, each characterized by distinct markers that are reproducible in vivo (Zhu et al., 2015; Lai et al., 2018; Mihaylova et al., 2018). The study by Zeng and colleagues further resolves neoblasts into 12 distinct subclusters, each possessing distinct expression profiles although their experimental validation remains pending. Single-cell sequencing has also enabled the organism-wide reconstruction of cell fate trajectories (Plass et al., 2018). Trajectory analyses were also used to computationally model the development of specific tissues such as the epidermis (Wurtzel et al., 2017) and the planarian nervous system (Molinaro et al., 2016), although a limitation of the latter study is its prone to biases due to the small number of cells profiled (<200 per library). More recently, single-cell RNA sequencing has been applied to examine the changes at the level of single-cells after manipulations such as wounding (Benham-Pyle et al., 2021) and the effects of a targeted gene knockdown (Cui et al., 2023). These applications collectively highlight the value of single-cell RNA-sequencing in the understanding of complex systems.

In this study, we generate single-cell expression atlases of irradiated planarians and compare them to an unirradiated control. Prior knowledge indicates that sub-lethally irradiated planarian stem cells face two main outcomes in vivo: repair and survival, or apoptosis (Sahu et al., 2021). Through single-cell sequencing, we aim to delineate these populations and individually assess their gene expression profiles. Simultaneously, we aim to explore the possibility of radiation-induced stem cell differentiation in planarians, considering the observed upregulation of known epidermal progeny markers in our post-irradiation bulk X1 transcriptome (further elaborated in Chapter 4). We also aim to evaluate potential radiation-responsive changes in cell fate trajectories, and to investigate the probable existence of transient radiation-induced cell states. By examining the planarian response to gamma radiation at a single-cell level, we aim to gain novel insights into the planarian radiation response and recovery process, which in turn may be broadly informative for how human stem and non-stem cells respond to ionizing radiation.

Selection of post-irradiation conditions for single-cell RNA sequencing

We selected four post-irradiation conditions alongside an unirradiated control for single-cell RNA-sequencing. The experimental conditions profiled were as follows:

1. Unirradiated control
2. 3 hours post-exposure to 5 Gy acute gamma radiation
3. 3 hours post-exposure to 10 Gy acute gamma radiation
4. 24 hours post-exposure to 5 Gy acute gamma radiation
5. 24 hours post-exposure to 10 Gy acute gamma radiation

The selection of irradiation dose and timepoints were rationalized by taking into account our existing understanding of neoblast kinetics post-irradiation. Using in situ hybridization, previous observations in our group have shown that at 3 hours post-irradiation, neoblast numbers remain at wild-type levels (Sahu et al., 2021). We postulate that this timepoint may represent an early stage of radiation response where planarian stem cells are engaged in a crucial decision phase, internally assessing whether the inflicted damage is reparable and determining whether to initiate repair or to undergo apoptosis. In contrast, the 24-hour timepoint represents a stage where stem cells can be seen undergoing a progressive reduction in number (Sahu et al., 2021). We infer that stem cells at this stage would have already made that crucial fate decision and are progressing along the elected route at this timepoint.

The choice of the two different gamma radiation doses, 5 Gy and 10 Gy, was guided by the expectation of observing dose-dependent responses in neoblasts. At the 5 Gy dose, we anticipated a stem cell response that leaned towards pro-survival, while at the more damaging 10 Gy dose, we hypothesized that the cellular response may be shifted towards one that is more pro-apoptotic. While the maximum tolerable acute dose for planarians is reported to be 15 Gy (Sahu et al., 2021), practical considerations regarding the collection of sufficient stem cell numbers for sequencing limited our investigation to the selected doses.

Generating single-cell expression atlases of irradiated planarians

We utilized Split Pool Ligation-based Transcriptome sequencing (SPLiT-seq) to generate single-cell libraries under the experimental conditions described. Developed by Rosenberg and colleagues, SPLiT-seq is a single-cell RNA sequencing method that incorporates combinatorial barcoding to index the cellular origin of RNA (Rosenberg et al., 2018). An advantage of SPLiT-seq is its cost-effectiveness in comparison to other single-cell sequencing methods, as this method eliminates the need for specialized instruments such as microfluidics-based devices for the partitioning of individual cells. Instead, SPLiT-seq relies on cells themselves for compartmentalization, with reverse transcription and subsequent barcode ligation all occurring in-cell. Cells go through three successive rounds of barcoding, with random pooling and redistribution of cells between each barcoding round. In our experiment, this process yields a total of 442,368 (48 x 96 x 96) distinct barcode combinations. We summarize our experimental workflow of SPLiT-seq library generation in Figure 6.

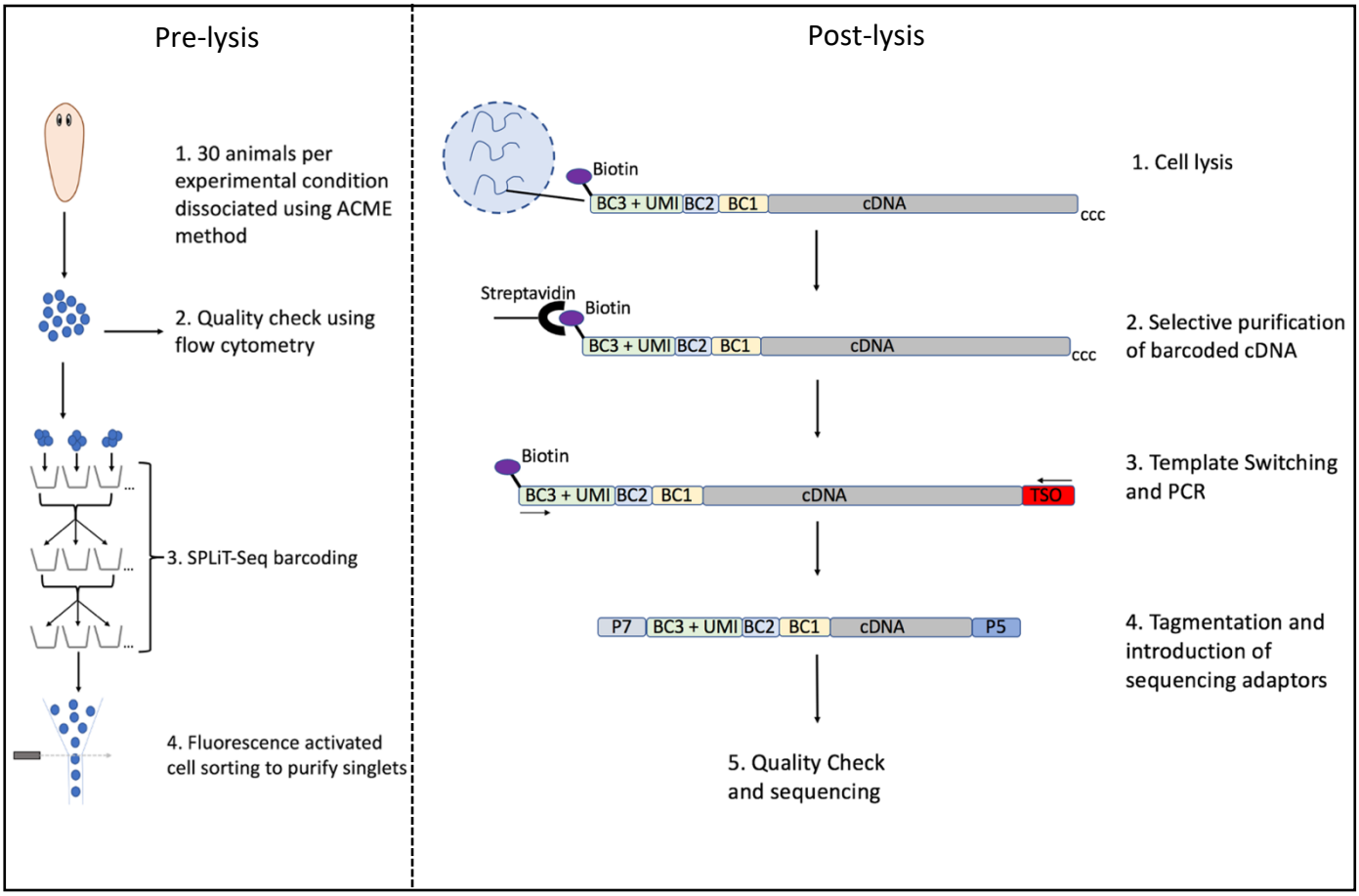

Figure 6. Schematic summary of single-cell library generation. For each experimental condition, 30 animals, either unirradiated or subjected to whole-body irradiation, were dissociated into cells using the ACME method (Garcia-Castro et al., 2021). Flow cytometry was used to assess the quality of dissociation and to measure the cell concentration of each suspension. Cells from different experimental conditions were then diluted to a fixed concentration and loaded, non-randomly, into a 48-well plate, where each well was equipped with oligodT primers appended to a well-specific barcode. To maximize stem cell collection for the 24-hour post-10 Gy sample, we allocated double the amount of input cells and first-round barcoding reagents to compensate for the anticipated reduction in stem cell numbers. An in-cell reverse transcription reaction was then initiated in each well, generating cDNA molecules that were adapted with a unique first cell barcode. After reverse transcription, cells from various conditions were then pooled together and randomly redistributed across a 96-well plate, each containing a unique second-cell barcode that is ligated onto the first barcode. The cells were then pooled and randomly redistributed once more into a final 96-well plate for the third round of barcoding. The third cell barcodes are contained within a DNA construct alongside an 8-bit Unique Molecular Identifier (UMI), as well as a 5' biotin modification, which are collectively concatenated onto the cDNA molecules. Fluorescence activated cell-sorting was then used to purify singlets that remained intact throughout the sequential barcoding process. The library synthesis process post-lysis of isolated singlets, consisting of selective cDNA purification using streptavidin beads, template switching, PCR, tagmentation, and adaptor ligation were conducted as previously described (Garcia-Castro et al., 2021). The illustration post-lysis depicts the bottom strand of DNA. Following PCR in step 3, the library exists as double-stranded DNA. Abbreviations: TSO = Template-switch oligo, BC = Barcode.

Despite its advantages with respect to cost and accessibility, a current pragmatic limitation of SPLiT-seq is the mechanically harsh nature of the sequential barcoding process on cells. In our experiment, we were able to recover 18,000 singlet cells by fluorescence activated cell-sorting (FACS) after the three cell-barcoding rounds. This number corresponds to only 11.42% of the initial input amount of singlet cells. This level of cell loss is comparable to previously described single-cell libraries that are multiplexed by combinatorial barcoding (Garcia-Castro et al., 2021; Cao et al., 2019). As the barcoding process generates substantial cell loss and hence a large amount of cellular debris, we implemented FACS to ensure that only singlet cells that have remained intact throughout the barcoding process are captured (Figure 6). This approach limits the carryover of cell debris and cell aggregates to later

stages of the workflow. Consequently, this modification allowed us to retain a significantly higher percentage of sequencing reads that passed the initial stringent quality control steps compared to a previous planarian SPLiT-seq study (Garcia-Castro et al., 2021). This is because we were able to reduce the presence of low-quality reads, truncated reads, and free barcodes without an associated cDNA in our sequencing data. Additionally, the implementation of FACS in our workflow has contributed to a higher proportion of reads being retained post-demultiplexing. This enhancement is likely attributed to FACS selectively filtering for transcripts encapsulated within intact cells, while concurrently reducing the undesired carry-over of ambient RNA.

Following initial sequence quality checks and data pre-processing, reads were computationally demultiplexed into their cell-of-origin based on the combination of the three appended cell-barcodes. Additionally, since cells from different conditions were loaded into defined wells containing well-specific first cell-barcodes, each cell can be assigned to their sample-of-origin based on the identity of the first cell-barcode. We achieved an overall mapping rate of 94.05%, a rate that is comparable to published planarian SPLiT-seq libraries (Garcia-Castro et al., 2021; Benham-Pyle et al., 2021).

As initially flagged by Garcia-Castro and colleagues, planarian SPLiT-seq libraries contain an over-representation of sequencing reads mapping to highly expressed genes encoding ribosomal RNAs or to repetitive intergenic regions (Garcia-Castro et al., 2021). Assessments of our library against the published planarian SPLiT-seq libraries reveal that the same over-represented reads can be found in our dataset at proportions comparable to the ones in the literature (Garcia-Castro et al., 2021; Benham-Pyle et al., 2021). To ensure the reliability of downstream analyses, we discarded the top 5 most represented reads in our library, which collectively accounted for 59.7% of the total sequenced reads (Figure 7A). Comparatively, these reads accounted for an average of 60.4% and 68.1% of the total sequenced reads in the libraries reported by Benham-Pyle et al. and Garcia-Castro et al., respectively (Figure 7B, 7C). These reads persist post-demultiplexing and are present in correlating proportions within the captured transcriptomes of individual cells (Figure 7D, 7E, 7F).

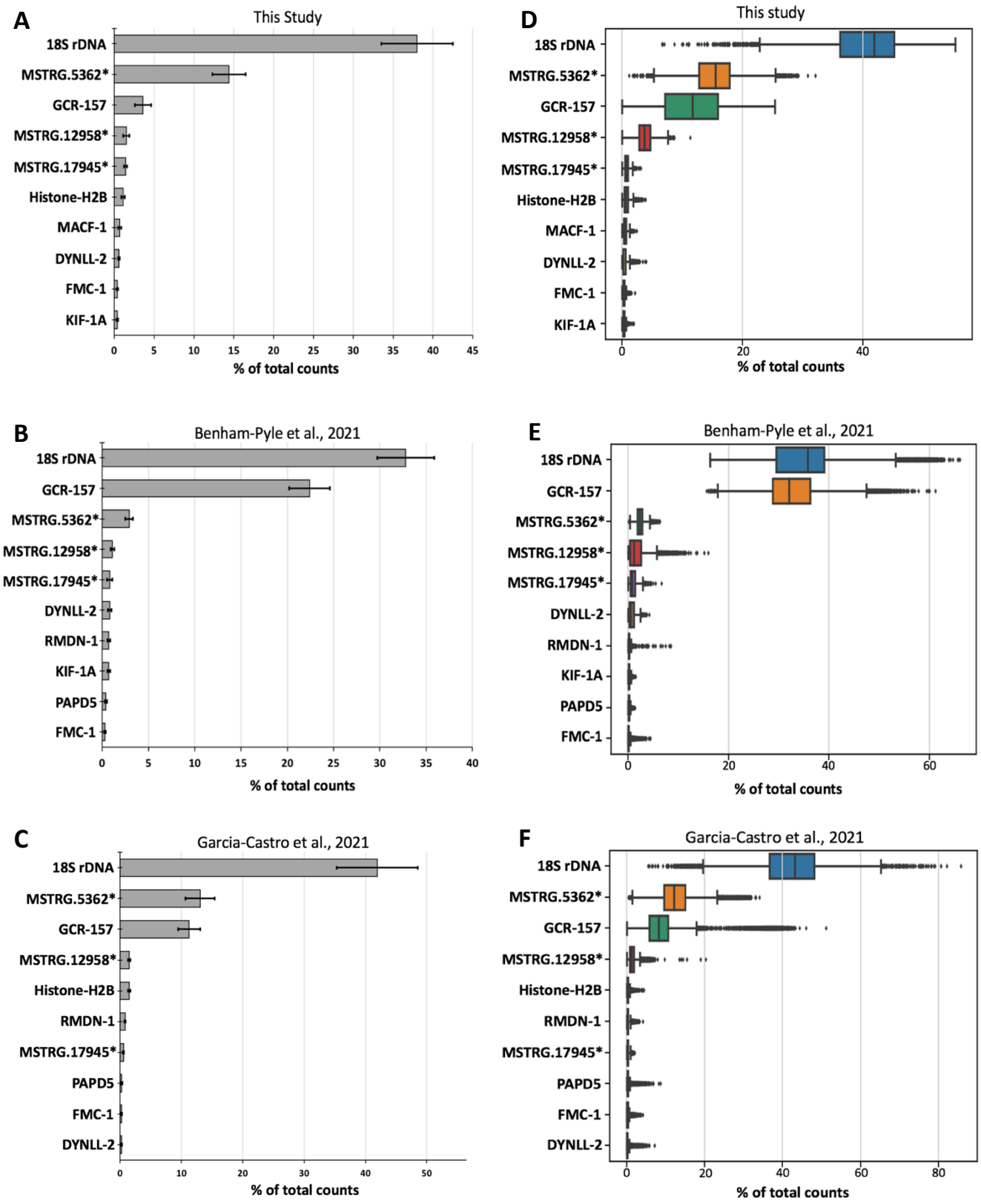

Figure 7. Overrepresented reads in planarian SPLiT-seq libraries. (A, B, C) Top 10 reads displaying the highest percentage of total counts averaged across sub-libraries in **(A)** present study, **(B)** Benham-Pyle et al., 2021 and **(C)** Garcia-Castro et al., 2021. **(D, E, F)** Box plots illustrating the reads' corresponding distributions within the captured transcriptomes of individual cells. All profiled cells from **(D)** present study, **(E)** Benham-Pyle et al., 2021, and **(F)** Garcia-Castro et al., 2021, were included. Asterisks (*) represent repetitive elements with an associated genomic identifier.

The presence of these artefacts reduces the informative reads present in our library, highlighting another limitation of SPLiT-seq in planarians to date. The origin of these over-represented reads cannot be explained by PCR biases since they persist even after duplicate removal by collapsing UMIs. Considering that most of these artefacts possess unique combinations of three cell-barcodes, we speculate that they may have originated from unique cDNA molecules, generated due to mis-priming during the initial reverse transcription stage. Currently, all primer and barcode sequences used for SPLiT-seq library generation in planarians are identical to those employed in mammalian SPLiT-seq studies. To mitigate the impact of these artefactual reads, careful primer sequence alterations would be necessary to prevent non-specific priming in the future, taking into account the AT-rich genome of planarians. Additionally, future applications of DASH (Depletion of Abundant Sequences by Hybridization) to deplete these overrepresented reads prior to sequencing (Gu et al., 2016) may improve the sensitivity of planarian SPLiT-seq libraries.

After filtering out these reads, we generated single-cell gene expression matrices for our data, which were then imported into the Seurat environment (Butler et al., 2018) for downstream analyses. To ensure data quality, we excluded cells with fewer than 125 detected genes and those with abnormally high UMI counts (>5000 UMIs per cell). The lower cut-off was aimed to exclude low-quality or ruptured cells, while the higher cut-off served to prevent the inclusion of cell aggregates and barcode collisions. These cut-off values were calibrated based on the correlation between the number of detected UMI's and the number of detected genes per cell (Figure 8C). Ultimately, we were able to retain and profile the transcriptomes of 15,463 single cells. Demultiplexing the cells into their sample-of-origin revealed the following cell counts: 3018 wild-type cells, 2519 cells from the 3-hour post-5 Gy sample, 2241 cells from the 3-hour post-10 Gy sample, 2684 cells from the 24-hour post-5 Gy sample, and 5001 cells from the 24-hour post-10 Gy sample.

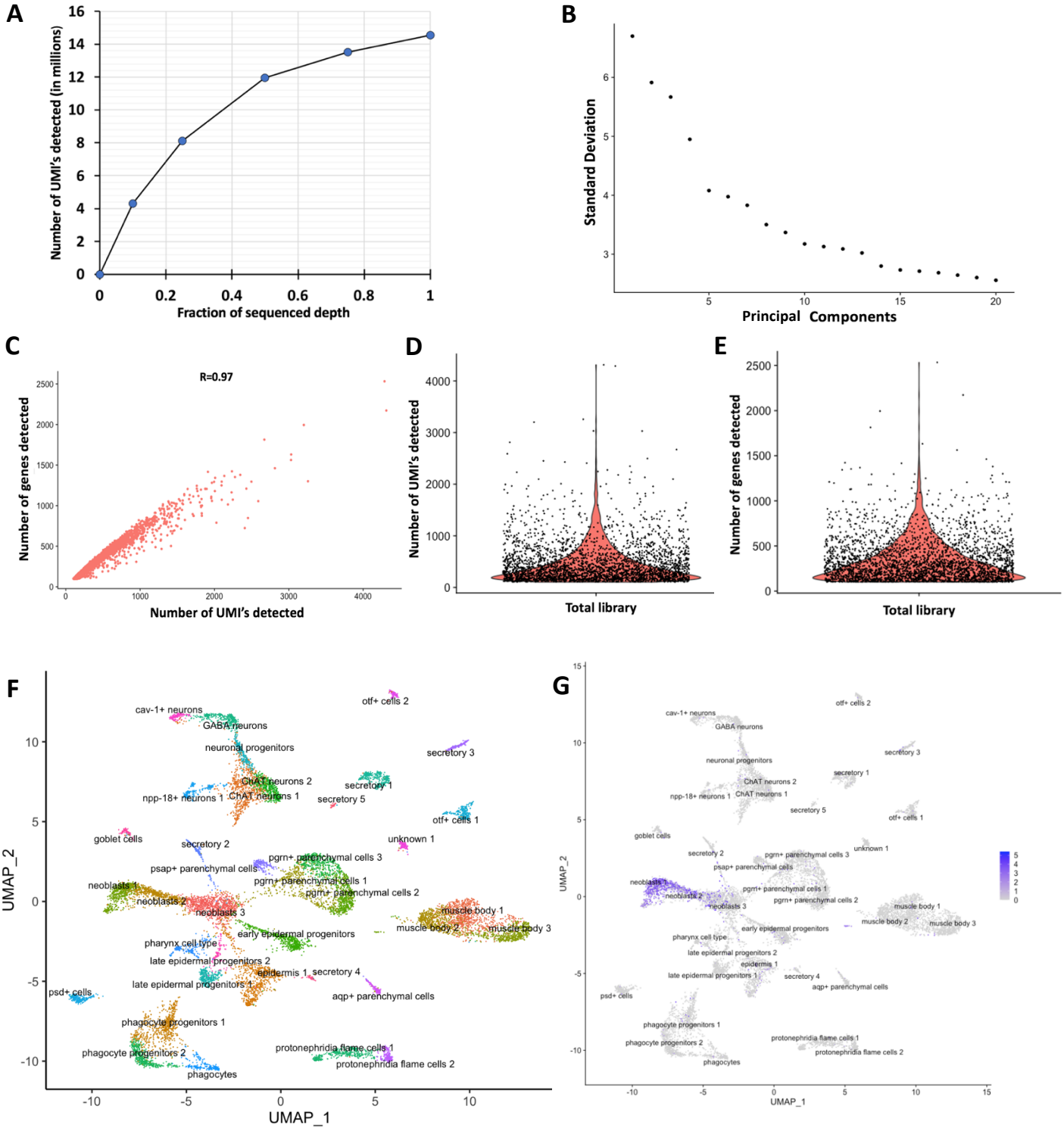

Figure 8. Single-cell library metrics. **(A)** UMI saturation curve at given fractions of complete sequencing depth. **(B)** Elbow plot ranking of principal components based on the amount of variance explained by each component. **(C)** Pearson correlation of the number of UMI's detected per cell against number of genes detected per cell. **(D and E)** Violin plots showing the distribution of **(D)** number of detected UMI's per cell and **(E)** the number of genes detected per cell. **(F)** Integrated UMAP representation of captured single cells spanning all five experimental conditions, with each dot representing an individual cell, coloured by cluster affiliation. **(G)** Expression pattern of the stem cell marker, Smedwi-1, colour-coded in blue. Scale bar represents natural log-normalized expression values [ln(UMI per 10000 +1)].

Assessments of sequencing saturation indicate that our library was approaching the plateau phase (Figure 8A), suggesting reasonable sequencing depth. On average, we detected 610 unique transcripts and 335 genes per cell across all samples (Figure 8D, 8E). We determined the dimensionality of the data and selected 20 of the most significant principal components to be retained for further analyses (Figure 8B). We then utilized the UMAP algorithm (McInnes et al., 2018; Becht et al., 2018) on our data to visualize the patterns of cell clustering in a two-dimensional space (Figure 8F).

Mechanistically, UMAP is a dimensional reduction technique which first uses a nearest-neighbour graphing method to embed the data in a high-dimensional space. Subsequently, the algorithm computes the critical features and relationships of the data to be preserved, and then uses gradient descent to find an optimal two-dimensional representation of the data (McInnes et al., 2018). By applying UMAP to our data at a resolution of 1.5, we were able to identify 37 distinct cell clusters (Figure 8F). To assign an identity to each cluster, we leveraged the FindAllMarkers function in Seurat (Butler et al., 2018), enabling us to identify the top 30 cluster-enriched genes functioning as markers to aid the classification process. We were able to associate most of the observed cell clusters to a specific planarian tissue or cell-type based on their expression of known tissue-specific marker genes. Cluster identities were further validated through comparisons with single-cell gene expression profiles obtained from existing planarian atlases of similar sensitivities (Plass et al., 2018; Garcia-Castro et al., 2021; Benham-Pyle et al., 2021).

Within our atlas, we identified three distinct neoblast clusters characterized by the presence of the stem cell marker, Smedwi-1 (Figure 8G). The segregation of neoblasts into three clusters was consistent across both irradiated and wild-type samples, suggesting that this mode of clustering is independent of radiation treatment. Upon investigation of marker genes associated with these clusters (Appendix Table 1), Neoblast clusters 1 and 2 appear to be exclusively composed of stem cells. This is because the marker genes characterizing these clusters displayed strong associations with planarian stemness, both in their known functions and from their spatial distribution in existing bulk and single-cell RNA sequencing datasets (Neiro et al., 2022; Plass et al., 2018; Benham-Pyle et al., 2021; Garcia-Castro et al., 2021). Specifically, Neoblast clusters 1 and 2 are both distinguished by the differential

expression of key stem cell genes – Smedwi-1, Smedwi-2 (Reddien et al., 2005b), Vasa-1 (Shibata et al., 1999; Wagner et al., 2012), Bruli (Guo et al., 2006; Solana et al., 2016), and core histones H2A (Rossi et al., 2007) as well as H2B (Solana et al., 2012). Analysing their distribution across bulk RNA-sequencing datasets reveal that markers of Neoblast clusters 1 and 2 exhibit >50% average proportional expression within the X1 FACS compartment, which is composed of stem cells in S/G2/M phase, corroborating their associations with planarian stemness (Figure 9A, 9B). Furthermore, marker genes characterizing Neoblast clusters 1 and 2 largely overlapped, although notable genes unique to each cluster could be observed. For instance, RAD50, a gene associated with mammalian replication (Bian et al., 2019); as well as BRG-1 and Smedwi-3, contributors to planarian stem cell differentiation (Trost et al., 2018; Kashima et al., 2020), were found to serve as markers for Neoblast cluster 2, but not for Neoblast cluster 1 (Appendix Table 1). Implications of these marker patterns were incorporated and further described in our model of action (Figure 16).

In contrast, Neoblast cluster 3 occupies a central location within the UMAP plot, connecting the Smedwi-1^{+} stem cells to other known planarian tissue-types (Figure 8F, 8G). Additionally, Neoblast cluster 3 displays a scattered expression pattern of neoblast markers as well as markers associated with various differentiated tissue-types (Appendix Table 1). Experimentally validated lineage-specific genes serving as markers for Neoblast cluster 3 include ACTB, expressed in intestinal cells and intestine-specialized neoblasts (Raz et al., 2021), Hmcn-1, expressed in muscle and pharyngeal cells (Lindsay-Mosher et al., 2020), pmp5, expressed in epidermal progeny cells (Zhu et al., 2015), and slc4a-1, expressed in secretory cells of the protonephridia (Vu et al., 2015). These observations led us to infer that Neoblast cluster 3 may encompass a mixture of post-mitotic stem and lineage-specified progenitor cells. Additionally, this cluster may contain pre-mitotic stem cells in G2 phase before asymmetric division, which have been found to co-express markers of stemness and markers of lineage specification (Raz et al., 2021). The presence of markers associated with differentiation in Neoblast cluster 3 is also reflected in their relative distribution within bulk RNA-sequencing datasets. Markers of this cluster display higher average proportional expression values in the X2 (comprising G1-stem cells and stem cell progeny) and Xins (comprising differentiated cell-types) FACS compartments relative to Neoblast clusters 1 and 2 (Figure 9).

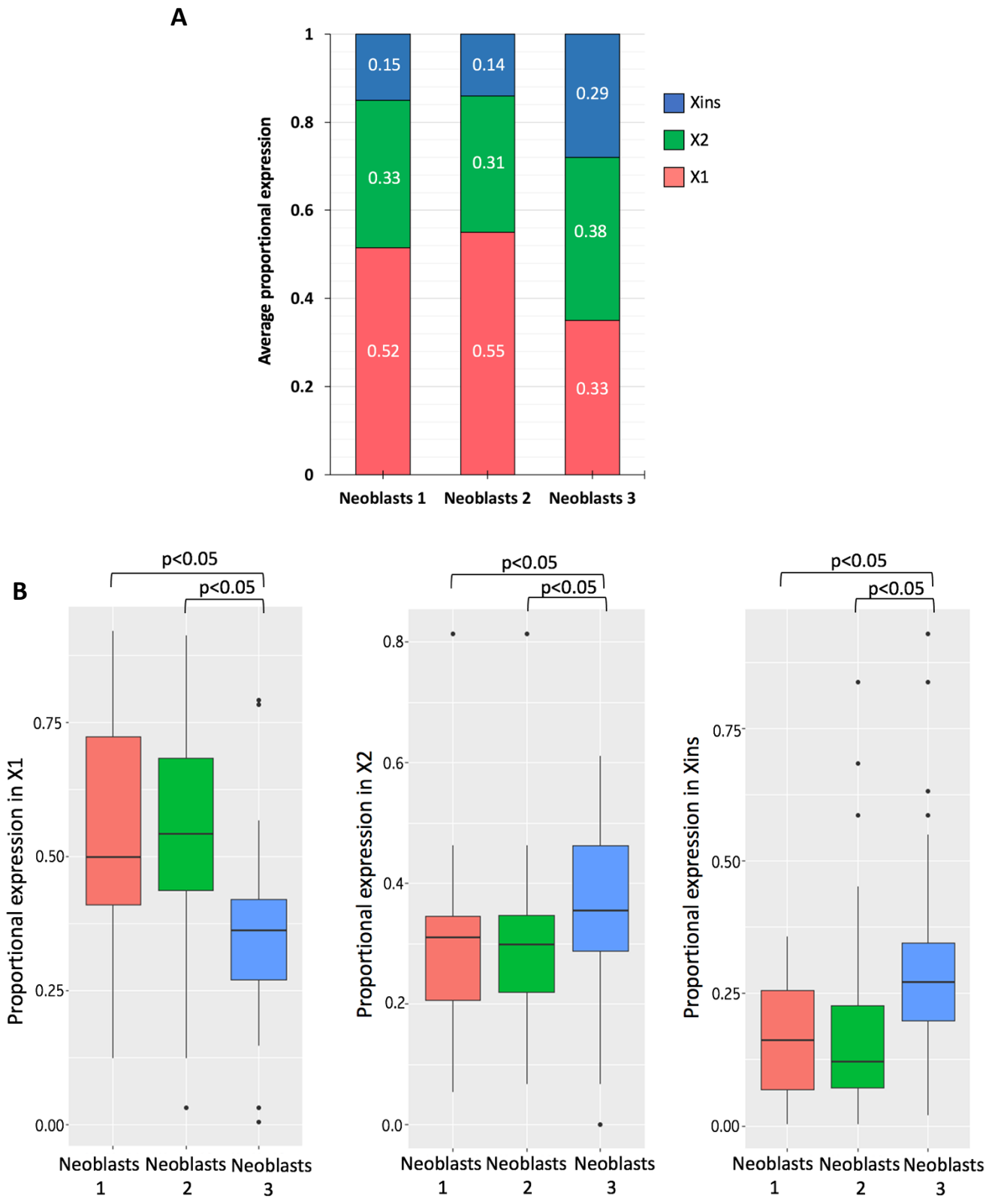

Figure 9. Markers of Neoblast clusters 1 and 2 display enriched expression in the X1 FACS compartment. (A) Average bulk proportional expression profiles of wild-type neoblast cluster markers in relation to the X1, X2, and Xins FACS compartments. **(B)** Box plots illustrating the relative distribution of wild-type neoblast cluster markers across X1, X2 and Xins FACS compartments. Statistically significant differences were observed between Neoblast clusters 1 and 2 against Neoblast cluster 3 (Kruskal-Wallis test, p-values < 0.05).

In the context of our atlas, Neoblast cluster 3 potentially represents a transitory state where cells withdraw from stemness before differentiation into various tissue-types. Such transitional states, featuring intricate overlaps between stem and progenitor cells, have been previously described in multiple planarian single-cell RNA-sequencing studies (Swapna et al., 2018; Fincher et al., 2018; Plass et al., 2018). The likely identities of cells that populate each neoblast cluster are examined in further detail, taking into consideration their responses to acute gamma radiation.

Differential sensitivity of neoblast clusters in response to gamma radiation

As previously described, elucidating the aberrant changes in cellular landscapes when comparing single-cell atlases of tissues in a healthy versus diseased state has emerged as a promising prognostic tool for understanding disease progression. Our single-cell RNA sequencing efforts enable the investigation of cellular landscape changes within planarians exposed to gamma radiation, offering valuable insights into the planarian radiation response and recovery process.

To explore whether distinct subpopulations of neoblasts exhibit differential sensitivities to gamma radiation, we compared the relative abundances of the three neoblast clusters in the unirradiated sample to their corresponding abundances after treatment with gamma radiation. Initially, we performed dataset integration (Stuart et al., 2019) using the Seurat environment to align similar cell states across different experimental samples. In this process, the algorithm identifies shared gene expression patterns, termed anchors, among different samples. These anchors facilitated the mapping of similar cell states or populations from distinct samples onto a shared two-dimensional space (Figure 8F). The UMAP plots were then split into their respective sample-of-origins, enabling us to visualize and assess the changes in the single-cell atlas following exposure to gamma radiation (Figure 10).

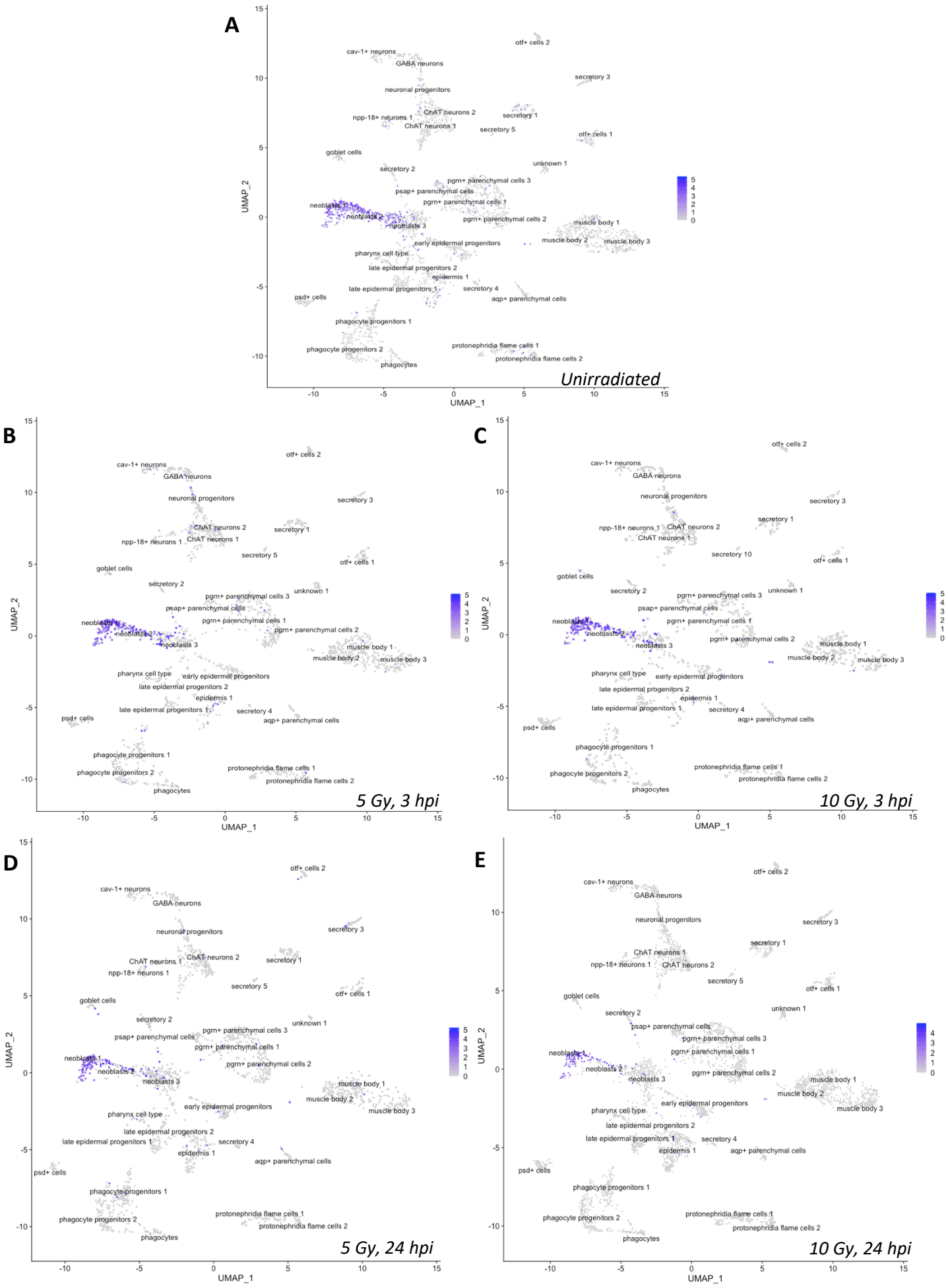

Figure 10. UMAP visualization of integrated single-cells partitioned by sample-of-origin. Conditions are: **(A)** Unirradiated, **(B)** 3 hours post 5 Gy irradiation, **(C)** 3 hours post 10 Gy irradiation, **(D)** 24 hours post 5 Gy irradiation, and **(E)** 24 hours post 10 Gy irradiation. Smedwi-1 expression profiles colour-coded in blue. Scale bars represent natural-log-normalized expression values as previously described.

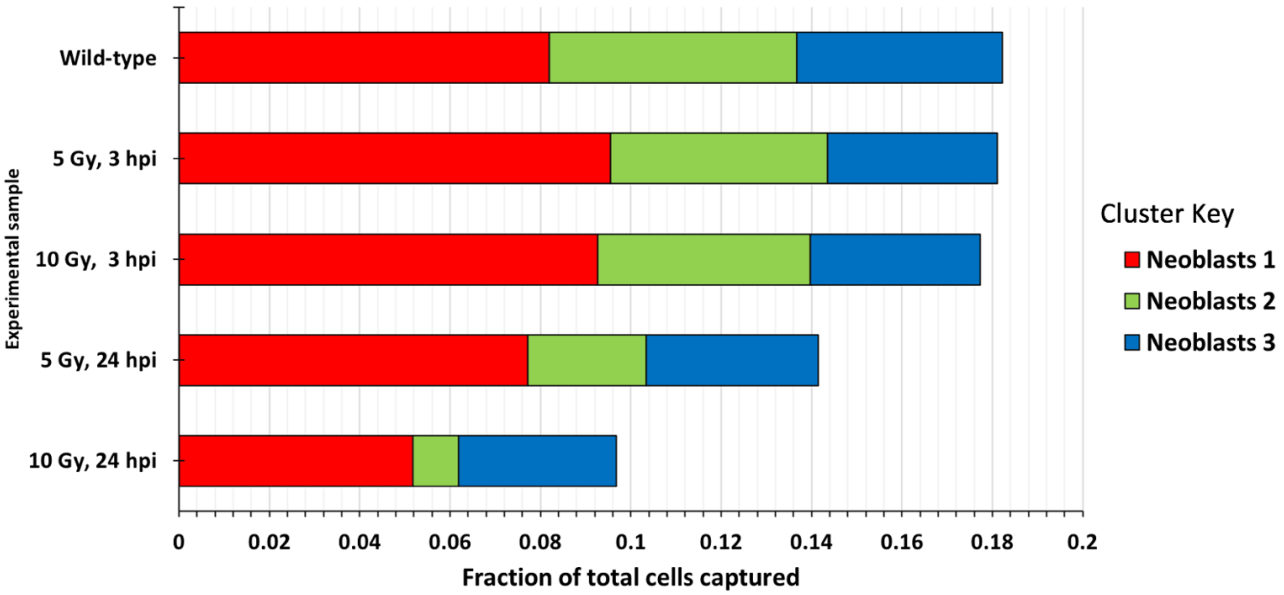

Figure 11. Changes in neoblast cluster proportions following exposure to gamma radiation. Stacked bar chart indicating the proportion sizes of Neoblast clusters 1, 2, and 3 with respect to the total cells captured in each experimental sample. Abbreviation: hpi – hours post irradiation.

Table 3. Proportions of Neoblast clusters 1, 2, and 3 with respect to the total cells captured in each experimental condition.

Condition	Percentage of total cells captured			
	Neoblasts 1	Neoblasts 2	Neoblasts 3	Others
Wild-type	8.18%	5.48%	4.55%	81.79%
5 Gy, 3 hpi	9.55%	4.80%	3.75%	81.89%
10 Gy, 3 hpi	9.26%	4.71%	3.76%	82.17%
5 Gy, 24 hpi	7.72%	2.62%	3.81%	85.85%
10 Gy, 24 hpi	5.18%	1.02%	3.49%	90.31%

We made several observations regarding the dynamic changes in neoblast cluster compositions in response to gamma radiation, both in a time and dose-dependent manner. In the unirradiated control sample, the three neoblast clusters collectively accounted for 18.21% of the total captured cells, with Neoblast cluster 1 representing 8.18% of captured cells, Neoblast cluster 2 representing 5.48% of captured cells, and Neoblast cluster 3 representing 4.55% of captured cells (Table 3).

At the three-hour timepoint post-irradiation, regardless of radiation dose, we found that the overall proportion of cells collectively comprising the three neoblast clusters remained relatively unchanged with respect to the unirradiated control (Figure 11). This observation is consistent with previous experimental findings, where in situ hybridization for the stem cell marker, Smedwi-1, revealed no significant reduction in stem cell numbers as of this timepoint (Sahu et al, 2021). In the 5 Gy sample, the three neoblast clusters collectively accounted for 18.11% of captured cells, while in the 10 Gy sample, they comprised 17.73% of captured cells. However, a noticeable difference that emerged in the three-hour post-irradiation samples compared to the unirradiated control is that the relative abundances of each individual neoblast cluster underwent changes (Figure 11). Specifically, we observed a decrease in the relative abundances of Neoblast cluster 2 (from 5.48% in the unirradiated sample to 4.80% and 4.71% in 5 Gy and 10 Gy samples, respectively) and Neoblast cluster 3 (from 4.55% in the unirradiated sample to 3.75% and 3.76% in 5 Gy and 10 Gy samples, respectively). The reduction in Neoblast clusters 2 and 3 was accompanied by an increase in the relative abundance of Neoblast cluster 1 at this timepoint (from 8.18% in the unirradiated sample to 9.55% and 9.26% in the 5 Gy and 10 Gy samples, respectively, as listed in Table 3).

However, at the 24-hour post-irradiation timepoint, we observed a more pronounced and dose-dependent decrease in the proportion of cells collectively residing within the three neoblast clusters. In the 24-hour post-5 Gy irradiation sample, neoblast clusters collectively accounted for 14.15% of captured cells, while in the 24-hour post-10 Gy irradiation sample, they represented only 9.69% of the captured cells (Figure 11). At this timepoint, we observed that individual neoblast clusters were disproportionally affected by gamma radiation. Neoblast cluster 2 appeared to exhibit the greatest sensitivity to gamma radiation, as the cluster experienced the greatest reduction in proportional abundance. Specifically, Neoblast cluster 2, accounting for 5.48% of captured cells in the unirradiated sample, accounted for only 2.62% and 1.02% of cells in the 24-hour post-5 Gy and 10 Gy irradiation samples, respectively (Table 3). The loss of cells in Neoblast cluster 2 at this timepoint is visually apparent in the UMAP, where this cluster, which typically serves as a bridge between Neoblast cluster 1 and Neoblast cluster 3, appears to be heavily depleted (Figure 10D, 10E). In contrast, Neoblast cluster 1 sustained a comparatively lesser impact in

response to gamma radiation, with a smaller relative decrease in proportional abundance compared to that of Neoblast cluster 2. The proportion of Neoblast cluster 1 decreased from 8.18% of captured cells in the unirradiated sample to 7.72% and 5.18% of captured cells in the 24-hour post-5 Gy and 10 Gy samples, respectively (Table 3).

In the case of Neoblast cluster 3, we observed a reduction in its proportion from 4.54% of cells captured in the unirradiated sample to 3.81% in the 24-hour post-5 Gy sample and 3.49% in the 24-hour post-10 Gy sample (Table 3). While this change in abundance may appear relatively small, it is crucial to interpret these observations cautiously due to the unique composition of Neoblast cluster 3. As previously described, Neoblast cluster 3 is inferred to be composed of a mixture of both stem cells and lineage-primed progenitor cells. It is plausible that within Neoblast cluster 3, the stem cells themselves are hyper-sensitive to gamma radiation, yet their loss is not significantly reflected in the overall change in cluster size due to the presence of progenitor cells that are known to be unaffected by radiation at these doses and timepoints.

To effectively investigate the existence of cluster-specific stem cell sensitivity to gamma radiation, it is important to establish a correlation between changes in relative cluster proportions with the changes in the proportion of Smedwi-1^{+} cells detected within each cluster. It should be noted, however, that a limitation of this approach is the possibility of false negatives due to sequencing dropouts of Smedwi-1, originating from the sparsity and stochasticity of captured transcripts in every cell. Nonetheless, we observed that in the unirradiated sample, Smedwi-1 transcripts were detected in 82.72% of cells in Neoblast cluster 1, 63.14% of cells in Neoblast cluster 2, while in Neoblast cluster 3, Smedwi-1 was detected in only 26.24% of cells (Figure 12). This decreasing proportion of observed Smedwi-1^{+} cells from Neoblast cluster 1 to Neoblast cluster 3 coincides with the heightened prevalence of lineage-associated markers in Neoblast cluster 3 (Figure 9). Collectively, these observations corroborate our hypothesis of an increasing proportion of progenitor states along this trajectory.

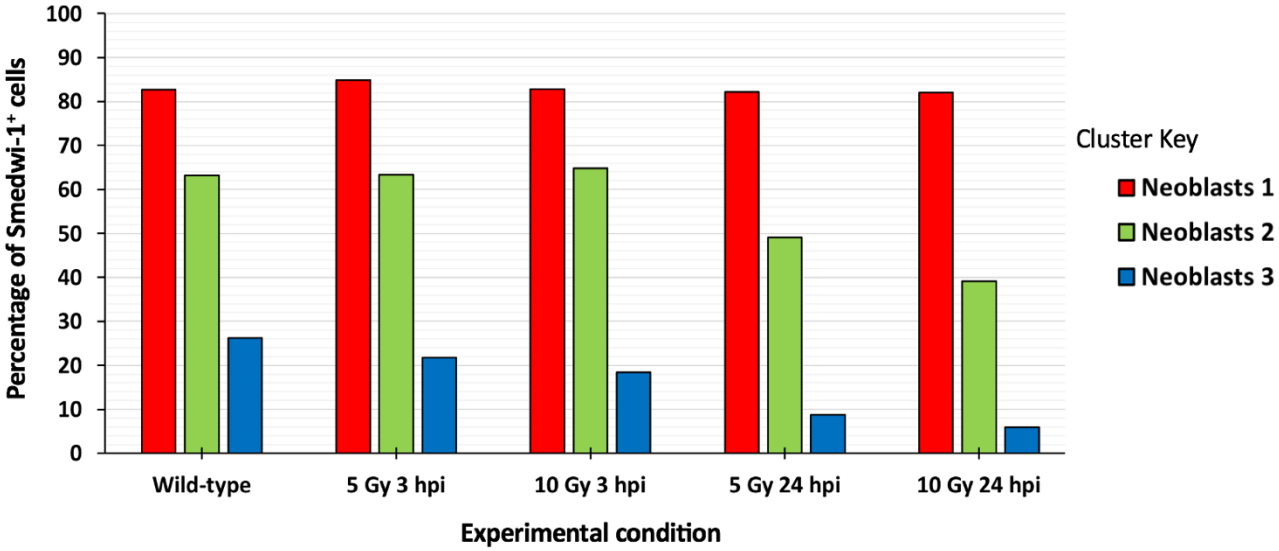

Figure 12. Percentage of cells with detectable Smedwi-1 expression within Neoblast clusters 1, 2, and 3 in each experimental condition.

At the three-hour post-irradiation timepoint, the proportion of observed Smedwi-1$^+$ cells within Neoblast clusters 1 and 2 remained relatively unchanged at both tested radiation doses. However, in Neoblast cluster 3, a dose-dependent reduction in Smedwi-1$^+$ cells was observed, with Smedwi-1 being detected in 21.78% of cells in the 3-hour post-5 Gy sample, and 18.37% in the 3-hour post-10 Gy sample (Figure 12).

At the 24-hour post-irradiation timepoint, more significant and dose-dependent reductions in the fraction of Smedwi-1$^+$ cells were observed in Neoblast clusters 2 and 3 compared to the unirradiated sample. Specifically, Smedwi-1 was detected in 49.09% and 39.06% of cells in Neoblast cluster 2 in the 24-hour post-5 Gy and 24-hour post-10 Gy samples, respectively. In Neoblast cluster 3, Smedwi-1 was detected in only 8.74% and 5.93% of cells in the same respective samples. Conversely, in Neoblast cluster 1, the proportion of cells where Smedwi-1 was detected remained relatively unchanged after irradiation, regardless of dose or timepoint, when compared to the unirradiated sample (Figure 12). As the mean number of UMI's and genes detected per cell in each neoblast cluster were consistent across different experimental conditions, it is unlikely that the differences observed in the percentage of detected Smedwi-1$^+$ cells following irradiation be attributed to technical artefacts arising from differences in sampling.

Taking into consideration the changes in cluster abundances and the proportions of detected Smedwi-1$^+$ cells per cluster, stem cells affiliated with Neoblast cluster 1 appear to be less impacted by gamma radiation exposure compared to those in Neoblast clusters 2 and 3. This phenomenon may be attributed to a greater propensity for stem cells in Neoblast clusters 2 and 3 towards radiation-induced apoptosis, suggesting that cells affiliated with Neoblast clusters 2 and 3 are more sensitive to gamma radiation, while stem cells in Neoblast cluster 1 exhibit a comparatively greater resilience. However, it is essential to explore alternative scenarios that may explain these observations. It remains plausible that all stem cells, regardless of their cluster affiliation, share equal sensitivity to gamma radiation. In this scenario, the observed changes in cluster abundances and Smedwi-1$^+$ cell proportions could be attributed to transcriptomic alterations induced by gamma radiation. These alterations may cause stem cells originally assigned to Neoblast clusters 2 and 3 in the unirradiated sample to acquire a transcriptomic profile that more closely resembles that of a Neoblast cluster 1 cell, causing them to now cluster with Neoblast cluster 1.

Subsequently, we conducted RNA velocity analyses to explore changes in neoblast cell fate trajectories in response to gamma radiation. Through this, we aim to further elucidate the underlying mechanisms that may drive the observed differences in cluster sensitivity to gamma radiation.

Reconstruction of cell fate trajectories in response to gamma radiation using RNA velocity

RNA velocity predicts the direction and speed of cell state transitions by using the relative abundance of pre-mRNA and mature mRNA, correlating them using a simple first-order differential equation (La Manno et al., 2018). This approach benefits from the fact that reads originating from pre-mRNA (un-spliced) or mature mRNA (spliced) can be distinguished from single-cell RNA-sequencing data due to the presence of introns in the former while the latter maps exclusively to exonic regions. By examining the collective transcriptional dynamics of all detected genes within a cell, two distinct cohorts of genes can be extrapolated to either increase or decrease in mRNA abundance in the cell's future state. This extrapolation is based on the abundance ratios of pre-mRNA to mature mRNA in a cell's current state. Specifically, an elevated ratio of pre-mRNA to mature mRNA counts

over steady-state indicates increased new transcription of a particular gene. Consequently, the cell is predicted to harbour increased levels of mature mRNA derived from that gene in the future, considering the temporal delay between the conversion of pre-mRNA to mature mRNA through splicing. Conversely, a decrease in the same ratio signifies gene suppression, and the future state of the cell is predicted to have reduced levels of mature mRNA derived from that gene, as transcripts degrade with diminished inputs.

In this study, we employed the dynamical model of RNA velocity (Bergen et al., 2020) to first investigate the relationship between the three neoblast clusters within the context of their developmental trajectories under unirradiated conditions. We then employed this method to characterize alterations in cell fate trajectories amongst these neoblast clusters in response to gamma radiation. An advantage of RNA velocity over alternative trajectory inference methods, such as the commonly used pseudotime analyses, lies in its ability to be performed in an unbiased and unsupervised manner. While pseudotime-based approaches require the manual designation of a root as the starting point (Trapnell et al., 2014; Street et al., 2018), RNA velocity operates without the need for any subjective input, and hence can be performed without prior knowledge of transitions in the system.

For each experimental condition, we performed RNA velocity analyses and superimposed the resultant velocity vectors, represented as streamlines with black arrowheads, onto the respective UMAP plots for visualization (Figure 13). These streamlines represent the inferred trajectories averaged across entire clusters, offering insights into the general direction of cell state transitions. For a more detailed examination, we also depicted the RNA velocities of individual cells in Figure 14. In Figure 14, stable cell states that are not predicted to undergo transitions are represented by dots, while the arrows indicate cells that are inferred to undergo transitions. The direction of the arrows depict the inferred direction of cell state transitions, while the length of the arrows represent the magnitude of the velocity vector. This magnitude, known as velocity length, serves as a metric for the inferred speed of transitions occurring within cells. The velocity lengths of individual cells are depicted in Figure 15, providing a chance to investigate the speed of inferred transitions at the level of single-cells, which would be highly valuable for a more comprehensive understanding of cell state changes in the system.

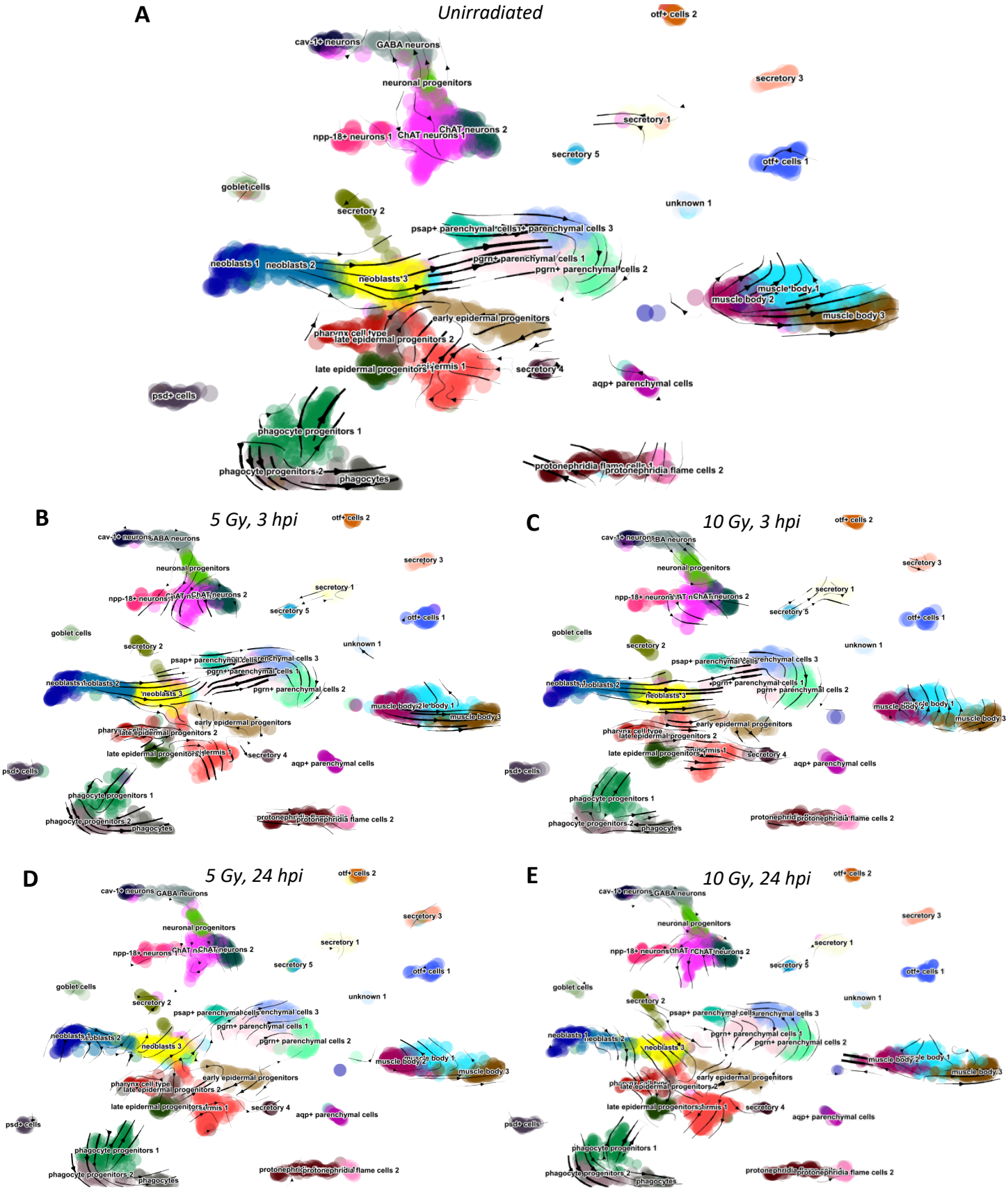

Figure 13. Velocity vector fields superimposed onto the UMAP showing the averaged differentiation trajectories of distinct subclusters. Subfigures separated by experimental condition: **(A)** Unirradiated, **(B)** 3 hours post 5 Gy gamma radiation, **(C)** 3 hours post 10 Gy gamma radiation, **(D)** 24 hours post 5 Gy gamma radiation, **(E)** 24 hours post 10 Gy gamma radiation.

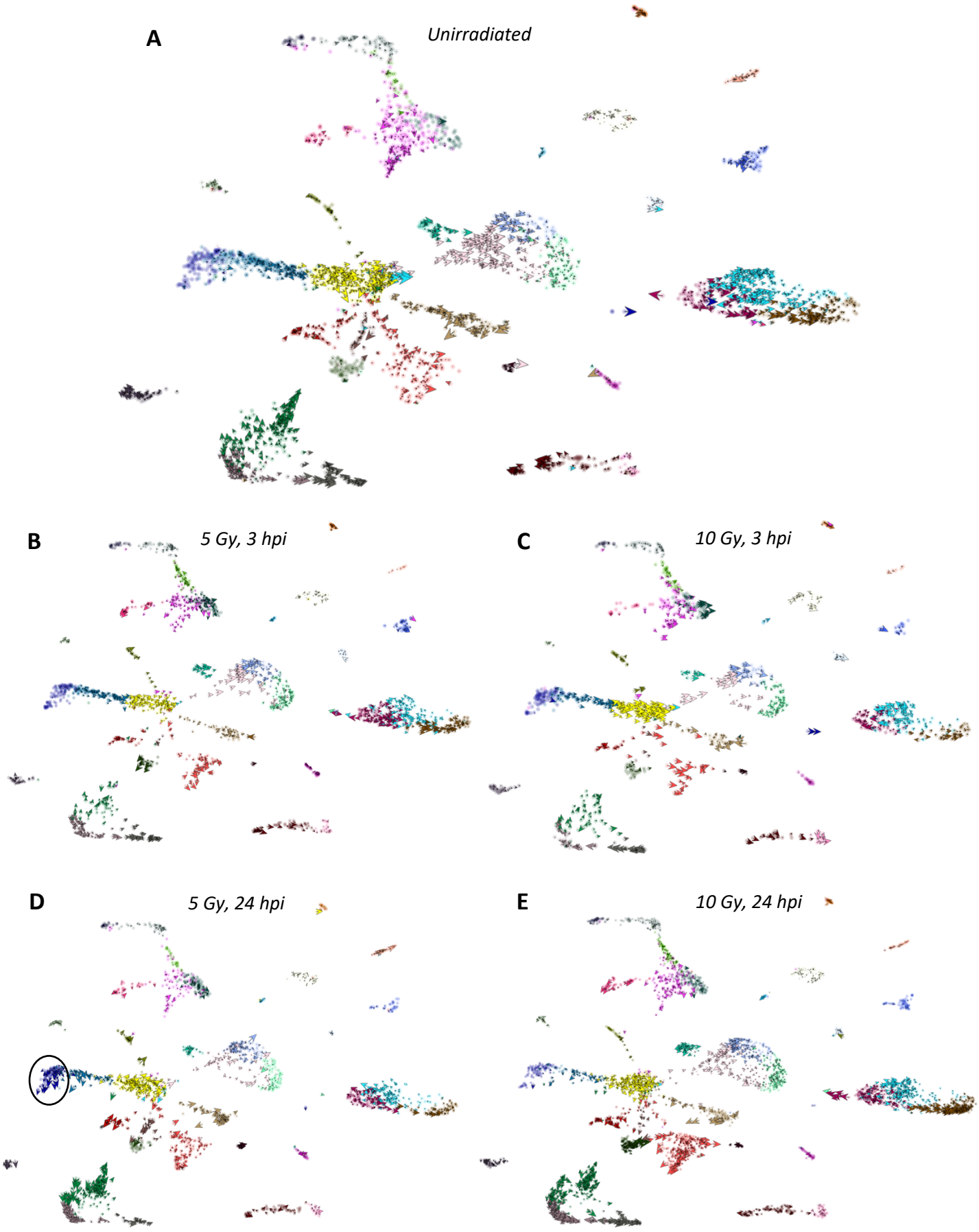

Figure 14. RNA velocities at single-cell resolution. Subfigures separated by experimental condition. **(A)** Unirradiated **(B)** 3 hours post 5 Gy gamma radiation, **(C)** 3 hours post 10 Gy gamma radiation, **(D)** 24 hours post 5 Gy gamma radiation, **(E)** 24 hours post 10 Gy gamma radiation. Cluster positions in the UMAP are identical to the positions shown in Figure 13.

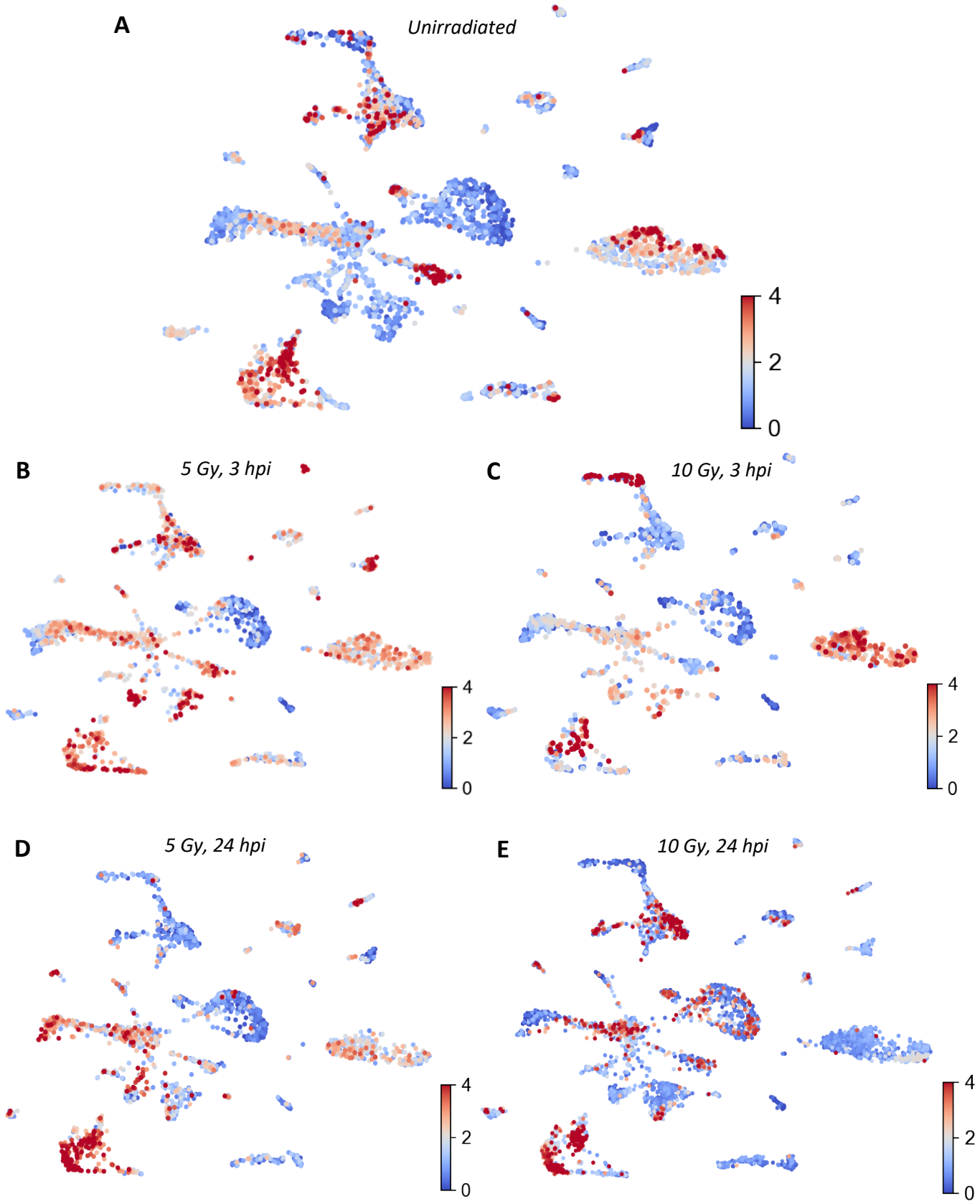

Figure 15. RNA velocity lengths at single-cell resolution. Subfigures separated by experimental condition: **(A)** Unirradiated, **(B)** 3 hours post 5 Gy gamma radiation, **(C)** 3 hours post 10 Gy gamma radiation, **(D)** 24 hours post 5 Gy gamma radiation, **(E)** 24 hours post 10 Gy gamma radiation. Cluster positions in the UMAP are identical to the positions shown in Figure 13. Scale bars represent the velocity values, defined as the statistical residual of observed over inferred steady-state ratios of gene expression kinetics within each cell. The full derivation of this value can be referenced to the work by Bergen and colleagues (Bergen et al., 2021).

In mammalian systems, root and terminal states, typically represented by quiescent stem cells and terminally differentiated cells respectively, often exhibit low RNA velocities and are implied as stable states. In contrast, intermediate states such as activated stem cells and lineage-specified progenitors commonly possess high velocity kinetics, implying cell states that are rapidly changing as differentiation takes place (La Manno et al., 2018; Svensson and Pachter, 2018; Zywitza et al., 2018). These insights aid in our application of RNA velocity in understanding the kinetics of cell state transitions in our atlas.

In the unirradiated sample, we observed unique patterns of RNA velocities associated with each neoblast cluster. Neoblast cluster 1 displayed low RNA velocities, evident by the absence of directional arrows (Figure 14A), and low values of RNA velocity lengths (Figure 15A) in its constituent cells. The low RNA velocity of Neoblast cluster 1 suggests that it represents a relatively stable state, potentially serving as the root of the system. In contrast, cells in Neoblast cluster 2 exhibited high velocities, suggesting an unstable and transitional nature of cells associated with this cluster (Figure 15A). Meanwhile, Neoblast cluster 3 consisted of a mixture of both high and low velocity cells (Figure 15A), potentially reflecting the heterogeneity in cell-types populating this cluster. The unique patterns of RNA velocities associated with each neoblast cluster provided valuable insights that contributed to our model of action, which is further discussed in Figure 16.

Regarding the directionality of the inferred developmental trajectory, we observed robust and unidirectional vector fields extending from Neoblast cluster 2 towards Neoblast cluster 3 (Figure 13A, 14A). This finding suggests a consistent and directional flow of cell state transitions from Neoblast cluster 2 towards Neoblast cluster 3 under wild-type conditions. Cells within Neoblast cluster 3 then appear to feed out towards differentiated tissue clusters, although a biased trajectory towards the parenchymal and epidermal lineages was observed in our atlas (Figure 13A, 14A). The underrepresentation of movement towards other cell lineages may be attributed to poor connectivity to those clusters. This may be caused by an under-sampling of transient intermediary cell states, potentially hindering the identification of complete trajectories. Alternatively, the poor connectivity could be due to inefficiencies in capturing a continuous spectrum of gene expression due to

the limited sensitivity of our method. Consequently, the discrete nature of captured genes may cause the disparities between tissue-types to be artefactually accentuated, as only the highly expressed tissue markers could be robustly defined as differentially expressed between distinct tissues.

Nevertheless, the directionality of cell state transitions between the neoblast clusters under wild-type conditions, inferred using RNA velocity, aligns with our previous observation of decreasing Smedwi-1^{+} cell proportions in the same direction. These RNA velocity observations corroborate our initial proposition of increasing progenitor-like cell states along the suggested developmental sequence originating from Neoblast cluster 1, through Neoblast cluster 2 and finally towards Neoblast cluster 3, before giving rise to other non-stem cell types.

At the three-hour post-irradiation timepoint, we observed that the inferred directionality of cell state transitions between the neoblast clusters remained unchanged relative to wild-type. RNA velocity analyses indicate the same unidirectional developmental sequence from Neoblast cluster 1, through Neoblast cluster 2, towards Neoblast cluster 3, at both the radiation doses tested (Figure 13B, 13C), mirroring the pattern observed in the unirradiated sample. However, observations of velocity length suggest that the RNA velocity of Neoblast cluster 3 had been altered from initially a mixture of high and low velocity cells in the unirradiated sample to a state where all cells within the cluster are homogenously high velocity (Figure 15B, 15C). The increase in RNA velocity at this timepoint was not restricted to Neoblast cluster 3 alone. Instead, a global elevation in cellular RNA velocities was observed across various tissue clusters, including an increase in velocities associated with putative terminally differentiated cell types. It is plausible that the heightened RNA velocities observed across multiple tissues at this timepoint reflect a surge in new transcription of early response genes following exposure to gamma radiation.

At the 24-hour timepoint post-irradiation, a notable shift in the neoblast cell fate trajectories was observed at both tested doses. The direction of cell state transitions had altered from a unidirectional pattern in the unirradiated sample (Figure 13A) to a state where no clear directionality between the neoblast clusters could be inferred (Figure 13D,

13E). This could be reflective of a state where the normal developmental sequence is temporarily halted while stem cells undergo either repair or apoptosis in response to gamma radiation.

At this timepoint, we also observed a dose-dependent distinction in the RNA velocity lengths of cells in Neoblast cluster 1, the cluster where affiliated stem cells are believed to exhibit the greatest resilience to gamma radiation. Namely, we observed high RNA velocity lengths for Neoblast cluster 1 in the 24-hour post-5 Gy irradiation sample (Figure 15D), while the velocity of the cluster remained low in the 24-hour post-10 Gy irradiation sample (Figure 15E). Underlying this distinction could be that cells in Neoblast cluster 1 are in a more advanced stage of the recovery process in the 5 Gy sample than in the 10 Gy sample. RNA velocity infers a highly transitional state associated with Neoblast cluster 1 in the 5 Gy sample, as cells in the cluster could be undergoing state transitions as part of the repopulation process at this specific dose and timepoint. In contrast, RNA velocity predicts a relatively stable and non-transitional Neoblast cluster 1 state in the 24-hour post 10 Gy-irradiation sample. Since the greater level of damage sustained by cells in this experimental sample would necessitate a longer repair phase, the low RNA velocities observed in Neoblast cluster 1 at this dose and timepoint may be reflective of cells still actively undergoing repair, and have yet to initialize the repopulation process. This hypothesis aligns with our previous observations of dose-dependency in the time required for neoblast cell-cycle re-entry after sublethal irradiation (Sahu et al., 2021).

In addition to the heightened cellular RNA velocities, the projected trajectory of cells within Neoblast cluster 1 at the 24-hour post-5 Gy irradiation timepoint deviates from the original path predicted in the unirradiated sample. The directional arrows in Neoblast cluster 1 during this post-irradiation state consistently point backwards, a direction that opposes that of Neoblast cluster 1 in the unirradiated sample. This indicates a trend towards the tip of the cluster that is situated farthest away from the other neoblast clusters (Figure 14D, circled). Considering the UMAP location, it is plausible that this tip region of Neoblast cluster 1 corresponds to the residence of stem cells in a more naïve state, and possibly even a pluripotent state. The observed shift in cell fate trajectories at this experimental condition may imply that neoblasts re-establish pluripotency before proliferating to replenish the

irradiated animal with new stem cells. Such plasticity aligns with the findings of Raz and colleagues (Raz et al., 2021), which revealed that neoblast fates can be reversed and re-specified with respect to their gene expression state.

Overall, RNA velocity analyses predict a unidirectional developmental sequence from Neoblast cluster 1, through Neoblast cluster 2, and ultimately towards Neoblast cluster 3 under wild-type conditions, with radiation treatment capable of inducing changes in the direction and speed of these inferred transitions.

Investigating neoblast cluster differences underlying their differential sensitivity to gamma radiation

Decoding the functional state of stem cells associated with each neoblast cluster would enhance our understanding of the observed differences in cluster sensitivity to gamma radiation. To explore this, we propose a model that incorporates information obtained from our single-cell atlas, our trajectory predictions, and insights derived from existing studies in the planarian literature (Figure 16).

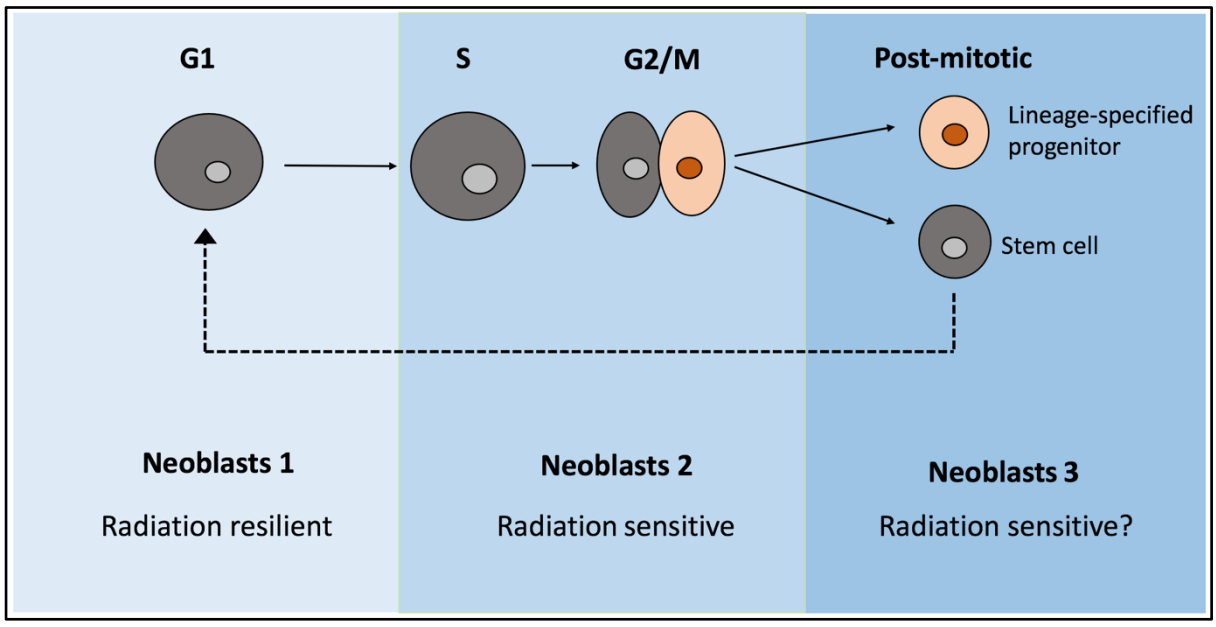

Figure 16. Model of action relating neoblast cluster affiliation, cell-cycle phase, and sensitivity to gamma radiation

Our model posits that neoblast cluster affiliation is closely linked to the cell's temporal position within the cell-cycle. We infer that the Neoblast cluster 1, exhibiting the greatest resilience to gamma radiation compared to stem cells in other clusters, consists primarily of stem cells in G1 phase. Conversely, Neoblast cluster 2, representing the cluster with the greatest susceptibility to gamma radiation, is inferred to be predominantly composed of stem cells in S/G2/M phases of the cell cycle. Neoblast cluster 3, characterized previously to be comprised of a mixture of both stem and progenitor cells, may represent the post-mitotic products of asymmetric stem cell divisions in our model, where one daughter cell retains stemness while the other acquires lineage specification (Figure 16).

Our model is relatable to findings from a previous study by Zeng and colleagues, who observed a correlation between neoblast cell-cycle phase and sensitivity to gamma radiation (Zeng et al., 2018). In their study, neoblasts were categorised into distinct subpopulations based on the detected levels of Smedwi-1 mRNA and protein in tandem using flow cytometry. Cells displaying high levels of both Smedwi-1 mRNA and protein were classified as the Piwi-high subgroup, the subgroup that exhibited the greatest sensitivity to gamma radiation. The Piwi-high subgroup was inferred to be made up of cycling stem cells based on their transcriptional profiles resembling the canonical X1 subgroup, a FACS-enriched population for stem cells in S/G2/M phases. In contrast, neoblasts displaying low levels of both Smedwi-1 mRNA and protein were assigned to the Piwi-low subgroup. Cells in this subgroup exhibited only mild sensitivity to gamma radiation and were proposed to be composed of a mixture of post-mitotic/G1 phase stem cells and fate-determined progenitor cells (Zeng et al., 2018).

In the same study, the authors also reported a small subset of Piwi-high cells that exhibited a relatively high tolerance to gamma radiation (Zeng et al., 2018). However, the authors did not elaborate further on this observation. This observation may have a key biological basis, as studies in mammalian systems have demonstrated that cells in late S phase exhibit heightened tolerance to ionizing radiation (Pawlik and Keyomarsi, 2004; Iliakis and Okayasu, 1990). This is because late S phase represents a time window where cells have completed replication and are free from replication stresses. At the same time, repair templates in the form of sister chromatids are present, enabling the use of homologous

recombination for double-stranded break repair. Considering these insights, it would be worthwhile to explore whether planarian stem cells in late S phase similarly possess heightened resistance to gamma radiation. Additionally, it would be valuable to correlate these observations with our atlas, namely whether Neoblast cluster 1 and Neoblast cluster 2 represent Piwi-low and Piwi-high cells respectively, while also investigating whether the residual surviving stem cells within Neoblast cluster 2 are more likely to be in late S phase. However, the binary output of Smedwi-1 detection in our atlas, instead of one that is graded, limits our ability to confidently distinguish Piwi-high or Piwi-low cells, preventing direct application of this correlation.

In the case of Neoblast cluster 3, analysis of our atlas indicates a notable decrease in the proportion of Smedwi-1^+ cells within said cluster following radiation exposure (Figure 12). Investigation of RNA velocity length reveals that Neoblast cluster 3 comprises cells exhibiting a mixture of high and low velocities (Figure 15A). A possible interpretation could be that high velocity cells correspond to highly transitional lineage-specified progenitor cells, while the low velocity cells may represent stable states in the form of post-mitotic stem cells. The observed reduction in Smedwi-1^+ cells within Neoblast cluster 3 following irradiation could be attributed to these post-mitotic stem cells transitioning back to G1 phase, causing them to associate with Neoblast cluster 1 (Figure 16). This results in an overall net loss in the number of post-mitotic stem cells in Neoblast cluster 3, since the input to this cluster is temporarily disconnected due to cell cycle arrest following radiation exposure.

Additionally, the RNA velocity-inferred directional sequence from Neoblast cluster 1, through Neoblast cluster 2, towards Neoblast cluster 3 (Figure 13A) may be reflective of cellular progression through the cell cycle. Velocity lengths representing the speed of cell state transitions were observed to be low in Neoblast cluster 1, inferred to be comprised of stem cells in G1 phase (Figure 15A). The low velocity lengths in G1 cells may be attributed to the long duration of this cell cycle phase. In contrast, the transitions from S phase to G2 and to M phase take place relatively rapidly, potentially explaining the high velocity lengths observed in cells of Neoblast cluster 2 (Figure 15A). Furthermore, this sequence of velocity vectors may not be exclusively tied to the cell cycle, but may also represent the gradual

acquisition of cell-fate specification as cells progress along the cell cycle. Recent proposals have suggested a tight coupling between planarian cell cycle progression and the acquisition of lineage specification (Raz et al., 2021). This hypothesis is based on the observation of heightened fate-specifying transcription factor (FSTF) expression in S/G2/M phases of the cell-cycle, while the expression of such factors were limited in G1 phase stem cells. It is speculated that FSTF expression is only initialized in S phase of the cell cycle (Raz et al., 2021), which may explain why the velocity vector fields originate from Neoblast cluster 2 rather than Neoblast cluster 1 in the wild-type sample of our atlas (Figure 13A). This suggests that Neoblast cluster 2 may comprise fate-specified stem cells that exhibit greater susceptibility to gamma radiation compared to the more naïve neoblasts that may populate Neoblast cluster 1. However, limited sensitivity of our atlas restricts further investigation at present as FSTF expression could not be robustly detected in our single-cell atlas.

Upon comparing the marker genes associated with each neoblast cluster under wild-type conditions, we observed that Smedwi-3 serves as a marker for Neoblast clusters 2 and 3, but not Neoblast cluster 1 (Appendix Table 1). It is proposed that Smedwi-3 plays a role in the differentiation of neoblast progeny (Palakodeti et al., 2008; Kashima et al., 2020), and its cluster associations may reflect a gradual withdrawal from stemness in accordance with the direction predicted in our trajectory analyses. Similarly, BRG-1 marks Neoblast clusters 2 and 3, but not Neoblast cluster 1 (Appendix Table 1). BRG-1 is inferred in planarians to promote the chromatin remodelling events needed during cell fate specification, and hence is implicated in planarian stem cell differentiation (Trost et al., 2018, Wiggans et al., 2023). Furthermore, RAD50, known in humans to regulate the DNA damage response and promote the repair of double-stranded breaks (Bian et al., 2019), was identified to exclusively serve as a marker for Neoblast cluster 2 (Appendix Table 1). This potentially reflects S phase cells as RAD50 may have a conserved role in the sensing and mitigation of replication stresses. Recent findings also suggest RAD50's direct involvement in promoting mitotic progression, independent of its repair functions (Völkening et al., 2020), and hence may also reflect G2/M phase cells. Overall, the presence of Smedwi-3, BRG-1 and RAD50 as markers Neoblast cluster 2 supports our hypothesis that this cluster is populated by S/G2/M phase stem cells.

Additionally, we conducted pseudo-bulk differential gene expression analyses, following the methodology outlined by Butler and colleagues (Butler et al., 2018), to further explore the differences between cells assigned to Neoblast clusters 1 and 2 under wild-type conditions. Using this method, transcript counts from all cells within wild-type Neoblast clusters 1 and 2 were separately aggregated and normalized, generating two independent bulk-like profiles for subsequent differential gene-expression testing. Our findings revealed the upregulation of additional DNA repair genes, replication-associated genes, and cell-cycle related genes in Neoblast cluster 2 (Log_2 Fold Change > 1, p-value < 0.05) [Figure 17A, Appendix table 2]. Such genes include DNA repair genes, ATR (Nam and Cortez, 2011) and Fanconi Anemia Group 1 protein [FANCI] (Jones and Huang, 2012), Structural Maintenance of Chromosomes family genes, SMC1 and SMC2 (Harvey et al., 2002), and the anaphase-promoting gene CDC16 (Tugendreich et al., 1995). The heightened prominence of DNA repair and SMC genes in Neoblast cluster 2 may reflect cells in S phase experiencing replication stresses, while CDC16 transcripts may originate from mitotic cells. Overall, these findings support our hypothesis that Neoblast cluster 2 is comprised of stem cells in S/G2/M phases. However, caution needs to be exercised when further interpreting these results, as single-cell differential gene expression analyses are prone to false discoveries due to the sparsity and stochasticity of captured transcripts (Squair et al., 2021).

Nonetheless, we conducted pseudo-bulk differential gene expression analyses to identify genes exhibiting differential expression in Neoblast cluster 1 following exposure to gamma radiation. We analysed the pseudo-bulk transcriptomes of Neoblast cluster 1 under varying post-irradiation conditions relative to wild-type, revealing genes upregulated in Neoblast cluster 1 following irradiation (Figure 17 B-E) [Appendix Tables 3-6]. These genes hold potential as candidate regulators enabling the cells within this cluster to display resilience to gamma radiation. We further explored their relevance in Chapter 4, where our pseudo-bulk findings are integrated with our bulk RNA-sequencing dataset of irradiated X1 cells, aiding in the selection of candidate genes for an RNAi screen as part of our efforts to identify novel regulators of planarian radiotolerance in vivo.

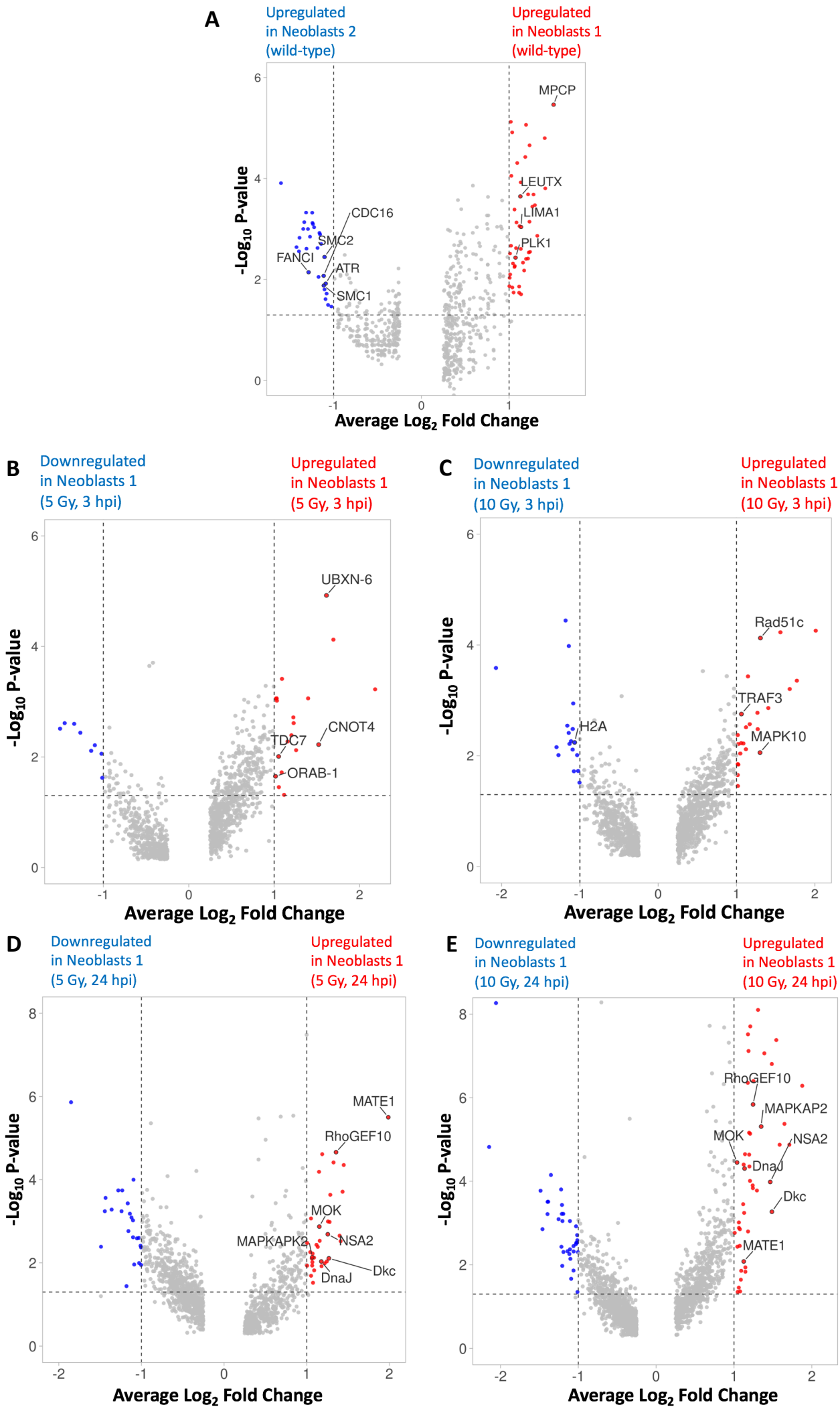
A
Upregulated in Neoblasts 2 (wild-type)
Upregulated in Neoblasts 1 (wild-type)
MPCP
LEUTX
LIMA1
PLK1
CDC16
SMC2
FANCI
ATR
SMC1
-Log10 P-value
Average Log2 Fold Change
B
Downregulated in Neoblasts 1 (5 Gy, 3 hpi)
Upregulated in Neoblasts 1 (5 Gy, 3 hpi)
UBXN-6
CNOT4
TDC7
ORAB-1
C
Downregulated in Neoblasts 1 (10 Gy, 3 hpi)
Upregulated in Neoblasts 1 (10 Gy, 3 hpi)
Rad51c
TRAF3
H2A
MAPK10
D
Downregulated in Neoblasts 1 (5 Gy, 24 hpi)
Upregulated in Neoblasts 1 (5 Gy, 24 hpi)
MATE1
RhoGEF10
MOK
MAPKAPK2
NSA2
Dkc
DnaJ
E
Downregulated in Neoblasts 1 (10 Gy, 24 hpi)
Upregulated in Neoblasts 1 (10 Gy, 24 hpi)
RhoGEF10
MAPKAP2
MOK
NSA2
DnaJ
Dkc
MATE1

Figure 17. Pseudo-bulk differential gene expression analyses between selected Neoblast clusters and conditions. (A) Volcano plot depicting the genes that are differentially expressed between Neoblast cluster 1 and Neoblast cluster 2 under wild-type conditions. Volcano plots depicting the genes that are differentially expressed in Neoblast Cluster 1 at **(B)** 3 hours post 5 Gy, **(C)** 3 hours post 10 Gy, **(D)** 24 hours post 5 Gy, and **(E)**, 24 hours post 10 Gy exposures relative to Neoblast Cluster 1 under wild-type conditions.

Chapter 3 – Conclusions and future perspectives

Our single-cell atlas reveals three distinct neoblast clusters exhibiting varying sensitivity to gamma radiation. In the unirradiated sample representing a wild-type condition, trajectory predictions indicate a unidirectional transitional sequence from Neoblast cluster 1, through Neoblast cluster 2, towards Neoblast cluster 3. However, this directional sequence becomes obscured and disjointed as of 24 hours post-irradiation. We propose a model suggesting that neoblast cluster affiliation is tied to the cell's position within cell cycle. We infer that Neoblast cluster 1 is primarily comprised of G1 phase stem cells exhibiting a relatively high resilience to gamma radiation, while Neoblast cluster 2 mainly consists of S/G2/M phase stem cells exhibiting the greatest sensitivity to gamma radiation.

It is important to acknowledge that our current atlas lacks the sensitivity required to robustly detect and quantify the expression of cell cycle genes and FSTFs at the level of single-cells. Additional sequencing efforts with improved sensitivity would be required to comprehensively explore the intricate relationship between cell cycle dynamics, fate specification, and sensitivity to gamma radiation. A more sensitive atlas may also allow us to distinguish stem cells based on their Smedwi-1 expression levels, and to decipher whether the expression level of Smedwi-1 can be a predictor of sensitivity to gamma radiation. A practical validatory solution using our current SPLiT-seq method could be the generation of single-cell atlases following cell-cycle manipulation. If our model holds true, blocking the G1/S transition would lead to an accumulation of cells clustering in Neoblast cluster 1,

whilst depleting cells in Neoblast clusters 2 and 3. Impeding the G2/M transition in turn would cause an accumulation of cells in Neoblast cluster 2, accompanied by a depletion of cells in Neoblast cluster 3.

Currently, the single-cell quantification of FSTF expression would necessitate the use of the highly sensitive albeit costly 10X genomics platform for single-cell sequencing. However, further improvements to SPLiT-seq technologies in planarians may enable the quantification of these genes in a more cost-effective manner. Measuring the expression of these genes at the level of single cells would enhance our understanding of resilient and sensitive cell states in response to gamma radiation, and potentially provide differential markers of these states for experimentally testing in vivo.

Nonetheless, through pseudo-bulk differential gene expression analyses, we identified genes that are upregulated in Neoblast cluster 1 following exposure to gamma radiation. Integrating these findings with our post-irradiation bulk transcriptome of X1 cells guided our selection of candidate genes for an RNAi screen, aimed to uncover novel regulators of planarian radiotolerance in vivo. Comprehensive information regarding this RNAi screen, including the methodology and findings as well as their broader implications is detailed in the following chapter.

Chapter 4: An RNA Interference Screen Reveals Critical Regulators of Radiotolerance in Planarians

Chapter 4 – Introduction

As first unveiled in the nematode *C. elegans* (Fire et al., 1998), RNAi permits the post-transcriptional silencing of target genes in planarians through sequence-specific degradation of endogenous mRNA (Sanchez-Alvarado and Newmark, 1999). Over the past two decades, RNAi has expanded to become a powerful reverse genetics tool enabling gene discovery in planarians. In this chapter, we conduct a primary RNAi screen with the aim to identify novel and potentially conserved regulators of planarian radiotolerance in vivo. Understanding the factors that contribute to planarian radiotolerance may shed light on the conserved mechanisms underpinning radiation resistance across the animal kingdom. Genes found to be important for planarian radiotolerance, while also exhibiting conservation in mammals, could emerge as prospective targets for therapeutic interventions. Such interventions could offer clinical advantages such as imparting radioprotection to normal stem cells, or sensitizing cancer stem cells to radiotherapy.

Selection of candidate genes for RNAi

Previous efforts in our group have assembled a post-irradiation transcriptome of the planarian X1 cell population (unpublished data, courtesy of Dr. Sounak Sahu). This cell population is a flow-cytometry-based compartment that is enriched for stem cells in S/G2/M phases (Hayashi et al., 2006). The genes within this cell population exhibiting differential expression following exposure to gamma radiation have been subjected to prior in silico characterization (data unpublished), however functional elucidation of these genes remains pending. The strategy used to generate this transcriptome is summarized in Figure 18A, which is of relevance to this present study, as this dataset serves as a key resource for our candidate gene selection process.

A

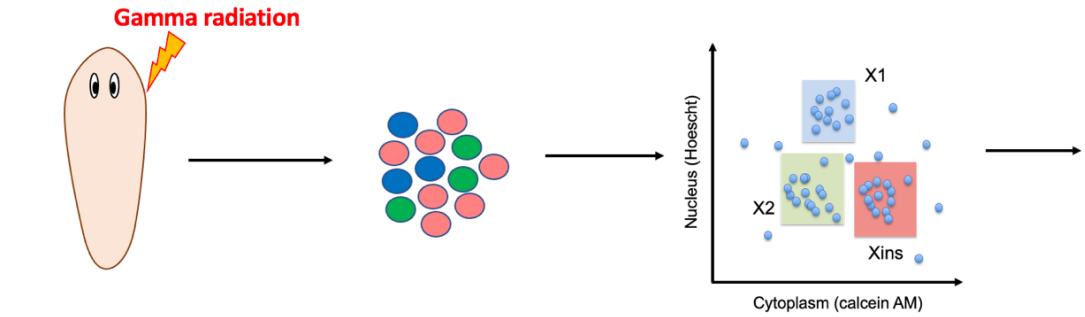

1. Whole-body 5 Gy gamma irradiation

2. Papain-based cell dissociation

3. FACS isolation of X1 cells

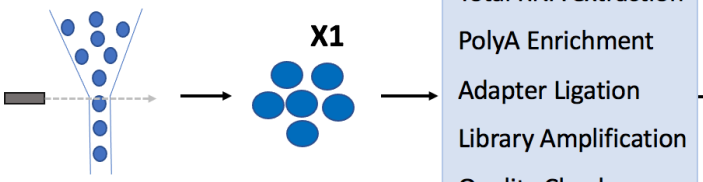

Total RNA extraction
PolyA Enrichment
Adapter Ligation
Library Amplification
Quality Check

RNA sequencing

Differential gene expression

4. Library preparation and sequencing

5. Assess transcriptional changes in response to gamma radiation

B

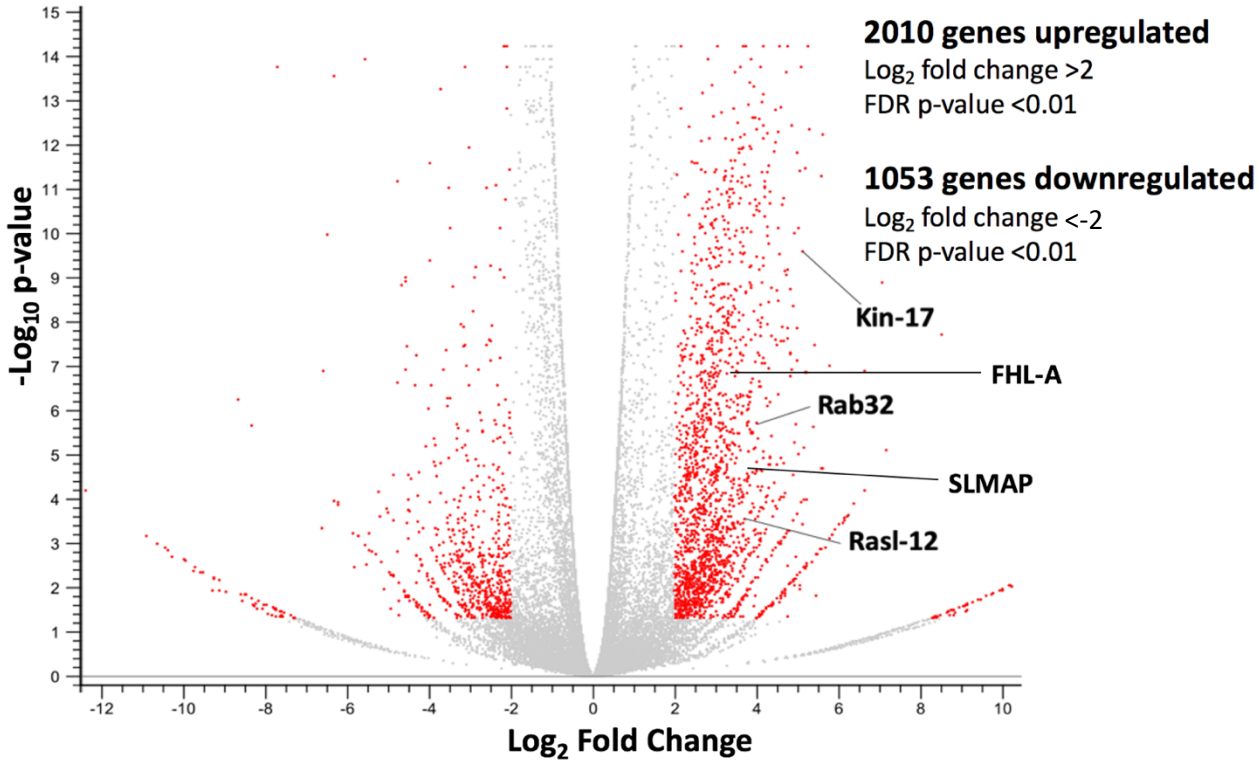

Figure 18. Transcriptional response of the X1 cell compartment to gamma radiation exposure. **(A)** Schematic overview of the strategy employed for the transcriptomic profiling of X1 cells in response to gamma radiation exposure. Animals were subjected to an acute 5 Gy dose of whole-body gamma radiation, and their cells were dissociated at 24 hours post-irradiation. Unirradiated animals were used as controls and dissociated in the same manner. Using fluorescence activated cell sorting, X1 populations were isolated from both irradiated and non-irradiated animals based on their nuclear-to-cytoplasmic ratios. Subsequently, RNA-sequencing was performed on the sorted cells to identify differentially expressed genes between the irradiated X1 cells against their unirradiated counterparts. DESeq2 (Love et al., 2014) was used for differential gene expression testing, which unveiled the upregulation of 2010 genes and the downregulation of 1053 genes in response to acute gamma radiation, illustrated in the accompanying volcano plot in **(B)**.

The genes selected for RNAi screening primarily originated from the cohort of genes displaying upregulation in the X1 cell fraction following exposure to acute gamma radiation (Figure 18B). Genes that are transcriptionally activated post-irradiation serve as attractive candidates for involvement in radiation response and survival mechanisms. Several criteria were evaluated in our candidate gene selection process, including assessing the magnitude of fold change post-irradiation, functional novelty, or novelty in the context of genotoxic damage as established by literature review, presence or absence of a mammalian orthologue, and the predicted functions of the gene. Emphasis was directed toward the screening of novel transcription factors, genes with putative regulatory DNA binding domains, and signalling regulators. The prioritization of these genes aimed to elucidate potential gene regulatory networks orchestrating planarian radiotolerance. Additionally, we incorporated selected platyhelminth-specific genes of uncharacterized functions that were upregulated in response to gamma radiation, recognizing these genes as potential platyhelminth innovations conferring radiotolerance to the animal. A list of the genes incorporated into our RNAi screen, along with a key describing the selected genes' features, are provided in Appendix Table 8.

As described in Chapter 3, our screen also incorporated genes that were upregulated following irradiation in Neoblast cluster 1 — the stem cell cluster within our single-cell atlas that showcased the greatest resilience to gamma radiation. However, the inclusion of these genes was weighed carefully, acknowledging the constraints of single-cell differential gene expression analyses previously discussed in Chapter 3. Candidate gene selection from this list involved assessing the post-irradiation changes in their pseudo-bulk gene expression levels, shifts in the percentage of cells with detectable expression of the gene, and their alignment with gene expression patterns observed in our bulk RNA sequencing data. A total of 8 genes – Dkc, MAPKKK3, NSA2, RhoGEF10, 14-3-3T, DnaJ, UMSBP, and YBX2, which concurrently showed upregulation in both the bulk X1 dataset and Neoblast cluster 1 post-irradiation, were incorporated into the screen (Chapter 3 – Figure 17, Appendix tables 5,6).

While our bulk RNA-sequencing efforts offer valuable insights into the transcriptional response of X1 cells to gamma radiation, we acknowledge a technical limitation of the assay that surfaced during our analysis. Specifically, we observed the upregulation of Prog-1 (Log_2 Fold-Change = +1.72) and Agat-1 (Log_2 Fold-Change = +3.49) at 24 hours post-irradiation relative to the unirradiated control. These genes represent canonical markers for early and late-stage stem cell progenies of the epidermal lineage, respectively (Eisenhoffer et al., 2008). Initially, this observed upregulation led us to consider the possibility of radiation-induced premature stem cell differentiation, a phenomenon documented in other systems (Monje et al., 2002; Schneider et al., 2013; Konířová et al., 2019; Wagle and Song, 2020). However, our attempts at in vivo experimental validation through whole-mount double in situ hybridization, co-staining for Prog-1/Smedwi-1 in one assay, and Agat-1/Smedwi-1 in another, failed to show a significant increase in the proportions of Smedwi-1^+ cells co-expressing either Prog-1 or Agat-1 post-irradiation (Figure 19). These observations suggest against the notion of radiation-induced stem cell differentiation, or the occurrence of a phenomenon where Smedwi-1^+ cells co-expressing these progeny markers are enriched, which could have implied that cells in this state possess heightened tolerance to gamma radiation.

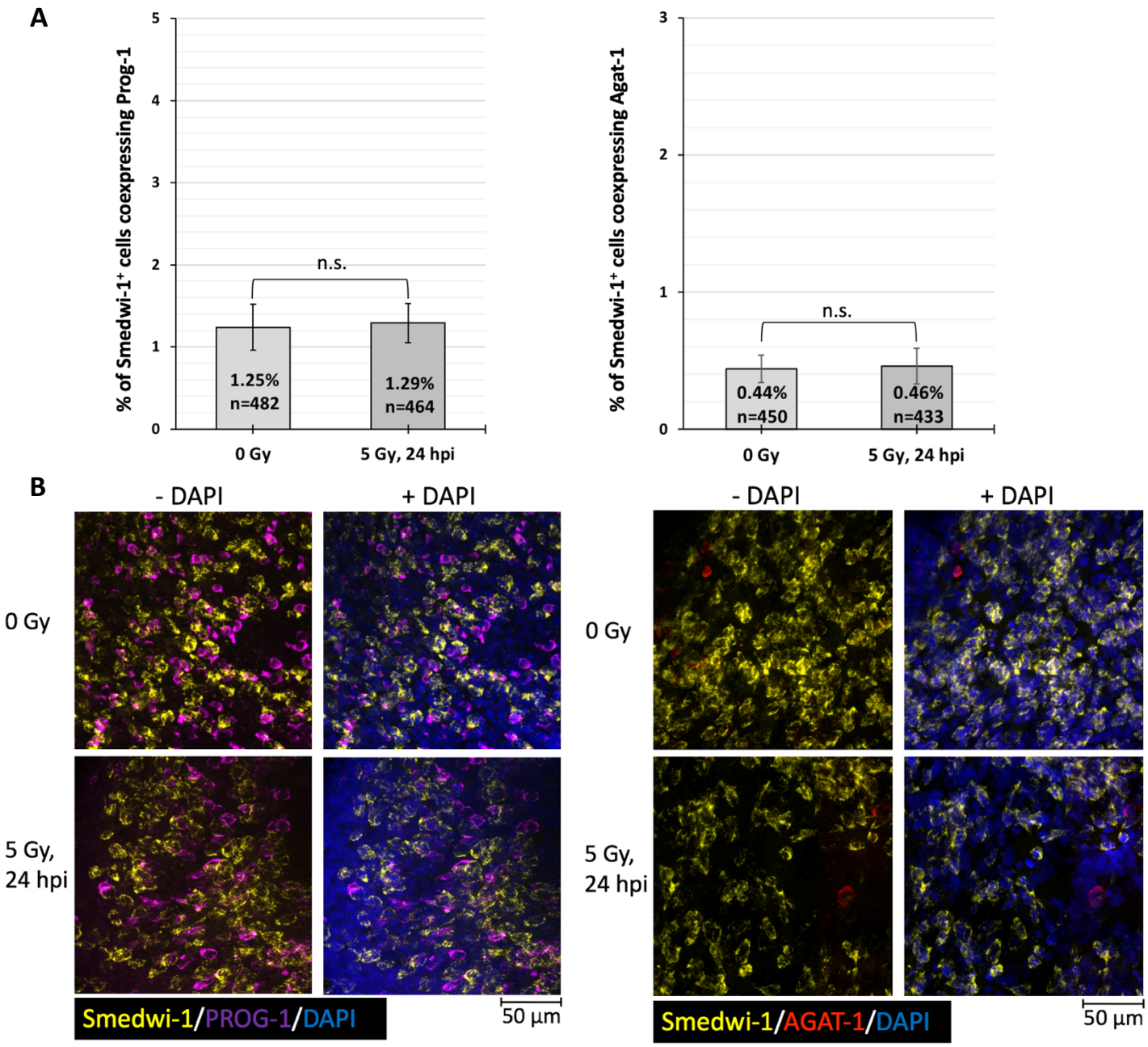

Figure 19. Absence of Prog-1 and Agat-1 upregulation in stem cells in vivo by 24 hours post 5 Gy irradiation. (A) Percentage of Smedwi-1$^+$ cells co-expressing either Prog-1 or Agat-1 compared between unirradiated animals and those 24 hours after exposure to 5 Gy acute gamma radiation. The observed differences were not statistically significant (unpaired t-test p-value >0.05). Co-expression analyses were performed using JaCoP colocalization finder (Bolte and Cordelieres, 2006), which uses Costes' method (Costes et al., 2004) for background subtraction and signal threshold establishment. The output of JaCOP was manually validated to ensure that occurrences of colocalization did not arise from overlapping cytoplasm of adjacent cells. The abbreviation 'n' denotes the total number of cells examined across five biological replicates per condition. **(B)** Representative dual fluorescence ins itu hybridisation images depicting the Smedwi-1/Prog-1 and Smedwi-1/Agat-1 expression patterns in non-irradiated and irradiated animals. Images shown capture the periphery of the stem cell compartment that intersects with the more superficial Prog-1$^+$ cell layer.

This discrepancy prompted us to consider potential technical factors contributing to the observed upregulation of Prog-1 and Agat-1 post-irradiation. The most likely reason is that FACS gating methods inadvertently leave progeny cells within the X1 gate. By 24 hours post-irradiation, these progeny cells become enriched, as their proportional abundances increase due to the radiation-induced depletion of true positive stem cells within the same target gate. Supporting the presence of progeny cells in the X1 gate and their subsequent enrichment post-irradiation, the genes – Mitochondrial Carrier Protein 1 (Mcp-1) [Log_2 fold change = +3.14], Ornithine Decarboxylase 1 (Odc-1) [Log_2 fold change = +3.61], and Cytochrome p450 1A1 (Cp1A1)[Log_2 fold change = +3.05], display a similar pattern of upregulation as Prog-1 and Agat-1 at 24 hours post-irradiation (Appendix Table 9). Akin to Agat-1, these three genes are classified as Category 3 markers, a signature of late-epidermal progeny cells (Eisenhoffer et al., 2008).

This technical limitation of impure gating can be seen in prior studies that employ control flow-cytometry gates with lethally irradiated animals. In such cases, residual cells could still be detected in the X1 gate even after the purging the animals of all stem cells via lethal irradiation (Hayashi et al., 2006; Eisenhoffer et al., 2008; Pearson and Sanchez-Alvarado, 2010). Eisenhoffer and colleagues indirectly evaluated the purity of this sorting approach, observing that only 80% of X1 cells were positive for the stem cell marker, Smedwi-1, through in situ hybridization of the sorted cell population (Eisenhoffer et al., 2008). The same study further revealed the presence of Prog-1^+ and Agat-1^+ cells, expressed in a manner that is mutually exclusive to the Smedwi-1^+ cells, via in situ hybridization of sorted X1 cell population. Specifically, Prog-1 and Agat-1 were detected in 0.7% and 2.4% of the sorted X1 cells, respectively (Eisenhoffer et al., 2008). Additionally, the authors also conducted cell-cycle analysis of the X1 cell population using a propidium iodide-based flow-cytometry approach, revealing that an average of 5.62% of X1 cells were in G1 phase (Eisenhoffer et al., 2008), which potentially includes some of these progeny cells. These findings collectively support our inference of artefactual progeny cell inclusion within the X1 gate.

To investigate the prominence of these carry-over progeny cells in our X1 data, we compared the transcripts per million (TPM) values of Prog-1, Agat-1, Odc-1, Mcp-1, and Cp1A1 in our wild-type samples with their corresponding TPM values extracted from publicly available X1 datasets (Zhu et al., 2015; van Wolfswinkel et al., 2014; Tu et al., 2015). We observed that the TPM values for these five genes in our control samples did not exhibit statistically significant differences when compared to their mean TPM values across the referenced public control datasets (Table 4). This suggests that our gating stringency did not permit a significantly greater influx of these progeny cells through the X1 gate than what was present in the public datasets.

Table 4. Comparison of TPM values for selected epidermal progeny genes within wild-type X1 RNA sequencing datasets from this study against published datasets.

Gene	**TPM values in wild-type X1 libraries**											
	Zhu et al., 2015		van Wolfswinkel et al., 2014		Tu et al., 2015				**Mean**	This study		**Mean**
	Rep 1	Rep 2	Rep 1	Rep 2	Rep 1	Rep 2	Rep 3	Rep 4		Rep 1	Rep 2	
Prog-1	35.16	34.89	19.29	22.80	16.34	15.41	16.39	15.20	**21.96**	21.32	20.03	**20.67**
Agat-1	9.38	10.34	5.39	4.16	6.25	5.86	7.84	7.25	**7.04**	6.68	5.50	**6.11**
Odc-1	28.47	28.58	24.78	22.66	11.45	9.88	12.22	9.37	**18.43**	20.37	19.20	**19.72**
Mcp-1	0.16	0.21	0.37	0.35	0.14	0.09	0.10	0.21	**0.22**	0.36	0.40	**0.38**
Cp1A1	1.02	1.37	1.15	0.83	0.77	0.98	2.02	2.56	**1.25**	0.97	1.28	**1.12**

Given these observations, we attribute the observed upregulation of progeny markers, Prog-1 and Agat-1, in our X1 dataset following irradiation to technical rather than biological reasons. Their upregulation is likely due to a rise in the proportional abundance of progeny cells within the X1 gate following irradiation, resulting from the radiation-induced ablation of true-positive stem cells that normally occupy the same gate.

In our process of selecting candidate genes, we took precautionary measures to reduce the impact of these artefacts on our results. We avoided the screening of differentially expressed genes with spatial expression profiles characteristic of these

progeny cell-types, as determined from single-cell gene expression data (Fincher et al., 2018; Plass et al., 2018) and a prior study that identified epidermal progenitor-associated genes (Zhu et al., 2015). We also prioritized the screening of genes with intrinsically high proportional expression in stem cells (Neiro et al., 2022), and whose expressions were further upregulated after gamma radiation exposure (Appendix Table 8). These strategies aimed to enhance the probability of screening differentially expressed genes originating from stem cells rather than the contaminant progeny cells post-irradiation. Additionally, we avoided the screening of genes with known pro-apoptotic functions, as we recognize that genes driving apoptosis may manifest as a prominent signature at the profiled timepoint. This exclusion aimed to ensure that our screen was targeted towards identifying genes that confer radiotolerance to the animals by promoting stem cell survival and recovery in response to gamma radiation. A list of the excluded genes, along with a key describing the genes' features, can be found in Appendix Table 9.

RNAi experimental strategy

In total, we performed 105 single-gene knockdowns in our primary RNAi screen, following the experimental strategy outlined in Figure 20. Each gene knockdown was evaluated for two distinct phenotypes. Firstly, we closely monitored five animals per gene knockdown for up to 50 days post-exposure to a 15 Gy dose of acute whole-body gamma radiation. The objective was to ascertain whether the combination of targeted gene knockdown and sub-lethal irradiation induced mortality or resulted in severe morphological changes in the animals. Concurrently, to establish a baseline, we maintained five animals per gene knockdown in a non-irradiated state to assess if the silencing of specific genes resulted in defects to animal homeostasis (Figure 20B). The second phenotypic assessment examines whether the gene knockdowns induce a delay in stem cell recovery following sub-lethal irradiation (Figure 20B). We implemented this assay to capture genes with potentially more subtle but nevertheless meaningful contributions to planarian radiotolerance. We also quantified the stem cell numbers in five non-irradiated animals per RNAi condition to assess whether any of the targeted gene knockdowns affected stem cell maintenance under homeostatic conditions.

A

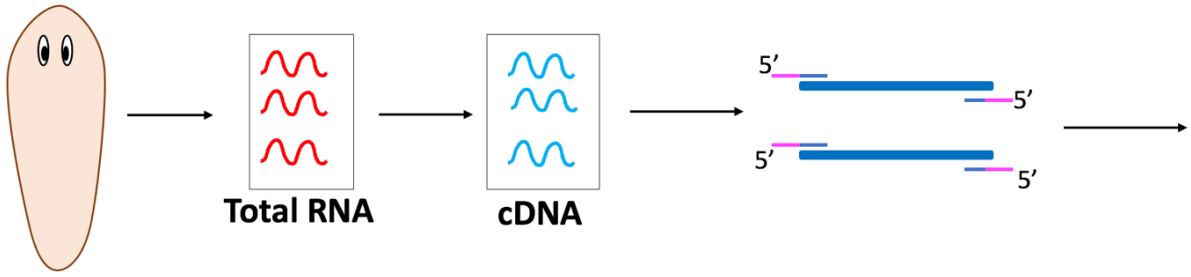

1. Trizol RNA extraction

2. Reverse transcription

3. Gene-specific PCR amplification from cDNA

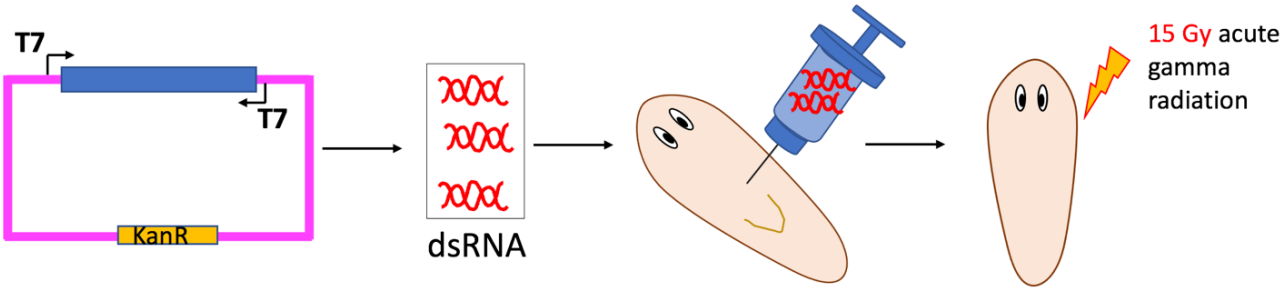

4. Cloning into PPR-T4P vector backbone

5. In-vitro transcription

6. Injection of dsRNA into planarian gut

7. Sub-lethal irradiation

B

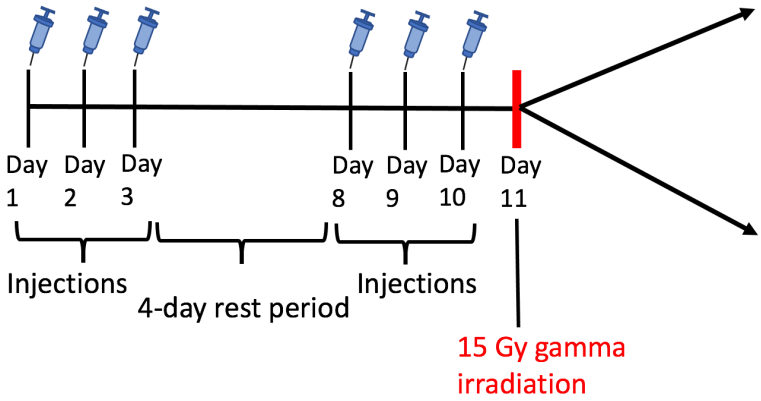

Phenotypic assessment 1: Lethality or severe morphological defects in either irradiated or unirradiated knockdown animals
Method: Bright-field microscopy monitoring up to 50 days post irradiation

Phenotypic assessment 2: Delay in stem cell recovery in irradiated knockdown animals or impaired stem cell maintenance in unirradiated knockdown animals
Method: In-situ hybridisation staining for stem cell marker, Smedwi-1, at 7 days post irradiation

Figure 20. RNAi screen to identify pivotal regulators of planarian radiotolerance in vivo.
(A) Schematic overview of the RNAi experimental workflow. Total RNA was extracted from planarians and reversed transcribed into cDNA. Genes-of-interest were amplified from cDNA using gene-specific primers adapted with sequences that are complementary to the target vector insertion site, facilitating their directional insertion into the PPR-T4P vector. Inserts cloned into the vector are flanked by opposing T7 promoter sites, enabling the synthesis of dsRNA through T7 RNA-polymerase-mediated in vitro transcription. 20 animals per gene were subjected to gene-specific knockdown, achieved by administering dsRNA directly into the planarian gut by microinjection, in accordance with the schedule described in (B).
(B) Timeline of each gene knockdown assay. 7-day-starved planarians were injected with dsRNA on three consecutive days, followed by a 4-day-rest period. A second set of dsRNA injections were administered over another three consecutive days. 10 RNAi-treated animals were exposed to sub-lethal irradiation 24 hours after the last injection dose, with the other half kept non-irradiated. Both the irradiated and non-irradiated RNAi-treated animals were assessed for two phenotypes, probing for their long-term survival and the timely recovery of their stem cells in the case of the irradiated batch; and for homeostatic defects in the unirradiated batch.

In our RNAi screen, we successfully identified six single-gene knockdowns that rendered planarians sensitive to sub-lethal irradiation in vivo, revealing their crucial roles in regulating planarian radiotolerance. These genes include – Sarcolemma membrane-associated protein (Slmap), Kin17 DNA/RNA binding protein (Kin-17), Dyskerin synthase (Dkc), Ras-related protein Rab-32 (Rab32), Ras-like family 12 (Rasl-12), and *Drosophila* Melanogaster X-Like 1 (DMXL-1). We uncovered an additional 20 genes whose knockdowns induced a delay in the recovery of stem cells following irradiation. Although RNAi of these 20 genes did not culminate in fatal outcomes for the animals, we acknowledge their potential contributions to planarian radiotolerance.

RNAi of Slmap, Kin-17, Dkc, Rab32, Rasl-12, and DMXL-1 sensitizes planarians to gamma radiation in vivo

Among the 105 genes subjected to knockdown, we observed that the individual silencing of Slmap, Kin-17, Dkc, Rab32, Rasl-12, and DMXL-1 enhanced planarian sensitivity to gamma radiation. These genes were initially selected as screening candidates due to their differential expression in silico post-irradiation. Namely, all six genes displayed upregulation in our post-irradiation bulk X1 dataset (Appendix Table 8), with Dkc additionally showing upregulation in Neoblast cluster 1 of our single-cell atlas at the 24-hour timepoint post both 5 Gy and 10 Gy irradiation (Chapter 3 – Figure 17, Appendix Tables 5 and 6).

While the individual gene knockdowns caused no observable defect to non-irradiated animals, the combination of RNAi and sub-lethal irradiation was lethal for the six genes described (Figure 21A). Specifically, 100% mortality (n=20) was observed amongst animals subjected to Slmap, Kin-17, Dkc, Rab32, and Rasl-12 single-RNAi in combination with sub-lethal irradiation. In the case of DMXL-1 RNAi, 80% or 16 out of 20 of the sub-lethally irradiated animals exhibited fatal outcomes (Figure 21B). All animals that died in the assay displayed anterior regression, ventral curling, and eventual tissue lysis (Figure 21A), a series of events reminiscent of the stereotypical ablation-in-stem-cell-function phenotype within planarians (Reddien et al., 2005; Rink, 2013). These observations suggest that the target genes play pivotal roles in the planarian radiation response and recovery process, although their functions may be dispensable for animal homeostasis.

In our assay, we knocked down GFP, a sequence that is absent from the planarian genome, to serve as a negative control. This is important to control for artefacts potentially caused by sequence-independent events upon introduction of foreign dsRNA into planarians. Simultaneously, this control helped validate that the technical micro-injection procedure did not cause excessive mechanical damage, thereby avoiding additional stress to the animal tissue. No instances of mortality nor aberrant morphological changes were observed among our negative control group. Conversely, we knocked down ATR, a DNA repair gene previously shown in our group to sensitize planarians to gamma radiation without lethality in unirradiated animals (Sahu et al., 2021), as a positive control. The efficacy of RNAi was validated using quantitative PCR, affirming successful reduction in target gene expression upon knockdown in our assay (Figure 21C).

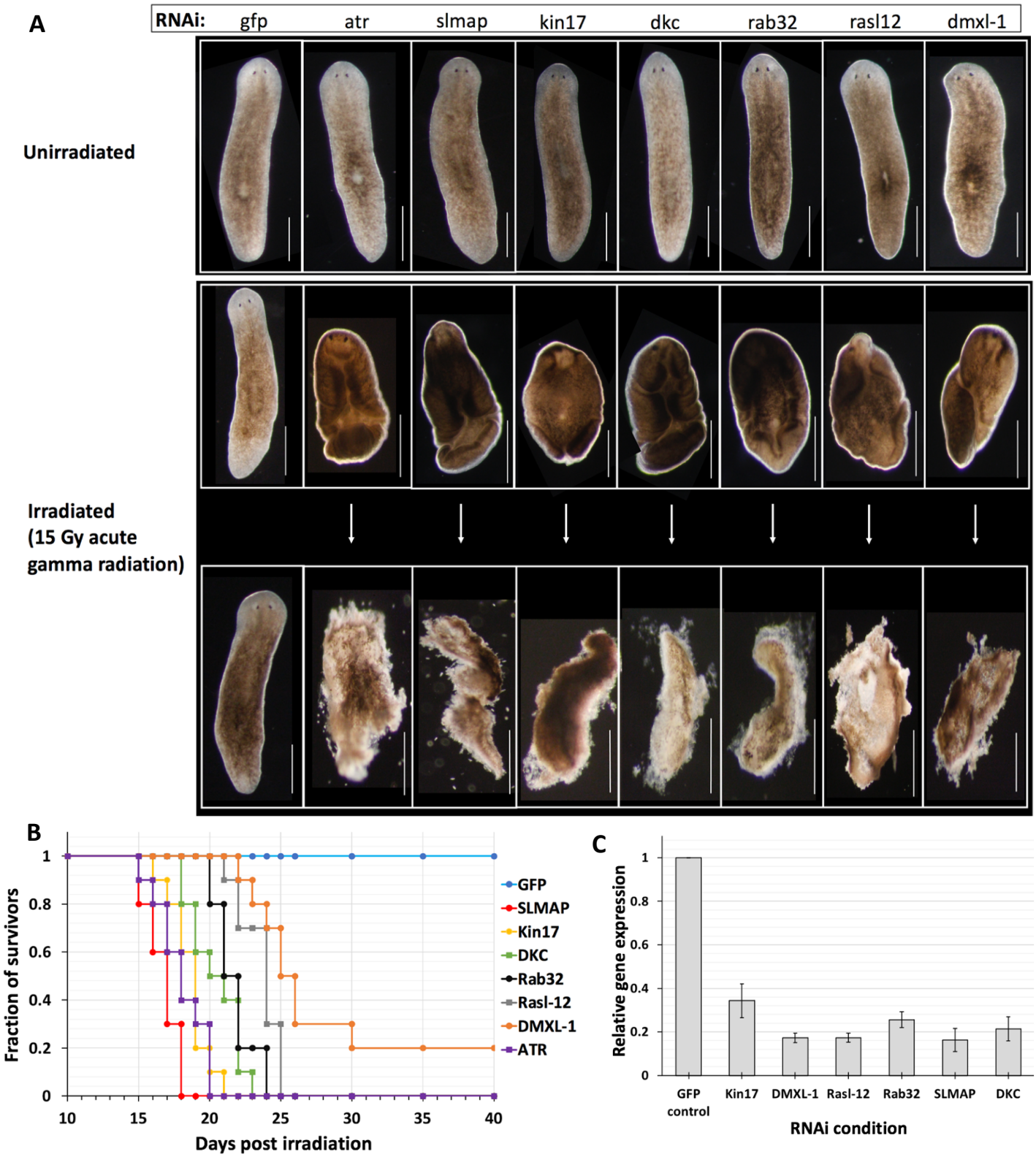

Figure 21. Combination of target gene RNAi and sub-lethal irradiation induces animal mortality.

(A) Morphology of animals subjected to RNAi with or without subsequent treatment with sub-lethal irradiation captured through brightfield microscopy. Scale bars represent 1 mm. Images of surviving animals were captured at the 50-day post-irradiation mark, while animals displaying morphological changes were documented at various timepoints in correlation with the survival curve outlined in (B). **(B)** Survival curves illustrating the outcomes for animals subjected to targeted gene RNAi and sub-lethal irradiation. n=20 for all conditions. **(C)** qPCR analysis investigating the efficacy of target gene knockdown. Gene expression levels were measured 24 hours post-irradiation in the RNAi-treated animals, using GAPDH as the reference gene.

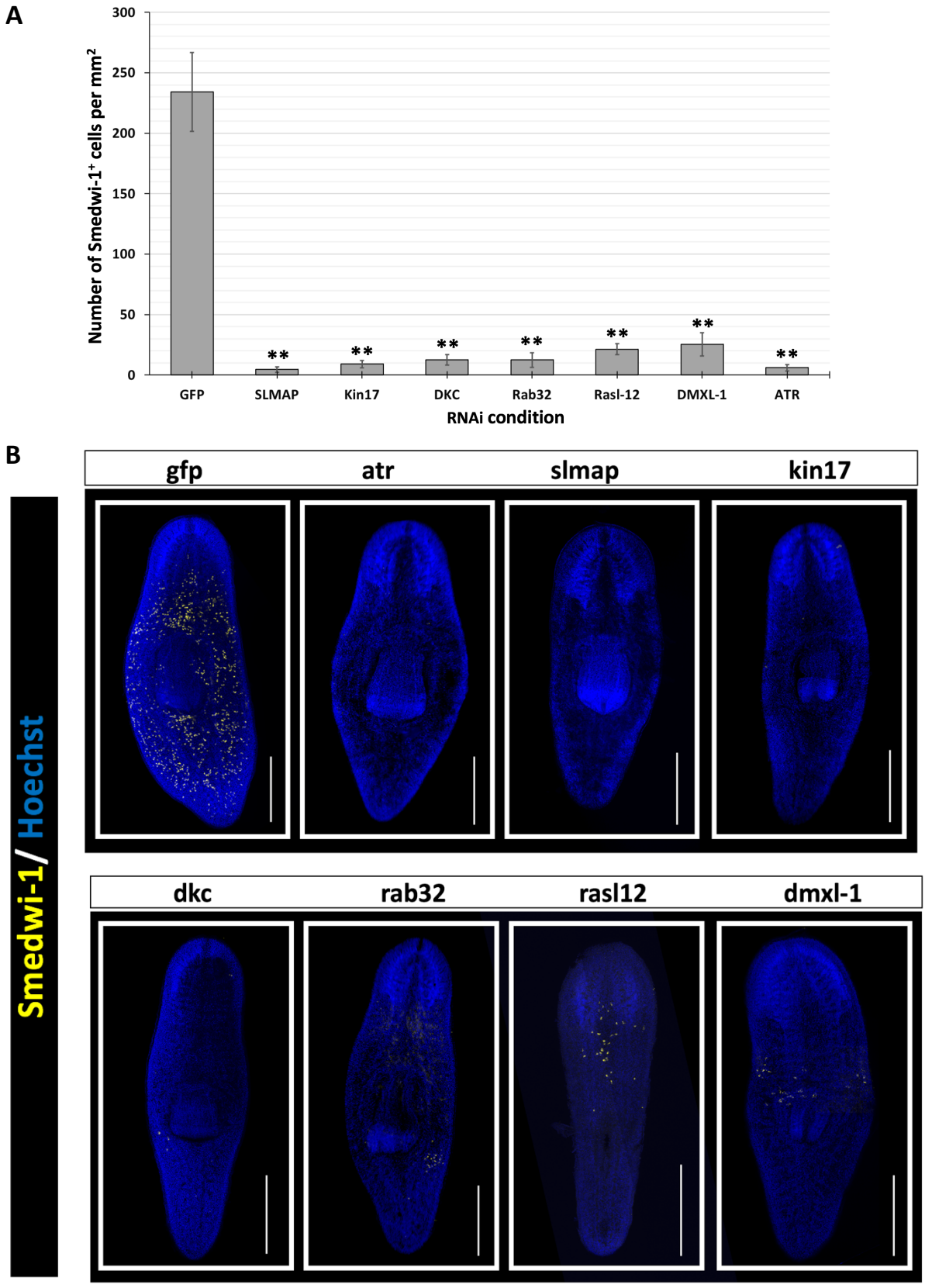

Figure 22. RNAi of Slmap, Kin-17, Dkc, Rab32, Rasl-12, and DMXL-1 impairs stem cell recovery following irradiation. (A) Quantification of stem cell numbers/mm^2 in the knockdown animals at 7 days post-exposure to 15 Gy acute gamma radiation. Results expressed as mean ± standard deviation. Double asterisks (**) indicate a statistically significant difference with an unpaired t-test p-value < 0.001 in relation to the GFP control. **(B)** Representative Smedwi-1 fluorescence in situ hybridization images of planarians subjected to targeted gene RNAi at 7 days post-irradiation. Scale bars represent 1 mm.

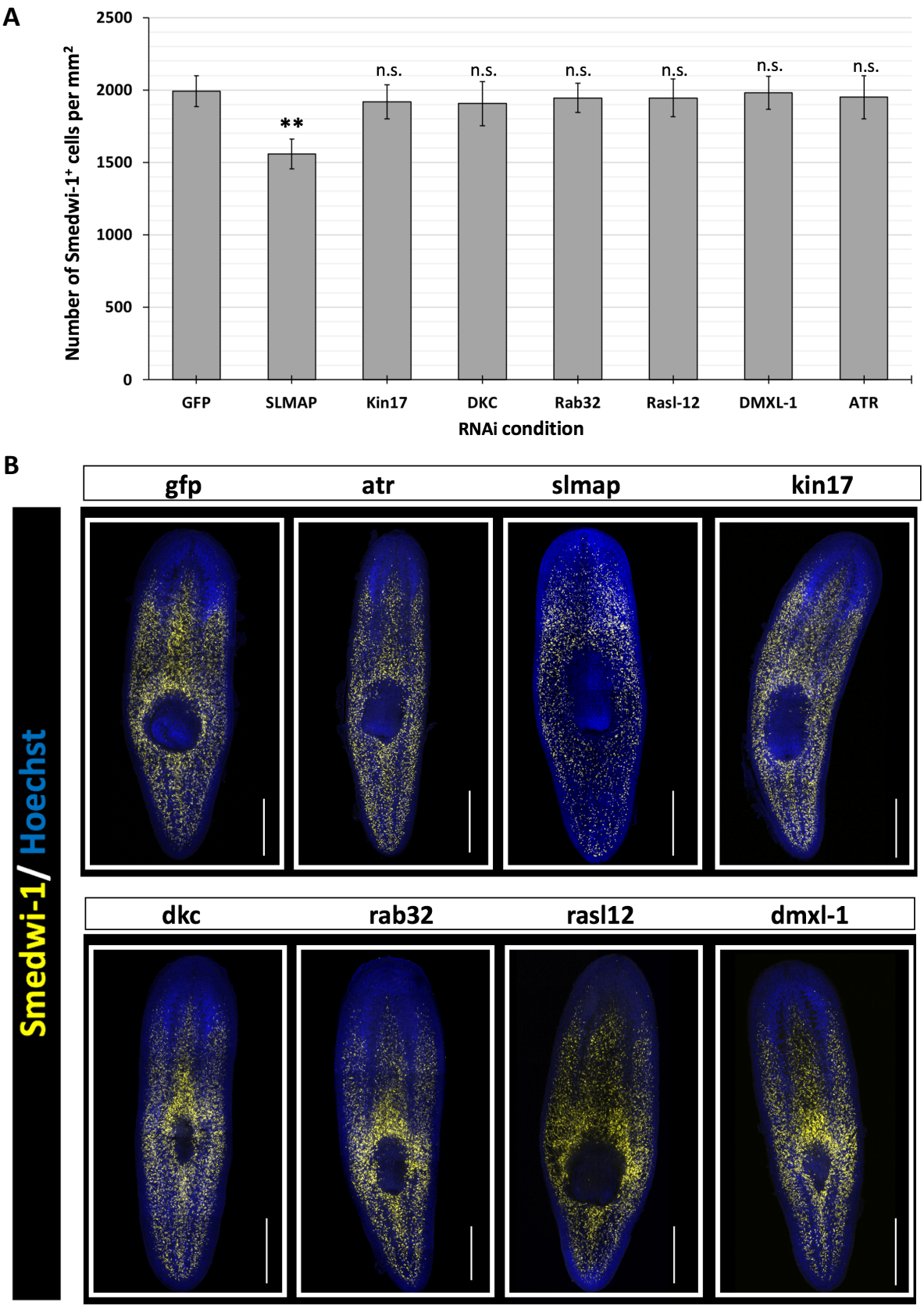

Figure 23. Slmap RNAi compromises stem cell maintenance under homeostatic conditions.

(A) Quantification of stem cell numbers/mm^2 in non-irradiated animals at the equivalent timepoint post RNAi as the irradiated subjects in Figure 22. Results expressed as mean ± standard deviation. Double asterisks (**) indicate a statistically significant difference with an unpaired t-test p-value <0.001 in relation to the GFP control. The abbreviation n.s. represents that the differences are not statistically significant in relation to the GFP control. **(B)** Representative Smedwi-1 fluorescence in situ hybridization images of non-irradiated animals subjected to targeted gene RNAi. Scale bars represent 1 mm.

Using in situ hybridization to target the stem cell marker, Smedwi-1, we uncovered evidence of impaired post-irradiation stem cell recovery in animals subjected to knockdown of these six genes. Specifically, at 7 days post sub-lethal irradiation, a timepoint where stem cells are expected to be in the phase of rapid repopulation, a markedly reduced number of stem cells were observed in the knockdown animals compared to the GFP control group (Figure 22).

Among the non-irradiated animals, RNAi knockdowns of Kin-17, Dkc, Rab32, Rasl-12, DMXL-1, and the positive control, ATR, did not cause significant reductions in stem cell numbers. However, a statistically significant 21.68% reduction in mean stem cell numbers was observed within planarians subjected to Slmap RNAi under homeostatic conditions (Figure 23). Despite this decrease, the knockdown of Slmap alone was insufficient to induce animal mortality without irradiation (Figure 21A). It is noteworthy that animals subjected to the combined treatment of Slmap RNAi and sub-lethal irradiation exhibited the shortest median lethal time amongst the various lethal combinations (Figure 21B). This finding might be linked to our observation of reduced stem cell numbers upon Slmap RNAi under non-irradiated conditions, as animals subjected to Slmap knockdown may harbour pre-existing stem cell defects even prior to irradiation treatment.

Taken together, these findings suggest that, apart from Slmap, the examined genes may not be essential for stem cell maintenance under homeostatic conditions. However, they appear to be vital for the stem cell recovery process following exposure to gamma radiation. To gain a more comprehensive understanding into the functions of these six genes, further investigations were conducted in Chapter 5. Our investigations encompassed phylogenetic analyses of the genes, reviewing their orthologues' reported functions where available, and a deeper exploration into their roles in radiation response and recovery in vivo using the planarian model system.

Targeted gene RNAi induces delayed stem cell recovery post gamma radiation exposure

As outlined in our experimental workflow (Figure 20), we conducted in situ hybridization targeting the stem cell marker, Smedwi-1, at 7 days post-irradiation. This was carried out to assess whether individual gene knockdowns incurred the phenotype of delay in stem cell recovery. For categorization, we applied a criterion that considered knockdowns with stem cell numbers falling below 50% of those observed in the GFP control at this timepoint as indicative of the delayed recovery phenotype. We identified 20 single-gene knockdowns that fell into this category (Figure 24). Despite inducing a delay in stem cell recovery, none of these 20 single-gene knockdowns resulted in the mortality of sub-lethally irradiated animals. Furthermore, these 20 genes do not appear to be essential for stem cell maintenance, as we did not observe any significant reduction in stem cell numbers in their respective knockdowns without irradiation (Appendix Table 10).

The observed delay in stem cell recovery post-irradiation without animal mortality suggests that the target genes contribute, but may not be ultimately necessary for planarian radiotolerance. Some of these observations might also reflect a pragmatic limitation of RNAi, namely the incompleteness of gene silencing, as discussed in RNAi experiments across various model systems (Reddien et al., 2005; Uprichard, 2005; Tomoyasu et al., 2008; Conte et al., 2015), and seen in our present study (Figure 21C). Although these knockdowns result in delayed stem cell recovery, residual activity of the target gene post RNAi-treatment may suffice to sustain animal survival post-irradiation. Redundancies with other proteins and pathways may also partially compensate for the loss of the target gene, averting fatal outcomes. We acknowledge the substantial error bars associated with our data, which may be attributed to the small sample sizes of n=5 for each condition. Stem cell number variability within the same RNAi condition might also reflect variability in the extent of target gene silencing, and hence knockdown potency, between different animal subjects. The six genes described in the previous section were excluded from this category since the combination of their targeted RNAi and sub-lethal irradiation led to animal mortality (Figure 21).

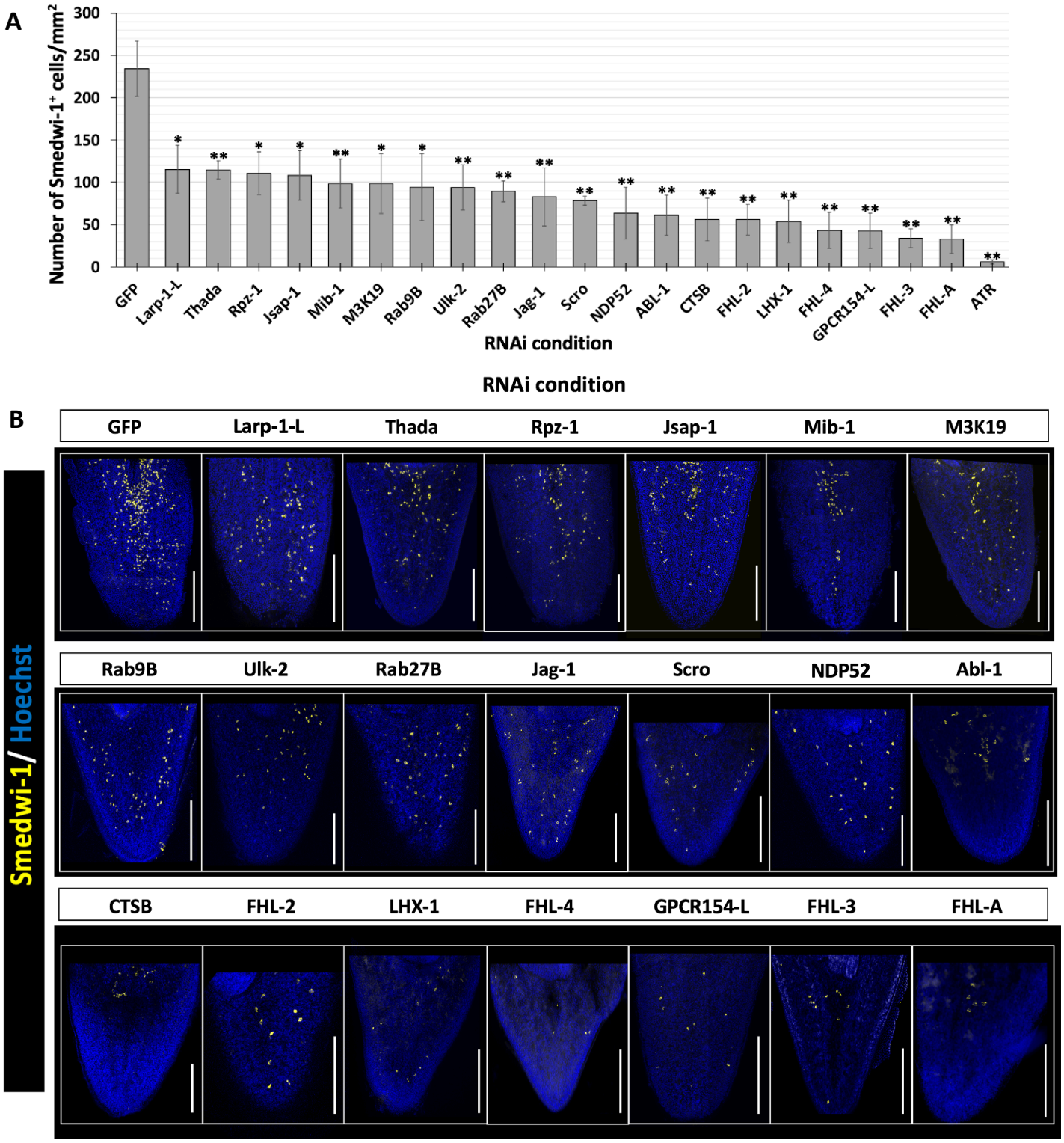

Figure 24. Targeted gene RNAi induces a delay in stem cell recovery following sublethal irradiation. **(A)** Quantification of stem cell numbers/mm^2 in the knockdown animals at 7 days post exposure to 15 Gy acute gamma radiation. Results expressed as mean ± standard deviation. Double asterisks (**) indicate a statistically significant difference with an unpaired t-test p-value <0.001 in relation to the GFP control. A single asterisk (*) denotes statistical significance with an unpaired t-test p-value of less than 0.005, but greater than 0.001. **(B)** Representative Smedwi-1 fluorescence in situ hybridization images of planarian tail regions derived from animals subjected to targeted gene RNAi at 7 days post irradiation. Scale bars represent 0.5 mm.

To gain insights into the roles of our target genes and how they might contribute to the post-irradiation stem cell recovery process, we explored the documented functions of their orthologues in other systems, where available. We first utilized the OrthoFinder (Emms and Kelly, 2019) and EggNOG 6.0 (Hernandez-Plaza et al., 2023) algorithms for orthologue identification. Orthology predictions made by these algorithms were consistent and were further validated using a reciprocal best-blast hit approach (Moreno-Hagelsieb and Latimer, 2008). Phylogenetic predictions indicate that our RNAi screen unveiled two platyhelminth-specific genes, which we have designated as La-Related Protein 1-like (Larp-1-like) and G-Protein Coupled Receptor 154-like (GPCR154-like), whose knockdowns delayed stem cell recovery following irradiation. These two platyhelminth-specific genes are inferred to originate from duplication events of the ancestral genes – Larp-1, and GPCR154, respectively (Figure 25). This inference is supported by the consistent return of Larp-1 and GPCR154 as the top blast hits for Larp-1-like and GPCR154-like, respectively, across diverse metazoans, including relatively closely related lineages such as molluscs and annelids within the same lophotrochozoan clade. Additionally, while orthologues of Larp-1 could be identified in fungi and plants, consistent with previous findings (Deragon and Bousquet-Antonelli, 2015), orthologues of GPCR154 were exclusive to the metazoan lineage. Nonetheless, although orthologues of the ancestral genes have been characterized in other model systems, neither the ancestral copies nor the platyhelminth-specific paralogues of these genes have been subjected to prior investigation in planarians.

Structural analyses reveal that both Larp-1-like and GPCR154-like possess the characteristic domains definitive of their respective protein groups (Figure 25B, 25D). Specifically, Larp-1-like features an La motif, an RNA-binding motif with a winged-helix-turn-helix architecture (Dong et al., 2004); while GPCR154-like possesses the hallmark seven transmembrane alpha-helices, a signature architecture of proteins within the GPCR superfamily (Filipek et al., 2003). However, notable differences between platyhelminth Larp-1-like and metazoan Larp-1 include the former being substantially shorter in length and lacking DM15 repeats at the protein's C-terminal region (Figure 25B). DM15 repeats aid in mRNA cap binding (Lahr et al., 2015), and are a highly conserved feature across metazoan Larp-1 copies, although it is absent from the fungal orthologue, consistent with recent analysis by Mansouri-Noori and colleagues (Mansouri-Noori et al., 2023).

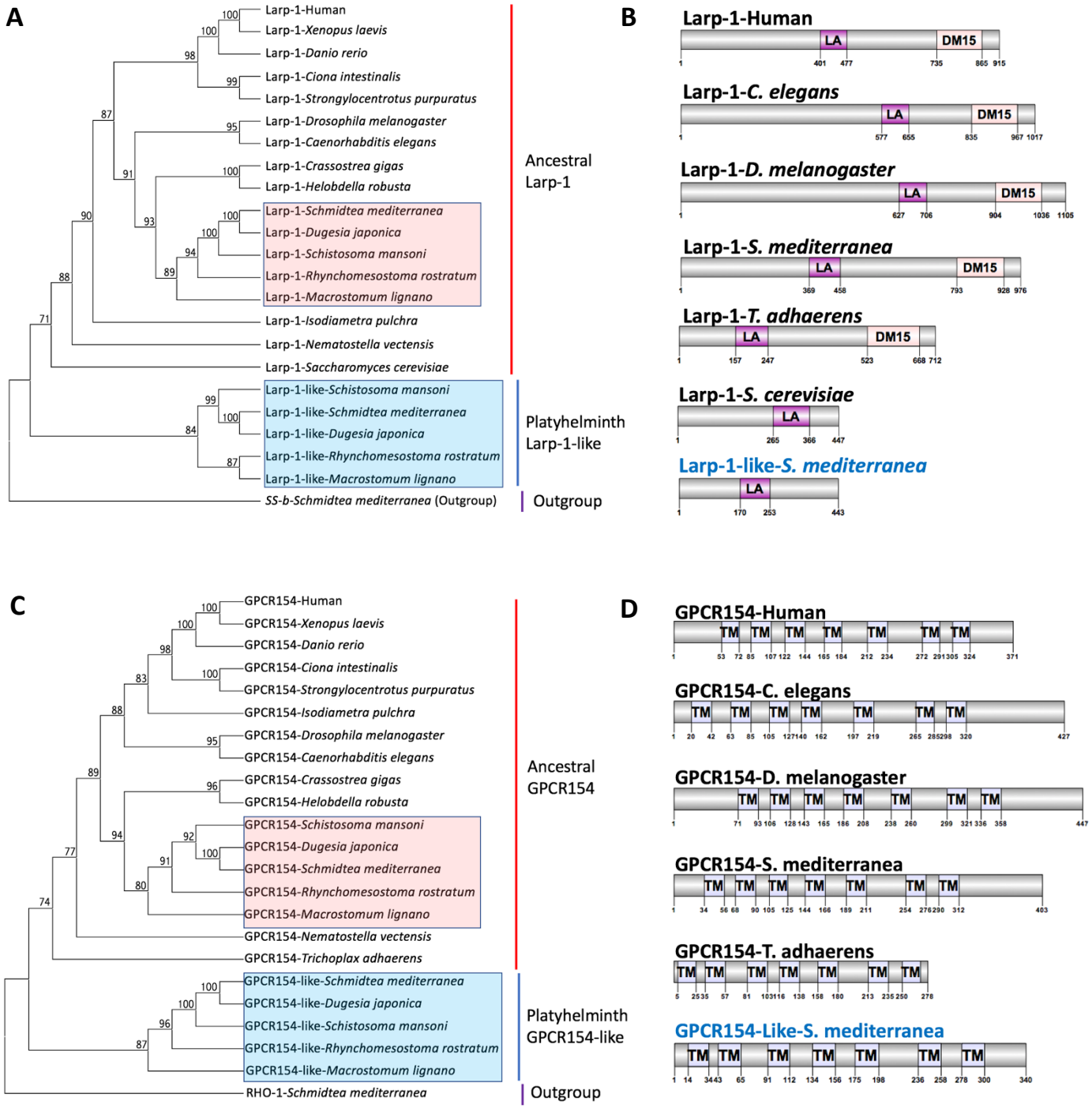

Figure 25. Phylogenetic and domain architecture analysis of Larp-1-like and GPCR154-like. **(A)** Maximum likelihood phylogenetic tree depicting the relationship between platyhelminth Larp-1-like and the ancestral Larp-1 copies, with SS-b, another conserved LA-domain-containing gene, as an outgroup. **(B)** Domain architecture analysis of Larp-1 and Larp-1-like, featuring selected species representatives. **(C)** Maximum likelihood phylogenetic tree depicting the relationship between platyhelminth GPCR154-like and ancestral GPCR154 copies, with RHO-1, another conserved rhodopsin-like GPCR family gene, as an outgroup. **(D)** Domain architecture analysis of GPCR154 and GPCR154-like, featuring selected species representatives.

Functionally, the mammalian orthologue of Larp-1 is implicated in tumorigenesis, cancer cell migration, and metastasis, primarily through the direct post-transcriptional regulation of mTOR (Hong et al., 2017; Mura et al., 2015; Hopkins et al., 2016). Similarly, through the post-transcriptional regulation of target genes, mammalian Larp-1 has been found to be crucial for regulated cell divisions and cell survival under non-cancerous contexts (Burrows et al., 2010). Furthermore, Larp-1 is reported to facilitate gametogenesis in both *Drosophila* and *C. elegans* by post-transcriptionally regulating the expression of key genes involved in meiosis (Nykamp et al., 2008; Ichihara et al., 2007; Blagden et al., 2009). The orthologue of Larp-1 has also been studied in yeasts, with a documented role in promoting oxidative stress resistance in *Saccharomyces cerevisiae* (Kershaw et al., 2015). Given that both Larp-1 and Larp-1-like in planarians retain the La RNA binding domain (Figure 25B), they may also be involved in the post-transcriptional regulation of target genes in planarians. Considering its knockdown phenotype (Figure 24), Larp-1-like may have a post-transcriptional regulatory role that contributes to the stem cell recovery process following irradiation, although the impact of DM15 repeat-loss on their ability to bind mRNA remains to be investigated.

Another platyhelminth-specific gene whose knockdown induced a strong delay in stem cell recovery after irradiation is GPCR154-like, which encodes a rhodopsin-like G-protein coupled receptor. GPCRs comprise a gene family recognized for their ability to transduce signals from extracellular ligands and activating intracellular G proteins as secondary messengers to modulate a wide array of biological functions (Rosenbaum et al., 2009). Despite limited mechanistic understanding of the gene, mutations in mammalian GPCR154 have been linked with an increased susceptibility to asthma (Pietras et al., 2011), sleep disorders (Xing et al., 2019), and inflammatory bowel diseases (D'amato et al., 2007). Expanding beyond GPCR154, although a direct role of the broader GPCR family genes in radiation resistance remains unexplored, GPCR involvement in proliferative signalling under both normal (New and Wong, 2007) and cancerous conditions (Chaudhary and Kim, 2021; O'Hayre et al., 2014) may potentially hold relevance for planarians. Whether their functions in proliferative signalling is extended to planarians and their precise contributions to the planarian stem cell recovery process after irradiation requires future investigation.

In addition to uncovering novel genes, our RNAi screen has unveiled key players of evolutionarily conserved signalling pathways whose knockdowns incurred the phenotype of delayed stem cell recovery following irradiation (Figure 24). Among these genes are the planarian orthologues of Jagged-1 (Jag-1) and Mindbomb-1 (Mib-1), both of which hold essential roles in Notch signalling across both vertebrates and invertebrates. Jagged-1 is classified as a canonical ligand for Notch signalling (D'Souza et al., 2010), while Mib-1 encodes an E3 ubiquitin ligase that drives the endocytosis of Notch ligands and receptors (Le Borgne et al., 2005; Lai et al., 2005). Both Jag-1 and Mib-1 were observed to be indispensable for Notch signalling activation (Grochowski et al., 2016; Lindsell et al., 1995; Koo et al., 2005; Itoh et al., 2003), with dysregulation of these genes resulting in either embryonic lethality or severe developmental defects in diverse model organisms (Xue et al., 1999; Koo et al., 2007; Itoh et al., 2003; Kiernan et al., 2006; Yang and Deng, 2018; High et al., 2008). In planarians, Notch signalling has been implicated in fine-tuning the balance between stem cell proliferation and apoptosis (Dong et al., 2021), as well as oogenesis in sexual strains (Khan and Newmark, 2022). The observed effects of Jag-1 and Mib-1 RNAi (Figure 24), coupled with the radio-sensitizing effect of DMXL-1 RNAi (Figure 21), a gene deemed indispensable for Notch signalling in *Drosophila* (Yan et al., 2009), collectively point to the potential importance of Notch signalling in the planarian stem cell recovery process after irradiation. These observations may in turn position planarians as an attractive in vivo model system to expand our understanding of Notch signalling function within the context of stem cell radiation response. Such understanding would be of biomedical significance, especially in light of reports regarding Notch-mediated cancer stem cell radiotolerance in glioma (Wang et al., 2010; Shen et al., 2015) and lung cancer (Theys et al., 2013; Hassan et al., 2013). Specifically, elevated levels of Notch signalling in both these cancer types have been observed to promote cancer stem cell survival and their subsequent proliferation after ionizing radiation exposure in vitro (Yahyanejad et al., 2016, Hassan et al., 2013, Wang et al., 2010), potentially implicating Notch signalling in driving radiotherapy resistance and disease recurrence in vivo.

Moreover, delay in stem cell recovery upon RNAi of Jnk/Sapk Associated Protein 1 (Jsap-1) and MAP Kinase Kinase Kinase 19 (M3K19) [Figure 24] implicates the JNK cascade as a potential contributor to the planarian post-irradiation recovery process, given their

established roles as regulators of JNK signalling in mammals (Engstrom et al., 2010, Hoang et al., 2020). The JNK cascade has been demonstrated in mammals and *Drosophila* to modulate both cellular apoptosis and proliferation in highly context-dependent manners (Behrens et al., 1999; Lin and Dibling, 2002; Dhanasekaran and Reddy, 2012; La Marca and Richardson, 2020). This property extends to planarians, as it has been shown that JNK signalling governs the regulated cell deaths and cell divisions during tissue regeneration and remodelling in *S. mediterranea* (Almuedo-Castillo et al., 2014). Moreover, the significance of JNK signalling in orchestrating precise tissue regeneration is reported not only in planarians (Tasaki et al., 2011; Tejada-Romero et al., 2015), but also in other model organisms such as *Drosophila* (Bergantinos et al., 2010) and Zebrafish (Ishida et al., 2010; Kawakami, 2010). In the context of radiation resistance, JNK generally promotes apoptosis in irradiated cancer cells (Chen et al., 1996; reviewed in Munshi and Ramesh, 2013), although instances of JNK-mediated radiation resistance have been reported as well (Wu et al., 2019, Eke et al., 2012; Li et al., 2016). Additionally, JNK signalling has been shown to confer protection against reactive oxygen species in *Drosophila* (Wang et al., 2003).

In future efforts, targeting other components of the Notch and JNK signalling pathways, even those that are not implicated by transcriptomics, would expand our understanding of these pathways in the regulation of planarian radiotolerance. In addition, exploring potential crosstalk between JNK and ERK signalling in this context would also be valuable. Both JNK and ERK pathways involve MAP kinase signalling cascades as the primary mode of signal transduction (Johnson and Lapadat, 2002), and evidence of their interplay has been documented in mammals, *Drosophila*, and *C. elegans*. In mammals, JNK and ERK pathways can simultaneously respond to the same stimulus, modulating a complex and graded cellular response (Zhang and Liu, 2002; Shen et al., 2003), while these two pathways in *Drosophila* (Ciapponi et al., 2001) and *C. elegans* (Okuyama et al., 2010; Oh et al., 2005) have been found to activate common downstream effectors. Such crosstalk between JNK and ERK might extend to planarians, and may be crucial for planarian radiotolerance, as JNK is implicated in stem cell recovery in this study (Figure 24), while ERK has been found to participate in a wound-response that promotes stem cell survival in irradiated planarians (Shiroor et al., 2020).

Furthermore, we observed that RNAi targeting the planarian orthologues of Rab9B and Rab27B, both belonging to the small GTPase class of signal transducers, caused a delay in stem cell recovery post-irradiation (Figure 24). These observations, coupled with our finding of radio-sensitization achieved through RNAi of other small GTPases – Rab32 and Rasl-12 (Figure 21), underscore the potential significance of this protein class in the planarian response and recovery process post-irradiation. The Rab family of small GTPases, renowned orchestrators of intracellular membrane and vesicular transport (Stenmark, 2009), plays fundamental roles in a myriad of developmental and homeostatic processes (reviewed in Homma et al., 2021). Although Rab9B remains functionally enigmatic, Rab27B was found to be upregulated in response to X-ray irradiation in glioblastoma cells, contributing to their radiotolerance both in vitro and in vivo by promoting the secretion of the epidermal growth factor, Epiregulin (Nishioka et al., 2020). Rab27B was also reported to promote the proliferation and metastasis of breast cancer cells (Hendrix et al., 2010). Conversely, the antagonization of Rab27B-signalling was found to be sufficient in quenching the invasiveness of the same breast cancer cell line in vitro (Wu et al., 2019).

The planarian orthologue of ABL-1 represents another signalling transducer in this phenotypic category (Figure 24). ABL-1 encodes a tyrosine kinase that is activated upon DNA damage (Shaul and Yehoyada, 2005) and oxidative stress (Li, 2005) to promote DNA repair in mammals. Mammalian ABL-1 has been reported to act immediately upstream of key DNA repair genes such as ATM and ATR (Wang et al., 2011), Rad51 (Yuan et al., 1998; Chen et al., 1999; Yuan et al., 2003), Rad52 (Kitao and Yuan, 2002), Parp1 (Bohio et al., 2019; Golovine et al., 2023), as well as DNA-PK (Kharbanda et al., 1997; Shangary et al., 2000), phosphorylating and modulating them in response to various sources of DNA damage. A potential similarity between ABL-1 in mammals and planarians could be its responsiveness to gamma radiation, as protein assays reveal the activation of ABL-1 upon gamma radiation exposure in human HEK293 cells (Tang et al., 2012), while we observed transcriptional upregulation of the gene in our planarian X1 post-irradiation dataset (Log_2 fold change +3.10, Appendix Table 8).

Taken together, our assay uncovered conserved signalling regulators whose knockdowns delayed the stem cell recovery process post-exposure to sub-lethal irradiation.

The documented roles of these genes, including Rab27B's contribution to radio-resistance and ABL-1's pro-DNA-repair functions, may potentially be extended to planarians, possibly serving as the underlying basis for the observed delay. Whether the planarian orthologues of these genes operate similarly to their mammalian counterparts, or have potentially evolved novel functions specific to planarians, requires further investigation.

Furthermore, our screen identified three autophagy-related genes, Unc-51-like kinase 2 [Ulk-2] (Lee and Tournier, 2011), Cathepsin-B [CTSB] (Man and Kanneganti, 2016), and Nuclear Domain 10 Protein 52 [NDP52] (Viret et al., 2018) that contribute to the stem cell recovery process following irradiation (Figure 24). While autophagy conventionally supports cell survival by eliminating stress-induced damaged biomolecules (Lum et al., 2005; Mizushima and Komatsu, 2011), autophagic pathways also participate in orchestrating the regulated apoptotic events during the development of many organisms (Das et al., 2012; Kang et al., 2007; Ryoo and Baehrecke, 2010). In cancer, autophagy can exhibit either tumour suppressive or oncogenic roles dependent on the context (Mathew et al., 2007; White, 2015; Yang et al., 2011; Levy et al., 2017). Autophagy appears to display dual functionality in planarians as well, contributing to both cell survival and apoptosis during tissue remodelling (Jin et al., 2022; Gonzalez-Estevez et al., 2007). In the context of radiation response, autophagy can uphold both pro-survival and pro-apoptotic roles, dependent on the crosstalk with other active pathways (Tam et al., 2017; Li et al., 2020). While the roles of Ulk-2 and NDP52 in irradiated cells remain unexplored, CTSB has been reported in *C. elegans* to aggravate the pathology of radiation-induced bystander effects in vivo (Peng et al., 2017). Conversely, inhibiting CTSB was found to confer radioprotection to *C. elegans* by dampening the severity of these bystander effects (Zheng et al., 2019). Further investigation into these three genes may provide valuable insights into the role of autophagy in the planarian radiation response.

In our study, we also identified genes linked to animal development that display novel functions in the context of radiation response, as their knockdowns led to delayed stem cell recovery post-irradiation (Figure 24). Among these genes is the planarian orthologue of Thyroid Transcription Factor-1 (TTF-1), which contains a homeobox DNA-binding domain and is recognized to be important for thyroid, lung, and brain

morphogenesis during mammalian development (Lazzaro et al., 1991; Trueba et al., 2005). Additionally, the *Drosophila* TTF-1 orthologue, Scarecrow (Scro), has been found to play crucial roles in brain development, with mutations in the gene causing severely malformed optic lobes (Yoo et al., 2020).

Another gene falling into this subcategory is the planarian orthologue of Rapunzel-1 (Rpz1). Its orthologue in zebrafish is reported to be vital for skeletal development, as homozygous gene mutants were embryonic lethal due to malformations in global bone structures (Goldsmith et al., 2003). Conversely, gain-of-function mutations involving the gene causes skeletal overgrowth in zebrafish (Green et al., 2009). Despite these observations, orthologues of Rpz1 remain functionally uncharacterized outside of the zebrafish model system. A third gene within this subcategory is the planarian orthologue of Thyroid Adenoma-Associated (THADA). THADA expression is enriched in the mammalian thyroid, with current understanding indicating that THADA contributes to thyroid cell differentiation, and the maintenance of thyroid cells in a differentiated state under homeostatic conditions (Kloth et al., 2011). THADA mutations have been implicated in triggering abnormal dedifferentiation events in the thyroid, predisposing individuals to thyroid cancer (Rippe et al., 2003; Tali et al., 2023; Kloth et al., 2011). The precise role of these genes in planarian development and homeostasis, as well as their links to the planarian radiation response and recovery process, remains to be uncovered.

Investigating the role of FHL family genes in planarian radiotolerance

In our RNAi screen, we discovered that the individual silencing of FHL-A, FHL-2, FHL-3, and FHL-4, members of the FHL (Four and a Half LIM domain) gene family, resulted in a significant delay in the recovery of stem cells following irradiation. Notably, the knockdowns involving FHL genes exerted the most profound effect among the 20 genes within this category, exhibiting some of the lowest average stem cell counts in relation to the GFP control at the 7-day post-irradiation mark (Figure 24A). Despite the substantial delay in stem cell recovery, knockdowns of these FHL genes individually did not reach the threshold required to trigger mortality in sub-lethally irradiated animals.

These four FHL genes were found to be upregulated en-masse at 24 hours post-irradiation in our X1 bulk dataset (Appendix Table 8). Furthermore, direct links between aberrant expression of FHL family members with various human cancers have been established (Wei and Zhang, 2020; Ding et al 2009; Hua et al., 2016; Wang et al., 2020; Huang et al, 2022; Jin et al 2018; Fu et al., 2020). Collectively, these factors position the FHL family genes as interesting candidates and hence their incorporation into our primary RNAi screen.

Phylogenetic predictions suggest that among the platyhelminth FHL genes, only FHL-A contains identifiable orthologues in other animals. Given our observations, we infer that FHL-A may represent the ancestral FHL gene that is conserved across metazoans. Paralogous genes – FHL-2, FHL-3, and FHL-4, identified in this study, alongside the previously unveiled FHL-1 gene by Wagner and colleagues (Wagner et al., 2012), are inferred to be exclusive to the platyhelminth lineage (Figure 26A). Supporting the emergence of these genes via duplication from the ancestral FHL-A, orthologues of FHL-A are consistently returned as the top blast hit when querying platyhelminth FHLs against the proteomes of diverse model systems. In our analysis, we also observed that vertebrate model systems encode an array of vertebrate-specific FHL gene paralogues, likely arising from whole-genome duplication events during the course of vertebrate evolution (Ohno, 1970; Garcia-Fernandez and Holland, 1994; Abi-Rached et al., 2002; Dehal and Boore, 2005; Putnam et al., 2008; Simakov et al., 2020). In contrast, only a solitary copy of the ancestral FHL gene could be identified within invertebrate model organisms. Phylogenetic tree analysis reveals clustering of Platyhelminth FHL-A with other invertebrate FHL-A copies (Figure 26A), supporting an orthologous relationship and its inferred ancestral status. Furthermore, FHL family members could not be identified in the genomes of fungi and plants, aligning with a previous finding suggesting that the FHL gene family is a metazoan-specific innovation (Koch et al., 2012).

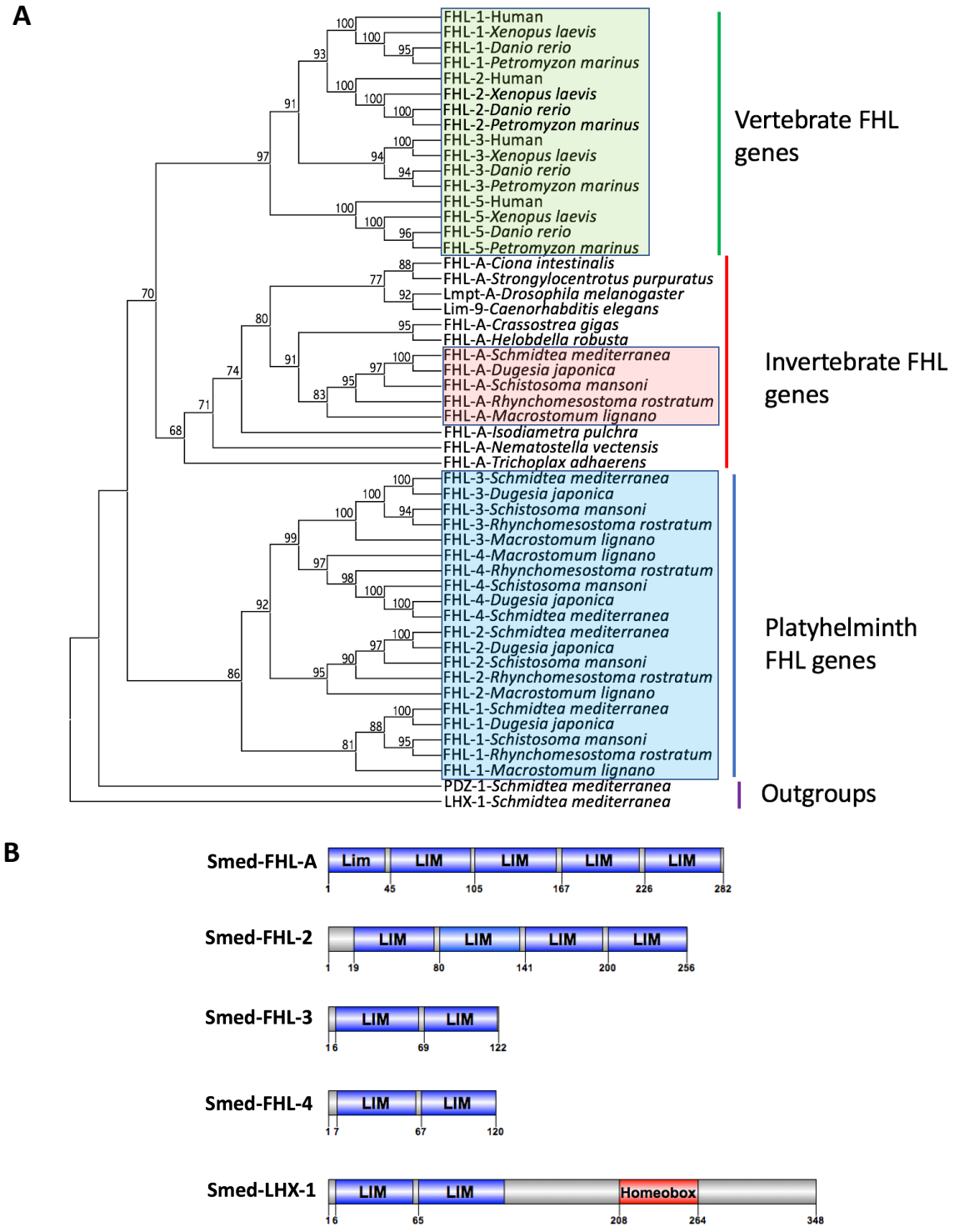

Figure 26. FHL-A is evolutionarily conserved, but the planarian paralogues of FHL-1, FHL-2, FHL-3, and FHL-4 are unique to platyhelminths. (A) Maximum likelihood phylogenetic tree depicting the phylogenetic relationships between FHL genes. Ancestral FHL-A copies within the platyhelminth group (red box), platyhelminth-specific FHL genes (blue box), and vertebrate FHL genes (green box) are highlighted. Outgroups are representatives from other conserved LIM-domain-containing gene families. **(B)** Illustration of domain architectures featured in planarian FHL genes and LHX-1, identified in this study. The use of uppercase letters (LIM) signifies complete LIM domains, while the use of lowercase (Lim) represents partial or half LIM domains.

Genes belonging to the FHL family are characterized by their possession of multiple LIM domains, without the presence of any other functional domain (Zheng and Zhao, 2007). The LIM domains themselves are characterized by a tandem zinc finger arrangement. These LIM-domain zinc fingers serve as binding sites for proteins (Dawid et al., 1995; Kuroda et al., 1996; Dawid et al., 1998), with no current evidence supporting their direct involvement in DNA binding. It is important to acknowledge that the visual representation of domain architecture in Figure 26B may inadvertently underrepresent the extent of variation between the platyhelminth FHL gene paralogues. This is because each LIM domain comprises a blend of conserved and highly variable sites. The conserved amino acids, positioned at regular intervals, play important structural roles in constructing the tandem zinc-finger arrangement and upholding domain stability (Kadrmas and Beckerle, 2004; Zheng and Zhao, 2007). Concurrently, LIM domains are also lined with regions of variable amino acids that impart target binding specificity (Kadrmas and Beckerle, 2004).

In mammals, FHL genes serve as pivotal adaptor proteins, and are known to orchestrate a wide variety of functions (Bach, 2000; Kadrmas and Beckerle; 2004; Shathasivam et al., 2010). These genes partake in an extensive network of interactions (reviewed in Shathasivam et al., 2010), directly engaging with various partners and influencing the expression of target genes such as p21 (Ding et al., 2009; Niu et al., 2011), c-myc (Ding et al., 2009), BRCA-1 (Yan et al., 2003), AKT-1 (Hua et al., 2016), HIF-1 (Hubbi et al., 2012) and VEGF (Lin et al., 2012). In planarians, the binding partners of the FHL gene paralogues and their associated target genes remain unexplored. Nevertheless, the similarities observed in this study regarding their effects upon single knockdown and sublethal irradiation, alongside the close phylogenetic relationships between the FHL gene paralogues, suggest the plausible existence of functional redundancies. Such redundancies amongst FHL gene paralogues would not be a novel phenomenon. Instances of redundancy between mammalian FHL paralogues are implied given that distinct mammalian FHL genes have been found to interact with the same proteins to regulate the same target genes. Noteworthy examples include the binding of human FHL-1, FHL-2, and FHL-3 to SMAD proteins in the regulation of both TGFß-responsive and TGFß-independent genes (Ding et al., 2009), as well as the binding of both FHL-2 and FHL-3 to CREB-1 for MyoD activation during muscle differentiation (Fimia et al., 2000; Kong et al., 1997).

In invertebrate model systems, orthologues of FHL-A have been characterized in *Drosophila* and *C. elegans*. The *Drosophila* FHL orthologue, Lmpt, was observed to exhibit enriched expression in heart and muscle tissue. Lmpt was determined to be an important regulator of embryonic heart development in *Drosophila*, evidenced by severe myocardial tissue deficiency in homozygous mutants (She et al., 2022). Similarly, the *C. elegans* FHL orthologue, Lim-9, exhibits enriched expression in muscle tissue, although its precise functions in nematode development and homeostasis remain enigmatic (Xiong et al, 2009). Nevertheless, the role of FHL genes in the context of radiation response and recovery has not been characterized prior to this study.

In addition, our primary screen unveiled another LIM-domain-containing protein, the planarian orthologue of Lim Homeobox-1 (LHX-1), whose knockdown similarly introduced a strong delay in post-irradiation stem cell recovery (Figure 24). The planarian orthologue of LHX-1 features two N-terminal LIM domains alongside a homeobox DNA-binding domain situated at the C-terminal region (Figure 26B), a structurally conserved arrangement that is shared by LHX-1 orthologues across metazoans (Hobert and Westphal, 2000). Distinguishing LHX genes from their counterparts in the FHL group is their capacity to bind DNA, enabling direct regulation of target gene expression through their homeobox domains. Orthologues of LHX-1 have emerged as indispensable elements in the embryonic development of the nervous and endocrine systems across diverse model organisms (Sibbritt et al., 2018; Zhao et al., 2007; DeLay et al., 2018; Espiritu et al., 2018; Winchell and Jacobs, 2013; Srivastava et al., 2010). Within planarians, LHX group genes – Islet-1 (Hayashi et al., 2011; Marz et al., 2013), Arrowhead (Roberts-Galbraith et al., 2016), and LHX1-5.1 (Currie and Pearson, 2013) have been found to contribute to brain regeneration, suggesting that the role of LHX genes in nervous system development extends to planarians. Besides malformed brains, RNAi of Islet-1 impaired the regeneration of dopaminergic and serotonergic neurons (Marz et al., 2013), while RNAi of LHX1-5.1 compromised regeneration of serotonergic and GABAnergic neurons (Currie and Pearson, 2013). Additionally, Islet-1 is implicated in anterior-posterior patterning as well as midline patterning (Hayashi et al., 2011). Despite available information regarding other members of the LHX group, the precise role of planarian LHX-1, identified to contribute to post-irradiation stem cell recovery in this study, remains to be fully uncovered.

To explore potential redundancies or compensatory mechanisms among the LIM-domain-containing genes identified in our primary screen, we incorporated the four FHL genes in conjunction with LHX-1 in a secondary screen involving paired gene knockdowns. As the effects of single-gene RNAi may have been dampened by the compensatory actions of functionally redundant genes, knocking down genes in pairs may unveil additional regulators and their interactions that confer radiotolerance to planarians in vivo.

In our secondary screen, we silenced the expression of FHL-A, FHL-2, FHL-3, FHL-4, and LHX-1 in all possible combinatorial pairings of two. This yielded 10 distinctive combinations of gene pairs, to which we identified four specific gene pairings that led to 100% planarian mortality (10 out of 10 animals) following double RNAi and sub-lethal irradiation. Namely, paired RNAi of FHL-A and FHL-3, FHL-2 and FHL-4, FHL-A and LHX-1, as well as FHL-4 and LHX-1, were found to render planarians sensitive to sub-lethal irradiation (Figure 27). We also found that paired RNAi of FHL-3 and LHX-1 resulted in 20% mortality (2 out of 10 animals) among sub-lethally irradiated animals (Figure 27B). This potentially indicates that the concurrent silencing of FHL-3 and LHX-1 brings the animals near the lethality threshold. All animals that died in the assay displayed anterior regression, ventral curling, and eventual tissue lysis (Figure 27A), a series of events reminiscent of the stereotypical loss-in-stem-cell-function phenotype within planarians.

In contrast, the remaining five RNAi pairs exhibited neither mortality nor morphological changes among sub-lethally irradiated animals. Moreover, paired RNAi targeting all ten gene combinations yielded no discernible effect on unirradiated animals. Taken together, our observations suggest that these LIM-domain-containing genes play important roles in the planarian radiation response and recovery process, but they may be dispensable for the maintenance of animal homeostasis.

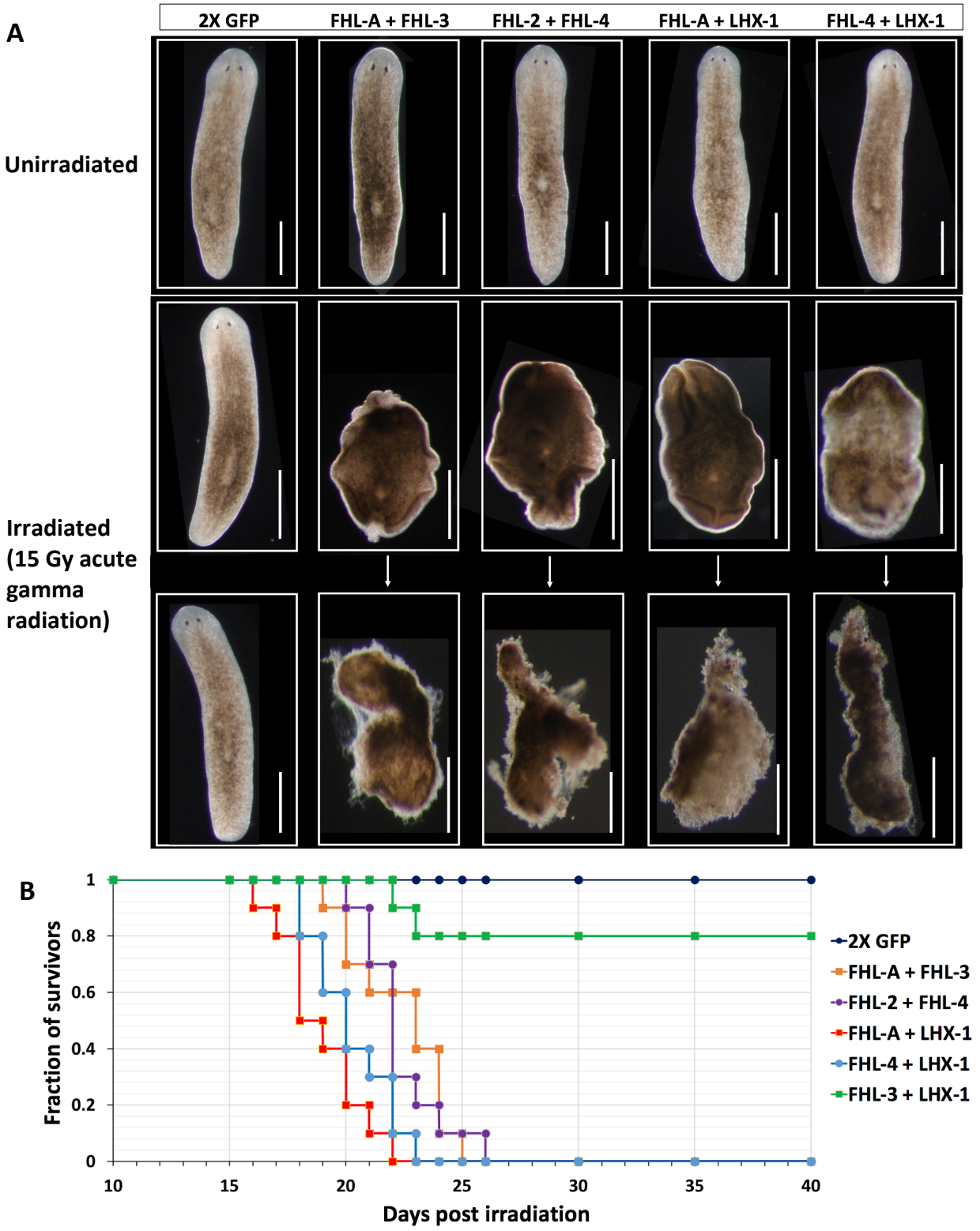

Figure 27. Paired gene knockdowns reveal novel FHL gene combinations that sensitize planarians to gamma radiation. (A) Morphology of animals subjected to double RNAi with or without treatment with sub-lethal irradiation, captured through brightfield microscopy. Scale bars represent 1 mm. Images of surviving animals were captured at the 50-day post-irradiation mark, while animals displaying morphological alterations were documented at various timepoints in correlation with the survival curves outlined in (B). **(B)** Survival curves illustrating the outcomes for animals subjected to selected RNAi pairs and sub-lethal irradiation. Only the RNAi pairs with incidences of mortality were shown. n=10 for all conditions.

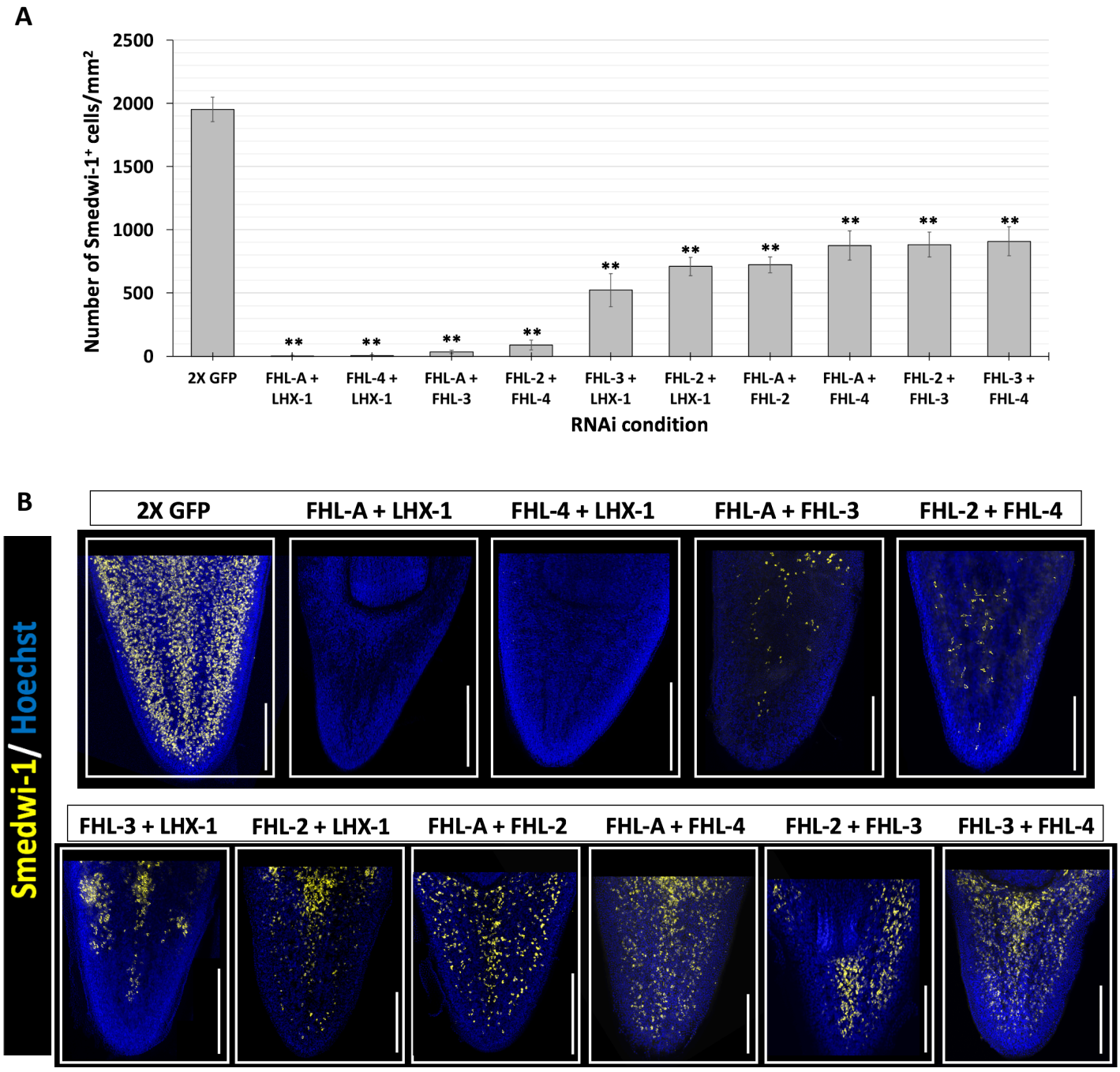

Figure 28. Impact of paired gene RNAi on the recovery of stem cells following irradiation.

(A) Quantification of stem cell numbers/mm^2 in the double-knockdown animals at 21 days post exposure to 15 Gy acute whole-body gamma radiation. Results expressed as mean ± standard deviation. Double asterisks (**) indicate a statistically significant difference with an unpaired t-test p-value <0.001 in relation to the GFP control. **(B)** Representative Smedwi-1 fluorescence in situ hybridization images of planarian tail regions derived from animals subjected to paired gene RNAi at 21 days post-irradiation. Scale bars represent 0.5 mm.

We performed in situ hybridization at 21 days post-irradiation targeting the stem cell marker, Smedwi-1. This investigation aimed to establish a correlation between our bright-field observations and the underlying stem cell activities of the animals subjected to double RNAi, both in the presence or absence of gamma radiation exposure. This specific timepoint was chosen because stem cell numbers in irradiated control animals are expected to return to wild-type levels per previous observations (Sahu et al., 2021).

Smedwi-1 in situ hybridization revealed heavily defective stem cell recovery within the subset of the four RNAi combinations that sensitized planarians to sub-lethal irradiation (Figure 28). In these four particular combinations, stem cell recovery was either entirely absent or only minimally evident. In contrast, the remaining six non-lethal RNAi combinations showcased a significant delay in stem cell recovery relative to the GFP RNAi controls following irradiation (Figure 28). Despite this delay, we infer that the level of stem cell activity remains adequate to support essential functions of the animals given their non-lethal outcomes. Furthermore, the non-irradiated animals subjected to double RNAi across all ten gene combinations exhibited no significant changes in stem cell numbers relative to controls. These observations suggest that the examined genes play important roles for the stem cell recovery process following irradiation, but they may be dispensable for stem cell maintenance under homeostatic conditions.

Our findings illuminate potential redundancy between FHL-A and FHL-3, as well as between FHL-2 and FHL-4, in the context of planarian radiotolerance. The rationale behind this inference is that the RNAi of these genes in tandem may nullify the compensatory effects that each gene exerts upon the other, ultimately sensitizing the animals to sub-lethal irradiation. The knockdown pairing of FHL-A and LHX-1, as well as the pairing of FHL-4 and LHX-1, may also signify functional overlaps between these gene sets given their observed lethal outcomes. However, the shorter median lethal times for RNAi pairs involving LHX-1 (Figure 27B) could imply a more potent or potentially additive impact.

Alternative to functional redundancy, the observed mortality of sub-lethally irradiated animals could potentially be explained by additive effects resulting from the dual knockdowns. Such an effect may arise from the gene pairs acting non-redundantly at

distinct stages of the stem cell recovery process. This recovery process presumptively encompasses initial survival signalling, DNA repair, cell-cycle re-entry, and finally controlled proliferation to replenish the depleted stem cell population. Additive effects could also materialize when distinct genes operate within separate pathways at the same stage of recovery. If the observed lethality arises from the additive effects of paired gene knockdowns, it is plausible that individual gene knockdowns might lack the potency required to induce lethality. However, when the genes are simultaneously knocked down in pairs, the disruption of more than one critical function could occur, ultimately leading to the observed adverse effects. Further investigation would be imperative to unravel the intricacies behind these gene interactions, and to elucidate their underlying functions within the context of planarian radiotolerance.

Chapter 4 – Conclusions and future perspectives

We conducted an RNAi screen with the objective of identifying novel regulators of planarian radiotolerance. Our primary screen encompassed the in vivo assessment of 105 single-gene knockdowns, probing their effects on animal survival and the timely recovery of stem cells following irradiation. The complete list of genes screened and their knockdown phenotypes are reported in Appendix Table 10. Through our screen, we successfully identified six distinct single-gene knockdowns, namely the RNAi of Slmap, Kin-17, Dkc, Rab32, Rasl-12, and DMXL-1, that rendered planarians sensitive to a physiologically sub-lethal dose of gamma radiation. These genes are characterized in greater detail in the following chapter.

Through our screen, we have also identified 20 single-gene knockdowns that introduced a delay in stem cell recovery following irradiation. Despite this effect, these knockdowns possessed insufficient potency to evoke mortality in the animal subjects. Within this subset, platyhelminth-specific genes of previously uncharacterized functions emerged, which we designated as Larp-1-like and GPCR154-like. This gene cohort also features a variety of conserved signalling regulators that are tied to the Notch and Jnk signalling pathways, respectively. Multiple small-GTPases, autophagy-related genes, as well as developmental-related genes, were also implicated in delaying the recovery of stem cells

upon knockdown and irradiation. While many of the conserved genes within this cohort have recognized functions across diverse biological contexts, their precise functions within the framework of radiation response and resistance remain enigmatic. The planarian model system offers an advantageous platform to further explore their radiation-related functions in an in vivo context. Additionally, silencing these genes in strategic pairs holds promise for uncovering synergistic or potential additive functions between these genes, thereby facilitating an investigation into the gene interactions that contribute to planarian radiotolerance.

Furthermore, we identified multiple members of the FHL gene family, along with another LIM-domain-containing protein, LHX-1, which collectively exhibited upregulation in our bulk transcriptomic profile of gamma-irradiated X1 cells. We incorporated these five genes into our primary RNAi screen, revealing that the individual silencing of these genes caused some of the strongest delays in stem cell recovery post-irradiation without crossing the threshold of lethality. Phylogenetic analyses suggest that within this ensemble of FHL genes, FHL-A likely represents the ancestral FHL gene copy that is conserved across diverse animal phyla. Similarly, we found that the planarian orthologue of LHX-1 is also well-conserved across the animal kingdom. In contrast, our phylogenetic assessments indicate that the planarian paralogues of FHL-2, FHL-3, and FHL-4 represent novel innovations that are unique to platyhelminth lineage.

We probed the existence of functional redundancy among these LIM-domain-containing genes through paired gene knockdown experiments. These efforts unveiled four specific gene pairings, specifically the dual-RNAi combinations of FHL-A and FHL-3, FHL-2 and FHL-4, FHL-A and LHX-1, as well as FHL-4 and LHX-1, that sensitized planarians to gamma radiation. Through in situ hybridization, we observed that these four RNAi combinations resulted in severely defective stem cell recovery post-irradiation, ultimately leading to fatal outcomes. Although stem cell recovery was observed to be delayed in the remaining six RNAi pairs, we infer that these animals harboured sufficient stem cell activity to sustain their essential functions, given their non-lethal outcomes.

In this chapter, we also determined that the planarian FHL-1 gene, previously identified in a study by Wagner and colleagues (Wagner et al., 2012), is exclusive to the flatworm lineage. Similar to the effects observed for the FHL genes unveiled in this study, RNAi targeting FHL-1 compromised stem cell expansion after irradiation (Wagner et al., 2012). Their study additionally reported incidences of mortality when FHL-1 RNAi was combined with sublethal irradiation. However, it is vital to consider a difference within the authors' study – they observed a 20% mortality rate amongst their negative control group. In contrast, our assay was calibrated to exhibit zero lethality within our negative controls after sublethal irradiation. This disparity potentially indicates that the animals in the assay conducted by Wagner and colleagues were subjected to a dose of gamma radiation that was higher than our sublethal dose, or encountered experimental conditions throughout the course of the assay that led to incidences of mortality in their control group. At present, our investigation into the planarian FHL-1 gene remains confined to phylogenetics and requires future replication using our experimental protocol. Furthermore, the future investigation of FHL-1 alongside the other FHL genes revealed in this chapter would be important to understand their interactions and to shed light on the role of the FHL gene family within the landscape of planarians.

Based on publicly available single-cell gene expression data, we observed distinct expression patterns for the FHL genes and LHX-1. FHL-A is mainly detected in neurons (Plass et al., 2018; Fincher et al., 2018), with the presence of the gene extending specifically to Neoblast cluster 10 in the atlas by Plass and colleagues. Conversely, FHL-4 expression appears to be restricted to the muscle lineage, while FHL-3 marks its presence in the pharynx and intestines. While FHL-A, FHL-3, and FHL-4 appear to showcase distinct tissue specificity, the single-cell gene expression patterns of FHL-2 and LHX-1 are comparatively less specific. Both FHL-2 and LHX-1 exhibit the highest single-cell gene expression within neuronal cell types, with detectable signals also observed in neoblasts, pharynx, secretory cells, and cells of the epidermal lineage (Plass et al., 2018; Fincher et al., 2018). While their expression patterns in single-cell atlases offer valuable insights, the implementation of in situ hybridization targeting these genes would be imperative for robust experimental validation. In this project, we attempted in situ hybridization targeting the FHL genes and LHX-1. However, we were not able to obtain good signal-to-noise ratios in these assays. A

plausible factor contributing to this challenge could be the relatively low expression levels of these genes. The exploration of higher sensitivity in situ techniques, such as those rooted upon Hybridization Chain Reaction-based methods (Choi et al., 2018), may hold promise for enhancing their detection capabilities in future studies.

To gain deeper insights into the influence of these LIM-domain-containing genes on potential signalling pathways and the regulation of target gene expression, investigating their binding partners could be a promising avenue for exploration. To achieve this, the utilization of pull-down assays represent a plausible approach, albeit one that poses challenges due to the need for high-quality, planarian-specific antibodies. The synthesis of such antibodies is expected to incur substantial costs, thereby reducing the feasibility of such methods in the near future. An alternative strategy for identifying potential binding partners of these genes could be the employment of proteomics involving cross-linking mass-spectrometry (XL-MS), an approach with circumvents the need for highly specialized antibodies. Uncovering their protein interactions could also reveal whether there is crosstalk between the LIM-domain-containing genes with the other genes highlighted in this study. In humans, FHL family members have reported interactions with ABL-1 (Wang et al., 2021), and with crucial components of the Notch signalling pathway (Qin et al., 2004; Liang et al., 2008). These findings in humans may be of relevance considering that silencing the planarian orthologues of ABL-1 and various Notch signalling components, similar to the FHL genes, led to a delay in stem cell recovery following irradiation.

To dissect the influence of the FHL genes and of LHX-1 on the regulation of gene expression in planarians, implementing a combined RNAi and RNA-sequencing approach could be feasible. This strategy can provide insight into the changes in cell transcriptomes following gene knockdown, thereby potentially revealing target genes that are co-activated or co-repressed by the FHL genes. In the case of LHX-1, this approach might also uncover direct influences on target gene expression via the gene's homeobox domain. Overall, future investigation into their spatial expression patterns, binding partners, and target genes under their influence, would significantly enhance our mechanistic understanding of the FHL genes and of LHX-1, both in the context of planarian homeostasis and in planarians exposed to gamma radiation.

Chapter 5: Characterizing Slmap, Kin-17, Dkc, Rab32, Rasl-12, and DMXL-1 functions in planarian radiotolerance

Chapter 5 – Introduction

In Chapter 4, our primary RNAi screen identified six genes with diverse functional profiles, namely Slmap, Kin-17, Dkc, Rab32, Rasl-12, and DMXL-1, whose knockdowns enhanced planarian sensitivity to gamma radiation. This chapter begins by investigating the evolutionary conservation of these genes through phylogenetic analyses and examining the documented functions of their orthologues in other systems, where applicable. We then leverage the planarian model system to investigate the roles of these genes within the context of adult stem cell radiation response and recovery in vivo. Our methodology involves probing the integrity of various recovery stages, encompassing DNA repair, cell-cycle re-entry, stem cell proliferation, and stem cell differentiation, with the objective of pinpointing the specific stage of recovery that is impacted by each targeted gene knockdown. Insights gained from our study of these genes may hold broader implications for understanding adult stem cell radiation responses across metazoans.

Evolutionary conservation of Slmap, Kin-17, Dkc, Rab32, Rasl-12, and DMXL-1

We employed the OrthoFinder (Emms and Kelly, 2019) and EggNOG 6.0 (Hernandez-Plaza et al., 2023) algorithms to evaluate the presence or absence of gene orthologues across various model organisms. Predictions of orthology made by these algorithms were consistent, and were validated using a conventional reciprocal best-blast hit approach (Moreno-Hagelsieb and Latimer, 2008).

Our phylogenetic analyses indicate widespread conservation of Slmap, Kin-17, Dkc, Rab32, and DMXL-1 across the animal kingdom. Among these genes, respective orthologues of Slmap, Kin-17, Dkc, and DMXL-1 could be identified in the fungal lineage, suggesting that their conservation extends beyond metazoans. However, this was not the case for metazoan Rab32, which lacks identifiable orthologues in fungi (Figure 29).

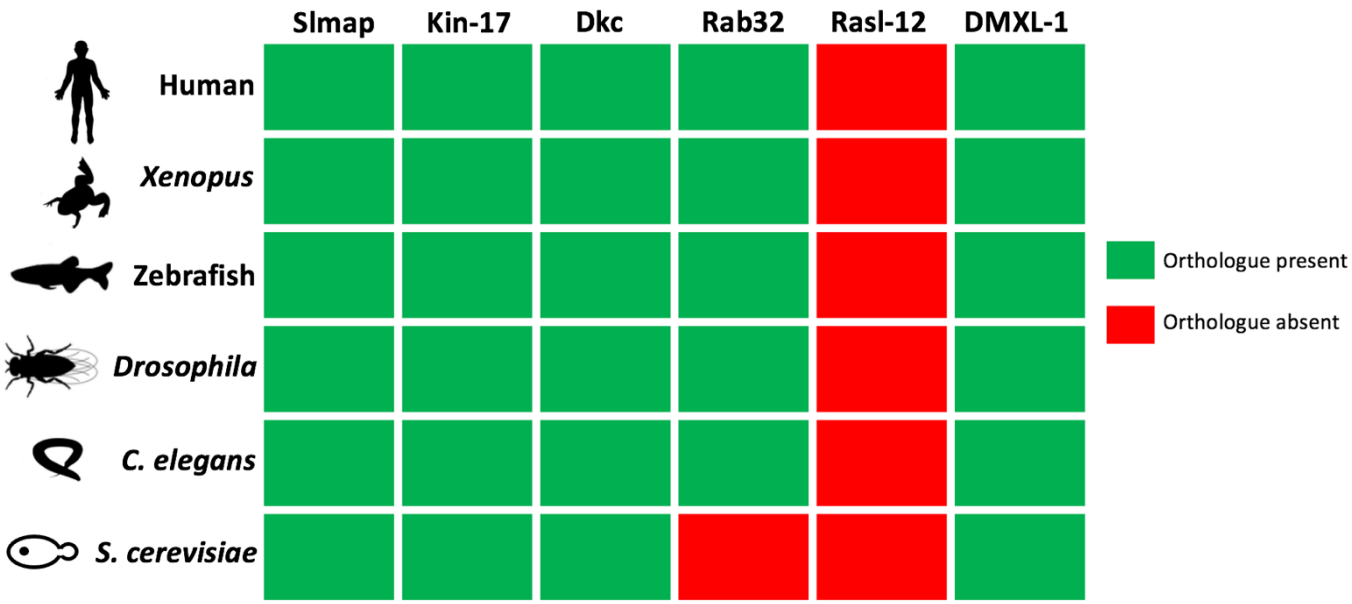

Figure 29. The genes Slmap, Kin-17, Dkc, Rab32, and DMXL-1 are conserved across metazoans, but Rasl-12 is unique to the platyhelminth lineage. Illustration depicts the presence (green) or absence (red) of gene orthologues to our target genes in selected model organisms.

In contrast, orthologues of platyhelminth Rasl-12 could not be found when queried against the proteomes of diverse vertebrate and invertebrate lineages, suggesting its exclusive presence within platyhelminths (Figure 30A). Both OrthoFinder and EggNOG 6.0, along with alternative orthology prediction algorithms – OMA (Altenhoff et al., 2021), and OrthoDB (Zdobnov et al., 2021), consistently place platyhelminth Rasl-12 into the orthogroup of Ras-like Estrogen Regulated Growth Inhibitor (RERG). RERG, another Ras-like small GTPase-encoding gene, is present in basal metazoans and is widely conserved across the animal kingdom (van Dam et al., 2011). Homology inference utilizing the integrated PlanMine feature (Rozanski et al., 2019) supports a paralogous relationship between RERG and Rasl-12 in platyhelminths, reinforcing the inferred origin of Rasl-12 via duplication involving the RERG gene during the course of platyhelminth evolution. This inference is further supported by the consistent return of RERG as the top blast hit for platyhelminth Rasl-12 in other invertebrate species, including closely related lineages such as molluscs and annelids within the same lophotrochozoan clade.

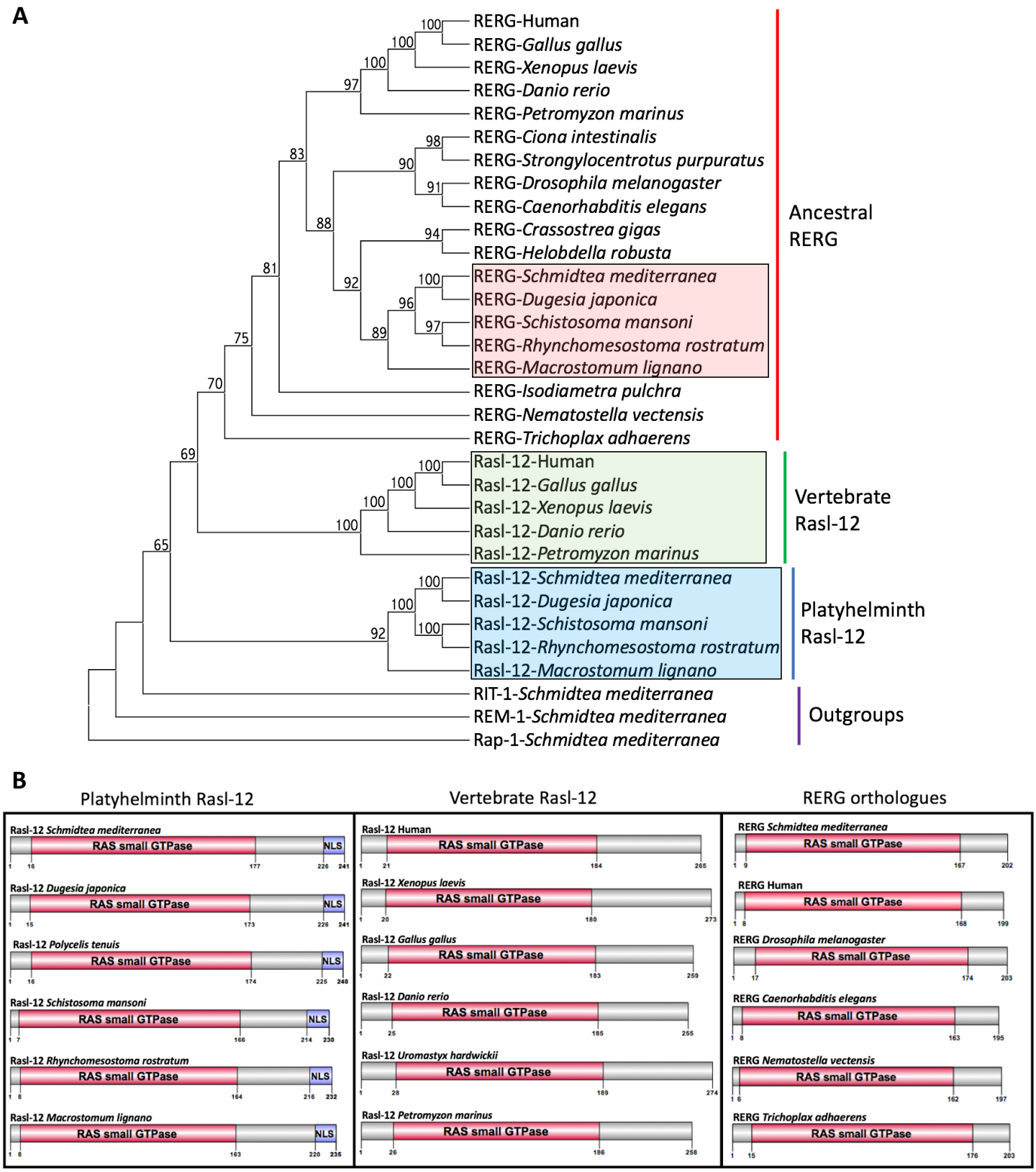

Figure 30. Phylogenetic analysis of platyhelminth and vertebrate Rasl-12. (A) Maximum likelihood tree depicting the phylogenetic relationships among platyhelminth Rasl-12, vertebrate Rasl-12, and the inferred ancestral RERG gene. Platyhelminth RERG (red), vertebrate Rasl-12 (green), and platyhelminth Rasl-12 (blue) are highlighted in boxes. Outgroups represent other conserved families within the group of Ras-like small GTPases. **(B)** Comparisons of domain architecture between platyhelminth Rasl-12, vertebrate Rasl-12, and the ancestral RERG gene. Abbreviation NLS: nuclear localization signal.

The nomenclature of platyhelminth Rasl-12, established in this study, is derived from its top blast hit in humans and other vertebrates, which is the vertebrate Rasl-12 gene. However, when querying vertebrate Rasl-12 against platyhelminth and other invertebrate proteomes, RERG is consistently returned as the top blast hit. Previous investigations into the evolutionary history of vertebrate Rasl-12 similarly suggest its emergence via duplication from the ancient RERG gene (van Dam et al., 2011). Furthermore, no orthologues of the vertebrate Rasl-12 gene have been identified outside of the vertebrate lineage (Diez et al., 2011). This implies that Rasl-12 in platyhelminths and vertebrates may represent two non-orthologous groups, each arising from independent duplication events of the ancestral RERG gene.

Despite their inferred independent origins, platyhelminth and vertebrate Rasl-12 share considerable sequence similarity in their Ras GTPase domains, with 62.67% sequence identity between *S. mediterranea* and human Rasl-12, potentially due to convergent evolution. However, the amino acid sequences downstream of this conserved domain diverge significantly between the two groups. Analysis of protein architecture using Pfam (Finn et al., 2014) and Prosite (Hulo et al., 2006) reveals additional non-conserved amino acid residues at the C-terminal regions of both platyhelminth and vertebrate Rasl-12 copies. These residues are absent from the ancestral RERG gene, causing RERG to be shorter than both platyhelminth and vertebrate Rasl-12. A key distinction between the two Rasl-12 groups is the presence of a bipartite nuclear localization signal (Lu et al., 2021) predicted at the C-terminus of platyhelminth Rasl-12 proteins, whereas the corresponding region of vertebrate Rasl-12 lacks known motifs (Figure 30B). Unlike vertebrate Rasl-12, the C-terminus of platyhelminth Rasl-12 is enriched with basic amino acids, characteristic of nuclear localization signals (Cokol et al., 2000). Specifically, Rasl-12 in different platyhelminth species possess 5 lysine residues and either 1 or 2 arginine residues in the terminal 14 bases of the protein, putatively facilitating its nuclear import.

Nevertheless, dissecting the reported functions of our target genes' orthologues in other systems, where present, may assist in identifying conserved functions in planarians. This in turn may shed preliminary insight into the mechanisms-of-action of our target genes in planarians both under homeostatic conditions and in response to gamma radiation.

Slmap

The human Slmap gene encodes a C-terminal tail-anchored protein that is post-translationally inserted into various intracellular membranes, in an isoform-specific manner (Byers et al., 2009). The protein's N-terminal region contains a Forkhead-associated (FHA) domain responsible for mediating protein-protein interactions, establishing Slmap as a signal transducer (Wielowieyski et al., 2000). Predictions of domain architecture indicate the conservation of both the C-terminal transmembrane coils and the N-terminal FHA domain between the human and planarian gene counterparts.

Functionally, orthologues of the Slmap gene have not been investigated in the context of radiation exposure or DNA damage. Nevertheless, dysregulated Slmap expression has been linked with the onset of diabetes in both humans (Upadhyay et al., 2015) and mice (Ding et al., 2005). Furthermore, Slmap has been documented to support normal cardiac functions in both humans and mice (Ishikawa et al., 2012; Nader et al., 2012; Mlynarova et al., 2019). Beyond metazoans, the Slmap orthologue in the budding yeast *S. cerevisiae* has been implicated in driving pheromone-responsive cell-cycle arrest (Kemp and Sprague, 2003). Additionally, in the filamentous fungus *Sordaria macrospora*, Slmap promotes sexual reproduction by facilitating hyphal fusion (Nordzieke et al., 2015).

One aspect of Slmap's function that may be pertinent to our study on adult stem cell radiation response is its proposed role as a key component and regulator of microtubule organizing centres. This is because distinct splice isoforms of the mouse Slmap gene have been identified to localize and function within centrosomes (Guzzo et al., 2004). Notably, overexpression of these isoforms, resulting in elevated centrosomal Slmap concentrations, has been found to induce lethality in mouse fibroblasts in vitro. Conversely, mutations that disable the protein's centrosomal targeting ability have been observed to inhibit cell proliferation by causing an aberrant accumulation of cells in G2/M phases of the cell cycle (Guzzo et al., 2004). The precise molecular mechanisms underlying these observations in mammals remain poorly characterized. Nonetheless, in this chapter, we aim to investigate a potentially novel role of Slmap in the context of adult stem cell radiation response.

Kin-17

Kin-17 is another gene that has emerged from our primary screen as a crucial regulator of planarian radiotolerance. In mammals, Kin-17 has been reported to possess a zinc finger domain and a tandem SH3 domain, enabling direct binding to DNA and RNA, respectively (Tissier et al., 1995; le Maire et al., 2006). Among our genes-of-interest, Kin-17 stands out as the sole gene that has previously undergone investigation within the context of radiation response and DNA damage. In various mammalian cell lines, Kin-17 was found to be transcriptionally upregulated following exposure to both gamma radiation (Biard et al., 1997) and non-ionizing UV-C radiation (Masson et al., 2003) in vitro. We observed a similar upregulation of Kin-17 in our transcriptomic profile of gamma-irradiated planarian X1 cells (Log_2 Fold Change = +4.37 at 24 hours post 5 Gy irradiation, Appendix Table 8).

Additionally, immunofluorescence targeting Kin-17 in a human carcinoma cell line revealed a major redistribution of the protein in response to gamma radiation in vitro. While the protein displayed a diffuse staining pattern within the nucleoplasm in non-irradiated cells, Kin-17 proteins aggregated to form large intranuclear foci following irradiation (Biard et al., 2002). Subsequently, knockdown of human Kin-17 was observed to significantly increase the radiosensitivity of the same cell line in vitro (Despras et al., 2003). Mechanistically, Kin-17 is proposed to enhance cell survival after irradiation by promoting efficient repair and resolution of double-stranded breaks (Le et al., 2016).

In multiple human cell lines under non-irradiated conditions, Kin-17 proteins were observed to undergo a similar redistribution to form intranuclear foci during S phase of the cell cycle (Miccoli et al., 2003). Kin-17 is understood to participate in replication factories, colocalizing with essential replication factors such as replication protein A, PCNA, and DNA polymerase alpha (Miccoli et al., 2003; Miccoli et al., 2005). Knockdown of Kin-17 causes an accumulation of cells in S phase, highlighting the gene's important role for cell cycle progression in vitro (Biard et al., 2002). It has recently been proposed that mammalian Kin-17 promotes both DNA replication and the subsequent repair of replication-induced DNA damage (Huang et al., 2023), although the molecular details of their functions remain enigmatic. The significance of Kin-17 in human DNA repair is further highlighted during class switch recombination in activated B cells (Le et al., 2016).

In the context of cancer, Kin-17 is observed to be upregulated in breast cancer (Zeng et al., 2011) and non-small cell lung cancer (Zhang et al., 2017), contributing to cancer cell proliferation in the former and cancer cell invasiveness in the latter. Additionally, Kin-17 has emerged as a potential therapeutic target in the treatment of both breast cancer (Gao et al., 2019) and cervical cancer (Su et al., 2022), as ablating Kin-17's activity promoted the apoptosis of both cancer cell types in vitro.

In planarians, Kin-17 expression is most pronounced in S/G2/M phase stem cells, with 67.18% of the Kin-17 transcripts, detected via bulk RNA-sequencing, originating from the X1 cell compartment. In contrast, the gene's relative expression in the X2 and Xins compartments stands at 21.56% and 11.25%, respectively (Neiro et al., 2022) [Appendix Table 8]. This enrichment in S/G2/M phase stem cells could suggest that the gene's observed functions in mammalian replication and repair may extend to planarian stem cells. Furthermore, the transcriptional upregulation of planarian Kin-17 after radiation exposure, coupled with the radio-sensitizing effect observed in vivo upon its knockdown, implies that its documented roles in mammalian radiation response and tolerance may be relevant to planarians as well.

Dkc

Another gene identified in Chapter 4, whose knockdown renders planarians sensitive to gamma radiation, is the planarian orthologue of Dkc. Dkc encodes an enzyme responsible for the synthesis of Dyskerin, an evolutionarily conserved RNA-binding protein that associates with various ribonucleoprotein complexes to drive a diverse range of cellular processes (Garus and Autexier, 2021). In mammals, these processes encompass Dyskerin's association with small nucleolar RNAs to facilitate ribosomal RNA and ribosome biogenesis (Ruggero et al., 2003), its interaction with Cajal bodies to regulate pre-mRNA splicing (Elsharawy et al., 2020), and its binding to the RNA component of telomerases to modulate telomere maintenance (Mitchell et al., 1999). Loss-of-function mutations in the human Dkc gene lead to dysfunctional telomere maintenance, resulting in the premature aging syndrome known as Dyskeratosis congenita (Knight et al., 1999). In contrast, gain-of-function mutations in the gene aberrantly increases ribosome biogenesis and enhances

telomerase activity, both of which have been implicated in the progression and poor clinical outcomes of multiple different human cancers (O'Brien et al., 2016; Ko et al., 2018; Elsharawy et al., 2020; Hou et al., 2020; Guerrieri et al., 2020).

Dkc function in ribosome biogenesis is found to be conserved between humans and *Drosophila* (Giordano et al., 1999). Additionally, the *Drosophila* Dkc gene is understood to be essential for the maintenance of both germline and intestinal stem cells. This is because tissue-specific knockouts of Dkc in either the *Drosophila* testes or midgut led to premature differentiation and consequently the depletion of resident stem cells, ultimately resulting in atrophy of the respective tissues (Kauffman et al., 2003; Vicidomini et al., 2017). It is proposed that the *Drosophila* Dkc gene maintains telomeres in a telomerase-independent pathway which remains unexplored to date (Vicidomini et al., 2017), given that telomere stability in *Drosophila* does not rely on conventional telomerase-based mechanisms (Pardue et al., 2005). The functions of Dkc in ribosome biogenesis and telomere maintenance extend beyond metazoans, as the gene's orthologue has been observed to uphold both these functions in *S. cerevisiae* (Zebarjadian et al., 1999; Hamma et al., 2005; Ungar et al., 2009).

In planarians, much like Kin-17, Dkc expression is most prominent in S/G2/M phase stem cells, with 60.20% of the Dkc transcripts, detected via bulk RNA-sequencing, to originate from the X1 cell compartment. In contrast, the gene's relative expression in the X2 and Xins compartments stands at 26.01% and 13.79%, respectively (Neiro et al., 2022) [Appendix Table 8]. This enriched expression in S/G2/M phase planarian stem cells could suggest an important role for the long-term self-renewal of neoblasts, should the function of Dkc in telomere maintenance be conserved in planarians. Furthermore, we observed upregulated Dkc expression in our bulk transcriptome of gamma-irradiated X1 cells (Log_2 fold change = +3.03 at 24 hours post 5 Gy irradiation, Appendix Table 8). Dkc was also observed to be upregulated at 24 hours post both 5 Gy and 10 Gy irradiation in Neoblast cluster 1 (Appendix Table 5,6), the stem cell cluster that exhibited the greatest resilience against gamma radiation in our single-cell atlas. These in silico observations, coupled with the radio-sensitizing effect on planarians in vivo upon its knockdown in Chapter 4, suggest a potential novel and conserved role of the gene in adult stem cell radiotolerance.

Rab32 and Rasl-12

Our RNAi screen also uncovered two small GTPases, Rab32 and Rasl-12, whose knockdowns rendered planarians more sensitive to gamma radiation in vivo. In humans, Rab32 functions as an inhibitor of apoptosis through multiple distinct pathways. Firstly, Rab32 contributes to the alleviation of endoplasmic reticulum (ER) stress by modulating ER calcium levels and promoting the accumulation of the chaperone calnexin at the ER (Bui et al., 2010). This mitigation of ER stress promotes cell survival, as ER stress readily signals the activation of cellular apoptosis (Sano and Reed, 2013).

Furthermore, Rab32 serves as a protein kinase A (PKA) anchoring protein and exerts its anti-apoptotic functions through PKA-dependent signalling (Alto et al., 2002). Specifically, Rab32 activation has been shown to promote PKA-mediated phosphorylation and subsequent suppression of the pro-apoptotic factor BAD (Bui et al., 2010). Additionally, PKA activation by Rab32 also leads to PKA-mediated phosphorylation and inactivation of Dynamin-related protein 1 (Drp-1). This in turn prevents the activation of Drp-1-mediated mitochondrial fission (Bui et al., 2010), thus preventing mitochondrial fission-induced apoptosis (Cribbs and Strack, 2007). Notably, this same pathway, which links Rab32 function to Drp1-mediated mitochondrial fission, was recently observed to promote the in vivo migration and invasiveness of glioblastoma cells in mice (Chen et al., 2023).

In addition to its anti-apoptotic functions, Rab32 is also recognized in humans as a contributor to autophagy (Hirota and Tanaka, 2009) and phagocytosis (Spano and Galan, 2012). The autophagic functions of Rab32 extend beyond mammals, as autophagic pathways driven by Rab32 have been reported in the respective orthologues of the gene in *Drosophila* (Wang et al., 2012) and *C. elegans* (Zhou et al., 2011). In the context of our study, the potential conservation of Rab32's anti-apoptotic and pro-autophagic functions in planarians may underscore the gene's observed effects on planarian radiotolerance. This chapter delves into Rab32's function within the context of planarian radiotolerance, while simultaneously exploring whether Rasl-12 represents a planarian-specific innovation to counteract genotoxic stresses.

DMXL-1

Our sixth gene-of-interest investigated in this chapter is DMXL-1. The DMXL-1 gene is strongly conserved across eukaryotes (Kraemer et al., 2000), and encodes a large WD-repeat protein known to regulate endosomal function in mammals, *Drosophila*, and Zebrafish. First identified in *Drosophila*, mutations in the DMXL-1 gene disrupt the regulated endocytosis of Notch signalling components from the cell membrane (Yan et al., 2009). As a result, tissue-specific mutagenesis of DMXL-1 in the *Drosophila* follicular epithelium, eye imaginal disc, and wing imaginal disc all led to developmental abnormalities in the respective tissues (Yan et al., 2009). Knockdown of the mammalian DMXL-1 gene was similarly found to attenuate Notch signalling in a keratinocyte cell line in vitro due to defects in endocytosis (Sethi et al., 2010). In Zebrafish, a loss-of-function mutation in DMXL-1 was observed to disrupt the endocytosis of Wnt signalling receptors in neural crest cells. This disruption resulted in diminished levels of Wnt signalling, impairing the activation of epithelial-to-mesenchymal transition, and subsequently leading to defects in neural crest migration in the developing zebrafish embryo (Tuttle et al., 2014). These insights suggest that DMXL-1 serves as a key regulator for various signalling pathways, and it may regulate crucial signalling pathways that impart radiotolerance to planarians.

Experimental strategy for characterization of target gene function

Leveraging our knowledge of radiation-induced responses in mammals (Maier et al., 2016), *Drosophila* (Su, 2019), *C. elegans* (Sakashita et al., 2010), as well as in planarians (Sahu et al., 2021), we can identify a conserved sequence of critical processes vital for organismal survival. We extrapolate these insights to our study, postulating that this fundamental chain of events, encompassing DNA repair, cell-cycle re-entry, stem cell proliferation, and stem cell differentiation, holds vital significance for planarian survival and recovery from gamma radiation exposure (Figure 31).

In this chapter, we harness the planarian model system to investigate the roles of our target genes within the framework of radiation response and recovery in vivo. Our methodology entails examining the functionality of the described recovery stages, aiming to pinpoint the specific stage(s) of recovery impacted by each targeted gene knockdown. Our study enables us to explore whether Kin-17's radiation-responsive roles in mammals extend to planarians, while also providing a unique opportunity to uncover novel and potentially conserved functions of the remaining genes within this context.

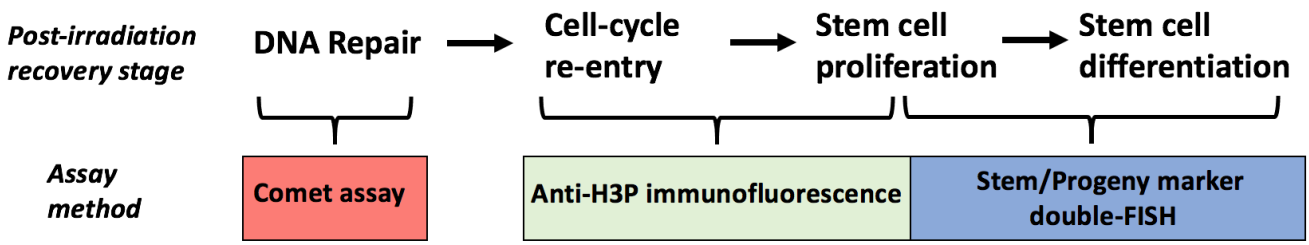

Figure 31. Sequence of events necessary for planarian recovery from sub-lethal irradiation and the experimental strategies to investigate them.

In our investigation, we silenced our genes-of-interest and exposed the animals to a sub-lethal 15 Gy dose of whole-body acute gamma radiation. The experimental workflow for dsRNA microinjection and dosimetry were consistent with the one outlined in our primary RNAi screen. To evaluate the impact of targeted gene knockdown on either stem cell expansion or differentiation, we compared the recovery kinetics of both stem cells and progeny cells in the treatment groups with those in the GFP RNAi negative control group. We accomplished this by performing double in situ hybridization over a time-course following irradiation, concurrently targeting the stem cell marker, Smedwi-1, and the early epidermal progenitor cell marker, Prog-1. Impaired recovery of Smedwi-1^{+} cells relative to controls would indicate that the targeted gene knockdown compromises stem cell recovery post-irradiation. In contrast, if we observe the recovery of Smedwi-1^{+} cells but not Prog-1^{+} cells, it would suggest that stem cell proliferation is taking place, but the knockdown impacts the differentiation process, preventing stem cells from giving rise to progeny.

To investigate the dynamics of neoblast cell-cycle re-entry following knockdown and irradiation, we conducted immunofluorescence targeting Phospho-Histone H3 (H3P), a marker for cells in late G2 and M phases (Hendzel et al., 1997), over a post-irradiation time-course. This assay would serve as a direct proxy for mitotic stem cell activity, as stem cells represent the sole proliferative cell-type within planarians (Newmark and Sanchez-Alvarado, 2000). Previous observations in our group showcased that sub-lethally irradiated wild-type planarians undergo a transient period of cell cycle arrest putatively allocated for DNA repair. The duration of this arrest is dose-dependent, with $H3P^{+}$ cells only reappearing in animals at 3 days post-exposure to a 15 Gy dose of acute gamma radiation (Sahu et al., 2021). In our assay, we also included immuno-staining for H3P at the 1-day post-irradiation timepoint to examine whether any of the knockdowns induced premature cell-cycle re-entry. The occurrence of this phenomenon would indicate that the targeted gene knockdown causes a form of checkpoint defect. Such a defect would be detrimental for cells because attempting mitosis despite the presence of un-repaired DNA damage would lead to death of the cell through mitotic catastrophe (Vakifahmetoglu et al., 2008).

Prior efforts in our group, which involved the knockdown of conserved DNA repair genes, have also established DNA repair as a critical process for planarian survival following exposure to gamma radiation (Sahu et al., 2021). To evaluate the impact of targeted gene knockdowns on the process of DNA repair, we conducted a series of alkaline Comet assays over a time-course post-irradiation. The fundamental principle of the Comet assay involves the migration of negatively charged DNA towards the anode during electrophoresis, with low molecular weight DNA fragments, generated due to strand breaks, migrating more readily compared to high molecular-weight intact DNA. This migration creates a distinct trail of DNA reminiscent of a comet's tail (Figure 36, further described in the corresponding section). The quantity of DNA contained within these comet tails following electrophoresis positively correlates with the extent of DNA strand breaks present within cells (Olive and Banath, 2006). Comparing the level of DNA damage in cells from animals subjected to targeted gene knockdown with that of negative controls may help unveil whether any of our genes-of-interest serve as important regulators of DNA strand-break repair in planarians.

Single-RNAi of Slmap, Kin-17, Dkc, Rab32, Rasl-12, and DMXL-1 impairs stem cell expansion following irradiation

We conducted dual fluorescence in situ hybridization simultaneously targeting the stem cell marker, Smedwi-1, and the lineage-specified progeny marker, Prog-1. In situ hybridization was performed on animals from both the experimental and control groups at five distinct timepoints – specifically, at 3, 7, 10, 14, and 21 days post-exposure to an acute 15 Gy dose of whole-body gamma radiation. The selection of post-irradiation timepoints for examination was guided by our prior knowledge of how stem cell numbers change in wild-type animals over time following exposure to 15 Gy gamma radiation. We incorporated the 3-day timepoint as the earliest post-irradiation stage for investigation, as this particular timepoint represents the phase where stem cell numbers in control animals are expected to be at their lowest. The latest timepoint we examined was the 21-day post-irradiation stage, at which stem cell numbers in control animals are projected to have fully recovered to levels comparable to those in non-irradiated animals (Sahu et al., 2021).

Our quantification of Smedwi-1^{+} cell numbers over time reveals that the individual silencing of our genes-of-interest, combined with sub-lethal irradiation, impairs stem cell recovery. We also observed that the modes and extent of impairment may vary depending on the specific gene targeted for knockdown. We can categorize our genes-of-interest into two subsets based on the observed effects on stem cell recovery.

Firstly, we observed that RNAi targeting Slmap, Kin-17, and Dkc, led to a reduced number of initial surviving stem cells at 3 days post-irradiation compared to the GFP control group (Figure 32A). Notably, RNAi of Slmap, which had been found to impact stem cell maintenance under non-irradiated conditions in Chapter 4, resulted in the lowest number of initial surviving stem cells among the genes we tested. Additionally, the residual surviving stem cells in animals subjected to Slmap, Kin-17, and Dkc single-RNAi in conjunction with 15 Gy gamma irradiation exhibited proliferation incompetency. This is evident as almost all animals subjected to these conditions displayed a complete lack of stem cell recovery (Figure 32B). The observed proliferation incompetency among residual surviving stem cells is comparable to what is observed in planarians exposed to lethal doses of gamma radiation (Sahu et al., 2021).

The second category pertains to the effects of Rab32, Rasl-12, and DMXL-1 RNAi on stem cell dynamics post-irradiation. In these cases, although no significant differences were observed in the number of surviving stem cells relative to the control group at the 3-day post-irradiation timepoint (Figure 32A), we observed a significantly delayed stem cell expansion phenotype (Figure 32B). In control animals, the number of stem cells began to rise at the 3-day post-irradiation mark. However, for Rasl-12 and DMXL-1 RNAi, increases in stem cell numbers were only detected at the 10-day post-irradiation timepoint. In the case of Rab32 RNAi, an increase in stem cell number was only detected at the 14-day post-irradiation mark (Figure 32B). Despite the increase in stem cell numbers, fatal outcomes persisted in animals subjected to the knockdown of these three genes in combination with 15 Gy gamma irradiation. This suggests that although some degree of stem cell recovery occurred, there was insufficient stem cell activity to sustain essential functions of the animals, culminating in their mortality.

Nevertheless, observing an increase in stem cell numbers within Rab32, Rasl-12, and DMXL-1 RNAi-treated animals indicate that some, if not all, of the surviving stem cells retained proliferative competency in these cases. However, the knockdown-induced impairments led to an abnormally prolonged state of cell-cycle arrest in the surviving stem cells, consequently delaying the stem cell recovery process. It is crucial to acknowledge a pragmatic limitation of RNAi that may contribute to this phenomenon of extended cell-cycle arrest, which is related to the transient nature of gene silencing by RNAi. It is possible that the inhibition of stem cell proliferation may gradually subside as gene silencing levels decrease over time due to the limited lifespan of dsRNA within cells.

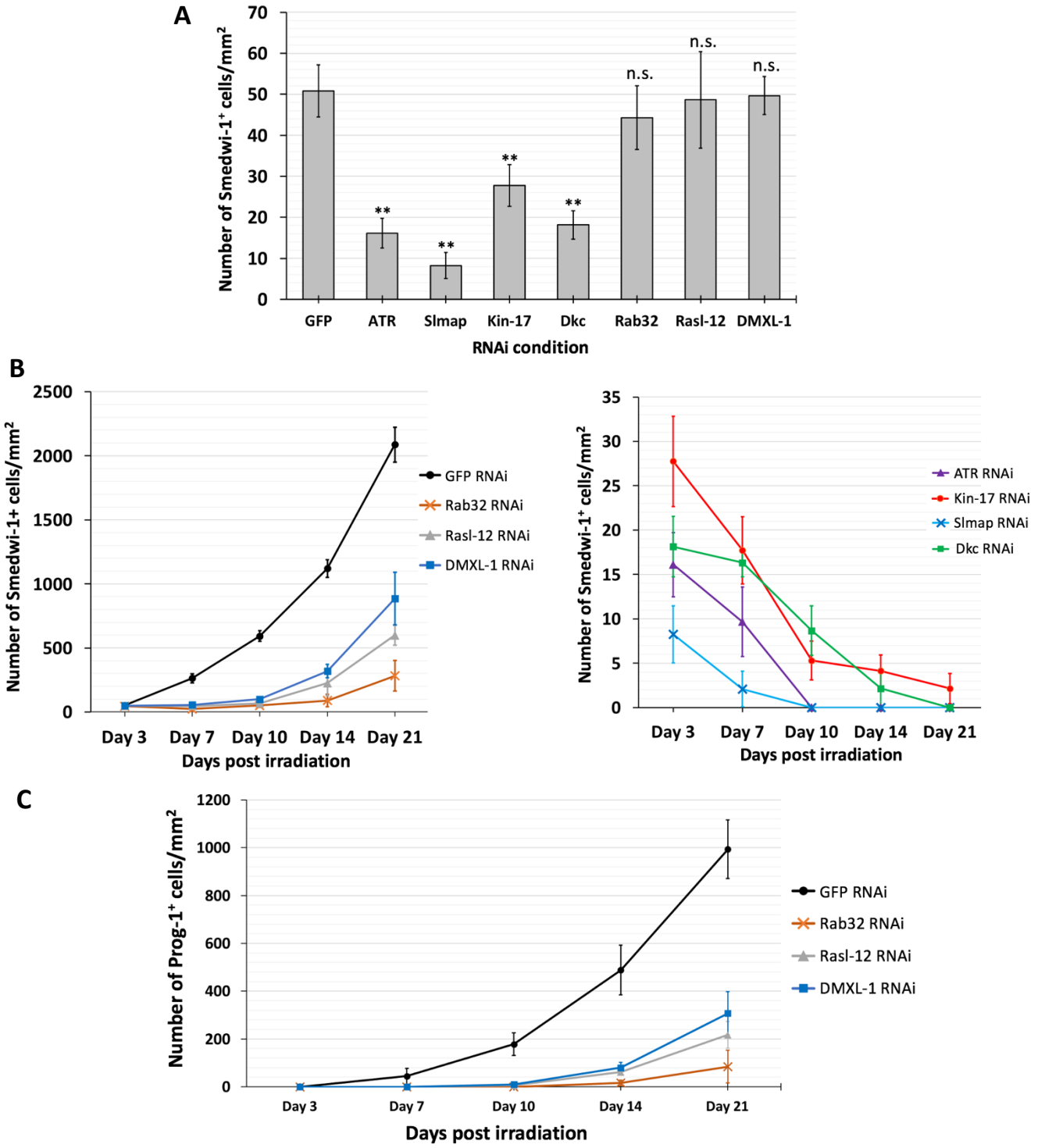

Figure 32. RNAi of Slmap, Kin-17, Dkc, Rab32, Rasl-12, and DMXL-1 impairs stem cell expansion after sub-lethal irradiation. (A) Quantification of Smedwi-1$^+$ cell numbers at 3 days post-irradiation in animals subjected to targeted gene RNAi. Asterisks (**) indicate a statistically significant difference with an unpaired t-test p-value <0.001 in relation to the GFP control. **(B, C)** Quantification of Smedwi-1$^+$ cell numbers **(B)** and Prog-1$^+$ cell numbers **(C)** at 3, 7, 10, 14, and 21 days post-irradiation in animals under various RNAi-treated backgrounds. All differences with the GFP control at each respective timepoint, except for the values at 3 days post-irradiation [refer to (A)], displayed statistical significance with unpaired t-test p-values <0.001. Graphs of Prog-1$^+$ counts over time for Slmap, Kin-17, Dkc RNAi-treated animals have been omitted as these animals displayed no increases in Prog-1$^+$ cells within the tested timeframe.

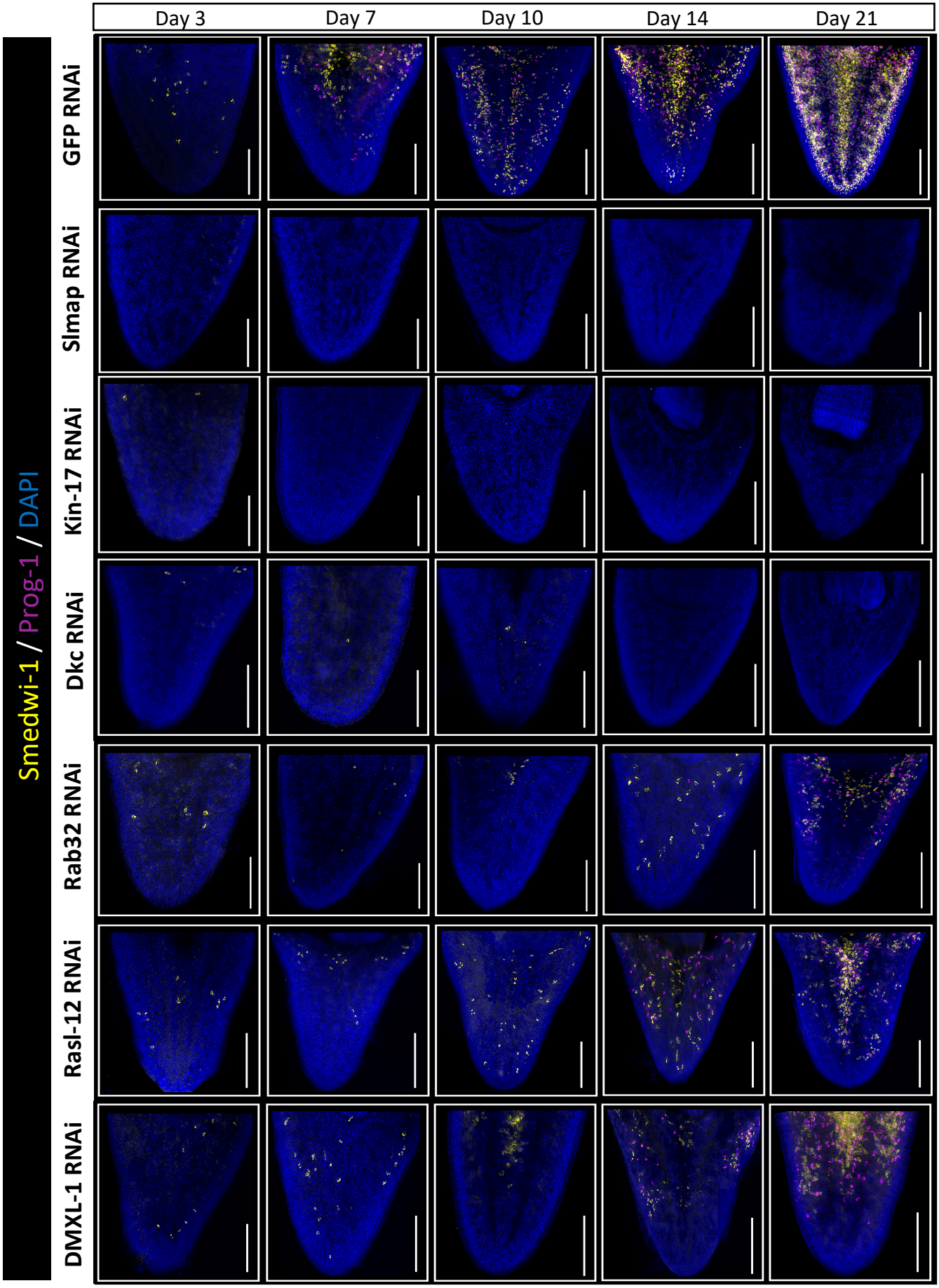

Figure 33. Dynamic expression patterns of Smedwi-1 and Prog-1 in RNAi-treated planarians exposed to sub-lethal irradiation. Representative dual fluorescence in situ hybridisation images of planarian tail regions, depicting the Smedwi/Prog-1 expression patterns, at 3, 7, 10, 14, and 21 days post 15 Gy irradiation in animals exposed to various RNAi treatments. Scale bars represent 0.5 mm.

In our evaluation of stem cell differentiation, we observed that the post-irradiation stem cell expansion and differentiation processes are temporally coupled. In control animals, although stem cell differentiation is preceded by stem cell proliferation, we observed the emergence of new progeny cells long before the full recovery of the stem cell compartment following irradiation. For instance, while stem cell numbers began to rise in control animals at 3 days post-irradiation, an increase in Prog-1$^+$ early-epidermal progeny cell numbers could be detected at 7 days post-irradiation. Both stem cell and progeny cell numbers increased concurrently in control animals during their road to recovery and survival (Figure 32B, 32C). These insights suggest that during the post-irradiation stem cell repopulation phase, stem cell divisions are not exclusively limited to symmetric divisions. Rather, asymmetric divisions also occur, giving rise to lineage-specified progeny.

In animals subjected to RNAi targeting Rab32, Rasl-12, and DMXL-1, we have observed the occurrence of post-irradiation stem cell differentiation, evidenced by the increases in Prog-1$^+$ cell numbers within the treated animals (Figure 32C). However, the emergence of Prog-1$^+$ cells occurred at varying timepoints, closely following the increase in stem cell numbers in all cases. The kinetics of stem cell differentiation in these RNAi-treated animals resemble those in the control group, as indicated by the similarities in the curve's gradient during the corresponding increment phases. The time interval between the onset of stem cell proliferation and differentiation is also comparable to that of the GFP control group, with Prog-1$^+$ cells emerging one experimental timepoint after the emergence of Smedwi-1$^+$ stem cells. Based on these observations, we attribute the mortality of the animals following targeted gene knockdown and sub-lethal irradiation to defects in stem cell expansion, rather than differentiation.

In cases where animals underwent RNAi targeting Slmap, Kin-17, and Dkc, where majority of the animals exhibited a complete lack of stem cell proliferation after sub-lethal irradiation (Figure 32B), we observed no incidence of Prog-1$^+$ cell recovery. This, in turn, indicates a lack of new stem cell differentiation post-irradiation. However, as cell-cycle re-entry and stem cell proliferation precede stem cell differentiation, it becomes challenging to assess the direct influence of these knockdowns on the post-irradiation stem cell differentiation process. It remains plausible that these genes also contribute to stem cell

differentiation during the animal's recovery from irradiation. However, any knockdown-induced impairments in the ability of stem cells to differentiate could be masked by the concurrent failure in stem cell proliferation in an underlying epistatic phenomenon.

Single-RNAi of Slmap, Kin-17, Dkc, Rab32, Rasl-12, and DMXL-1 impairs neoblast cell-cycle re-entry after irradiation

Defects in neoblast cell-cycle re-entry may underpin the observed deficiencies in stem cell proliferation following targeted gene RNAi in combination with sub-lethal irradiation. To investigate and compare the dynamics of cell-cycle re-entry in planarians undergoing these treatments, we performed immunofluorescence assays over a post-irradiation time-course targeting H3P, a marker of stem cells in G2/M phase. In the non-targeting GFP RNAi control group, we observed the emergence of $H3P^+$ cells at the 3-day timepoint post-exposure to an acute 15 Gy dose of whole-body gamma radiation. Subsequently, the count of $H3P^+$ cells continued to rise, indicative of ongoing stem cell proliferation (Figure 34B). The $H3P^+$ cell counts over time following irradiation in our negative control group align with kinetics previously observed for wild-type planarians irradiated at the same dose (Sahu et al., 2021). Furthermore, the emergence of $H3P^+$ cells at 3 days post-irradiation corresponds to the onset of stem cell number expansion observed in our present study (Figure 32B, 34B).

In contrast, animals subjected to RNAi targeting Slmap, Kin-17, Dkc, and Rab32 failed to produce any $H3P^+$ cells up to the final timepoint examined, which was day 10 post-irradiation (Figure 34A). These findings align with the absence of an increase in stem cell numbers at these timepoints for the four gene knockdowns in question (Figure 32B). In the cases of Rasl-12 and DMXL-1 RNAi, $H3P^+$ cells emerged in the animals at the 10-day post-irradiation timepoint (Figure 34B), coinciding with the onset of stem cell number expansion in the RNAi-treated animals (Figure 32B).

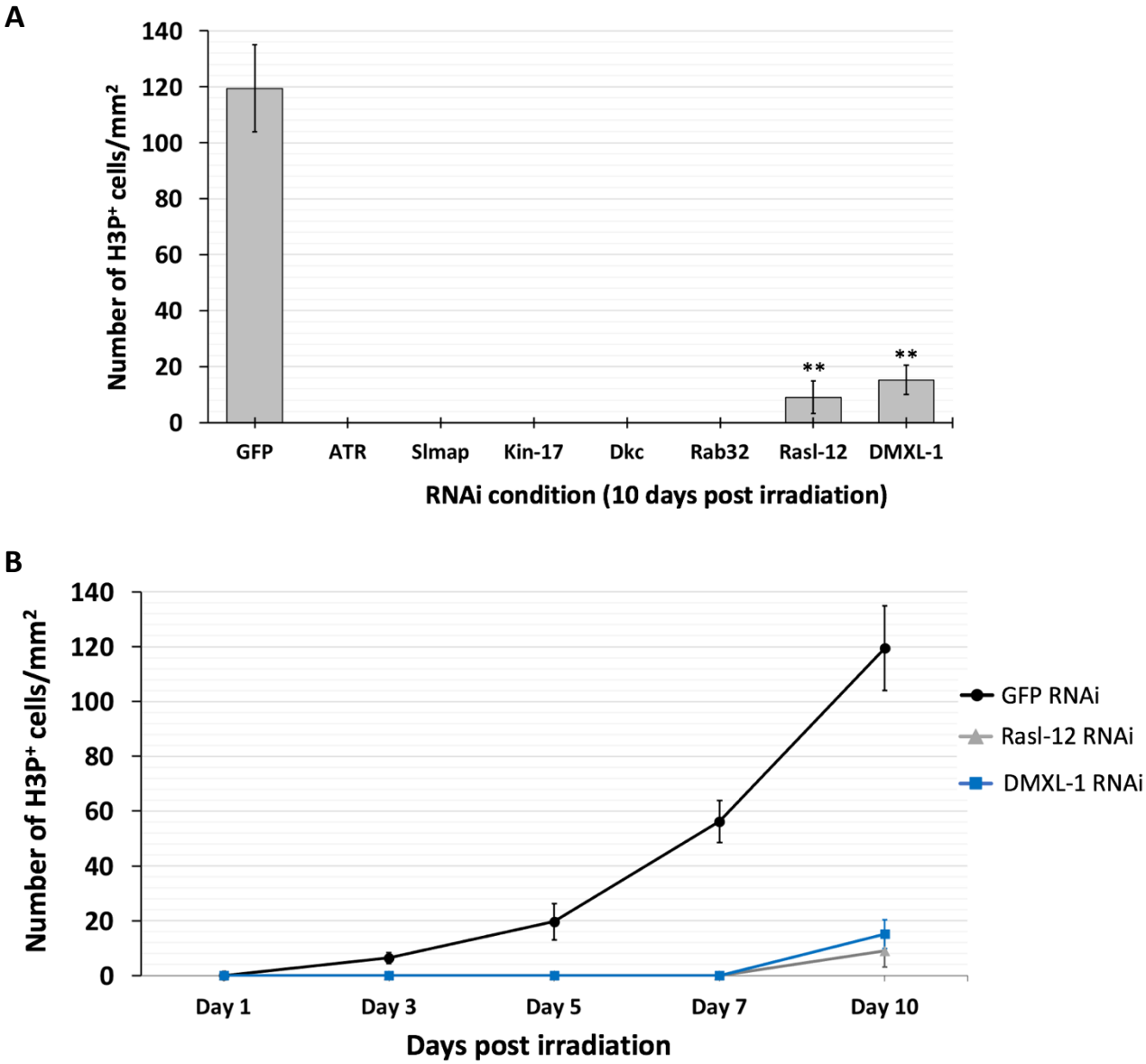

Figure 34. RNAi of Slmap, Kin-17, Dkc, Rab32, Rasl-12 and DMXL-1 impairs neoblast cell-cycle re-entry after sub-lethal irradiation. (A) Quantification of $H3P^+$ cell numbers at 10 days post-irradiation in animals subjected to targeted gene RNAi. Asterisks (**) indicate a statistically significant difference with an unpaired t-test p-value <0.001 in relation to the GFP control. **(B)** Quantification of $H3P^+$ cell numbers at 1, 3, 5, 7, and 10 days post-irradiation in animals under various RNAi-treated backgrounds. Except for values at 1-day post-irradiation, where all conditions including the GFP control registered zero $H3P^+$ cell counts, all differences with the GFP control at each respective timepoint showed statistical significance with unpaired t-test p-values <0.001. Graphs of $H3P^+$ counts over time for Slmap, Kin-17, Dkc and Rab32 RNAi-treated animals have been omitted as these animals displayed no increases in $H3P^+$ cells within the tested timeframe.

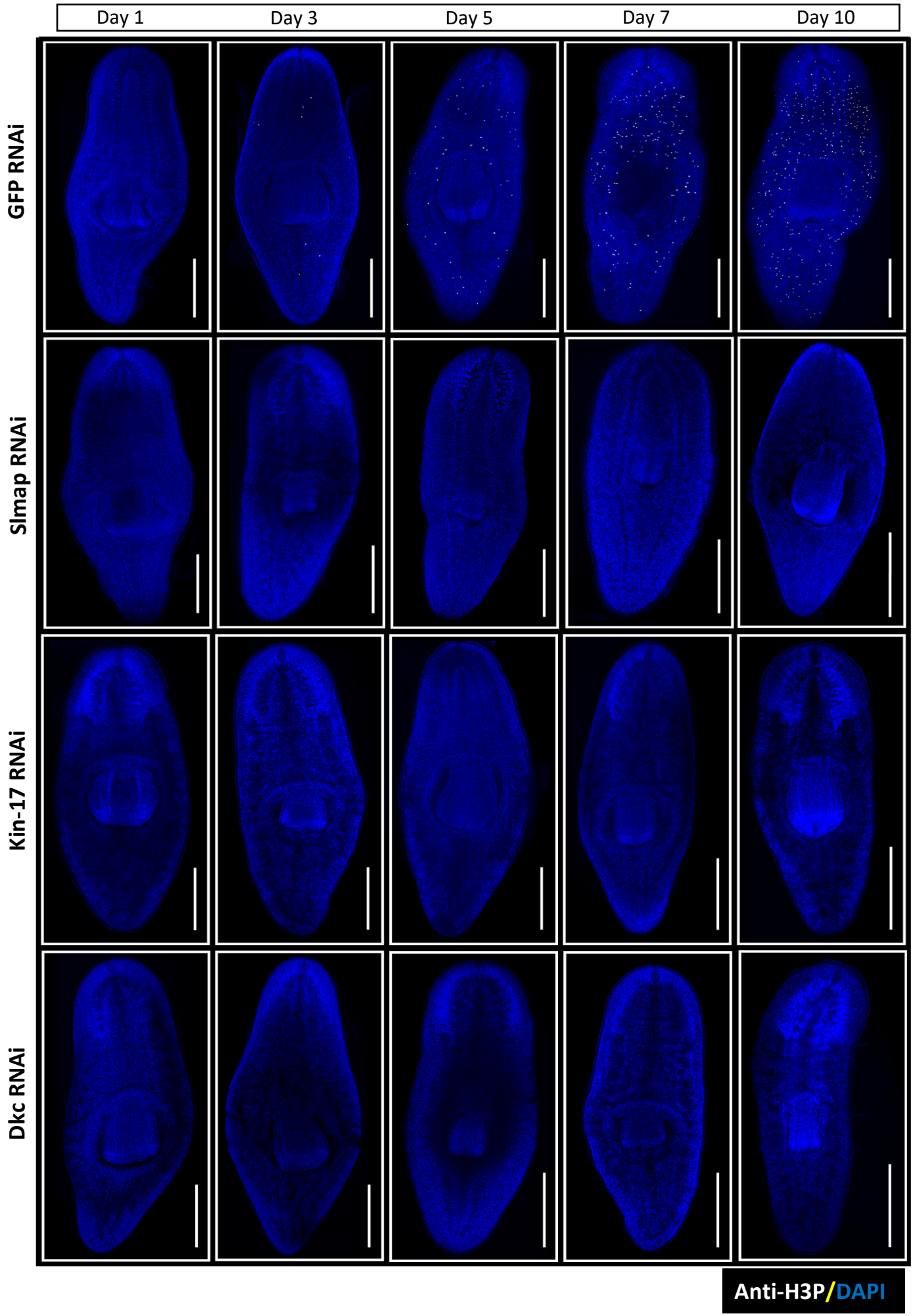
Day 1
Day 3
Day 5
Day 7
Day 10
GFP RNAi
Slmap RNAi
Kin-17 RNAi
Dkc RNAi
Anti-H3P/DAPI

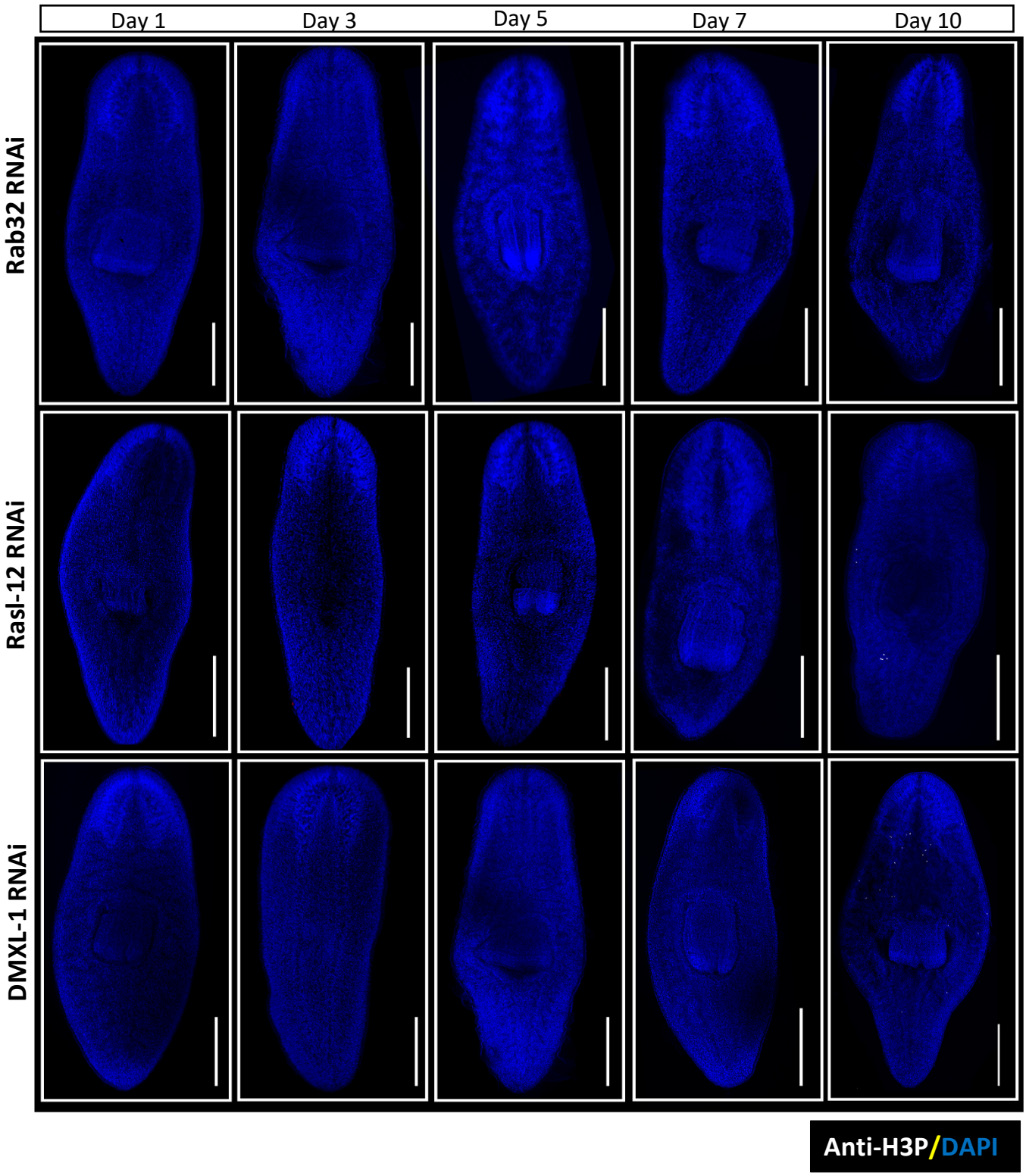

Figure 35. Dynamic expression patterns of H3P in RNAi-treated planarians exposed to sub-lethal irradiation. Representative immunofluorescence images of planarians, depicting the H3P expression patterns, at 1, 3, 5, 7, and 10 days post 15 Gy irradiation in animals exposed to various RNAi treatments. Scale bars represent 1 mm.

Insights from this assay suggest that the knockdowns either inhibit or significantly delay neoblast cell-cycle re-entry following irradiation. This inhibition underlies the observed impairment in stem cell recovery, ultimately leading to mortality of the treated animals. Additionally, the results from this assay enable us to deductively exclude several other processes that might have been impacted by the knockdowns. For instance, the absence of $H3P^+$ cells at the 1 day-post irradiation timepoint for all genes tested indicates that the knockdowns did not induce premature cell-cycle re-entry due to a potential checkpoint defect. Furthermore, there was no abnormal accumulation of $H3P^+$ cells in the knockdown animals post-irradiation. This would have meant a situation where $H3P^+$ cell counts increased without subsequent stem cell number expansion, an occurrence that may have signified a potential defect in the G2-to-M phase transition step or a mitotic defect.

RNAi of Dkc impairs post-irradiation DNA strand break repair

One potential factor contributing to the observed defects in neoblast cell-cycle re-entry following irradiation could be a knockdown-induced impairment in DNA repair. Failure to repair damaged DNA leads to persistent DNA damage response signalling, a phenomenon that sustains cell-cycle arrest (Rodier et al., 2009). Moreover, prolonged DNA damage response signalling, resulting from the continued presence of unrepaired DNA, could even trigger apoptosis directly in affected cells (Hoeijmakers, 2009). To investigate the post-irradiation DNA repair capacities of animals subjected to targeted gene knockdown, we employed the alkaline Comet assay, a method that allows us to measure the extent of DNA strand breaks within individual cells. The experimental procedure first involved subjecting animals to targeted gene knockdown and exposing them to a whole-body 15 Gy acute dose of gamma radiation. Subsequently, animals were dissociated into single-cells at 3, 24, 48, 72, and 96 hours post-irradiation. The cells were then embedded on agarose-coated glass microscope slides in preparation for electrophoresis. Our approach aimed to quantitatively assess the amount of DNA strand breaks present within cells over time following irradiation, serving as an informative indicator on whether any of the knockdowns impacted the progression of DNA repair.

In the non-targeting GFP control group, we observed a gradual decrease in the average percentage of DNA within comet tails throughout the tested timepoints (Figure 36C, 36D). This observation suggests that ongoing DNA strand break repair mechanisms are at play. For our positive control, we employed dual knockdowns of ATR and Parp-1, ensuring the induction of a robust defective-DNA-repair phenotype by targeting both double-stranded and single-stranded break repair pathways. In our positive control, we recorded higher average percentages of comet tail DNA across all tested timepoints in relation to our negative control, which indicates successful hindrance of DNA strand-break repair by knockdown (Figure 36C, 36D).

In our negative control group, we observed that by the 96-hour post-irradiation mark, the percentage of DNA in comet tails had returned to levels similar to those in non-irradiated control samples, which was set as our baseline (Figure 37A). Specifically, we recorded an average of 5.32% DNA in comet tails within our non-irradiated negative control sample, a baseline value consistent with a prior study conducted by our group (Sahu et al., 2021). It is worth highlighting that baseline damage levels in Comet assays of planarian cells exhibit variability across different research groups. For instance, Yin and colleagues reported lower baseline values compared to our study (Yin et al., 2016), while baselines exceeding 10% DNA in comet tails were reported in two separate studies (Peiris et al., 2016c; Barghouth et al., 2022).

This baseline level of detected DNA damage in unirradiated samples may arise from both endogenous DNA damage inherent within cells and pragmatic limitations of the assay that could introduce artefactual DNA damage to cells during the experimental procedure. These artefacts may include mechanical or enzymatic damage inflicted upon DNA during the cell dissociation process. Additional DNA damage may also be introduced during the electrophoresis step, as DNA at this stage is devoid of its protective cellular environment, rendering it more susceptible to damage from sources such as heat and light (Olive and Banath, 2006). We took measures to mitigate the impact of non-endogenous DNA damage by employing a gentler dissociation process, and by conducting electrophoresis under cold conditions while ensuring the samples were shielded from light.

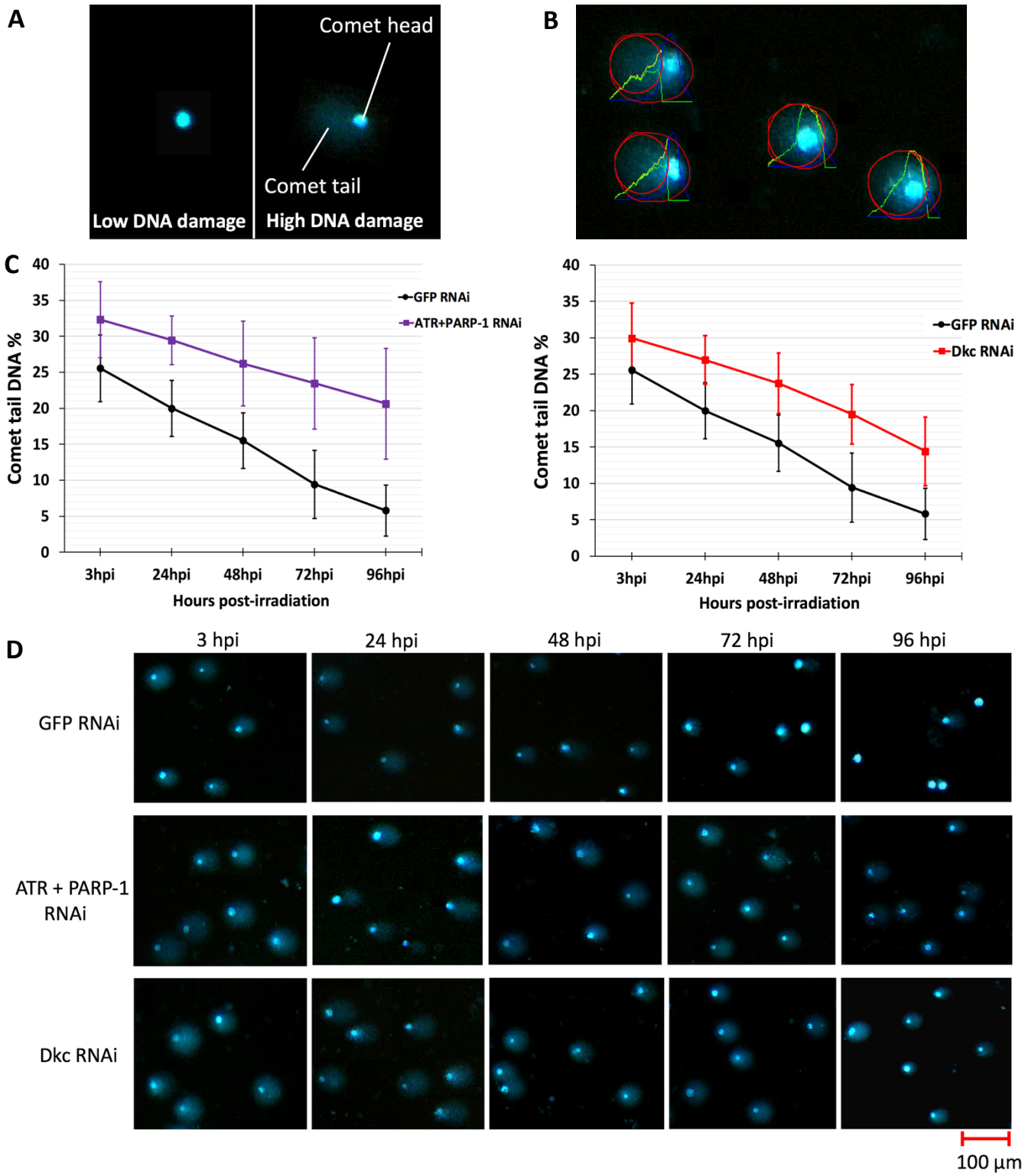

Figure 36. Comet assay reveals defective DNA stand break repair in Dkc RNAi-treated animals.

(A) Visual representation of either an undamaged or damaged nucleus post-electrophoresis. **(B)** Demonstration of Comet finding and analysis using OpenComet software (Gyori et al., 2014), measuring head and tail parameters and their respective intensities. **(C)** Quantification of percentage comet tail DNA over time in GFP (negative control), ATR + Parp-1 (positive control) and Dkc RNAi-treated animals. Statistically significant differences, with unpaired t-test p-values <0.001, were observed at each corresponding timepoint compared to the GFP control. **(D)** Representative fluorescence images showing the extent of comet tail formation at various timepoints after irradiation in Dkc and control RNAi samples. Abbreviation – hpi: hours post-irradiation.

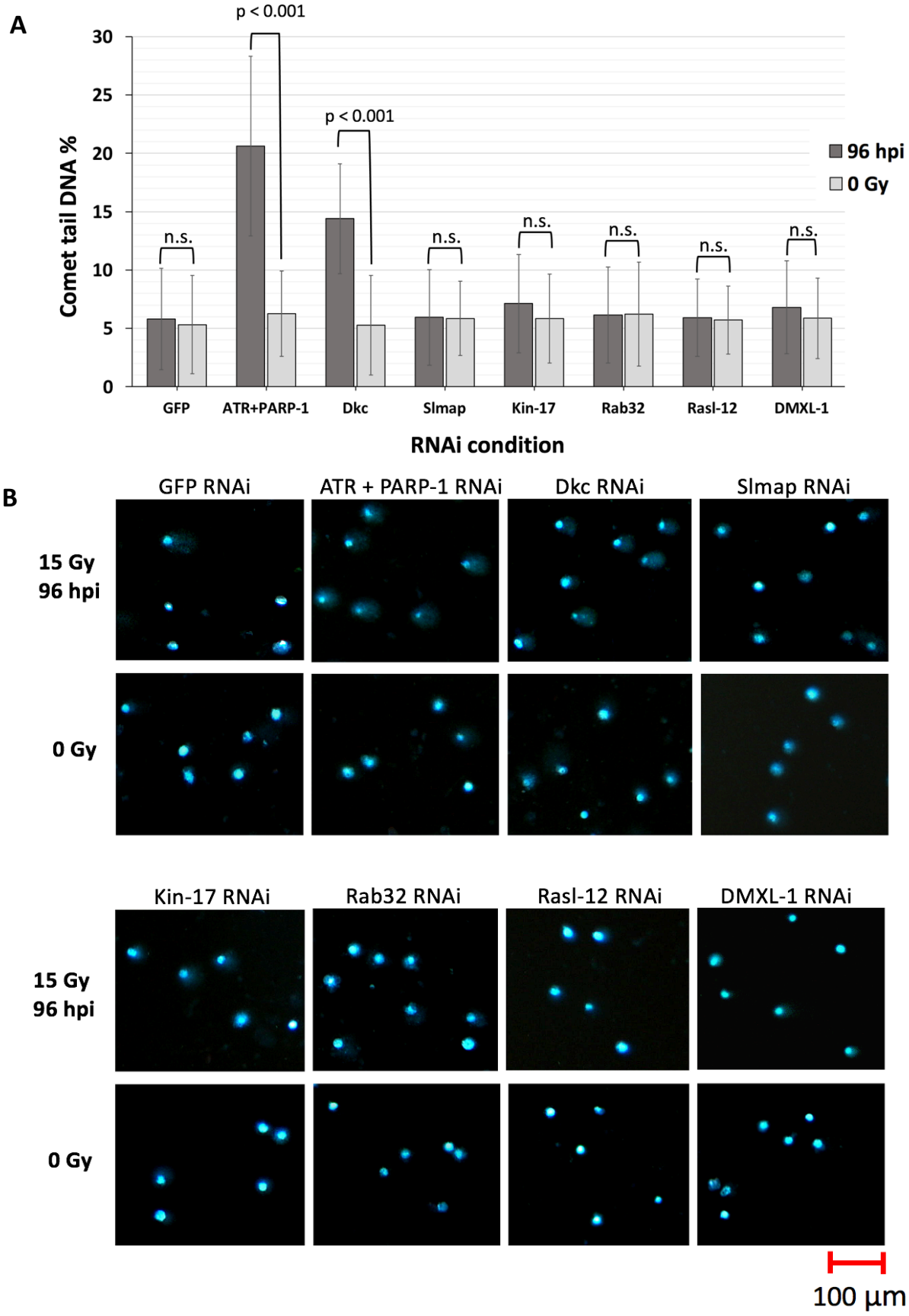

Figure 37. Comet assay analysis of DNA stand break repair capacity in cells under various RNAi-treated backgrounds. (A) Quantification of the average percentage of comet tail DNA in cells at 96 hours post-irradiation (hpi) and in non-irradiated samples across different RNAi treatments. **(B)** Representative fluorescence images showing the extent of comet tail formation in cells, both at 96 hpi and under non-irradiated conditions, under different RNAi-treated backgrounds.

In the assessments of our genes-of-interest, we observed that samples subjected to Dkc RNAi in conjunction with sub-lethal irradiation exhibited delayed DNA repair kinetics when compared to the non-targeting GFP control. This delay is evidenced, with statistical significance, by the consistently higher average percentages of DNA within comet tails at all tested timepoints following irradiation in the Dkc RNAi group, relative to the negative control group (Figure 36C). Moreover, the level of DNA damage did not return to baseline levels by 96 hours post-irradiation in cells subjected to Dkc RNAi (Figure 36C, Figure 37A). The reduced rate of DNA strand break repair in Dkc RNAi-treated animals implicates the gene as a novel and potentially conserved regulator of this process following irradiation.

However, in the cases of cells subjected to single-RNAi of Slmap, Kin-17, Rab32, Rasl-12, and DMXL-1, we observed that their post-irradiation DNA strand-break repair kinetics closely resembled those of our negative control group. This is supported by the absence of statistically significant differences in the percentages of comet tail DNA relative to negative controls at each corresponding timepoint following irradiation. Furthermore, akin to the negative control group, the percentage of comet tail DNA in samples subjected to RNAi of Slmap, Kin-17, Rab32, Rasl-12, and DMXL-1 returned to baseline levels at the 96-hour post-irradiation timepoint (Figure 37A). Our findings indicate that these five genes are not essential for repairing DNA strand breaks in planarians following irradiation.

Concurrently, we evaluated the extent of DNA strand breaks in cells subjected to each gene knockdown under non-irradiated conditions. We achieved this by performing the Comet assay on unirradiated samples taken at 24 hours after the final injection dose. This experiment aimed to investigate whether any of our genes-of-interest play a role in DNA strand break repair and thus contribute to the preservation of genomic stability during homeostasis. Our observations revealed that all gene knockdowns, including our positive control, exhibited baseline levels of DNA damage, with no significant differences observed compared to our negative control group (Figure 37A). This observation suggests that our genes-of-interest are not essential for maintaining genomic stability under non-irradiated conditions. Alternatively, it is possible that the assay lacks the necessary sensitivity to detect relatively low levels of DNA damage in the absence of a genotoxic agent, such as gamma radiation.

Taken together, our assay has unveiled a novel and potentially vital role of Dkc in the repair of DNA strand breaks in planarians following irradiation. In contrast, for animals subjected to RNAi targeting Slmap, Kin-17, Rab32, Rasl-12, and DMXL-1, the observed defects in neoblast cell-cycle re-entry may be attributed to factors unrelated to DNA strand break repair, necessitating further exploration. While the Comet assay demonstrates that the knockdown of these five genes does not compromise DNA strand break repair, it is important to recognize that DNA strand breaks represent only one of the many forms of DNA damage that can occur in the genome after irradiation (Reisz et al., 2014). One limitation of the Comet assay is its restricted ability to detect only DNA strand breaks, hence potentially overlooking other forms of DNA damage that can result from exposure to gamma radiation. Such lesions can include crosslinks, oxidative damage, and erroneous base modifications (Breimer, 1988; Reisz et al., 2014; Cadet and Davies, 2017), whose ongoing presence could inhibit stem cell proliferation. Furthermore, although our assay provides evidence of functional DNA strand break repair in animals subjected to RNAi of Slmap, Kin-17, Rab32, Rasl-12, and DMXL-1, the assay does not offer insights into repair fidelity. Thus, it remains plausible that our genes-of-interest continue to uphold important roles in the broader DNA repair process, potentially contributing to the repair of lesions beyond strand breaks, as well as potentially influencing repair fidelity.

Another constraint inherent to our assay is its inability to pinpoint the specific cell-of-origin for each comet. While our assay offers valuable insights into global DNA strand break repair in planarians subjected to targeted gene knockdown coupled with irradiation, it lacks the capacity to distinguish and measure DNA damage specifically occurring in stem cells or non-stem cells. It is conceivable that the effects of these gene knockdowns on the DNA repair process vary between stem and non-stem cells. Therefore, our assessment of global DNA strand break repair, while informative, cannot be directly extrapolated to stem cells without further investigation.

RNAi of Slmap, Kin-17, and Dkc renders planarians sensitive to 10 Gy acute gamma radiation

In Chapter 4, our primary RNAi screen revealed that individually silencing Slmap, Kin-17, Dkc, Rab32, Rasl-12, and DMXL-1 rendered planarians sensitive to a 15 Gy dose of acute whole-body gamma radiation. Recognizing that the impact of each of these six genes on planarian radiotolerance may vary, we investigated the survival of planarians subjected to targeted gene knockdown in conjunction with a 10 Gy dose of whole-body acute gamma irradiation. Notably, the 10 Gy dose employed in this experiment was intentionally set lower than the sub-lethal 15 Gy dose previously used in our RNAi screen and subsequent gene characterization assays. One aim of this experiment was to identify and categorize target genes capable of rendering planarians sensitive to 10 Gy gamma irradiation upon knockdown. Such an effect would elucidate a subgroup of knockdowns that demonstrate a more pronounced degree of radio-sensitization, thereby exerting a stronger influence on planarian radiotolerance as compared to genes whose RNAi effects are only penetrant at the 15 Gy dose.

In addition, this assay provided an opportunity to validate whether bottleneck effects influenced our earlier observations of animal mortality when gene knockdown was combined with 15 Gy irradiation. In our 15 Gy experiments, our negative control group displayed an average initial stem cell survival rate of 2.86% (Figure 32A), closely mirroring the 3.01% previously recorded in our group for wild-type planarians irradiated at the same dose (Sahu et al., 2021). Given the relatively small number of surviving stem cells at the 15 Gy dose, there was a potential for bottleneck effects to arise, particularly in the context of RNAi targeting Slmap, Kin-17, and Dkc. In these three cases, even fewer stem cells initially survived the 15 Gy dose (Figure 32A), possibly leading to a scenario where no rescue-competent stem cells remained due to random chance, characteristic of a bottleneck effect. Conducting the combined RNAi and irradiation assay at a lower dose, such as the 10 Gy dose, where an initial stem cell survival rate of 13.40% was previously recorded for wild-type planarians (Sahu et al., 2021), would make the stem cell recovery process less susceptible to the influence of bottleneck effects.

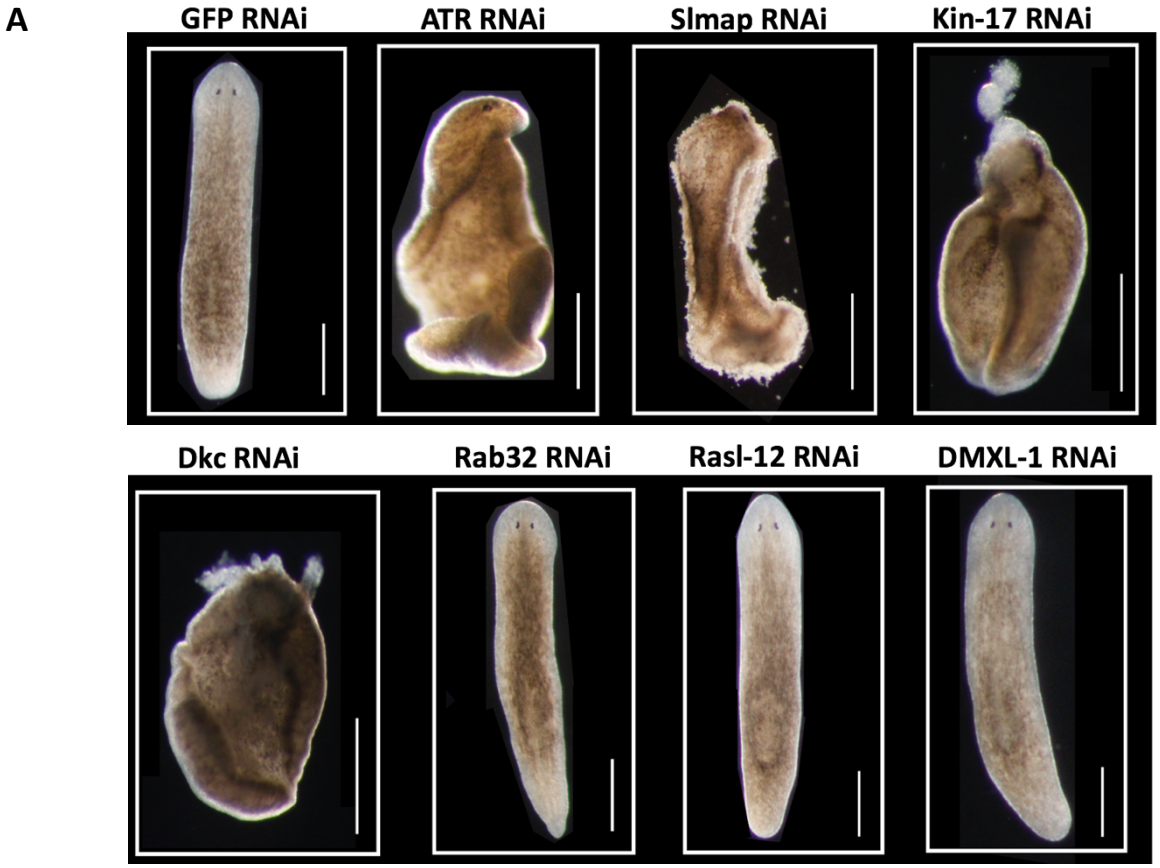
A
GFP RNAi
ATR RNAi
Slmap RNAi
Kin-17 RNAi
Dkc RNAi
Rab32 RNAi
Rasl-12 RNAi
DMXL-1 RNAi

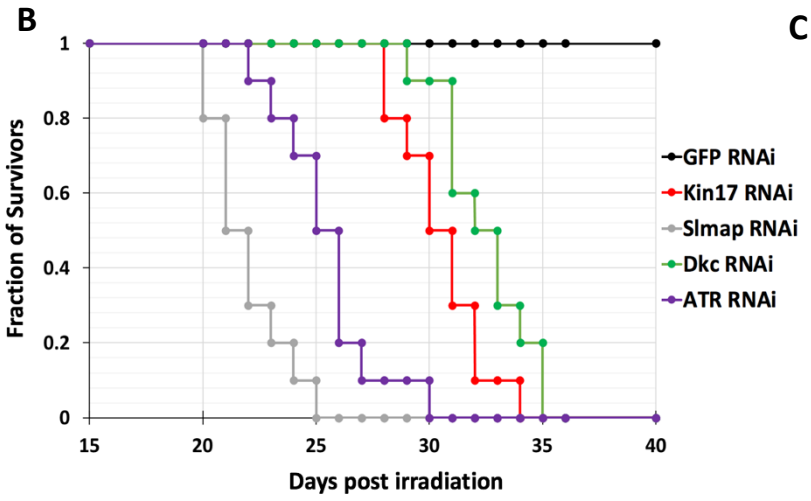
B
Fraction of Survivors
Days post irradiation
GFP RNAi
Kin17 RNAi
Slmap RNAi
Dkc RNAi
ATR RNAi

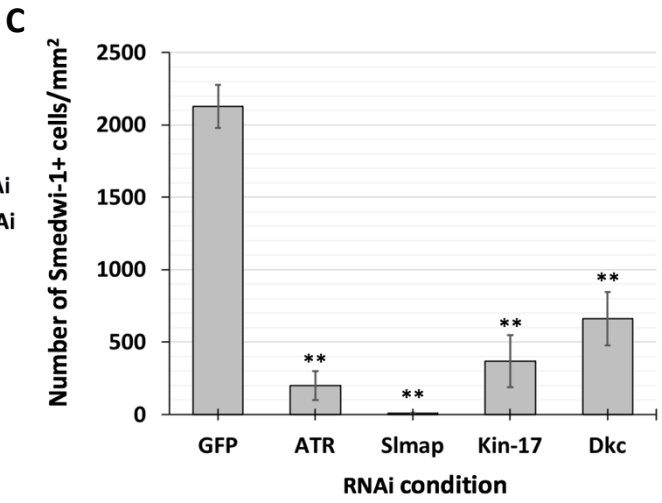
C
Number of Smedwi-1+ cells/mm²
RNAi condition
GFP
ATR
Slmap
Kin-17
Dkc

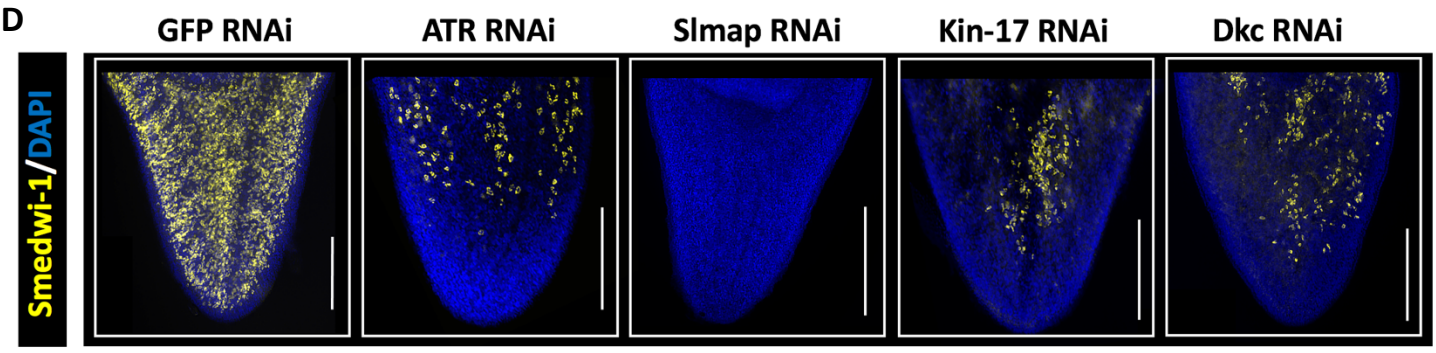
D
GFP RNAi
ATR RNAi
Slmap RNAi
Kin-17 RNAi
Dkc RNAi
Smedwi-1/DAPI

Figure 38. RNAi of Slmap, Kin-17 and Dkc renders planarians sensitive to 10 Gy gamma irradiation **(A)** Morphology of animals subjected to targeted RNAi in combination with 10 Gy acute gamma irradiation, captured through brightfield microscopy. n=10 for all conditions. Scale bars represent 1 mm. Images of surviving animals were captured at the 50-day post-irradiation mark, while animals displaying morphological changes were documented at various timepoints in correlation with the survival curves outlined in (B). **(B)** Survival curves showing the outcomes for animals subjected to targeted gene RNAi and sub-lethal irradiation. n=10 for all conditions. Survival curves for Rab32, Rasl-12, and DMXL-1 RNAi were omitted as these knockdowns coupled with 10 Gy irradiation failed to show any instances of animal mortality. **(C)** Quantification of Smedwi-1^{+} cells/mm^{2} in various RNAi-treated animals at 21 days post-exposure to 10 Gy gamma radiation. Asterisks (**) indicate statistically significant differences compared to the GFP control with unpaired t-test p-values <0.001. **(D)** Representative Smedwi-1 fluorescence in situ hybridisation images of planarian tail regions derived from animals subjected to targeted RNAi at 21 days post-irradiation. Scale bars represent 0.5 mm.

In our assay, we observed that single-RNAi targeting Slmap, Kin-17, and Dkc efficiently rendered planarians sensitive to a 10 Gy dose of acute whole-body gamma radiation. Specifically, we documented a 100% mortality rate (n=10) among animals subjected to the individual knockdown of these three genes in combination with 10 Gy irradiation (Figure 38B). All animals that perished in this assay displayed anterior regression, ventral curling, and eventual tissue lysis (Figure 38A), a sequence of events reminiscent of the stereotypical ablation-in-stem-cell-function phenotype within planarians (Reddien et al., 2005; Rink, 2013). In contrast, no instances of mortality nor abnormal morphological changes were observed in animals subjected to single-RNAi treatments targeting Rab32, Rasl-12, and DMXL-1 in conjunction with 10 Gy gamma irradiation (Figure 38A).

These findings place Slmap, Kin-17, and Dkc in a distinct category due to their more potent radio-sensitizing effects upon gene knockdown. Our observations further emphasize their crucial roles as indispensable regulators of planarian radiotolerance. In addition, achieving 100% lethality following the combined treatment of gene knockdown and 10 Gy irradiation provides confidence that the knockdown-induced impairments in the planarian stem cell recovery process are not caused by bottleneck effects.

Furthermore, we conducted in situ hybridization at 21 days post-irradiation targeting the stem cell marker, Smedwi-1. This investigation aimed to establish a correlation between our observations of animal mortality and the underlying stem cell activities in animals subjected to Slmap, Kin-17, and Dkc RNAi coupled with 10 Gy gamma irradiation. While we had previously observed a complete abolition of stem cell recovery in Slmap, Kin-17, and Dkc RNAi-treated animals at 15 Gy (Figure 32B, Figure 33), we also observed disruptions in post-irradiation stem cell recovery at 10 Gy, albeit with varying degrees of impairment among different genes. Specifically, the complete absence of stem cell recovery at 15 Gy for Slmap-RNAi-treated animals was observed to extend to the 10 Gy dose, as no stem cells were detected within these animals at 21 days post-irradiation (Figure 38C, 38D). The effects of Slmap-RNAi also appeared to be stronger than that of our positive-control, which consisted of ATR RNAi-treated animals exposed to 10 Gy irradiation, as some degree of stem cell recovery was observed in the latter (Figure 38C, 38D). This finding may be linked to our earlier observation of impacted stem cell maintenance upon Slmap RNAi under non-irradiated conditions (Chapter 4 – Figure 23), as Slmap RNAi-treated animals may harbour pre-existing stem cell defects even prior to irradiation treatment.

In the cases of Kin-17 and Dkc RNAi, the animals displayed a delayed stem cell expansion phenotype following 10 Gy irradiation. These animals exhibited a reduced number of stem cells compared to the non-targeting GFP control at 21 days post-irradiation, with the differences being statistically significant (Figure 38C, 38D). Although some degree of stem cell recovery was observed in animals subjected to RNAi of ATR, Kin-17, and Dkc in conjunction with 10 Gy irradiation, we infer that the level of stem cell activity within these animals was inadequate to sustain their essential functions, ultimately leading to the observed fatal outcomes.

Chapter 5 – Conclusion and future perspectives

In this chapter, we analysed the phylogeny and investigated the radiation-responsive functions of Slmap, Kin-17, Dkc, Rab32, Rasl-12, and DMXL-1. These six genes were selected for investigation given their observed capacity to sensitize planarians to gamma radiation upon knockdown, as detailed in Chapter 4. Phylogenetic analyses revealed that the Rasl-12 gene in our study represents a platyhelminth-specific innovation. In contrast, Slmap, Kin-17, Dkc, Rab32, and DMXL-1 were identified to exhibit strong conservation across metazoans. To shed preliminary insight into the functions of our target genes, we conducted a thorough literature review to understand the documented functions of their orthologues, where present. These genes were discerned to uphold diverse functions across various model systems, with Kin-17 standing out as the only gene that had been directly linked to radiation response or DNA repair processes prior to this study.

We then utilized the planarian model system to examine the in vivo functions of these six genes in the context of adult stem cell radiation response and recovery. Our approach involved probing the functionality of various recovery stages, encompassing DNA strand break repair, cell-cycle re-entry, stem cell proliferation, and stem cell differentiation, to pinpoint the specific stage of recovery that is impacted by each targeted gene knockdown.

Collectively, our findings enable us to categorize our genes-of-interest into two distinct groups based on their impact on planarian stem cell dynamics following knockdown and irradiation. Firstly, the application of RNAi targeting Slmap, Kin-17, and Dkc led to a state of proliferation incompetency within the residual population of surviving stem cells, as stem cell recovery was completely abolished within the RNAi-treated animals exposed to 15 Gy gamma irradiation. In contrast, assessments of Smedwi-1^{+} and H3P^{+} cell dynamics in animals subjected to RNAi targeting Rab32, Rasl-12, and DMXL-1 revealed that some, if not all, of the surviving stem cells retained the capacity to proliferate after exposure to the same dose. However, these knockdowns induced an aberrantly prolonged state of neoblast cell-cycle arrest, resulting in a substantial delay in the stem cell recovery process. This

categorization of genes, with Slmap, Kin-17, and Dkc in one subset and Rab32, Rasl-12, and DMXL-1 in another, can also be extended to their effects on planarian survival after exposure to a lower, 10 Gy dose of acute gamma radiation. Specifically, RNAi of Slmap, Kin-17, and Dkc induced a more pronounced radio-sensitizing effect in planarians by rendering them sensitive to 10 Gy irradiation. In contrast, the latter group of gene knockdowns did not possess such potency.

In both these assays, incorporating additional intermediate timepoints would improve the precision of recovery kinetics analysis for stem cells, progeny cells, and mitotic cells in response to both knockdown and irradiation. For instance, our initial stem cell number measurement was conducted at 3 days post-irradiation, with the primary focus on examining the stem cell recovery phase. However, this assay does not capture the kinetics of stem cell number decline immediately after irradiation. In the future, evaluating stem cell numbers at multiple timepoints between exposure and the 3-day post-irradiation mark can help us understand whether any of the knockdowns influence the pattern of stem cell decline. This in turn may illuminate knockdown-induced defects that affect the decision-making process of stem cells regarding their fate post-irradiation.

Furthermore, the penultimate and final timepoints where stem cell numbers were measured were at day 14 and day 21 post-irradiation, respectively. There is a relatively large gap between these two timepoints, and our extrapolation of stem cell numbers over this period may cause us to overlook crucial details, particularly in the cases involving Rab32, Rasl-12, and DMXL-1 RNAi. This is because stem cell numbers were observed to be in the early incremental phase in these three cases. Examining the dynamics of both stem cell and $H3P^{+}$ cell counts more precisely during the progression of this phase may provide insight into whether the rate of stem cell proliferation is affected by the knockdowns once the state of cell-cycle arrest is eventually withdrawn. This may clarify whether proliferation defects, additional to the abnormally prolonged state of cell-cycle arrest, contribute to the overall delay in stem cell recovery.

Subsequently, we conducted alkaline Comet assays to assess whether knockdown-induced impairments in DNA stand break repair might be responsible for the observed deficiencies in stem cell proliferation post-irradiation. We observed that RNAi of Dkc hindered global DNA strand break repair following exposure to 15 Gy gamma radiation. However, animals subjected to RNAi targeting Slmap, Kin-17, Rab32, Rasl-12, and DMXL-1 did not display post-irradiation DNA strand break repair defects.

One limitation of the alkaline Comet assay is that it measures both single-stranded and double-stranded breaks collectively (Olive and Banath, 2006). Given that most DNA breaks formed after irradiation are single-stranded (Roots et al., 1985), there is a potential oversight in assessing the repair of double-stranded breaks. Deficiencies in double-stranded break repair due to knockdown may be substantially less apparent due to the disproportionate ratio between these two types of lesions. Future optimization of the neutral Comet assay, which specifically quantifies DNA double-stranded breaks (Olive and Banath, 2006), could be beneficial. By integrating the results of the neutral Comet assay with existing data from the alkaline Comet assay, we can clarify the distinction between the repair of single-stranded and double-stranded breaks. This in turn can inform us on whether any of our genes-of-interest contribute to either or both of these crucial processes.

Another recognized limitation of our Comet assay strategy is its inability to specifically quantify DNA strand breaks and their repair within stem cells. To address this challenge, studying the effects of targeted gene knockdown on stem cell DNA strand-break repair could involve immunofluorescence assays targeting DNA repair factors such as yH2AX, Rad51, and PAR, in combination with the stem cell marker, Smedwi-1. Notably, within our research group, commercially available guinea pig polyclonal Rad51 antibodies and rabbit polyclonal PAR antibodies have proven successful in generating signals within planarian tissue sections. The next phase entails generating and optimizing an antibody that reacts specifically with planarian Smedwi-1, and co-staining it alongside Rad51 or PAR. As for yH2AX, a marker for double-strand breaks, commercially available antibodies targeting human yH2AX have demonstrated cross-reactivity with planarian yH2AX in the literature (Yin et al., 2016; Thiruvalluvan et al., 2018), albeit with suboptimal signal-to-noise quality ratios. However, our prior attempts using human, *Drosophila*, and a custom-made planarian

antibody to target planarian yH2AX were unsuccessful, necessitating further optimization efforts.

Besides DNA repair, neoblast cell-cycle re-entry, proliferation, and differentiation, another vital cellular process for animal recovery from gamma radiation is the mitigation of oxidative stress. This is because a significant source of cytotoxic damage following exposure to gamma radiation is attributed to the activity of reactive oxygen species (ROS), whose intracellular concentrations surge after radiation exposure (Azzam et al., 2012). Exploring whether the heightened radiosensitivity of planarians can be linked to knockdown-induced deficiencies in oxidative stress-relief pathways could be beneficial. Efforts by Jaenen and colleagues have successfully optimized the use of Carboxy-H2DCFDA and PO1 to measure ROS levels within planarian cells in vivo (Jaenen et al., 2021). Replicating these methods in future studies can allow us to assess the ROS scavenging capabilities of planarians under various RNAi-treated backgrounds, shedding light on the potential role of our target genes in antioxidant pathways.

Another informative experiment for future exploration involves examining whether our genes-of-interest similarly contribute to tolerance against other genotoxic agents. Alternative to gamma radiation, chemical alkylating agents such as Methyl methane-sulfonate (MMS) and Nitrosoguanidine (MNNG) have been previously dose-calibrated in planarians (Hollenbach et al., 2011; Stevens et al., 2017; Knakievicz et al., 2008). These agents could be used to study their effects on planarians under specific RNAi-treated backgrounds. Identifying genes that collectively impart tolerance against multiple genotoxic agents would reinforce their potential roles in the broader DNA repair process.

While this study has established our genes-of-interest as important regulators of planarian radiotolerance in vivo, whether these genes also impart chemoresistance to planarians is another area of interest. This is especially pertinent for the genes – Slmap, Kin-17, Dkc, Rab32, and DMXL-1, which are conserved in humans. Exploring whether these genes influence planarian stem cell responses to select anti-tumour drugs in vivo may offer valuable insights into how their respective human gene counterparts function in normal and cancer stem cells during chemotherapy.

Taken together, the experiments conducted thus far have offered valuable insight into the roles of our target genes in various cellular processes critical for recovery from sub-lethal irradiation. However, a more comprehensive understanding of their contributions to planarian radiotolerance requires a deeper molecular investigation. To achieve this, a combinatorial RNAi and RNA-sequencing approach in the future could be useful. In multiple model systems, Kin-17 and Dkc have been observed to directly interact with DNA, while Rab32, Rasl-12, Slmap and DMXL-1 have documented roles as signalling transducers in essential pathways. Silencing these genes and examining the resulting changes in cellular transcriptomes, both with and without exposure to gamma radiation, could be insightful to understand how our genes-of-interest influence signalling pathways and gene regulatory networks that potentially govern planarian radiotolerance. To specifically examine the regulatory functions of these genes in stem cells, conducting RNA-sequencing on sorted stem cells derived from RNAi-treated animals would be a practical approach.

In the wider framework, examining the orthologous genes in other model systems to understand their potential contributions to radiotolerance holds significant value. This approach could unveil novel and conserved regulators of radiation resistance that may be widely employed by different animals to counteract the detrimental effects of gamma radiation. Notably, the genes – Slmap, Kin-17, Dkc, Rab32, and DMXL-1, conserved between planarians and mammals, could also be of biomedical relevance. Currently, we are actively collaborating with Dr. Sounak Sahu (Sharan group, NIH) to investigate the functions of Rab32, Kin-17, and FHL-A (elaborated in Chapter 4) in human U2OS osteosarcoma cells. Ongoing experiments involve siRNA knockdowns of these three genes, followed by two phenotypic assessments in vitro. The first involves quantifying how the knockdowns influence cell survival rates after exposure to a sub-lethal dose of gamma radiation. The second aspect involves yH2AX staining to assess whether the knockdowns impact the process of double-stranded break repair in vitro. Our future plans include expanding the investigation to encompass the remaining genes identified in this study as crucial for planarian radiotolerance. Any observations of radio-sensitization from this primary assay in U2OS cells will lead to further study of the gene's effects on tumour organoids in secondary assays.

Overall, conserved genes found to also regulate the mammalian stem cell response to gamma radiation could emerge as prospective targets for therapeutic interventions. Such interventions could involve pharmaceutical modifications to their activity, potentially offering clinical advantages such as imparting radioprotection to normal stem cells, or by sensitizing cancer stem cells to radiotherapy

Concluding remarks

In this project, we adopted a functional genomics approach to investigate the mechanisms employed by planarian stem cells to withstand relatively high doses of acute gamma radiation. Planarians, which harbour abundant populations of experimentally tractable adult stem cells, served as an attractive in vivo model system for advancing our comprehension of stem cell radiation response and tolerance. Our primary objectives were to understand the transcriptomic responses of planarian stem cells when challenged with acute gamma radiation, and to identify novel regulators of planarian radiotolerance in vivo.

In the introductory chapter, we provided a brief description of DNA damage and the DNA damage response. We then discussed the genotoxic effects of ionizing radiation, followed by examining how normal and cancer stem cells in mammals differentially respond to ionizing radiation exposure. We conducted a thorough literature review of acute ionizing radiation tolerance across metazoans and discussed the use of alternative model organisms in the study of radiotolerance. We outlined the distinctive traits that make planarians an attractive in vivo model system to expand our understanding of adult stem cell radiation response and tolerance.

In Chapter 3, we generated SPLiT-Seq libraries of irradiated planarians. Our single-cell gene expression atlases unveiled three distinct neoblast clusters exhibiting varying sensitivity to gamma radiation. Additionally, RNA velocity analyses unveiled time and dose-dependent changes in neoblast fate trajectories following irradiation. By investigating the markers enriched in each neoblast cluster and integrating these findings with the inferred cell fate transitions, we proposed a model linking neoblast cluster affiliation with cell cycle stage, with stem cells in S/G2/M phases being more susceptible to acute gamma radiation.

In Chapter 4, we integrated our single-cell data with our previous post-irradiation transcriptome of bulk X1 cells to select candidate genes for an RNAi screen. Our RNAi screen, which encompassed the silencing of 105 single genes, unveiled six genes – Slmap, Kin-17, Dkc, Rab32, Rasl-12, and DMXL-1 – whose knockdowns heightened planarian sensitivity to gamma radiation in vivo. Our screen also unveiled 20 additional single-gene

knockdowns that significantly delayed the stem cell recovery process following sub-lethal irradiation, although these knockdowns alone were insufficient to cause animal mortality. Notably, multiple members of the FHL family and another LIM-domain-containing protein, LHX-1, collectively upregulated in our RNA-sequencing dataset of gamma-irradiated X1 cells, were among the gene knockdowns causing this delay phenotype. To probe for redundancies between these genes, we silenced their expression in all possible combinatorial pairs, revealing four RNAi pairs – FHL-A + FHL-3, FHL-A + LHX-1, FHL-2 + FHL-4, and FHL-4 + LHX-1, that sensitized planarians to gamma radiation.

In Chapter 5, we investigated the in vivo functions of Slmap, Kin-17, Dkc, Rab32, Rasl-12, and DMXL-1 in the regulation of planarian radiotolerance. We first determined that the genes – Slmap, Kin-17, Dkc, Rab32, and DMXL-1 were conserved across metazoans. The documented functions of their orthologues in other model systems were reviewed. Furthermore, we identified that the Rasl-12 gene in our study represents a platyhelminth-specific innovation. In our in vivo assessments of gene function, we assessed the integrity of various post-irradiation recovery phases, encompassing DNA strand break repair, neoblast cell-cycle re-entry, proliferation, and differentiation. We found that the residual surviving stem cells in Slmap, Kin-17, and Dkc RNAi-treated animals were proliferation incompetent after exposure to 15 Gy acute gamma radiation. Additionally, single-RNAi targeting these three genes were sufficiently potent to sensitize planarians to 10 Gy acute gamma radiation. In contrast, RNAi of Rab32, Rasl-12, and DMXL-1 led to an abnormally prolonged state of cell-cycle arrest in the remaining stem cells, resulting in significantly delayed stem cell recovery that ultimately prevented animal survival. Through the alkaline Comet assay, we were able to establish a link between the failure in neoblast cell-cycle re-entry and impaired DNA strand-break repair in animals subjected to Dkc RNAi.

Future work aims to enhance our bulk and single-cell RNA-sequencing datasets by implementing higher sensitivity methods, enabling a more comprehensive understanding of the gene regulatory networks that may drive planarian radiotolerance. Moreover, applying omics-based approaches to the study of our genes-of-interest in the future could improve our mechanistic understanding of their functions in planarians both under homeostatic and irradiated conditions. Additionally, future efforts could include testing the genes identified

in this study as crucial for planarian radiotolerance in other model organisms, potentially revealing conserved mechanisms employed by animals to counteract the deleterious effects of gamma radiation. The potential conservation of these mechanisms in mammals may also hold biomedical relevance, as targeting these genes could be explored for imparting radioprotection to normal stem cells, or to sensitize cancer stem cells to radiotherapy.

References

Abi-Rached, L., Gilles, A., Shiina, T., Pontarotti, P., & Inoko, H. (2002). Evidence of en bloc duplication in vertebrate genomes. *Nature genetics*, 31(1), 100–105. https://doi.org/10.1038/ng855

Aboobaker, A. A. (2011). Planarian stem cells: a simple paradigm for regeneration. *Trends in cell biology*, *21*(5), 304–311. https://doi.org/10.1016/j.tcb.2011.01.005

Acharya, M., Lan, M., Kan, V., Patel, N., Giedzinski, E., Tseng, B. & Limoli, C. (2010). Consequences of ionizing radiation-induced damage in human neural stem cells. *Free Radical Biology and Medicine*, 49(12), pp.1846-1855. https://doi.org/10.1016/j.freeradbiomed.2010.08.021

Adler, C., Seidel, C., McKinney, S. & Sánchez Alvarado, A. (2014). Selective amputation of the pharynx identifies a FoxA-dependent regeneration program in planaria. *eLife*, *3*, e02238. https://doi.org/10.7554/eLife.02238

Agata, K. (2003). Regeneration and gene regulation in planarians. *Current opinion in genetics & development*, *13*(5), 492–496. https://doi.org/10.1016/j.gde.2003.08.009

Ahmad, M., & Taqawi, I. H. (1978). Effect of gamma-rays on the life-shortening of the lizard Uromastix hardwickii. *Radiobiologia, radiotherapia*, *19*(5), 606–611.

Ahmed, S., Carruthers, R., Gilmour, L., Yildirim, S., Watts, C. & Chalmers, A. (2015). Selective Inhibition of Parallel DNA Damage Response Pathways Optimizes Radiosensitization of Glioblastoma Stem-like Cells. *Cancer Research*, 75(20), pp.4416-4428. https://doi.org/10.1158/0008-5472.CAN-14-3790

Almuedo-Castillo, M., Crespo-Yanez, X., Seebeck, F., Bartscherer, K., Salò, E., & Adell, T. (2014). JNK controls the onset of mitosis in planarian stem cells and triggers apoptotic cell death required for regeneration and remodeling. *PLoS genetics*, *10*(6), e1004400. https://doi.org/10.1371/journal.pgen.1004400

Altenhoff, A. M., Train, C. M., Gilbert, K. J., Mediratta, I., Mendes de Farias, T., Moi, D., Nevers, Y., Radoykova, H. S., Rossier, V., Warwick Vesztrocy, A., Glover, N. M., & Dessimoz, C. (2021). OMA orthology in 2021: website overhaul, conserved isoforms, ancestral gene order and more. *Nucleic acids research*, *49*(D1), D373–D379. https://doi.org/10.1093/nar/gkaa1007

Alto, N. M., Soderling, J., & Scott, J. D. (2002). Rab32 is an A-kinase anchoring protein and participates in mitochondrial dynamics. *The Journal of cell biology*, *158*(4), 659–668. https://doi.org/10.1083/jcb.200204081

Anderson, S. L., Harrison, F. L., Chan, G., & Moore, D. H. (1990). Comparison of cellular and whole-animal bioassays for estimation of radiation effects in the polychaete worm Neanthes arenaceodentata (Polychaeta). *Archives of environmental contamination and toxicology*, *19*(2), 164–174. https://doi.org/10.1007/BF01056083

Andrews, S. (2010). FastQC: A Quality Control Tool for High Throughput Sequence Data. Available at https://github.com/s-andrews/FastQC

Andrieu-Abadie, N., & Levade, T. (2002). Sphingomyelin hydrolysis during apoptosis. *Biochimica et biophysica acta*, *1585*(2-3), 126–134. https://doi.org/10.1016/s1388-1981(02)00332-3

Anoud, M., Delagoutte, E., Helleu, Q., Brion, A., Duvernois-Berthet, E., As, M., Marques, X., Lamribet, K., Senamaud, C., Jourdren, L., Adrait, A., Heinrich, S., Toutirais, G., Hamlaoui, S., Gropplero, G., Giovannini, I., Ponger, L., Gèze, M., Blugeon, C., Coute, Y., Guidetti, R., Rebecchi, L., Giovannangeli, C., De Cian, A., Concordet, J. (2024). Comparative transcriptomics reveal a novel tardigrade specific DNA binding protein induced in response to ionizing radiation. *eLife 13:RP92621*. https://doi.org/10.7554/eLife.92621.1

Antosh, M., Fox, D., Hasselbacher, T., Lanou, R., Neretti, N., & Cooper, L. N. (2014). Drosophila melanogaster show a threshold effect in response to radiation. *Dose-response : a publication of International Hormesis Society*, *12*(4), 551–581. https://doi.org/10.2203/dose-response.13-047.Antosh

Aravin, A. A., Hannon, G. J., & Brennecke, J. (2007). The Piwi-piRNA pathway provides an adaptive defense in the transposon arms race. *Science (New York, N.Y.)*, *318*(5851), 761–764. https://doi.org/10.1126/science.1146484

Ash, P. (1980). The influence of radiation on fertility in man. *The British journal of radiology*, *53*(628), 271–278. https://doi.org/10.1259/0007-1285-53-628-271

Avery, O. T., Macleod, C. M., & McCarty, M. (1944). Studies on the chemical nature of the substance inducing transformation of Pneumococcal Types: Induction of transformation by a Deoxyribonucleic acid fraction isolated from Pneumococcus Type III. *The Journal of experimental medicine*, *79*(2), 137–158. https://doi.org/10.1084/jem.79.2.137

Aylon, Y. & Oren, M. (2007). Living with p53, Dying of p53. *Cell*, 130(4), pp.597-600. https://doi.org/10.1016/j.cell.2007.08.005

Ayrapetov, M., Gursoy-Yuzugullu, O., Xu, C., Xu, Y. & Price, B. (2014). DNA double-strand breaks promote methylation of histone H3 on lysine 9 and transient formation of repressive chromatin. *Proceedings of the National Academy of Sciences*, 111(25), pp.9169-9174. https://doi.org/10.1073/pnas.1403565111

Azzam, E. I., Jay-Gerin, J. P., & Pain, D. (2012). Ionizing radiation-induced metabolic oxidative stress and prolonged cell injury. *Cancer letters*, *327*(1-2), 48–60. https://doi.org/10.1016/j.canlet.2011.12.012

Bach, I. (2000). The LIM domain: regulation by association. *Mechanisms of development*, *91*(1-2), 5–17. https://doi.org/10.1016/s0925-4773(99)00314-7

Baguna, J., & Romero, R. (1981). Quantitative analysis of cell types during growth, degrowth and regeneration in the Planarians dugesia mediterranea and Dugesia Tigrina. *The Biology of the Turbellaria*, 181-194. doi:10.1007/978-94-009-8668-8_25

Baguna, J., Saló, E., & Auladell, C. (1989). Regeneration and pattern formation in Planarians: III. evidence that neoblasts are totipotent stem cells and the source of Blastema Cells. *Development*, 107(1), 77-86. doi:10.1242/dev.107.1.77

Banin, S., Moyal, L., Shieh, S., Taya, Y., Anderson, C. W., Chessa, L., Smorodinsky, N. I., Prives, C., Reiss, Y., Shiloh, Y., & Ziv, Y. (1998). Enhanced phosphorylation of p53 by ATM in response to DNA damage. *Science (New York, N.Y.)*, *281*(5383), 1674–1677. https://doi.org/10.1126/science.281.5383.1674

Bao, S., Wu, Q., McLendon, R., Hao, Y., Shi, Q., Hjelmeland, A., Dewhirst, M., Bigner, D. & Rich, J. (2006). Glioma stem cells promote radioresistance by preferential activation of the DNA damage response. *Nature*, 444(7120), pp.756-760. https://doi.org/10.1038/nature05236

Bardeen, C., & Baetjer, F. (1904). The inhibitive action of Roentgen rays on regeneration in planarians. *J Exp Zool.* 1904;1:191–195. doi: 10.1002/jez.1400010107.

Barghouth, P. G., Rojas, S., O'Dell, L. R., Betancourt, A. M., & Oviedo, N. J. (2022). Analysis of DNA Double-Stranded Breaks Using the Comet Assay in Planarians. *Methods in molecular biology (Clifton, N.J.)*, *2450*, 479–491. https://doi.org/10.1007/978-1-0716-2172-1_25

Barghouth, P. G., Thiruvalluvan, M., LeGro, M., & Oviedo, N. J. (2019). DNA damage and tissue repair: What we can learn from planaria. *Seminars in cell & developmental biology*, *87*, 145–159. https://doi.org/10.1016/j.semcdb.2018.04.013

Bartucci, M., Svensson, S., Romania, P., Dattilo, R., Patrizii, M., Signore, M., Navarra, S., Lotti, F., Biffoni, M., Pilozzi, E., Duranti, E., Martinelli, S., Rinaldo, C., Zeuner, A., Maugeri-Saccà, M., Eramo, A. & De Maria, R. (2011). Therapeutic targeting of Chk1 in NSCLC stem cells during chemotherapy. *Cell Death & Differentiation*, 19(5), pp.768-778. https://doi.org/10.1038/cdd.2011.170

Beausejour, C. (2003). Reversal of human cellular senescence: roles of the p53 and p16 pathways. *The EMBO Journal*, 22(16), pp.4212-4222. https://doi.org/10.1093/emboj/cdg417

Becht, E., McInnes, L., Healy, J., Dutertre, C. A., Kwok, I. W. H., Ng, L. G., Ginhoux, F., & Newell, E. W. (2018). Dimensionality reduction for visualizing single-cell data using UMAP. *Nature biotechnology*, 10.1038/nbt.4314. https://doi.org/10.1038/nbt.4314

Becker, D., Elsässer, T., Tonn, T., Seifried, E., Durante, M., Ritter, S. & Fournier, C. (2009). Response of human hematopoietic stem and progenitor cells to energetic carbon ions. *International Journal of Radiation Biology*, 85(11), pp.1051-1059. https://doi.org/10.3109/09553000903232850

Behrens, A., Sibilia, M., & Wagner, E. F. (1999). Amino-terminal phosphorylation of c-Jun regulates stress-induced apoptosis and cellular proliferation. *Nature genetics*, *21*(3), 326–329. https://doi.org/10.1038/6854

Beltrán-Pardo, E., Jönsson, K. I., Harms-Ringdahl, M., Haghdoost, S., & Wojcik, A. (2015). Tolerance to Gamma Radiation in the Tardigrade Hypsibius dujardini from Embryo to Adult Correlate Inversely with Cellular Proliferation. *PloS one*, *10*(7), e0133658. https://doi.org/10.1371/journal.pone.0133658

Benham-Pyle, B. W., Brewster, C. E., Kent, A. M., Mann, F. G., Jr, Chen, S., Scott, A. R., Box, A. C., & Sánchez Alvarado, A. (2021). Identification of rare, transient post-mitotic cell states that are induced by injury and required for whole-body regeneration in Schmidtea mediterranea. *Nature cell biology*, *23*(9), 939–952. https://doi.org/10.1038/s41556-021-00734-6

Bergantiños, C., Corominas, M., & Serras, F. (2010). Cell death-induced regeneration in wing imaginal discs requires JNK signalling. *Development (Cambridge, England)*, *137*(7), 1169–1179. https://doi.org/10.1242/dev.045559

Bergen, V., Lange, M., Peidli, S., Wolf, F. A., & Theis, F. J. (2020). Generalizing RNA velocity to transient cell states through dynamical modeling. *Nature biotechnology*, *38*(12), 1408–1414. https://doi.org/10.1038/s41587-020-0591-3

Bergen, V., Soldatov, R. A., Kharchenko, P. V., & Theis, F. J. (2021). RNA velocity-current challenges and future perspectives. *Molecular systems biology*, *17*(8), e10282. https://doi.org/10.15252/msb.202110282

Bertolini, S., Wang, B., Meier, B., Hong, Y., & Gartner, A. (2017). *Caenorhabditis elegans* BUB-3 and SAN-1/MAD3 Spindle Assembly Checkpoint Components Are Required for Genome Stability in Response to Treatment with Ionizing Radiation. *G3 (Bethesda, Md.)*, *7*(12), 3875–3885. https://doi.org/10.1534/g3.117.1122

Bhadra, M., Horikoshi, N., Pushpavallipvalli, S., Sarkar, A., Bag, I., Krishnan, A., Lucchesi, J., Kumar, R., Yang, Q., Pandita, R., Singh, M., Bhadra, U., Eissenberg, J. & Pandita, T. (2011). The role of MOF in the ionizing radiation response is conserved in Drosophila melanogaster. *Chromosoma*, 121(1), pp.79-90. https://doi.org/10.1007/s00412-011-0344-7

Bhargavan, M. (2008). Trends in the utilization of medical procedures that use ionizing radiation. *Health physics*, *95*(5), 612–627. https://doi.org/10.1097/01.HP.0000327659.4261

Bian, L., Meng, Y., Zhang, M., & Li, D. (2019). MRE11-RAD50-NBS1 complex alterations and DNA damage response: implications for cancer treatment. *Molecular cancer*, *18*(1), 169. https://doi.org/10.1186/s12943-019-1100-5

Biard, D. S., Miccoli, L., Despras, E., Frobert, Y., Creminon, C., & Angulo, J. F. (2002). Ionizing radiation triggers chromatin-bound kin17 complex formation in human cells. *The Journal of biological chemistry*, *277*(21), 19156–19165. https://doi.org/10.1074/jbc.M200321200

Biard, D. S., Saintigny, Y., Maratrat, M., Paris, F., Martin, M., & Angulo, J. F. (1997). Enhanced expression of the Kin17 protein immediately after low doses of ionizing radiation. *Radiation research*, *147*(4), 442–450. https://doi.org/10.2307/3579501

Biedka, M., Kuźba-Kryszak, T., Nowikiewicz, T., & Żyromska, A. (2016). Fertility impairment in radiotherapy. *Contemporary oncology* 20(3), 199–204. https://doi.org/10.5114/wo.2016.57814

Blagden, S. P., Gatt, M. K., Archambault, V., Lada, K., Ichihara, K., Lilley, K. S., Inoue, Y. H., & Glover, D. M. (2009). Drosophila Larp associates with poly(A)-binding protein and is required for male fertility and syncytial embryo development. *Developmental biology*, *334*(1), 186–197. https://doi.org/10.1016/j.ydbio.2009.07.016

Bohio, A. A., Sattout, A., Wang, R., Wang, K., Sah, R. K., Guo, X., Zeng, X., Ke, Y., Boldogh, I., & Ba, X. (2019). c-Abl-Mediated Tyrosine Phosphorylation of PARP1 Is Crucial for Expression of Proinflammatory Genes. *Journal of immunology (Baltimore, Md. : 1950)*, *203*(6), 1521–1531. https://doi.org/10.4049/jimmunol.1801616

Bolte, S., & Cordelières, F. P. (2006). A guided tour into subcellular colocalization analysis in light microscopy. *Journal of microscopy*, *224*(Pt 3), 213–232. https://doi.org/10.1111/j.1365-2818.2006.01706.x

Bonham, K., & Palumbo, R. (1951). Effects of x-rays on snails, crustacea, and algae. *Growth, 15(3),* 155–188.

Boutet, E., Lieberherr, D., Tognolli, M., Schneider, M., & Bairoch, A. (2007). UniProtKB/Swiss-Prot. *Methods in molecular biology (Clifton, N.J.)*, *406*, 89–112. https://doi.org/10.1007/978-1-59745-535-0_4

Bracker, T. U., Giebel, B., Spanholtz, J., Sorg, U. R., Klein-Hitpass, L., Moritz, T., & Thomale, J. (2006). Stringent regulation of DNA repair during human hematopoietic differentiation: a gene expression and functional analysis. *Stem cells (Dayton, Ohio)*, *24*(3), 722–730. https://doi.org/10.1634/stemcells.2005-0227

Bradshaw, B., Thompson, K., & Frank, U. (2015). Distinct mechanisms underlie oral vs aboral regeneration in the cnidarian Hydractinia echinata. *eLife*, *4*, e05506. https://doi.org/10.7554/eLife.05506

Brandl, H., Moon, H., Vila-Farré, M., Liu, S. Y., Henry, I., & Rink, J. C. (2016). PlanMine--a mineable resource of planarian biology and biodiversity. *Nucleic acids research*, *44*(D1), D764–D773. https://doi.org/10.1093/nar/gkv1148

Breimer, L. (1988). Ionizing radiation-induced mutagenesis. *British journal of cancer*, *57*(1), 6–18. https://doi.org/10.1038/bjc.1988.2

Brenner, M., & Hearing, V. J. (2008). The protective role of melanin against UV damage in human skin. *Photochemistry and photobiology*, *84*(3), 539–549. https://doi.org/10.1111/j.1751-1097.2007.00226.x

Brentnall, M., Rodriguez-Menocal, L., De Guevara, R. L., Cepero, E., & Boise, L. H. (2013). Caspase-9, caspase-3 and caspase-7 have distinct roles during intrinsic apoptosis. *BMC cell biology*, *14*, 32. https://doi.org/10.1186/1471-2121-14-32

Broad Institute. (2018). Picard Toolkit. Retrieved from http://broadinstitute.github.io/picard/

Brown, D. D. R., & Pearson, B. J. (2017). A Brain Unfixed: Unlimited Neurogenesis and Regeneration of the Adult Planarian Nervous System. *Frontiers in neuroscience*, *11*, 289. https://doi.org/10.3389/fnins.2017.00289

Bui, M., Gilady, S. Y., Fitzsimmons, R. E., Benson, M. D., Lynes, E. M., Gesson, K., Alto, N. M., Strack, S., Scott, J. D., & Simmen, T. (2010). Rab32 modulates apoptosis onset and mitochondria-associated membrane (MAM) properties. *The Journal of biological chemistry*, *285*(41), 31590–31602. https://doi.org/10.1074/jbc.M110.101584

Bujarrabal-Dueso, A., Sendtner, G., Meyer, D. H., Chatzinikolaou, G., Stratigi, K., Garinis, G. A., & Schumacher, B. (2023). The DREAM complex functions as conserved master regulator of somatic DNA-repair capacities. *Nature structural & molecular biology*, *30*(4), 475–488. https://doi.org/10.1038/s41594-023-00942-8

Burma, S., Chen, B., Murphy, M., Kurimasa, A. & Chen, D. (2001). ATM Phosphorylates Histone H2AX in Response to DNA Double-strand Breaks. *Journal of Biological Chemistry*, 276(45), pp.42462-42467. https://doi.org/10.1074/jbc.C100466200

Burrows, C., Abd Latip, N., Lam, S., Carpenter, L., Sawicka, K., Tzolovsky, G., Gabra, H., Bushel, M., Glover, D., Willis, A., Blagden, S. (2010). The RNA binding protein Larp1 regulates cell division, apoptosis and cell migration. *Nucleic Acids Res*. Sep;38(16):5542-53. doi: 10.1093/nar/gkq294.

Bushnell, B. (2014). BBMap: A Fast, Accurate, Splice-Aware Aligner. Lawrence Berkeley National Laboratory. LBNL-7065E. Retrieved from http://escholarship.org/uc/item/1h3515gn.

Butler, A., Hoffman, P., Smibert, P., Papalexi, E., & Satija, R. (2018). Integrating single-cell transcriptomic data across different conditions, technologies, and species. *Nature biotechnology*, *36*(5), 411–420. https://doi.org/10.1038/nbt.4096

Byers, J. T., Guzzo, R. M., Salih, M., & Tuana, B. S. (2009). Hydrophobic profiles of the tail anchors in SLMAP dictate subcellular targeting. *BMC cell biology*, *10*, 48. https://doi.org/10.1186/1471-2121-10-48

Bylicky, M., Mueller, G. & Day, R. (2018). Radiation resistance of normal human astrocytes: the role of non-homologous end joining DNA repair activity. *Journal of Radiation Research*, 60(1), pp.37-50. https://doi.org/10.1093/jrr/rry084

Cadet, J. & Wagner, J. (2013). DNA Base Damage by Reactive Oxygen Species, Oxidizing Agents, and UV Radiation. *Cold Spring Harbor Perspectives in Biology*, 5(2), pp.a012559-a012559. https://doi.org/10.1101/cshperspect.a012559

Cadet, J., & Davies, K. J. A. (2017). Oxidative DNA damage & repair: An introduction. *Free radical biology & medicine*, *107*, 2–12. https://doi.org/10.1016/j.freeradbiomed.2017.03.030

Canman, C. E., Lim, D. S., Cimprich, K. A., Taya, Y., Tamai, K., Sakaguchi, K., Appella, E., Kastan, M. B., & Siliciano, J. D. (1998). Activation of the ATM kinase by ionizing radiation and phosphorylation of p53. *Science (New York, N.Y.)*, *281*(5383), 1677–1679. https://doi.org/10.1126/science.281.5383.1677

Cannan, W. & Pederson, D. (2015). Mechanisms and Consequences of Double-Strand DNA Break Formation in Chromatin. *Journal of Cellular Physiology*, 231(1), pp.3-14. https://doi.org/10.1002/jcp.25048

Cao, J., Spielmann, M., Qiu, X., Huang, X., Ibrahim, D. M., Hill, A. J., Zhang, F., Mundlos, S., Christiansen, L., Steemers, F. J., Trapnell, C., & Shendure, J. (2019). The single-cell transcriptional landscape of mammalian organogenesis. *Nature*, *566*(7745), 496–502. https://doi.org/10.1038/s41586-019-0969-x

Carruthers, R., Ahmed, S., Strathdee, K., Gomez-Roman, N., Amoah-Buahin, E., Watts, C. & Chalmers, A. (2014). Abrogation of radioresistance in glioblastoma stem-like cells by inhibition of ATM kinase. *Molecular Oncology*, 9(1), pp.192-203. https://doi.org/10.1016/j.molonc.2014.08.003

Castedo, M., Perfettini, J., Roumier, T., Andreau, K., Medema, R. & Kroemer, G. (2004). Cell death by mitotic catastrophe: a molecular definition. *Oncogene*, 23(16), pp.2825-2837. https://doi.org/10.1038/sj.onc.1207528

Cebria, F., Nakazawa, M., Mineta, K., Ikeo, K., Gojobori, T. & Agata, K. (2002). Dissecting planarian central nervous system regeneration by the expression of neural-specific genes. *Development, Growth and Differentiation*, 44(2), pp.135-146. https://doi.org/10.1046/j.1440-169x.2002.00629.x

Chan, Y. & West, S. (2015). GEN1 promotes Holliday junction resolution by a coordinated nick and counter-nick mechanism. *Nucleic Acids Research*, 43(22), pp.10882-10892. https://doi.org/10.1093/nar/gkv1207

Chang, C., Chen, Y., Chou, S., Han, C., Chen, Y., Yang, C., Huang, C. & Lo, J. (2014). Distinct Subpopulations of Head and Neck Cancer Cells with Different Levels of Intracellular Reactive Oxygen Species Exhibit Diverse Stemness, Proliferation, and Chemosensitivity. *Cancer Research*, 74(21), pp.6291-6305. https://doi.org/10.1158/0008-5472.CAN-14-0626

Chang, L., Graham, P., Hao, J., Ni, J., Deng, J., Bucci, J., Malouf, D., Gillatt, D., & Li, Y. (2016). Cancer stem cells and signalling pathways in radioresistance. *Oncotarget*, *7*(10), 11002–11017. https://doi.org/10.18632/oncotarget.6760

Chatterjee, N., & Walker, G. C. (2017). Mechanisms of DNA damage, repair, and mutagenesis. *Environmental and molecular mutagenesis*, 58(5), 235–263. https://doi.org/10.1002/em.22087

Chaudhary, P. K., & Kim, S. (2021). An Insight into GPCR and G-Proteins as Cancer Drivers. *Cells*, 10(12), 3288. https://doi.org/10.3390/cells10123288

Chavez, C., Cruz-Becerra, G., Fei, J., Kassavetis, G. & Kadonaga, J. (2019). The tardigrade damage suppressor protein binds to nucleosomes and protects DNA from hydroxyl radicals. *eLife*, 8, e47682. https://doi.org/10.7554/eLife.47682

Chen, G., Yuan, S. S., Liu, W., Xu, Y., Trujillo, K., Song, B., Cong, F., Goff, S. P., Wu, Y., Arlinghaus, R., Baltimore, D., Gasser, P. J., Park, M. S., Sung, P., & Lee, E. Y. (1999). Radiation-induced assembly of Rad51 and Rad52 recombination complex requires ATM and c-Abl. *The Journal of biological chemistry*, *274*(18), 12748–12752. https://doi.org/10.1074/jbc.274.18.12748

Chen, L., Nievera, C., Lee, A. & Wu, X. (2008). Cell Cycle-dependent Complex Formation of BRCA1·CtIP·MRN Is Important for DNA Double-strand Break Repair. *Journal of Biological Chemistry*, 283(12), pp.7713-7720. https://doi.org/10.1074/jbc.M710245200

Chen, M. F., Lin, C. T., Chen, W. C., Yang, C. T., Chen, C. C., Liao, S. K., Liu, J. M., Lu, C. H., & Lee, K. D. (2006). The sensitivity of human mesenchymal stem cells to ionizing radiation. *International journal of radiation oncology, biology, physics,* 66(1), 244–253. https://doi.org/10.1016/j.ijrobp.2006.03.062

Chen, P., Lu, Y., He, B., Xie, T., Yan, C., Liu, T., Wu, S., Yeh, Y., Li, Z., Huang, W., & Zhang, X. (2023). Rab32 promotes glioblastoma migration and invasion via regulation of ERK/Drp1-mediated mitochondrial fission. *Cell death & disease*, *14*(3), 198. https://doi.org/10.1038/s41419-023-05721-3

Chen, Y. R., Wang, X., Templeton, D., Davis, R. J., & Tan, T. H. (1996). The role of c-Jun N-terminal kinase (JNK) in apoptosis induced by ultraviolet C and gamma radiation. Duration of JNK activation may determine cell death and proliferation. *The Journal of biological chemistry*, *271*(50), 31929–31936. https://doi.org/10.1074/jbc.271.50.31929

Chen, Y., Li, D., Wang, D., Liu, X., Yin, N., Song, Y., Lu, S. H., Ju, Z., & Zhan, Q. (2012). Quiescence and attenuated DNA damage response promote survival of esophageal cancer stem cells. *Journal of cellular biochemistry*, *113*(12), 3643–3652. https://doi.org/10.1002/jcb.24228

Chen, Y., Su, Y., Chou, P., Chiang, W., Chang, M., Wang, L., Teng, S. & Wu, K. (2005). Overexpression of NBS1 Contributes to Transformation through the Activation of Phosphatidylinositol 3-Kinase/Akt. *Journal of Biological Chemistry*, 280(37), pp.32505-32511. https://doi.org/10.1074/jbc.M501449200

Cheng, L., Wu, Q., Huang, Z., Guryanova, O., Huang, Q., Shou, W., Rich, J. & Bao, S. (2011). L1CAM regulates DNA damage checkpoint response of glioblastoma stem cells through NBS1. *The EMBO Journal*, 30(5), pp.800-813. https://doi.org/10.1038/emboj.2011.10

Cheung, T. & Rando, T. (2013). Molecular regulation of stem cell quiescence. *Nature Reviews Molecular Cell Biology*, 14(6), pp.329-340. https://doi.org/10.1038/nrm3591

Choi, H. M. T., Schwarzkopf, M., Fornace, M. E., Acharya, A., Artavanis, G., Stegmaier, J., Cunha, A., & Pierce, N. A. (2018). Third-generation *in situ* hybridization chain reaction: multiplexed, quantitative, sensitive, versatile, robust. *Development (Cambridge, England)*, *145*(12), dev165753. https://doi.org/10.1242/dev.165753

Ciapponi, L., Jackson, D. B., Mlodzik, M., & Bohmann, D. (2001). Drosophila Fos mediates ERK and JNK signals via distinct phosphorylation sites. *Genes & development*, *15*(12), 1540–1553. https://doi.org/10.1101/gad.886301

Cmielova, J., Havelek, R., Soukup, T., Jiroutová, A., Visek, B., Suchánek, J., Vavrova, J., Mokry, J., Muthna, D., Bruckova, L., Filip, S., English, D. & Rezacova, M. (2012). Gamma radiation induces senescence in human adult mesenchymal stem cells from bone marrow and periodontal ligaments. *International Journal of Radiation Biology*, 88(5), pp.393-404. https://doi.org/10.3109/09553002.2012.666001

Cokol, M., Nair, R., & Rost, B. (2000). Finding nuclear localization signals. *EMBO reports*, *1*(5), 411–415. https://doi.org/10.1093/embo-reports/kvd092

Conger, A. & Clinton, J. (1973). Nuclear Volumes, DNA Contents, and Radiosensitivity in Whole-Body-Irradiated Amphibians. *Radiation Research*, 54(1), p.69. https://doi.org/10.2307/3573867

Conte, D., Jr, MacNeil, L. T., Walhout, A. J. M., & Mello, C. C. (2015). RNA Interference in Caenorhabditis elegans. *Current protocols in molecular biology*, *109*, 26.3.1–26.3.30. https://doi.org/10.1002/0471142727.mb2603s109

Cook, P., Ju, B., Telese, F., Wang, X., Glass, C. & Rosenfeld, M. (2009). Tyrosine dephosphorylation of H2AX modulates apoptosis and survival decisions. *Nature*, 458(7238), pp.591-596. https://doi.org/10.1038/nature07849

Corrado, G., Salutari, V., Palluzzi, E., Distefano, M. G., Scambia, G., & Ferrandina, G. (2017). Optimizing treatment in recurrent epithelial ovarian cancer. *Expert review of anticancer therapy*, 17(12), 1147–1158. https://doi.org/10.1080/14737140.2017.1398088

Costes, S. V., Daelemans, D., Cho, E. H., Dobbin, Z., Pavlakis, G., & Lockett, S. (2004). Automatic and quantitative measurement of protein-protein colocalization in live cells. *Biophysical journal*, *86*(6), 3993–4003. https://doi.org/10.1529/biophysj.103.038422

Cowles, M. W., Brown, D. D., Nisperos, S. V., Stanley, B. N., Pearson, B. J., & Zayas, R. M. (2013). Genome-wide analysis of the bHLH gene family in planarians identifies factors required for adult neurogenesis and neuronal regeneration. *Development (Cambridge, England)*, *140*(23), 4691–4702. https://doi.org/10.1242/dev.098616

Cribbs, J. T., & Strack, S. (2007). Reversible phosphorylation of Drp1 by cyclic AMP-dependent protein kinase and calcineurin regulates mitochondrial fission and cell death. *EMBO Reports*, *8*(10), 939–944. https://doi.org/10.1038/sj.embor.7401062

Cui, G., Dong, K., Zhou, J. Y., Li, S., Wu, Y., Han, Q., Yao, B., Shen, Q., Zhao, Y. L., Yang, Y., Cai, J., Zhang, S., & Yang, Y. G. (2023). Spatiotemporal transcriptomic atlas reveals the dynamic characteristics and key regulators of planarian regeneration. *Nature communications*, *14*(1), 3205. https://doi.org/10.1038/s41467-023-39016-0

Currie, K. W., & Pearson, B. J. (2013). Transcription factors lhx1/5-1 and pitx are required for the maintenance and regeneration of serotonergic neurons in planarians. *Development (Cambridge, England)*, *140*(17), 3577–3588. https://doi.org/10.1242/dev.098590

Currie, K. W., Molinaro, A. M., & Pearson, B. J. (2016). Neuronal sources of *hedgehog* modulate neurogenesis in the adult planarian brain. *eLife*, *5*, e19735. https://doi.org/10.7554/eLife.19735

Czerneková, M., & Jönsson, K. (2016). Mitosis in storage cells of the eutardigrade *Richtersius coronifer*. *Zool. J. Linn. Soc*., 178, pp. 888-896. https://doi.org/10.1111/zoj.12440

D'Amato, M., Bruce, S., Bresso, F., Zucchelli, M., Ezer, S., Pulkkinen, V., Lindgren, C., Astegiano, M., Rizzetto, M., Gionchetti, P., Riegler, G., Sostegni, R., Daperno, M., D'Alfonso, S., Momigliano-Richiardi, P., Torkvist, L., Puolakkainen, P., Lappalainen, M., Paavola-Sakki, P., Halme, L., … Kere, J. (2007). Neuropeptide S receptor 1 gene polymorphism is associated with susceptibility to inflammatory bowel disease. *Gastroenterology*, *133*(3), 808–817. https://doi.org/10.1053/j.gastro.2007.06.012

Dallas, L., Keith-Roach, M., Lyons, B. & Jha, A. (2012). Assessing the Impact of Ionizing Radiation on Aquatic Invertebrates: A Critical Review. *Radiation Research*, 177(5), pp.693-716. https://doi.org/10.1667/rr2687.1

Das, G., Shravage, B. V., & Baehrecke, E. H. (2012). Regulation and function of autophagy during cell survival and cell death. *Cold Spring Harbor perspectives in biology*, *4*(6), a008813. https://doi.org/10.1101/cshperspect.a008813

Dattani, A., Kao, D., Mihaylova, Y., Abnave, P., Hughes, S., Lai, A., Sahu, S., & Aboobaker, A. A. (2018). Epigenetic analyses of planarian stem cells demonstrate conservation of bivalent histone modifications in animal stem cells. *Genome research*, *28*(10), 1543–1554. https://doi.org/10.1101/gr.239848.118

Dawid, I. B., Breen, J. J., & Toyama, R. (1998). LIM domains: multiple roles as adapters and functional modifiers in protein interactions. *Trends in genetics : TIG*, *14*(4), 156–162. https://doi.org/10.1016/s0168-9525(98)01424-3

Dawid, I. B., Toyama, R., & Taira, M. (1995). LIM domain proteins. *Comptes rendus de l'Academie des sciences. Serie III, Sciences de la vie*, *318*(3), 295–306.

de Freitas Tallarico, L., Okazaki, K., Kawano, T., de Bragança Pereira, C. A., & Nakano, E. (2004). Dominant lethal effect of 60Co gamma radiation in Biomphalaria glabrata (SAY, 1818). *Mutation research*, *561*(1-2), 139–145. https://doi.org/10.1016/j.mrgentox.2004.05.002

De Mulder, K., Kuales, G., Pfister, D., Egger, B., Seppi, T., Eichberger, P., Borgonie, G., & Ladurner, P. (2010). Potential of Macrostomum lignano to recover from gamma-ray irradiation. *Cell and tissue research*, *339*(3), 527–542. https://doi.org/10.1007/s00441-009-0915-6

De Mulder, K., Kuales, G., Pfister, D., Willems, M., Egger, B., Salvenmoser, W., Thaler, M., Gorny, A. K., Hrouda, M., Borgonie, G., & Ladurner, P. (2009). Characterization of the stem cell system of the acoel Isodiametra pulchra. *BMC developmental biology*, *9*, 69. https://doi.org/10.1186/1471-213X-9-69

Dehal, P., & Boore, J. L. (2005). Two rounds of whole genome duplication in the ancestral vertebrate. *PLoS biology*, *3*(10), e314. https://doi.org/10.1371/journal.pbio.0030314

DeLay, B. D., Corkins, M. E., Hanania, H. L., Salanga, M., Deng, J. M., Sudou, N., Taira, M., Horb, M. E., & Miller, R. K. (2018). Tissue-Specific Gene Inactivation in *Xenopus laevis*: Knockout of *lhx1* in the Kidney with CRISPR/Cas9. *Genetics*, *208*(2), 673–686. https://doi.org/10.1534/genetics.117.300468

Derényi, I. & Szöllősi, G. (2017). Hierarchical tissue organization as a general mechanism to limit the accumulation of somatic mutations. *Nature Communications*, 8(1). https://doi.org/10.1038/ncomms14545

Desouky, O., Ding, N. & Zhou, G. (2015). Targeted and non-targeted effects of ionizing radiation. *Journal of Radiation Research and Applied Sciences*, 8(2), pp.247-254. Hyyp://doi.org/10.1016/j.jrras.2015.03.003

Despras, E., Miccoli, L., Créminon, C., Rouillard, D., Angulo, J. F., & Biard, D. S. (2003). Depletion of KIN17, a human DNA replication protein, increases the radiosensitivity of RKO cells. *Radiation research*, *159*(6), 748–758. https://doi.org/10.1667/0033-7587(2003)159[0748:dokahd]2.0.co;2

Dhanasekaran, D. N., & Reddy, E. P. (2008). JNK signaling in apoptosis. *Oncogene*, *27*(48), 6245–6251. https://doi.org/10.1038/onc.2008.301

DiCarlo, A., Maher, C., Hick, J., Hanfling, D., Dainiak, N., Chao, N., Bader, J., Coleman, C. & Weinstock, D. (2011). Radiation Injury After a Nuclear Detonation: Medical Consequences and the Need for Scarce Resources Allocation. *Disaster Medicine and Public Health Preparedness*, 5(S1), pp.S32-S44. https://doi.org/10.1001/dmp.2011.17

Diehn, M., Cho, R., Lobo, N., Kalisky, T., Dorie, M., Kulp, A., Qian, D., Lam, J., Ailles, L., Wong, M., Joshua, B., Kaplan, M., Wapnir, I., Dirbas, F., Somlo, G., Garberoglio, C., Paz, B., Shen, J., Lau, S., Quake, S., Brown, J., Weissman, I. & Clarke, M. (2009). Association of reactive oxygen species levels and radioresistance in cancer stem cells. *Nature*, 458(7239), pp.780-783. https://doi.org/10.1038/nature07733

Díez, D., Sánchez-Jiménez, F., & Ranea, J. A. (2011). Evolutionary expansion of the Ras switch regulatory module in eukaryotes. *Nucleic acids research*, *39*(13), 5526–5537. https://doi.org/10.1093/nar/gkr154

Ding, H., Howarth, A. G., Pannirselvam, M., Anderson, T. J., Severson, D. L., Wiehler, W. B., Triggle, C. R., & Tuana, B. S. (2005). Endothelial dysfunction in Type 2 diabetes correlates with deregulated expression of the tail-anchored membrane protein SLMAP. *American journal of physiology. Heart and circulatory physiology*, *289*(1), H206–H211. https://doi.org/10.1152/ajpheart.00037.2005

Ding, L., Wang, Z., Yan, J., Yang, X., Liu, A., Qiu, W., Zhu, J., Han, J., Zhang, H., Lin, J., Cheng, L., Qin, X., Niu, C., Yuan, B., Wang, X., Zhu, C., Zhou, Y., Li, J., Song, H., Huang, C., … Ye, Q. (2009). Human four-and-a-half LIM family members suppress tumor cell growth through a TGF-beta-like signaling pathway. *The Journal of clinical investigation*, *119*(2), 349–361. https://doi.org/10.1172/JCI35930

Dingli, D., Traulsen, A. & Pacheco, J. (2007). Compartmental Architecture and Dynamics of Hematopoiesis. *PLoS ONE*, 2(4), p.e345. https://doi.org/10.1371/journal.pone.0000345

Dobin, A., Davis, C. A., Schlesinger, F., Drenkow, J., Zaleski, C., Jha, S., Batut, P., Chaisson, M., & Gingeras, T. R. (2013). STAR: ultrafast universal RNA-seq aligner. *Bioinformatics (Oxford, England)*, *29*(1), 15–21. https://doi.org/10.1093/bioinformatics/bts635

Dong, G., Chakshusmathi, G., Wolin, S. L., & Reinisch, K. M. (2004). Structure of the La motif: a winged helix domain mediates RNA binding via a conserved aromatic patch. *The EMBO journal*, *23*(5), 1000–1007. https://doi.org/10.1038/sj.emboj.7600115

Dong, Z., Huo, J., Liang, A., Chen, J., Chen, G., & Liu, D. (2021). Gamma-Secretase Inhibitor (DAPT), a potential therapeutic target drug, caused neurotoxicity in planarian regeneration by inhibiting Notch signaling pathway. *The Science of the total environment*, *781*, 146735. https://doi.org/10.1016/j.scitotenv.2021.146735

D'Souza, B., Meloty-Kapella, L., & Weinmaster, G. (2010). Canonical and non-canonical Notch ligands. *Current topics in developmental biology*, 92, 73–129. https://doi.org/10.1016/S0070-2153(10)92003-6

Dubois, C., Pophillat, M., Audebert, S., Fourquet, P., Lecomte, C., Dubourg, N., Galas, S., Camoin, L., & Frelon, S. (2019). Differential modification of the C. elegans proteome in response to acute and chronic gamma radiation: Link with reproduction decline. *The Science of the total environment*, *676*, 767–781. https://doi.org/10.1016/j.scitotenv.2019.04.039

Dudley, D., Chaudhuri, J., Bassing, C. H., & Alt, F. W. (2005). Mechanism and control of V(D)J recombination versus class switch recombination: similarities and differences. *Advances in immunology*, *86*, 43–112. https://doi.org/10.1016/S0065-2776(04)86002-4

Duffner, P. (2004). Long-term effects of radiation therapy on cognitive and endocrine function in children with leukemia and brain tumors. *The neurologist*, *10*(6), 293–310. https://doi.org/10.1097/01.nrl.0000144287.35993.96

Dumitru, R., Gama, V., Fagan, B., Bower, J., Swahari, V., Pevny, L. & Deshmukh, M. (2012). Human Embryonic Stem Cells Have Constitutively Active Bax at the Golgi and Are Primed to Undergo Rapid Apoptosis. *Molecular Cell*, 46(5), pp.573-583. https://doi.org/10.1016/j.molcel.2012.04.002

Duncan, E. M., Chitsazan, A. D., Seidel, C. W., & Sánchez Alvarado, A. (2015). Set1 and MLL1/2 Target Distinct Sets of Functionally Different Genomic Loci In Vivo. *Cell reports*, *13*(12), 2741–2755. https://doi.org/10.1016/j.celrep.2015.11.059

Duvaud, S., Gabella, C., Lisacek, F., Stockinger, H., Ioannidis, V., & Durinx, C. (2021). Expasy, the Swiss Bioinformatics Resource Portal, as designed by its users. *Nucleic acids research*, *49*(W1), W216–W227. https://doi.org/10.1093/nar/gkab225

Edgar R. C. (2022). Muscle5: High-accuracy alignment ensembles enable unbiased assessments of sequence homology and phylogeny. *Nature communications*, *13*(1), 6968. https://doi.org/10.1038/s41467-022-34630-w

Eichholz, G., Bogdanov, A. & Dwinell, L. (1991). Radiation sensitivity of pine wood nematodes in woodchips. *International Journal of Radiation Applications and Instrumentation. Part A. Applied Radiation and Isotopes*, 42(2), pp.177-179. https://doi.org/10.1016/0883-2889(91)90070-H

Eisenhoffer, G. T., Kang, H., & Sánchez Alvarado, A. (2008). Molecular analysis of stem cells and their descendants during cell turnover and regeneration in the planarian Schmidtea mediterranea. *Cell stem cell*, *3*(3), 327–339. https://doi.org/10.1016/j.stem.2008.07.002

Eke, I., Deuse, Y., Hehlgans, S., Gurtner, K., Krause, M., Baumann, M., Shevchenko, A., Sandfort, V., & Cordes, N. (2012). β_1Integrin/FAK/cortactin signaling is essential for human head and neck cancer resistance to radiotherapy. *The Journal of clinical investigation*, *122*(4), 1529–1540. https://doi.org/10.1172/JCI61350

Elsharawy, K. A., Mohammed, O. J., Aleskandarany, M. A., Hyder, A., El-Gammal, H. L., Abou-Dobara, M. I., Green, A. R., Dalton, L. W., & Rakha, E. A. (2020). The nucleolar-related protein Dyskerin pseudouridine synthase 1 (DKC1) predicts poor prognosis in breast cancer. *British journal of cancer*, *123*(10), 1543–1552. https://doi.org/10.1038/s41416-020-01045-7

Emms, D. M., & Kelly, S. (2019). OrthoFinder: phylogenetic orthology inference for comparative genomics. *Genome biology*, *20*(1), 238. https://doi.org/10.1186/s13059-019-1832-y

Engel, D. (1967). Effect of single and continuous exposures of gamma radiation on the survival and growth of the blue crab, Callinectes sapidus. *Radiation research*, *32*(4), 685–691. https://doi.org/10.2307/3572280

Engström, W., Ward, A., & Moorwood, K. (2010). The role of scaffold proteins in JNK signalling. *Cell proliferation*, *43*(1), 56–66. https://doi.org/10.1111/j.1365-2184.2009.00654.x

Enoch, T., & Norbury, C. (1995). Cellular responses to DNA damage: cell-cycle checkpoints, apoptosis and the roles of p53 and ATM. *Trends in biochemical sciences*, *20*(10), 426–430. https://doi.org/10.1016/s0968-0004(00)89093-3

Espiritu, E. B., Crunk, A. E., Bais, A., Hochbaum, D., Cervino, A. S., Phua, Y. L., Butterworth, M. B., Goto, T., Ho, J., Hukriede, N. A., & Cirio, M. C. (2018). The Lhx1-Ldb1 complex interacts with Furry to regulate microRNA expression during pronephric kidney development. *Scientific reports*, *8*(1), 16029. https://doi.org/10.1038/s41598-018-34038-x

Eze, U. C., Bhaduri, A., Haeussler, M., Nowakowski, T. J., & Kriegstein, A. R. (2021). Single-cell atlas of early human brain development highlights heterogeneity of human neuroepithelial cells and early radial glia. *Nature neuroscience*, *24*(4), 584–594. https://doi.org/10.1038/s41593-020-00794-1

Fabbrizi, M., Meyer, B., Misri, S., Raj, S., Zobel, C., Hallahan, D. & Sharma, G. (2018b). Transient PP2A inhibition alleviates normal tissue stem cell susceptibility to cell death during radiotherapy. *Cell Death & Disease*, 9(5). https://doi.org/10.1038/s41419-018-0559-0

Fabbrizi, M., Warshowsky, K., Zobel, C., Hallahan, D. & Sharma, G. (2018a). Molecular and epigenetic regulatory mechanisms of normal stem cell radiosensitivity. *Cell Death Discovery*, 4(1). https://doi.org/10.1038/s41420-018-0132-8

Ferrezuelo, F., Colomina, N., Futcher, B., & Aldea, M. (2010). The transcriptional network activated by Cln3 cyclin at the G1-to-S transition of the yeast cell cycle. *Genome biology*, *11*(6), R67. https://doi.org/10.1186/gb-2010-11-6-r67

Filipek, S., Teller, D. C., Palczewski, K., & Stenkamp, R. (2003). The crystallographic model of rhodopsin and its use in studies of other G protein-coupled receptors. *Annual review of biophysics and biomolecular structure*, *32*, 375–397. https://doi.org/10.1146/annurev.biophys.32.110601.

Fimia, G. M., De Cesare, D., & Sassone-Corsi, P. (2000). A family of LIM-only transcriptional coactivators: tissue-specific expression and selective activation of CREB and CREM. *Molecular and cellular biology*, *20*(22), 8613–8622. https://doi.org/10.1128/MCB.20.22.8613-8622.2000

Fincher, C. T., Wurtzel, O., de Hoog, T., Kravarik, K. M., & Reddien, P. W. (2018). Cell type transcriptome atlas for the planarian *Schmidtea mediterranea*. *Science (New York, N.Y.)*, *360*(6391), eaaq1736. https://doi.org/10.1126/science.aaq1736

Finn, R. D., Bateman, A., Clements, J., Coggill, P., Eberhardt, R. Y., Eddy, S. R., Heger, A., Hetherington, K., Holm, L., Mistry, J., Sonnhammer, E. L., Tate, J., & Punta, M. (2014). Pfam: the protein families database. *Nucleic acids research*, *42*, D222–D230. https://doi.org/10.1093/nar/gkt1223

Fire, A., Xu, S., Montgomery, M. K., Kostas, S. A., Driver, S. E., & Mello, C. C. (1998). Potent and specific genetic interference by double-stranded RNA in Caenorhabditis elegans. *Nature,* 391(6669), 806–811. https://doi.org/10.1038/35888

Forsthoefel, D. J., Park, A. E., & Newmark, P. A. (2011). Stem cell-based growth, regeneration, and remodeling of the planarian intestine. *Developmental biology*, *356*(2), 445–459. https://doi.org/10.1016/j.ydbio.2011.05.669

Forsthoefel, D. J., Ross, K. G., Newmark, P. A., & Zayas, R. M. (2018). Fixation, Processing, and Immunofluorescent Labeling of Whole Mount Planarians. *Methods in molecular biology (Clifton, N.J.)*, *1774*, 353–366. https://doi.org/10.1007/978-1-4939-7802-1_10

Fortunato, A., Fleming, A., Aktipis, A. and Maley, C. (2021b). Upregulation of DNA repair genes and cell extrusion underpin the remarkable radiation resistance of Trichoplax adhaerens. *PLOS Biology*, 19(11), p.e3001471. https://doi.org/10.1371/journal.pbio.3001471

Fortunato, A., Taylor, J., Scirone, J., Aktipis, A. and Maley, C., (2021a). Sponges are highly resistant to radiation exposure and cancer. *BioRxiv*: https://doi.org/10.1101/2021.03.17.435910

Frank, S., Gaume, B., Bergmann-Leitner, E. S., Leitner, W. W., Robert, E. G., Catez, F., Smith, C. L., & Youle, R. J. (2001). The role of dynamin-related protein 1, a mediator of mitochondrial fission, in apoptosis. *Developmental cell*, *1*(4), 515–525. https://doi.org/10.1016/s1534-5807(01)00055-7

Friedländer, M. R., Adamidi, C., Han, T., Lebedeva, S., Isenbarger, T. A., Hirst, M., Marra, M., Nusbaum, C., Lee, W. L., Jenkin, J. C., Sánchez Alvarado, A., Kim, J. K., & Rajewsky, N. (2009). High-resolution profiling and discovery of planarian small RNAs. *Proceedings of the National Academy of Sciences of the United States of America*, *106*(28), 11546–11551. https://doi.org/10.1073/pnas.0905222106

Fu, Y., Xu, M., Cui, Z., Yang, Z., Zhang, Z., Yin, X., Huang, X., Zhou, M., Wang, X., & Chen, C. (2020). Genome-wide identification of FHL1 as a powerful prognostic candidate and potential therapeutic target in acute myeloid leukaemia. *EBioMedicine*, *52*, 102664. https://doi.org/10.1016/j.ebiom.2020.102664

Fujita, S. & Egami, N. (1984). Effect of Gamma Irradiation on the Reproductive System of the Pond Snail Physa acuta. *Radiation Research*, 98(2), p.362. https://doi.org/10.2307/3576243

Fuller, N., Lerebours, A., Smith, J. & Ford, A. (2015). The biological effects of ionising radiation on Crustaceans: A review. *Aquatic Toxicology*, 167, pp.55-67. https://doi.org/10.1016/j.aquatox.2015.07.013

Fuma, S., Watanabe, Y., Kawaguchi, I., Takata, T., Kubota, Y., Ban-nai, T. & Yoshida, S. (2012). Derivation of hazardous doses for amphibians acutely exposed to ionising radiation. *Journal of Environmental Radioactivity*, 103(1), pp.15-19. https://doi.org/10.1016/j.jenvrad.2011.09.004

Gager, C. S., & Blakeslee, A. F. (1927). Chromosome and Gene Mutations in Datura Following Exposure to Radium Rays. *Proceedings of the National Academy of Sciences of the United States of America*, *13*(2), 75–79. https://doi.org/10.1073/pnas.13.2.75

Gao, X., Liu, Z., Zhong, M., Wu, K., Zhang, Y., Wang, H., & Zeng, T. (2019). Knockdown of DNA/RNA-binding protein KIN17 promotes apoptosis of triple-negative breast cancer cells. *Oncology letters*, *17*(1), 288–293. https://doi.org/10.3892/ol.2018.9597

García-Castro, H., Kenny, N. J., Iglesias, M., Álvarez-Campos, P., Mason, V., Elek, A., Schönauer, A., Sleight, V. A., Neiro, J., Aboobaker, A., Permanyer, J., Irimia, M., Sebé-Pedrós, A., & Solana, J. (2021). ACME dissociation: a versatile cell fixation-dissociation method for single-cell transcriptomics. *Genome biology*, *22*(1), 89. https://doi.org/10.1186/s13059-021-02302-5

Garcia-Fernández, J., & Holland, P. W. (1994). Archetypal organization of the amphioxus Hox gene cluster. *Nature*, 370(6490), 563–566. https://doi.org/10.1038/370563a0

Garus, A., & Autexier, C. (2021). Dyskerin: an essential pseudouridine synthase with multifaceted roles in ribosome biogenesis, splicing, and telomere maintenance. *RNA (New York, N.Y.)*, *27*(12), 1441–1458. https://doi.org/10.1261/rna.078953.121

Gaugler, R. & Boush, G. (1979). Effects of γ-radiation on the entomogenous nematode, Neoaplectana carpocapsae. *Journal of Invertebrate Pathology*, 33(1), pp.121-123. https://doi.org/10.1016/0022-2011(79)90142-3

Giordano, E., Peluso, I., Senger, S., & Furia, M. (1999). minifly, a Drosophila gene required for ribosome biogenesis. *The Journal of cell biology*, *144*(6), 1123–1133. https://doi.org/10.1083/jcb.144.6.1123

Gladyshev, E., & Meselson, M. (2008). Extreme resistance of bdelloid rotifers to ionizing radiation. *Proceedings of the National Academy of Sciences of the United States of America*, *105*(13), 5139–5144. https://doi.org/10.1073/pnas.0800966105

Goldsmith, M. I., Fisher, S., Waterman, R., & Johnson, S. L. (2003). Saltatory control of isometric growth in the zebrafish caudal fin is disrupted in long fin and rapunzel mutants. *Developmental biology*, *259*(2), 303–317. https://doi.org/10.1016/s0012-1606(03)00186-6

Golovine, K., Abalakov, G., Lian, Z., Chatla, S., Karami, A., Chitrala, K. N., Madzo, J., Nieborowska-Skorska, M., Huang, J., & Skorski, T. (2023). ABL1 kinase as a tumor suppressor in AML1-ETO and NUP98-PMX1 leukemias. *Blood cancer journal*, *13*(1), 42. https://doi.org/10.1038/s41408-023-00810-0

González-Estévez, C., Felix, D. A., Aboobaker, A. A., & Saló, E. (2007). Gtdap-1 promotes autophagy and is required for planarian remodeling during regeneration and starvation. *Proceedings of the National Academy of Sciences of the United States of America*, *104*(33), 13373–13378. https://doi.org/10.1073/pnas.0703588104

González-Estévez, C., Felix, D. A., Rodríguez-Esteban, G., & Aboobaker, A. A. (2012). Decreased neoblast progeny and increased cell death during starvation-induced planarian degrowth. *The International journal of developmental biology*, *56*(1-3), 83–91. https://doi.org/10.1387/ijdb.113452cg

Green, J., Taylor, J. J., Hindes, A., Johnson, S. L., & Goldsmith, M. I. (2009). A gain of function mutation causing skeletal overgrowth in the rapunzel mutant. *Developmental biology*, *334*(1), 224–234. https://doi.org/10.1016/j.ydbio.2009.07.025

Grochowski, C. M., Loomes, K. M., & Spinner, N. B. (2016). Jagged1 (JAG1): Structure, expression, and disease associations. *Gene*, *576*(1 Pt 3), 381–384. https://doi.org/10.1016/j.gene.2015.10.065

Grohme, M. A., Schloissnig, S., Rozanski, A., Pippel, M., Young, G. R., Winkler, S., Brandl, H., Henry, I., Dahl, A., Powell, S., Hiller, M., Myers, E., & Rink, J. C. (2018). The genome of Schmidtea mediterranea and the evolution of core cellular mechanisms. *Nature*, *554*(7690), 56–61. https://doi.org/10.1038/nature25473

Gross, V., Bährle, R. & Mayer, G. (2018). Detection of cell proliferation in adults of the water bear Hypsibius dujardini (Tardigrada) via incorporation of a thymidine analog. *Tissue and Cell*, 51, pp.77-8. https://doi.org/10.1016/j.tice.2018.03.005

Grudniewska, M., Mouton, S., Simanov, D., Beltman, F., Grelling, M., de Mulder, K., Arindrarto, W., Weissert, P. M., van der Elst, S., & Berezikov, E. (2016). Transcriptional signatures of somatic neoblasts and germline cells in *Macrostomum lignano*. *eLife*, *5*, e20607. https://doi.org/10.7554/eLife.20607

Gu, W., Crawford, E. D., O'Donovan, B. D., Wilson, M. R., Chow, E. D., Retallack, H., & DeRisi, J. L. (2016). Depletion of Abundant Sequences by Hybridization (DASH): using Cas9 to remove unwanted high-abundance species in sequencing libraries and molecular counting applications. *Genome biology*, *17*, 41. https://doi.org/10.1186/s13059-016-0904-5

Guerrieri, A. N., Zacchini, F., Onofrillo, C., Di Viggiano, S., Penzo, M., Ansuini, A., Gandin, I., Nobe, Y., Taoka, M., Isobe, T., Treré, D., & Montanaro, L. (2020). DKC1 Overexpression Induces a More Aggressive Cellular Behavior and Increases Intrinsic Ribosomal Activity in Immortalized Mammary Gland Cells. *Cancers*, *12*(12), 3512. https://doi.org/10.3390/cancers12123512

Guo, T., Peters, A. H., & Newmark, P. A. (2006). A Bruno-like gene is required for stem cell maintenance in planarians. *Developmental cell*, *11*(2), 159–169. https://doi.org/10.1016/j.devcel.2006.06.004

Guo, X., Sun, J., Bian, P., Chen, L., Zhan, F., Wang, J., Xu, A., Wang, Y., Hei, T. & Wu, L. (2013). Radiation-Induced Bystander Signaling from Somatic Cells to Germ Cells in Caenorhabditis elegans. *Radiation Research*, 180(3), p.268. https://doi.org/10.1667/RR3218.1

Guzzo, R. M., Sevinc, S., Salih, M., & Tuana, B. S. (2004). A novel isoform of sarcolemmal membrane-associated protein (SLMAP) is a component of the microtubule organizing centre. *Journal of cell science*, *117*(Pt 11), 2271–2281. https://doi.org/10.1242/jcs.01079

Gyori, B. M., Venkatachalam, G., Thiagarajan, P. S., Hsu, D., & Clement, M. V. (2014). OpenComet: an automated tool for comet assay image analysis. *Redox biology*, *2*, 457–465. https://doi.org/10.1016/j.redox.2013.12.020

Hakem, R. (2008). DNA-damage repair; the good, the bad, and the ugly. *The EMBO Journal*, 27(4), pp.589-605. https://doi.org/10.1038/emboj.2008.15

Hall, R. N., Weill, U., Drees, L., Leal-Ortiz, S., Li, H., Khariton, M., Chai, C., Xue, Y., Rosental, B., Quake, S. R., Sánchez Alvarado, A., Melosh, N. A., Fire, A. Z., Rink, J. C., & Wang, B. (2022). Heterologous reporter expression in the planarian Schmidtea mediterranea through somatic mRNA transfection. *Cell reports methods*, 2(10), 100298. https://doi.org/10.1016/j.crmeth.2022.100298

Hamma, T., Reichow, S. L., Varani, G., & Ferré-D'Amaré, A. R. (2005). The Cbf5-Nop10 complex is a molecular bracket that organizes box H/ACA RNPs. *Nature structural & molecular biology*, *12*(12), 1101–1107. https://doi.org/10.1038/nsmb1036

Han, J., Won, E. J., Lee, B. Y., Hwang, U. K., Kim, I. C., Yim, J. H., Leung, K. M., Lee, Y. S., & Lee, J. S. (2014). Gamma rays induce DNA damage and oxidative stress associated with impaired growth and reproduction in the copepod Tigriopus japonicus. *Aquatic toxicology (Amsterdam, Netherlands)*, *152*, 264–272. https:/doi.org/10.1016/j.aquatox.2014.04.005

Han, K., Pierce, S. E., Li, A., Spees, K., Anderson, G. R., Seoane, J. A., Lo, Y. H., Dubreuil, M., Olivas, M., Kamber, R. A., Wainberg, M., Kostyrko, K., Kelly, M. R., Yousefi, M., Simpkins, S. W., Yao, D., Lee, K., Kuo, C. J., Jackson, P. K., Sweet-Cordero, A., … Bassik, M. C. (2020). CRISPR screens in cancer spheroids identify 3D growth-specific vulnerabilities. *Nature*, *580*(7801), 136–141. https://doi.org/10.1038/s41586-020-2099-x

Hao, Y., Hao, S., Andersen-Nissen, E., Mauck, W. M., 3rd, Zheng, S., Butler, A., Lee, M. J., Wilk, A. J., Darby, C., Zager, M., Hoffman, P., Stoeckius, M., Papalexi, E., Mimitou, E. P., Jain, J., Srivastava, A., Stuart, T., Fleming, L. M., Yeung, B., Rogers, A. J., Satija, R. (2021). Integrated analysis of multimodal single-cell data. *Cell*, *184*(13), 3573–3587.e29. https://doi.org/10.1016/j.cell.2021.04.048

Harper, J. & Elledge, S. (2007). The DNA Damage Response: Ten Years After. *Molecular Cell*, 28(5), pp.739-745. https://doi.org/10.1016/j.molcel.2007.11.015

Harvey, S. H., Krien, M. J., & O'Connell, M. J. (2002). Structural maintenance of chromosomes (SMC) proteins, a family of conserved ATPases. *Genome biology*, *3*(2), REVIEWS3003. https://doi.org/10.1186/gb-2002-3-2-reviews3003

Hashimoto, T., Horikawa, D., Saito, Y., Kuwahara, H., Kozuka-Hata, H., Shin-I, T., Minakuchi, Y., Ohishi, K., Motoyama, A., Aizu, T., Enomoto, A., Kondo, K., Tanaka, S., Hara, Y., Koshikawa, S., Sagara, H., Miura, T., Yokobori, S., Miyagawa, K., Suzuki, Y., Kubo, T., Oyama, M., Kohara, Y., Fujiyama, A., Arakawa, K., Katayama, T., Toyoda, A. & Kunieda, T. (2016). Extremotolerant tardigrade genome and improved radiotolerance of human cultured cells by tardigrade-unique protein. *Nature Communications*, 7(1). 12808. https://doi.org/10.1038/ncomms12808

Hassan, K. A., Wang, L., Korkaya, H., Chen, G., Maillard, I., Beer, D. G., Kalemkerian, G. P., & Wicha, M. S. (2013). Notch pathway activity identifies cells with cancer stem cell-like properties and correlates with worse survival in lung adenocarcinoma. *Clinical cancer research : an official journal of the American Association for Cancer Research*, *19*(8), 1972–1980. https://doi.org/10.1158/1078-0432.CCR-12-0370

Hayashi, T., Asami, M., Higuchi, S., Shibata, N., & Agata, K. (2006). Isolation of planarian X-ray-sensitive stem cells by fluorescence-activated cell sorting. *Development, growth & differentiation*, *48*(6), 371–380. https://doi.org/10.1111/j.1440-169X.2006.00876.x

Hayashi, T., Motoishi, M., Yazawa, S., Itomi, K., Tanegashima, C., Nishimura, O., Agata, K., & Tarui, H. (2011). A LIM-homeobox gene is required for differentiation of Wnt-expressing cells at the posterior end of the planarian body. *Development (Cambridge, England)*, *138*(17), 3679–3688. https://doi.org/10.1242/dev.060194

Hayman, T. J., Baro, M., MacNeil, T., Phoomak, C., Aung, T. N., Cui, W., Leach, K., Iyer, R., Challa, S., Sandoval-Schaefer, T., Burtness, B. A., Rimm, D. L., & Contessa, J. N. (2021). STING enhances cell death through regulation of reactive oxygen species and DNA damage. *Nature communications*, *12*(1), 2327. https://doi.org/10.1038/s41467-021-22572-8

He, X., Lindsay-Mosher, N., Li, Y., Molinaro, A. M., Pellettieri, J., & Pearson, B. J. (2017). FOX and ETS family transcription factors regulate the pigment cell lineage in planarians. *Development (Cambridge, England)*, *144*(24), 4540–4551. https://doi.org/10.1242/dev.156349

Hendrix, A., Maynard, D., Pauwels, P., Braems, G., Denys, H., Van den Broecke, R., Lambert, J., Van Belle, S., Cocquyt, V., Gespach, C., Bracke, M., Seabra, M. C., Gahl, W. A., De Wever, O., & Westbroek, W. (2010). Effect of the secretory small GTPase Rab27B on breast cancer growth, invasion, and metastasis. *Journal of the National Cancer Institute*, *102*(12), 866–880. https://doi.org/10.1093/jnci/djq153

Hendzel, M. J., Wei, Y., Mancini, M. A., Van Hooser, A., Ranalli, T., Brinkley, B. R., Bazett-Jones, D. P., & Allis, C. D. (1997). Mitosis-specific phosphorylation of histone H3 initiates primarily within pericentromeric heterochromatin during G2 and spreads in an ordered fashion coincident with mitotic chromosome condensation. *Chromosoma*, *106*(6), 348–360. https://doi.org/10.1007/s004120050256

Hernández-Plaza, A., Szklarczyk, D., Botas, J., Cantalapiedra, C. P., Giner-Lamia, J., Mende, D. R., Kirsch, R., Rattei, T., Letunic, I., Jensen, L. J., Bork, P., von Mering, C., & Huerta-Cepas, J. (2023). eggNOG 6.0: enabling comparative genomics across 12 535 organisms. *Nucleic acids research*, *51*(D1), D389–D394. https://doi.org/10.1093/nar/gkac1022

Herr, P., Lundin, C., Evers, B., Ebner, D., Bauerschmidt, C., Kingham, G., Palmai-Pallag, T., Mortusewicz, O., Frings, O., Sonnhammer, E., & Helleday, T. (2015). A genome-wide IR-induced RAD51 foci RNAi screen identifies CDC73 involved in chromatin remodeling for DNA repair. *Cell discovery*, *1*, 15034. https://doi.org/10.1038/celldisc.2015.34

Hershey, A. D., & Chase, M. (1952). Independent functions of viral protein and nucleic acid in growth of bacteriophage. *The Journal of general physiology*, *36*(1), 39–56. https://doi.org/10.1085/jgp.36.1.39

Heylmann, D., Rödel, F., Kindler, T. & Kaina, B. (2014). Radiation sensitivity of human and murine peripheral blood lymphocytes, stem and progenitor cells. *Biochimica et Biophysica Acta (BBA) - Reviews on Cancer*, 1846(1), pp.121-129.

High, F. A., Lu, M. M., Pear, W. S., Loomes, K. M., Kaestner, K. H., & Epstein, J. A. (2008). Endothelial expression of the Notch ligand Jagged1 is required for vascular smooth muscle development. *Proceedings of the National Academy of Sciences of the United States of America*, *105*(6), 1955–1959. https://doi.org/10.1073/pnas.0709663105

Hill, M. A. (2018). Track to the future: historical perspective on the importance of radiation track structure and DNA as a radiobiological target. *International journal of radiation biology*, *94*(8), 759–768. https://doi.org/10.1080/09553002.2017.1387304

Hirota, Y., & Tanaka, Y. (2009). A small GTPase, human Rab32, is required for the formation of autophagic vacuoles under basal conditions. *Cellular and molecular life sciences : CMLS*, *66*(17), 2913–2932. https://doi.org/10.1007/s00018-009-0080-9

Hoang, V. T., Nyswaner, K., Torres-Ayuso, P., & Brognard, J. (2020). The protein kinase MAP3K19 phosphorylates MAP2Ks and thereby activates ERK and JNK kinases and increases viability of KRAS-mutant lung cancer cells. *The Journal of biological chemistry*, *295*(25), 8470–8479. https://doi.org/10.1074/jbc.RA119.012365

Hobert, O., & Westphal, H. (2000). Functions of LIM-homeobox genes. *Trends in genetics : TIG*, *16*(2), 75–83. https://doi.org/10.1016/s0168-9525(99)01883-1

Hoeijmakers, J. H. (2009). DNA damage, aging, and cancer. *The New England journal of medicine*, *361*(15), 1475–1485. https://doi.org/10.1056/NEJMra0804615

Hoffman, P. (2020). SeuratDisk v0.0.0.9015. Retrieved from: https://github.com/mojaveazure/seurat-disk

Hollenbach, J. P., Resch, A. M., Palakodeti, D., Graveley, B. R., & Heinen, C. D. (2011). Loss of DNA mismatch repair imparts a selective advantage in planarian adult stem cells. *PloS one*, *6*(7), e21808. https://doi.org/10.1371/journal.pone.0021808

Homma, Y., Hiragi, S., & Fukuda, M. (2021). Rab family of small GTPases: an updated view on their regulation and functions. *The FEBS journal*, *288*(1), 36–55. https://doi.org/10.1111/febs.15453

Hong, S., Freeberg, M. A., Han, T., Kamath, A., Yao, Y., Fukuda, T., Suzuki, T., Kim, J. K., & Inoki, K. (2017). LARP1 functions as a molecular switch for mTORC1-mediated translation of an essential class of mRNAs. *eLife*, *6*, e25237. https://doi.org/10.7554/eLife.25237

Hopkins, T., Mura, M., Al-Ashtal, H., Lahr, R., Abd-Latip, N., Sweeney, K., Lu, H., Weir, J., El-Bahrawy, M., Steel, J., Ghaem-Maghami, S., Aboagye, O., Berman, A., Blagden, S. (2016). The RNA-binding protein LARP1 is a post-transcriptional regulator of survival and tumorigenesis in ovarian cancer. *Nucleic Acids Res*. Feb 18;44(3):1227-46. http://doi.org/10.1093/nar/gkv1515.

Horikawa, D. D., Kunieda, T., Abe, W., Watanabe, M., Nakahara, Y., Yukuhiro, F., Sakashita, T., Hamada, N., Wada, S., Funayama, T., Katagiri, C., Kobayashi, Y., Higashi, S., & Okuda, T. (2008). Establishment of a rearing system of the extremotolerant tardigrade Ramazzottius varieornatus: a new model animal for astrobiology. *Astrobiology*, *8*(3), 549–556. https://doi.org/10.1089/ast.2007.0139

Horikawa, D. D., Sakashita, T., Katagiri, C., Watanabe, M., Kikawada, T., Nakahara, Y., Hamada, N., Wada, S., Funayama, T., Higashi, S., Kobayashi, Y., Okuda, T., & Kuwabara, M. (2006). Radiation tolerance in the tardigrade Milnesium tardigradum. *International journal of radiation biology*, *82*(12), 843–848. https://doi.org/10.1080/09553000600972956

Horvath, M., Wang, X., Resnick, M. & Bell, D. (2007). Divergent Evolution of Human p53 Binding Sites: Cell Cycle Versus Apoptosis. *PLoS Genetics*, 3(7), p.e127. https://doi.org/10.1371/journal.pgen.0030127

Hou, P., Shi, P., Jiang, T., Yin, H., Chu, S., Shi, M., Bai, J., & Song, J. (2020). DKC1 enhances angiogenesis by promoting HIF-1α transcription and facilitates metastasis in colorectal cancer. *British journal of cancer*, *122*(5), 668–679. https://doi.org/10.1038/s41416-019-0695-z

Hua, G., He, C., Lv, X., Fan, L., Wang, C., Remmenga, S. W., Rodabaugh, K. J., Yang, L., Lele, S. M., Yang, P., Karpf, A. R., Davis, J. S., & Wang, C. (2016). The four and a half LIM domains 2 (FHL2) regulates ovarian granulosa cell tumor progression via controlling AKT1 transcription. *Cell death & disease*, *7*(7), e2297. https://doi.org/10.1038/cddis.2016.207

Huang, X., Dai, Z., Li, Q., Lin, X., Huang, Q., & Zeng, T. (2023). Roles and regulatory mechanisms of KIN17 in cancers (Review). *Oncology letters*, *25*(4), 137. https://doi.org/10.3892/ol.2023.13723

Huang, Z., Yu, C., Yu, L., Shu, H., & Zhu, X. (2022). The Roles of FHL3 in Cancer. *Frontiers in oncology*, *12*, 887828. https://doi.org/10.3389/fonc.2022.887828

Hubbi, M. E., Gilkes, D. M., Baek, J. H., & Semenza, G. L. (2012). Four-and-a-half LIM domain proteins inhibit transactivation by hypoxia-inducible factor 1. *The Journal of biological chemistry*, *287*(9), 6139–6149. https://doi.org/10.1074/jbc.M111.278630

Huebner, E. A., & Strittmatter, S. M. (2009). Axon regeneration in the peripheral and central nervous systems. *Results and problems in cell differentiation*, *48*, 339–351. https://doi.org/10.1007/400_2009_19

Huerta-Cepas, J., Szklarczyk, D., Heller, D., Hernández-Plaza, A., Forslund, S. K., Cook, H., Mende, D. R., Letunic, I., Rattei, T., Jensen, L. J., von Mering, C., & Bork, P. (2019). eggNOG 5.0: a hierarchical, functionally and phylogenetically annotated orthology resource based on 5090 organisms and 2502 viruses. *Nucleic acids research*, *47*(D1), D309–D314. https://doi.org/10.1093/nar/gky1085

Hulo, N., Bairoch, A., Bulliard, V., Cerutti, L., De Castro, E., Langendijk-Genevaux, P. S., Pagni, M., & Sigrist, C. J. (2006). The PROSITE database. *Nucleic acids research*, *34*(Database issue), D227–D230. https://doi.org/10.1093/nar/gkj063

Ichihara, K., Shimizu, H., Taguchi, O., Yamaguchi, M., & Inoue, Y. H. (2007). A Drosophila orthologue of larp protein family is required for multiple processes in male meiosis. *Cell structure and function*, *32*(2), 89–100. https://doi.org/10.1247/csf.07027

Iliakis, G. E., & Okayasu, R. (1990). Radiosensitivity throughout the cell cycle and repair of potentially lethal damage and DNA double-strand breaks in an X-ray-sensitive CHO mutant. *International journal of radiation biology*, *57*(6), 1195–1211. https://doi.org/10.1080/09553009014551291

Ishida, T., Nakajima, T., Kudo, A., & Kawakami, A. (2010). Phosphorylation of Junb family proteins by the Jun N-terminal kinase supports tissue regeneration in zebrafish. *Developmental biology*, *340*(2), 468–479. https://doi.org/10.1016/j.ydbio.2010.01.036

Ishikawa, T., Sato, A., Marcou, C. A., Tester, D. J., Ackerman, M. J., Crotti, L., Schwartz, P. J., On, Y. K., Park, J. E., Nakamura, K., Hiraoka, M., Nakazawa, K., Sakurada, H., Arimura, T., Makita, N., & Kimura, A. (2012). A novel disease gene for Brugada syndrome: sarcolemmal membrane-associated protein gene mutations impair intracellular trafficking of hNav1.5. *Circulation. Arrhythmia and electrophysiology*, *5*(6), 1098–1107. https://doi.org/10.1161/CIRCEP.111.969972

Itoh, M., Kim, C. H., Palardy, G., Oda, T., Jiang, Y. J., Maust, D., Yeo, S. Y., Lorick, K., Wright, G. J., Ariza-McNaughton, L., Weissman, A. M., Lewis, J., Chandrasekharappa, S. C., & Chitnis, A. B. (2003). Mind bomb is a ubiquitin ligase that is essential for efficient activation of Notch signaling by Delta. *Developmental cell*, *4*(1), 67–82. https://doi.org/10.1016/s1534-5807(02)00409-4

Jaafar, L., Podolsky, R. H., & Dynan, W. S. (2013). Long-term effects of ionizing radiation on gene expression in a zebrafish model. *PloS one*, *8*(7), e69445. https://doi.org/10.1371/journal.pone.0069445

Jacobs, K., Misri, S., Meyer, B., Raj, S., Zobel, C., Sleckman, B., Hallahan, D. & Sharma, G. (2016). Unique epigenetic influence of H2AX phosphorylation and H3K56 acetylation on normal stem cell radioresponses. *Molecular Biology of the Cell*, 27(8), pp.1332-1345. https://doi.org/10.1091/mbc.E16-01-0017

Jaenen, V., Fraguas, S., Bijnens, K., Heleven, M., Artois, T., Romero, R., Smeets, K., & Cebrià, F. (2021). Reactive oxygen species rescue regeneration after silencing the MAPK-ERK signalling pathway in Schmidtea mediterranea. *Scientific reports*, *11*(1), 881. https://doi.org/10.1038/s41598-020-79588-1

Jafer, A., Sylvius, N., Adewoye, A. B., & Dubrova, Y. E. (2020). The long-term effects of exposure to ionising radiation on gene expression in mice. *Mutation research*, *821*, 111723. https://doi.org/10.1016/j.mrfmmm.2020.111723

Jagadeesh, K. A., Dey, K. K., Montoro, D. T., Mohan, R., Gazal, S., Engreitz, J. M., Xavier, R. J., Price, A. L., & Regev, A. (2022). Identifying disease-critical cell types and cellular processes by integrating single-cell RNA-sequencing and human genetics. *Nature genetics*, *54*(10), 1479–1492. https://doi.org/10.1038/s41588-022-01187-9

Jeggo, P. A., & Löbrich, M. (2006). Contribution of DNA repair and cell cycle checkpoint arrest to the maintenance of genomic stability. *DNA repair*, *5*(9-10), 1192–1198. https://doi.org/10.1016/j.dnarep.2006.05.011

Ji, J., Yu, Y., Li, Z. L., Chen, M. Y., Deng, R., Huang, X., Wang, G. F., Zhang, M. X., Yang, Q., Ravichandran, S., Feng, G. K., Xu, X. L., Yang, C. L., Qiu, M. Z., Jiao, L., Yang, D., & Zhu, X. F. (2018). XIAP Limits Autophagic Degradation of Sox2 and Is A Therapeutic Target in Nasopharyngeal Carcinoma Stem Cells. *Theranostics*, *8*(6), 1494–1510. https://doi.org/10.7150/thno.21717

Jin, B., Ren, J., Chen, J., Dong, Z., Chen, G., & Liu, D. (2022). Autophagy-related DjAtg1-1 plays critical role in planarian regeneration by regulating proliferation and cell death. *Cell and tissue research*, *388*(2), 273–286. https://doi.org/10.1007/s00441-022-03591-3

Jin, X., Jiao, X., Jiao, J., Zhang, T., & Cui, B. (2018). Increased expression of FHL2 promotes tumorigenesis in cervical cancer and is correlated with poor prognosis. *Gene*, *669*, 99–106. https://doi.org/10.1016/j.gene.2018.05.087

Joanito, I., Wirapati, P., Zhao, N., Nawaz, Z., Yeo, G., Lee, F., Eng, C. L. P., Macalinao, D. C., Kahraman, M., Srinivasan, H., Lakshmanan, V., Verbandt, S., Tsantoulis, P., Gunn, N., Venkatesh, P. N., Poh, Z. W., Nahar, R., Oh, H. L. J., Loo, J. M., Chia, S., … Tan, I. B. (2022). Single-cell and bulk transcriptome sequencing identifies two epithelial tumor cell states and refines the consensus molecular classification of colorectal cancer. *Nature genetics*, *54*(7), 963–975. https://doi.org/10.1038/s41588-022-01100-4

Johnson, G. L., & Lapadat, R. (2002). Mitogen-activated protein kinase pathways mediated by ERK, JNK, and p38 protein kinases. *Science (New York, N.Y.)*, *298*(5600), 1911–1912. https://doi.org/10.1126/science.1072682

Johnson, T. E., & Hartman, P. S. (1988). Radiation effects on life span in Caenorhabditis elegans. *Journal of gerontology*, *43*(5), B137–B141. https://doi.org/10.1093/geronj/43.5.b137

Johnston, L. H., & Lowndes, N. F. (1992). Cell cycle control of DNA synthesis in budding yeast. *Nucleic acids research*, *20*(10), 2403–2410. https://doi.org/10.1093/nar/20.10.2403

Jones, M. J., & Huang, T. T. (2012). The Fanconi anemia pathway in replication stress and DNA crosslink repair. *Cellular and molecular life sciences : CMLS*, *69*(23), 3963–3974. https://doi.org/10.1007/s00018-012-1051-0

Jones, P., Binns, D., Chang, H. Y., Fraser, M., Li, W., McAnulla, C., McWilliam, H., Maslen, J., Mitchell, A., Nuka, G., Pesseat, S., Quinn, A. F., Sangrador-Vegas, A., Scheremetjew, M., Yong, S. Y., Lopez, R., & Hunter, S. (2014). InterProScan 5: genome-scale protein function classification. *Bioinformatics (Oxford, England)*, *30*(9), 1236–1240. https://doi.org/10.1093/bioinformatics/btu031

Jönsson, K. I., Harms-Ringdahl, M., & Torudd, J. (2005). Radiation tolerance in the eutardigrade Richtersius coronifer. *International journal of radiation biology*, *81*(9), 649–656. https://doi.org/10.1080/09553000500368453

Jönsson, K. I., Hygum, T. L., Andersen, K. N., Clausen, L. K., & Møbjerg, N. (2016). Tolerance to Gamma Radiation in the Marine Heterotardigrade, Echiniscoides sigismundi. *PloS one*, *11*(12), e0168884. https://doi.org/10.1371/journal.pone.0168884

Jovic, D., Liang, X., Zeng, H., Lin, L., Xu, F., & Luo, Y. (2022). Single-cell RNA sequencing technologies and applications: A brief overview. *Clinical and translational medicine*, *12*(3), e694. https://doi.org/10.1002/ctm2.694

Kadrmas, J. L., & Beckerle, M. C. (2004). The LIM domain: from the cytoskeleton to the nucleus. *Nature reviews. Molecular cell biology*, *5*(11), 920–931. https://doi.org/10.1038/nrm1499

Kang, C., You, Y. J., & Avery, L. (2007). Dual roles of autophagy in the survival of Caenorhabditis elegans during starvation. *Genes & development*, *21*(17), 2161–2171. https://doi.org/10.1101/gad.1573107

Karlsson, M., Zhang, C., Méar, L., Zhong, W., Digre, A., Katona, B., Sjöstedt, E., Butler, L., Odeberg, J., Dusart, P., Edfors, F., Oksvold, P., von Feilitzen, K., Zwahlen, M., Arif, M., Altay, O., Li, X., Ozcan, M., Mardinoglu, A., Fagerberg, L., … Lindskog, C. (2021). A single-cell type transcriptomics map of human tissues. *Science advances*, *7*(31), eabh2169. https://doi.org/10.1126/sciadv.abh2169

Kashima, M., Agata, K., & Shibata, N. (2020). What is the role of PIWI family proteins in adult pluripotent stem cells? Insights from asexually reproducing animals, planarians. *Development, growth & differentiation*, *62*(6), 407–422. https://doi.org/10.1111/dgd.12688

Katoh, O., Tauchi, H., Kawaishi, K., Kimura, A., & Satow, Y. (1995). Expression of the vascular endothelial growth factor (VEGF) receptor gene, KDR, in hematopoietic cells and inhibitory effect of VEGF on apoptotic cell death caused by ionizing radiation. *Cancer research*, *55*(23), 5687–5692.

Kauffman, T., Tran, J., & DiNardo, S. (2003). Mutations in Nop60B, the Drosophila homolog of human dyskeratosis congenita 1, affect the maintenance of the germ-line stem cell lineage during spermatogenesis. *Developmental biology*, *253*(2), 189–199. https://doi.org/10.1016/s0012-1606(02)00013-1

Kawakami A. (2010). Stem cell system in tissue regeneration in fish. *Development, growth & differentiation*, *52*(1), 77–87. https://doi.org/10.1111/j.1440-169X.2009.01138.x

Kemp, H. A., & Sprague, G. F. (2003). Far3 and five interacting proteins prevent premature recovery from pheromone arrest in the budding yeast Saccharomyces cerevisiae. *Molecular and cellular biology*, *23*(5), 1750–1763. https://doi.org/10.1128/MCB.23.5.1750-1763.2003

Kershaw, C. J., Costello, J. L., Castelli, L. M., Talavera, D., Rowe, W., Sims, P. F., Ashe, M. P., Hubbard, S. J., Pavitt, G. D., & Grant, C. M. (2015). The yeast La related protein Slf1p is a key activator of translation during the oxidative stress response. *PLoS genetics*, *11*(1), e1004903. https://doi.org/10.1371/journal.pgen.1004903

Khan, U. W., & Newmark, P. A. (2022). Somatic regulation of female germ cell regeneration and development in planarians. *Cell reports*, *38*(11), 110525. https://doi.org/10.1016/j.celrep.2022.110525

Khanna, K. K., & Jackson, S. P. (2001). DNA double-strand breaks: signalling, repair and the cancer connection. *Nature genetics*, *27*(3), 247–254. https://doi.org/10.1038/85798

Khanna, K. K., Lavin, M. F., Jackson, S. P., & Mulhern, T. D. (2001). ATM, a central controller of cellular responses to DNA damage. *Cell death and differentiation*, *8*(11), 1052–1065. https://doi.org/10.1038/sj.cdd.4400874

Kharbanda, S., Pandey, P., Jin, S., Inoue, S., Bharti, A., Yuan, Z. M., Weichselbaum, R., Weaver, D., & Kufe, D. (1997). Functional interaction between DNA-PK and c-Abl in response to DNA damage. *Nature*, *386*(6626), 732–735. https://doi.org/10.1038/386732a0

Kiernan, A. E., Xu, J., & Gridley, T. (2006). The Notch ligand JAG1 is required for sensory progenitor development in the mammalian inner ear. *PLoS genetics*, *2*(1), e4. https://doi.org/10.1371/journal.pgen.0020004

Kim, N., Kim, H. K., Lee, K., Hong, Y., Cho, J. H., Choi, J. W., Lee, J. I., Suh, Y. L., Ku, B. M., Eum, H. H., Choi, S., Choi, Y. L., Joung, J. G., Park, W. Y., Jung, H. A., Sun, J. M., Lee, S. H., Ahn, J. S., Park, K., Ahn, M. J., … Lee, H. O. (2020). Single-cell RNA sequencing demonstrates the molecular and cellular reprogramming of metastatic lung adenocarcinoma. *Nature communications*, *11*(1), 2285. https://doi.org/10.1038/s41467-020-16164-1

King, R. S., & Newmark, P. A. (2013). In situ hybridization protocol for enhanced detection of gene expression in the planarian Schmidtea mediterranea. *BMC developmental biology*, *13*, 8. https://doi.org/10.1186/1471-213X-13-8

Kitao, H., & Yuan, Z. M. (2002). Regulation of ionizing radiation-induced Rad52 nuclear foci formation by c-Abl-mediated phosphorylation. *The Journal of biological chemistry*, *277*(50), 48944–48948. https://doi.org/10.1074/jbc.M208151200

Kloth, L., Belge, G., Burchardt, K., Loeschke, S., Wosniok, W., Fu, X., Nimzyk, R., Mohamed, S. A., Drieschner, N., Rippe, V., & Bullerdiek, J. (2011). Decrease in thyroid adenoma associated (THADA) expression is a marker of dedifferentiation of thyroid tissue. *BMC clinical pathology*, *11*, 13. https://doi.org/10.1186/1472-6890-11-13

Knakievicz, T., Alves da Silveira, P., & Ferreira, H. B. (2008). Planarian neoblast micronucleus assay for evaluating genotoxicity. *Chemosphere*, *72*(9), 1267–1273. https://doi.org/10.1016/j.chemosphere.2008.04.058

Knight, S. W., Heiss, N. S., Vulliamy, T. J., Greschner, S., Stavrides, G., Pai, G. S., Lestringant, G., Varma, N., Mason, P. J., Dokal, I., & Poustka, A. (1999). X-linked dyskeratosis congenita is predominantly caused by missense mutations in the DKC1 gene. *American journal of human genetics*, *65*(1), 50–58. https://doi.org/10.1086/302446

Ko, E., Kim, J. S., Ju, S., Seo, H. W., Chang, Y., Kang, J. A., Park, S. G., & Jung, G. (2018). Oxidatively Modified Protein-Disulfide Isomerase-Associated 3 Promotes Dyskerin Pseudouridine Synthase 1-Mediated Malignancy and Survival of Hepatocellular Carcinoma Cells. *Hepatology (Baltimore, Md.)*, *68*(5), 1851–1864. https://doi.org/10.1002/hep.30039

Kobayashi, K., Hashiguchi, T., Ichikawa, T., Ishino, Y., Hoshi, M., & Matsumoto, M. (2008). Neoblast-enriched fraction rescues eye formation in eye-defective planarian 'menashi' Dugesia ryukyuensis. Development, growth & differentiation, 50(8), 689–696. https://doi.org/10.1111/j.1440-169X.2008.01066.x

Koch, B. J., Ryan, J. F., & Baxevanis, A. D. (2012). The diversification of the LIM superclass at the base of the metazoa increased subcellular complexity and promoted multicellular specialization. *PloS one*, *7*(3), e33261. https://doi.org/10.1371/journal.pone.0033261

Kong, Y., Flick, M. J., Kudla, A. J., & Konieczny, S. F. (1997). Muscle LIM protein promotes myogenesis by enhancing the activity of MyoD. *Molecular and cellular biology*, *17*(8), 4750–4760. https://doi.org/10.1128/MCB.17.8.4750

Konířová, J., Cupal, L., Jarošová, Š., Michaelidesová, A., Vachelová, J., Davídková, M., Bartůněk, P., & Zíková, M. (2019). Differentiation Induction as a Response to Irradiation in Neural Stem Cells In Vitro. *Cancers*, *11*(7), 913. https://doi.org/10.3390/cancers11070913

Koo, B. K., Lim, H. S., Song, R., Yoon, M. J., Yoon, K. J., Moon, J. S., Kim, Y. W., Kwon, M. C., Yoo, K. W., Kong, M. P., Lee, J., Chitnis, A. B., Kim, C. H., & Kong, Y. Y. (2005). Mind bomb 1 is essential for generating functional Notch ligands to activate Notch. *Development (Cambridge, England)*, *132*(15), 3459–3470. https://doi.org/10.1242/dev.01922

Koo, B. K., Yoon, M. J., Yoon, K. J., Im, S. K., Kim, Y. Y., Kim, C. H., Suh, P. G., Jan, Y. N., & Kong, Y. Y. (2007). An obligatory role of mind bomb-1 in notch signaling of mammalian development. *PloS one*, *2*(11), e1221. https://doi.org/10.1371/journal.pone.0001221

Kraemer, C., Enklaar, T., Zabel, B., & Schmidt, E. R. (2000). Mapping and structure of DMXL1, a human homologue of the DmX gene from Drosophila melanogaster coding for a WD repeat protein. *Genomics*, *64*(1), 97–101. https://doi.org/10.1006/geno.1999.6050

Krisko, A., Leroy, M., Radman, M. & Meselson, M. (2012). Extreme anti-oxidant protection against ionizing radiation in bdelloid rotifers. *Proceedings of the National Academy of Sciences*, 109(7), pp.2354-2357. https://doi.org/10.1073/pnas.1119762109

Kuribayashi, K., Finnberg, N., Jeffers, J., Zambetti, G. & El-Deiry, W. (2011). The relative contribution of pro-apoptotic p53-target genes in the triggering of apoptosis following DNA damage in vitro and in vivo. *Cell Cycle*, 10(14), pp.2380-2389. https://doi.org/10.4161/cc.10.14.16588

Kuroda, S., Tokunaga, C., Kiyohara, Y., Higuchi, O., Konishi, H., Mizuno, K., Gill, G. N., & Kikkawa, U. (1996). Protein-protein interaction of zinc finger LIM domains with protein kinase C. *The Journal of biological chemistry*, *271*(49), 31029–31032. https://doi.org/10.1074/jbc.271.49.31029

La Manno, G., Soldatov, R., Zeisel, A., Braun, E., Hochgerner, H., Petukhov, V., Lidschreiber, K., Kastriti, M. E., Lönnerberg, P., Furlan, A., Fan, J., Borm, L. E., Liu, Z., van Bruggen, D., Guo, J., He, X., Barker, R., Sundström, E., Castelo-Branco, G., Cramer, P., … Kharchenko, P. V. (2018). RNA velocity of single cells. *Nature*, *560*(7719), 494–498. https://doi.org/10.1038/s41586-018-0414-6

La Marca, J. E., & Richardson, H. E. (2020). Two-Faced: Roles of JNK Signalling During Tumourigenesis in the *Drosophila* Model. *Frontiers in cell and developmental biology*, *8*, 42. https://doi.org/10.3389/fcell.2020.00042

Lahr, R. M., Mack, S. M., Héroux, A., Blagden, S. P., Bousquet-Antonelli, C., Deragon, J. M., & Berman, A. J. (2015). The La-related protein 1-specific domain repurposes HEAT-like repeats to directly bind a 5'TOP sequence. *Nucleic acids research*, *43*(16), 8077–8088. https://doi.org/10.1093/nar/gkv748

Lai, A. G., Kosaka, N., Abnave, P., Sahu, S., & Aboobaker, A. A. (2018). The abrogation of condensin function provides independent evidence for defining the self-renewing population of pluripotent stem cells. *Developmental biology*, *433*(2), 218–226. https://doi.org/10.1016/j.ydbio.2017.07.023

Lai, E. C., Roegiers, F., Qin, X., Jan, Y. N., & Rubin, G. M. (2005). The ubiquitin ligase Drosophila Mind bomb promotes Notch signaling by regulating the localization and activity of Serrate and Delta. *Development (Cambridge, England)*, *132*(10), 2319–2332. https://doi.org/10.1242/dev.01825

Lakin, N. D., & Jackson, S. P. (1999). Regulation of p53 in response to DNA damage. *Oncogene*, 18(53), 7644–7655. https://doi.org/10.1038/sj.onc.1203015

Landreth, H. F., Dunaway, P. B., & Cosgrove, G. E. (1974). Effects of whole-body gamma irradiation on various life stages of the toad, Bufo woodhousei fowleri. *Radiation research*, *58*(3), 432–438.

Lapan, S. W., & Reddien, P. W. (2011). dlx and sp6-9 Control optic cup regeneration in a prototypic eye. *PLoS genetics*, *7*(8), e1002226. https://doi.org/10.1371/journal.pgen.1002226

Lapan, S. W., & Reddien, P. W. (2012). Transcriptome analysis of the planarian eye identifies ovo as a specific regulator of eye regeneration. *Cell reports*, *2*(2), 294–307. https://doi.org/10.1016/j.celrep.2012.06.018

Latz, D., Fleckenstein, K., Eble, M., Blatter, J., Wannenmacher, M., & Weber, K. J. (1998). Radiosensitizing potential of gemcitabine (2',2'-difluoro-2'-deoxycytidine) within the cell cycle in vitro. *International journal of radiation oncology, biology, physics*, *41*(4), 875–882. https://doi.org/10.1016/s0360-3016(98)00105-9

Lazzaro, D., Price, M., de Felice, M., & Di Lauro, R. (1991). The transcription factor TTF-1 is expressed at the onset of thyroid and lung morphogenesis and in restricted regions of the foetal brain. *Development (Cambridge, England)*, *113*(4), 1093–1104. https://doi.org/10.1242/dev.113.4.1093

Le Borgne, R., Remaud, S., Hamel, S., & Schweisguth, F. (2005). Two distinct E3 ubiquitin ligases have complementary functions in the regulation of delta and serrate signalling in Drosophila. *PLoS biology*, *3*(4), e96. https://doi.org/10.1371/journal.pbio.0030096

Le Maire, A., Schiltz, M., Stura, E. A., Pinon-Lataillade, G., Couprie, J., Moutiez, M., Gondry, M., Angulo, J. F., & Zinn-Justin, S. (2006). A tandem of SH3-like domains participates in RNA binding in KIN17, a human protein activated in response to genotoxics. *Journal of molecular biology*, *364*(4), 764–776. https://doi.org/10.1016/j.jmb.2006.09.033

Le Michael, X., Haddad, D., Ling, A. K., Li, C., So, C. C., Chopra, A., Hu, R., Angulo, J. F., Moffat, J., & Martin, A. (2016). Kin17 facilitates multiple double-strand break repair pathways that govern B cell class switching. *Scientific reports*, *6*, 37215. https://doi.org/10.1038/srep37215

Leduc, A., Chaouni, S., Pouzoulet, F., De Marzi, L., Megnin-Chanet, F., Corre, E., Stefan, D., Habrand, J. L., Sichel, F., & Laurent, C. (2021). Differential normal skin transcriptomic response in total body irradiated mice exposed to scattered versus scanned proton beams. *Scientific reports*, *11*(1), 5876. https://doi.org/10.1038/s41598-021-85394-0

Lee, E. J., & Tournier, C. (2011). The requirement of uncoordinated 51-like kinase 1 (ULK1) and ULK2 in the regulation of autophagy. *Autophagy*, *7*(7), 689–695. https://doi.org/10.4161/auto.7.7.15450

Lei, K., Thi-Kim Vu, H., Mohan, R. D., McKinney, S. A., Seidel, C. W., Alexander, R., Gotting, K., Workman, J. L., & Sánchez Alvarado, A. (2016). Egf Signaling Directs Neoblast Repopulation by Regulating Asymmetric Cell Division in Planarians. *Developmental cell*, *38*(4), 413–429. https://doi.org/10.1016/j.devcel.2016.07.012

Lei, K., Zhang, W., Chen, J., McKinney, S. A., Ross, E. J., Lee, H. C., & Sánchez Alvarado, A. (2023). Pluripotency retention and exogenous mRNA introduction in planarian stem cells in culture. *iScience*, *26*(2), 106001. https://doi.org/10.1016/j.isci.2023.106001

Levy, J. M. M., Towers, C. G., & Thorburn, A. (2017). Targeting autophagy in cancer. *Nature reviews. Cancer*, *17*(9), 528–542. https://doi.org/10.1038/nrc.2017.53

Li, B. (2005). c-Abl in oxidative stress, aging and cancer. *Cell cycle (Georgetown, Tex.)*, *4*(2), 246–248. https://doi.org/10.4161/cc.4.2.1490

Li, F., Zheng, X., Liu, Y., Li, P., Liu, X., Ye, F., Zhao, T., Wu, Q., Jin, X., & Li, Q. (2016). Different Roles of CHOP and JNK in Mediating Radiation-Induced Autophagy and Apoptosis in Breast Cancer Cells. *Radiation research*, *185*(5), 539–548. https://doi.org/10.1667/RR14344.1

Li, L., Liu, W. L., Su, L., Lu, Z. C., & He, X. S. (2020). The Role of Autophagy in Cancer Radiotherapy. *Current molecular pharmacology*, *13*(1), 31–40. https://doi.org/10.2174/1874467212666190809154518

Liang, L., Zhang, H. W., Liang, J., Niu, X. L., Zhang, S. Z., Feng, L., Liang, Y. M., & Han, H. (2008). KyoT3, an isoform of murine FHL1, associates with the transcription factor RBP-J and represses the RBP-J-mediated transactivation. *Biochimica et biophysica acta*, *1779*(12), 805–810. https://doi.org/10.1016/j.bbagrm.2008.08.001

Liao, Y., Smyth, G. K., & Shi, W. (2014). featureCounts: an efficient general purpose program for assigning sequence reads to genomic features. *Bioinformatics (Oxford, England)*, *30*(7), 923–930. https://doi.org/10.1093/bioinformatics/btt656

Lieber, M. (2010). The Mechanism of Double-Strand DNA Break Repair by the Nonhomologous DNA End-Joining Pathway. *Annual Review of Biochemistry*, 79(1), pp.181-211. https://doi.org/10.1146/annurev.biochem.052308.093131

Lin, A., & Dibling, B. (2002). The true face of JNK activation in apoptosis. *Aging cell*, *1*(2), 112–116. https://doi.org/10.1046/j.1474-9728.2002.00014.x

Lin, J., Qin, X., Zhu, Z., Mu, J., Zhu, L., Wu, K., Jiao, H., Xu, X., & Ye, Q. (2012). FHL family members suppress vascular endothelial growth factor expression through blockade of dimerization of HIF1α and HIF1β. *IUBMB life*, *64*(11), 921–930. https://doi.org/10.1002/iub.1089

Lindahl, T. & Barnes, D. (2000). Repair of Endogenous DNA Damage. *Cold Spring Harbor Symposia on Quantitative Biology*, 65(0), pp.127-134. https://doi.org/10.1101/sqb.2000.65.127

Lindsay-Mosher, N., Chan, A., & Pearson, B. J. (2020). Planarian EGF repeat-containing genes megf6 and hemicentin are required to restrict the stem cell compartment. *PLoS genetics*, 16(2), e1008613. https://doi.org/10.1371/journal.pgen.1008613

Lindsell, C. E., Shawber, C. J., Boulter, J., & Weinmaster, G. (1995). Jagged: a mammalian ligand that activates Notch1. *Cell*, *80*(6), 909–917. https://doi.org/10.1016/0092-8674(95)90294-5

Love, M. I., Huber, W., & Anders, S. (2014). Moderated estimation of fold change and dispersion for RNA-seq data with DESeq2. *Genome biology*, *15*(12), 550. https://doi.org/10.1186/s13059-014-0550-8

Lu, J., Wu, T., Zhang, B., Liu, S., Song, W., Qiao, J., & Ruan, H. (2021). Types of nuclear localization signals and mechanisms of protein import into the nucleus. *Cell communication and signaling : CCS*, *19*(1), 60. https://doi.org/10.1186/s12964-021-00741-y

Lum, J. J., DeBerardinis, R. J., & Thompson, C. B. (2005). Autophagy in metazoans: cell survival in the land of plenty. *Nature reviews. Molecular cell biology*, *6*(6), 439–448. https://doi.org/10.1038/nrm1660

Lundholm, L., Hååg, P., Zong, D., Juntti, T., Mörk, B., Lewensohn, R., & Viktorsson, K. (2013). Resistance to DNA-damaging treatment in non-small cell lung cancer tumor-initiating cells involves reduced DNA-PK/ATM activation and diminished cell cycle arrest. *Cell death & disease*, 4(1), e478. https://doi.org/10.1038/cddis.2012.211

Ma, Y., Pannicke, U., Schwarz, K. & Lieber, M. (2002). Hairpin Opening and Overhang Processing by an Artemis/DNA-Dependent Protein Kinase Complex in Nonhomologous End Joining and V(D)J Recombination. *Cell*, 108(6), pp.781-794. https://doi.org/10.1016/s0092-8674(02)00671-2

Macia i Garau, M., Lucas-Calduch, A. & López, E. (2011). Radiobiology of the acute radiation syndrome. *Reports of Practical Oncology & Radiotherapy*, 16(4), pp.123-130. https://doi.org/10.1016/j.rpor.2011.06.001

Maier, P., Hartmann, L., Wenz, F. & Herskind, C. (2016). Cellular Pathways in Response to Ionizing Radiation and Their Targetability for Tumor Radiosensitization. *International Journal of Molecular Sciences*, 17(1), p.102. https://doi.org/10.3390/ijms17010102

Malloy, K. D., Holman, M. A., Mitchell, D., & Detrich, H. W. (1997). Solar UVB-induced DNA damage and photoenzymatic DNA repair in antarctic zooplankton. *Proceedings of the National Academy of Sciences of the United States of America*, *94*(4), 1258–1263. https://doi.org/10.1073/pnas.94.4.1258

Man, S. M., & Kanneganti, T. D. (2016). Regulation of lysosomal dynamics and autophagy by CTSB/cathepsin B. *Autophagy*, *12*(12), 2504–2505. https://doi.org/10.1080/15548627.2016.1239679

Mansouri-Noori, F., Pircher, A., Bilodeau, D., Siniavskaia, L., Grigull, J., Rissland, O. S., & Bayfield, M. A. (2023). The LARP1 homolog Slr1p controls the stability and expression of proto-5'TOP mRNAs in fission yeast. *Cell reports*, *42*(10), 113226. https://doi.org/10.1016/j.celrep.2023.113226

Marnett, L. & Plastaras, J. (2001). Endogenous DNA damage and mutation. *Trends in Genetics*, 17(4), pp.214-221. https://doi.org/10.1016/s0168-9525(01)02239-9

Martin, F. J., Amode, M. R., Aneja, A., Austine-Orimoloye, O., Azov, A. G., Barnes, I., Becker, A., Bennett, R., Berry, A., Bhai, J., Bhurji, S. K., Bignell, A., Boddu, S., Branco Lins, P. R., Brooks, L., Ramaraju, S. B., Charkhchi, M., Cockburn, A., Da Rin Fiorretto, L., Davidson, C., … Flicek, P. (2023). Ensembl 2023. *Nucleic acids research*, *51*(D1), D933–D941. https://doi.org/10.1093/nar/gkac958

Martin, M. (2011). Cutadapt removes adapter sequences from high-throughput sequencing reads. *EMBnet.journal, 17*(1), pp. 10-12. https://doi.org/10.14806/ej.17.1.200

Martin, M., Vulin, A. & Hendry, J. (2016). Human epidermal stem cells: Role in adverse skin reactions and carcinogenesis from radiation. *Mutation Research/Reviews in Mutation Research*, 770, pp.349-368. https://doi.org/10.1016/j.mrrev.2016.08.004

März, M., Seebeck, F., & Bartscherer, K. (2013). A Pitx transcription factor controls the establishment and maintenance of the serotonergic lineage in planarians. *Development (Cambridge, England)*, *140*(22), 4499–4509. https://doi.org/10.1242/dev.100081

Masson, C., Menaa, F., Pinon-Lataillade, G., Frobert, Y., Chevillard, S., Radicella, J. P., Sarasin, A., & Angulo, J. F. (2003). Global genome repair is required to activate KIN17, a UVC-responsive gene involved in DNA replication. *Proceedings of the National Academy of Sciences of the United States of America*, *100*(2), 616–621. https://doi.org/10.1073/pnas.0236176100

Mathew, R., Karantza-Wadsworth, V., & White, E. (2007). Role of autophagy in cancer. *Nature reviews. Cancer*, *7*(12), 961–967. https://doi.org/10.1038/nrc2254

Mavragani, I. V., Nikitaki, Z., Kalospyros, S. A., & Georgakilas, A. G. (2019). Ionizing Radiation and Complex DNA Damage: From Prediction to Detection Challenges and Biological Significance. *Cancers*, *11*(11), 1789. https://doi.org/10.3390/cancers11111789

Maynard, S., Swistowska, A. M., Lee, J. W., Liu, Y., Liu, S. T., Da Cruz, A. B., Rao, M., de Souza-Pinto, N. C., Zeng, X., & Bohr, V. A. (2008). Human embryonic stem cells have enhanced repair of multiple forms of DNA damage. *Stem cells (Dayton, Ohio)*, *26*(9), 2266–2274. https://doi.org/10.1634/stemcells.2007-1041

McCord, A., Jamal, M., Williams, E., Camphausen, K., & Tofilon, P. (2009). CD133+ glioblastoma stem-like cells are radiosensitive with a defective DNA damage response compared with established cell lines. *Clinical cancer research : an official journal of the American Association for Cancer Research*, *15*(16), 5145–5153.

McFerrin, M. B., Turner, K. L., Cuddapah, V. A., & Sontheimer, H. (2012). Differential role of IK and BK potassium channels as mediators of intrinsic and extrinsic apoptotic cell death. *American journal of physiology. Cell physiology*, *303*(10), C1070–C1078. https://doi.org/10.1152/ajpcell.00040.2012

McInnes, L., Healy, J., & Melville, J. (2018). UMAP: uniform manifold approximation and projection for dimension reduction. *arXiv*:1802.03426. http://doi.org/10.48550/arXiv.1802.03426

Mellinger, P., Schultz, V. & James, D. (1975). Ionizing radiation and wild birds: A review. *C R C Critical Reviews in Environmental Control*, 5(3), pp.397-421. https://doi.org/10.1080/10643387509381629

Meyer, B., Fabbrizi, M., Raj, S., Zobel, C., Hallahan, D. & Sharma, G. (2016). Histone H3 Lysine 9 Acetylation Obstructs ATM Activation and Promotes Ionizing Radiation Sensitivity in Normal Stem Cells. *Stem Cell Reports*, 7(6), pp.1013-1022. https://doi.org/10.1016/j.stemcr.2016.11.004

Miccoli, L., Biard, D. S., Frouin, I., Harper, F., Maga, G., & Angulo, J. F. (2003). Selective interactions of human kin17 and RPA proteins with chromatin and the nuclear matrix in a DNA damage- and cell cycle-regulated manner. *Nucleic acids research*, *31*(14), 4162–4175. https://doi.org/10.1093/nar/gkg459

Miccoli, L., Frouin, I., Novac, O., Di Paola, D., Harper, F., Zannis-Hadjopoulos, M., Maga, G., Biard, D. S., & Angulo, J. F. (2005). The human stress-activated protein kin17 belongs to the multiprotein DNA replication complex and associates in vivo with mammalian replication origins. *Molecular and cellular biology*, *25*(9), 3814–3830. https://doi.org/10.1128/MCB.25.9.3814-3830.2005

Mihaylova, Y., Abnave, P., Kao, D., Hughes, S., Lai, A., Jaber-Hijazi, F., Kosaka, N., & Aboobaker, A. A. (2018). Conservation of epigenetic regulation by the MLL3/4 tumour suppressor in planarian pluripotent stem cells. *Nature communications*, *9*(1), 3633. https://doi.org/10.1038/s41467-018-06092-6

Mitchell, J. R., Wood, E., & Collins, K. (1999). A telomerase component is defective in the human disease dyskeratosis congenita. *Nature*, *402*(6761), 551–555. https://doi.org/10.1038/990141

Mix, M. C., & Sparks, A. K. (1970). Studies on the histopathological effects of ionizing radiation on the oyster Crassostrea gigas. I. The degenerative phase involving digestive diverticulae, stomach, and gut. *Journal of invertebrate pathology*, *16*(1), 14–37. https://doi.org/10.1016/0022-2011(70)90201-6

Mizushima, N., & Komatsu, M. (2011). Autophagy: renovation of cells and tissues. *Cell*, *147*(4), 728–741. https://doi.org/10.1016/j.cell.2011.10.026

Mlynarova, J., Trentin-Sonoda, M., Gaisler da Silva, F., Major, J. L., Salih, M., Carneiro-Ramos, M. S., & Tuana, B. S. (2019). SLMAP3 isoform modulates cardiac gene expression and function. *PloS one*, *14*(4), e0214669. https://doi.org/10.1371/journal.pone.0214669

Molina, M. D., & Cebrià, F. (2021). Decoding Stem Cells: An Overview on Planarian Stem Cell Heterogeneity and Lineage Progression. *Biomolecules*, *11*(10), 1532. https://doi.org/10.3390/biom11101532

Molinaro, A. M., & Pearson, B. J. (2016). In silico lineage tracing through single cell transcriptomics identifies a neural stem cell population in planarians. *Genome biology*, *17*, 87. https://doi.org/10.1186/s13059-016-0937-9

Monje, M. L., Mizumatsu, S., Fike, J. R., & Palmer, T. D. (2002). Irradiation induces neural precursor-cell dysfunction. *Nature medicine*, *8*(9), 955–962. https://doi.org/10.1038/nm749

Moore, N., & Lyle, S. (2011). Quiescent, slow-cycling stem cell populations in cancer: a review of the evidence and discussion of significance. *Journal of oncology*, *2011*, 396076. https://doi.org/10.1155/2011/396076

Moreno-Hagelsieb, G., & Latimer, K. (2008). Choosing BLAST options for better detection of orthologs as reciprocal best hits. *Bioinformatics (Oxford, England)*, *24*(3), 319–324. https://doi.org/10.1093/bioinformatics/btm585

Morgan, T. (1901). Regeneration. *Columbia University Biological series: Vol. VII*. New York: The Macmillan Company.

Morgan, W. F., & Sowa, M. B. (2005). Effects of ionizing radiation in nonirradiated cells. *Proceedings of the National Academy of Sciences of the United States of America*, *102*(40), 14127–14128. https://doi.org/10.1073/pnas.0507119102

Mori, R., Matsuya, Y., Yoshii, Y. & Date, H. (2018). Estimation of the radiation-induced DNA double-strand breaks number by considering cell cycle and absorbed dose per cell nucleus. *Journal of Radiation Research*, 59(3), pp.253-260. https://doi.org/10.1093/jrr/rrx097

Muller, H. J. (1927). Artificial Transmutation of the Gene. *Science (New York, N.Y.)*, *66*(1699), 84–87. https://doi.org/10.1126/science.66.1699.84

Muller, H. J. (1928). The Production of Mutations by X-Rays. *Proceedings of the National Academy of Sciences of the United States of America*, *14*(9), 714–726. https://doi.org/10.1073/pnas.14.9.714

Munshi, A., & Ramesh, R. (2013). Mitogen-activated protein kinases and their role in radiation response. *Genes & cancer*, *4*(9-10), 401–408. https://doi.org/10.1177/1947601913485414

Mura, M., Hopkins, T. G., Michael, T., Abd-Latip, N., Weir, J., Aboagye, E., Mauri, F., Jameson, C., Sturge, J., Gabra, H., Bushell, M., Willis, A. E., Curry, E., & Blagden, S. P. (2015). LARP1 post-transcriptionally regulates mTOR and contributes to cancer progression. *Oncogene*, *34*(39), 5025–5036. https://doi.org/10.1038/onc.2014.428

Nabors, L. B., Ammirati, M., Bierman, P. J., Brem, H., Butowski, N., Chamberlain, M. C., DeAngelis, L. M., Fenstermaker, R. A., Friedman, A., Gilbert, M. R., Hesser, D., Holdhoff, M., Junck, L., Lawson, R., Loeffler, J. S., Maor, M. H., Moots, P. L., Morrison, T., Mrugala, M. M., Newton, H. B., … National Comprehensive Cancer Network (2013). Central nervous system cancers. *Journal of the National Comprehensive Cancer Network* : JNCCN, 11(9), 1114–1151. https://doi.org/10.6004/jnccn.2013.0132

Nader, M., Westendorp, B., Hawari, O., Salih, M., Stewart, A. F., Leenen, F. H., & Tuana, B. S. (2012). Tail-anchored membrane protein SLMAP is a novel regulator of cardiac function at the sarcoplasmic reticulum. *American journal of physiology. Heart and circulatory physiology*, *302*(5), H1138–H1145. https://doi.org/10.1152/ajpheart.00872.2011

Nam, E. A., & Cortez, D. (2011). ATR signalling: more than meeting at the fork. *The Biochemical journal*, *436*(3), 527–536. https://doi.org/10.1042/BJ20102162

Narciso, L., Fortini, P., Pajalunga, D., Franchitto, A., Liu, P., Degan, P., Frechet, M., Demple, B., Crescenzi, M., & Dogliotti, E. (2007). Terminally differentiated muscle cells are defective in base excision DNA repair and hypersensitive to oxygen injury. *Proceedings of the National Academy of Sciences of the United States of America*, *104*(43), 17010–17015. https://doi.org/10.1073/pnas.0701743104

National Research Council. (2006). Health Risks from Exposure to Low Levels of Ionizing Radiation: BEIR VII Phase *2*. *Washington, DC: The National Academies Press*. https://doi.org/10.17226/11340.

Neiro, J., Sridhar, D., Dattani, A., & Aboobaker, A. (2022). Identification of putative enhancer-like elements predicts regulatory networks active in planarian adult stem cells. *eLife*, *11*, e79675. https://doi.org/10.7554/eLife.79675

Nelson, R. & Stafford, E. (1972). Effects of gamma radiation on the biology and population suppression of the two-spotted spider mite, *Tetranychus urticae* Koch. *Hilgardia* 41(12):299-341.

New, D. C., & Wong, Y. H. (2007). Molecular mechanisms mediating the G protein-coupled receptor regulation of cell cycle progression. *Journal of molecular signaling*, *2*, 2. https://doi.org/10.1186/1750-2187-2-2

Newmark, P. A., & Sánchez Alvarado, A. (2000). Bromodeoxyuridine specifically labels the regenerative stem cells of planarians. *Developmental biology*, *220*(2), 142–153. https://doi.org/10.1006/dbio.2000.9645

Nicolas, E., Simion, P., Guérineau, M., Terwagne, M., Colinet, M., Virgo, J., Lingurski, M., Boutsen, A., Dieu, M., Hallet, B., & Van Doninck, K. (2023). Horizontal acquisition of a DNA ligase improves DNA damage tolerance in eukaryotes. *Nature communications*, *14*(1), 7638. https://doi.org/10.1038/s41467-023-43075-8

Nikjoo, H., Bolton, C. E., Watanabe, R., Terrissol, M., O'Neill, P., & Goodhead, D. T. (2002). Modelling of DNA damage induced by energetic electrons (100 eV to 100 keV). *Radiation protection dosimetry*, *99*(1-4), 77–80. https://doi.org/10.1093/oxfordjournals.rpd.a006843

Nikjoo, H., O'Neill, P., Goodhead, D. T., & Terrissol, M. (1997). Computational modelling of low-energy electron-induced DNA damage by early physical and chemical events. *International journal of radiation biology*, *71*(5), 467–483. https://doi.org/10.1080/095530097143798

Nikjoo, H., O'Neill, P., Wilson, W. E., & Goodhead, D. T. (2001). Computational approach for determining the spectrum of DNA damage induced by ionizing radiation. *Radiation research*, *156*(5 Pt 2), 577–583. https://doi.org/10.1667/0033-7587(2001)156

Nishioka, S., Wu, P. H., Yakabe, T., Giaccia, A. J., Le, Q. T., Aoyama, H., Shimizu, S., Shirato, H., Onodera, Y., & Nam, J. M. (2020). Rab27b contributes to radioresistance and exerts a paracrine effect via epiregulin in glioblastoma. *Neuro-oncology advances*, *2*(1), vdaa091. https://doi.org/10.1093/noajnl/vdaa091

Niu, C., Liang, C., Guo, J., Cheng, L., Zhang, H., Qin, X., Zhang, Q., Ding, L., Yuan, B., Xu, X., Li, J., Lin, J., & Ye, Q. (2012). Downregulation and growth inhibitory role of FHL1 in lung cancer. *International journal of cancer*, *130*(11), 2549–2556. https://doi.org/10.1002/ijc.26259

Nordzieke, S., Zobel, T., Fränzel, B., Wolters, D. A., Kück, U., & Teichert, I. (2015). A fungal sarcolemmal membrane-associated protein (SLMAP) homolog plays a fundamental role in development and localizes to the nuclear envelope, endoplasmic reticulum, and mitochondria. *Eukaryotic cell*, *14*(4), 345–358. https://doi.org/10.1128/EC.00241-14

Nykamp, K., Lee, M. H., & Kimble, J. (2008). C. elegans La-related protein, LARP-1, localizes to germline P bodies and attenuates Ras-MAPK signaling during oogenesis. *RNA (New York, N.Y.)*, *14*(7), 1378–1389. https://doi.org/10.1261/rna.1066008

O'Brien, R., Tran, S. L., Maritz, M. F., Liu, B., Kong, C. F., Purgato, S., Yang, C., Murray, J., Russell, A. J., Flemming, C. L., von Jonquieres, G., Pickett, H. A., London, W. B., Haber, M., Gunaratne, P. H., Norris, M. D., Perini, G., Fletcher, J. I., & MacKenzie, K. L. (2016). MYC-Driven Neuroblastomas Are Addicted to a Telomerase-Independent Function of Dyskerin. *Cancer research*, *76*(12), 3604–3617. https://doi.org/10.1158/0008-5472.CAN-15-0879

O'Driscoll, M., & Jeggo, P. A. (2006). The role of double-strand break repair - insights from human genetics. *Nature reviews. Genetics*, *7*(1), 45–54. https://doi.org/10.1038/nrg1746

O'Hayre, M., Degese, M. S., & Gutkind, J. S. (2014). Novel insights into G protein and G protein-coupled receptor signaling in cancer. *Current opinion in cell biology*, *27*, 126–135. https://doi.org/10.1016/j.ceb.2014.01.005

Oda, E., Ohki, R., Murasawa, H., Nemoto, J., Shibue, T., Yamashita, T., Tokino, T., Taniguchi, T., & Tanaka, N. (2000). Noxa, a BH3-only member of the Bcl-2 family and candidate mediator of p53-induced apoptosis. *Science (New York, N.Y.)*, *288*(5468), 1053–1058. https://doi.org/10.1126/science.288.5468.1053

Oh, S. W., Mukhopadhyay, A., Svrzikapa, N., Jiang, F., Davis, R. J., & Tissenbaum, H. A. (2005). JNK regulates lifespan in Caenorhabditis elegans by modulating nuclear translocation of forkhead transcription factor/DAF-16. *Proceedings of the National Academy of Sciences of the United States of America*, *102*(12), 4494–4499. https://doi.org/10.1073/pnas.0500749102

Ohno, S. (1970). Evolution by Gene Duplcation. Springer-Verlag.

Okuyama, T., Inoue, H., Ookuma, S., Satoh, T., Kano, K., Honjoh, S., Hisamoto, N., Matsumoto, K., & Nishida, E. (2010). The ERK-MAPK pathway regulates longevity through SKN-1 and insulin-like signaling in Caenorhabditis elegans. *The Journal of biological chemistry*, *285*(39), 30274–30281. https://doi.org/10.1074/jbc.M110.146274

Olive, P. (1998). The Role of DNA Single- and Double-Strand Breaks in Cell Killing by Ionizing Radiation. *Radiation Research*, 150(5), p.S42.

Olive, P., & Banáth, J. (2006). The comet assay: a method to measure DNA damage in individual cells. *Nature protocols*, *1*(1), 23–29. https://doi.org/10.1038/nprot.2006.5

Oliver, L., Hue, E., Séry, Q., Lafargue, A., Pecqueur, C., Paris, F. & Vallette, F. (2013). Differentiation-Related Response to DNA Breaks in Human Mesenchymal Stem Cells. *Stem Cells*, 31(4), pp.800-807. https://doi.org/10.1002/stem.1336

Otani, K., Naito, Y., Sakaguchi, Y., Seo, Y., Takahashi, Y., Kikuta, J., Ogawa, K., & Ishii, M. (2016). Cell-cycle-controlled radiation therapy was effective for treating a murine malignant melanoma cell line in vitro and in vivo. *Scientific reports*, *6*, 30689. https://doi.org/10.1038/srep30689

Oviedo, N. J., & Beane, W. S. (2009). Regeneration: The origin of cancer or a possible cure?. *Seminars in cell & developmental biology*, *20*(5), 557–564. https://doi.org/10.1016/j.semcdb.2009.04.005

Oviedo, N. J., Newmark, P. A., & Sánchez Alvarado, A. (2003). Allometric scaling and proportion regulation in the freshwater planarian Schmidtea mediterranea. *Developmental dynamics : an official publication of the American Association of Anatomists*, *226*(2), 326–333. https://doi.org/10.1002/dvdy.10228

Oviedo, N. J., Pearson, B. J., Levin, M., & Sánchez Alvarado, A. (2008). Planarian PTEN homologs regulate stem cells and regeneration through TOR signaling. *Disease models & mechanisms*, *1*(2-3), 131–141. https://doi.org/10.1242/dmm.000117

Paithankar, J., Ghodke, T. & Patil, R. (2021). Insight into the evolutionary profile of radio-resistance among insects having intrinsically evolved defence against radiation toxicity. *International Journal of Radiation Biology*, 98(6), pp.1012-1024. https://doi.org/10.1080/09553002.2020.1859153

Palakodeti, D., Smielewska, M., Lu, Y. C., Yeo, G. W., & Graveley, B. R. (2008). The PIWI proteins SMEDWI-2 and SMEDWI-3 are required for stem cell function and piRNA expression in planarians. *RNA (New York, N.Y.)*, *14*(6), 1174–1186. https://doi.org/10.1261/rna.1085008

Pardue, M. L., Rashkova, S., Casacuberta, E., DeBaryshe, P. G., George, J. A., & Traverse, K. L. (2005). Two retrotransposons maintain telomeres in Drosophila. *Chromosome research : an international journal on the molecular, supramolecular and evolutionary aspects of chromosome biology*, *13*(5), 443–453. https://doi.org/10.1007/s10577-005-0993-6

Park, H. H., Lo, Y. C., Lin, S. C., Wang, L., Yang, J. K., & Wu, H. (2007). The death domain superfamily in intracellular signaling of apoptosis and inflammation. *Annual review of immunology*, *25*, 561–586. https://doi.org/10.1146/annurev.immunol.25.022106.141656

Pascual-Carreras, E., Marín-Barba, M., Castillo-Lara, S., Coronel-Córdoba, P., Magri, M. S., Wheeler, G. N., Gómez-Skarmeta, J. L., Abril, J. F., Saló, E., & Adell, T. (2023). Wnt/β-catenin signalling is required for pole-specific chromatin remodeling during planarian regeneration. *Nature communications*, *14*(1), 298. https://doi.org/10.1038/s41467-023-35937-y

Paull, T., Rogakou, E., Yamazaki, V., Kirchgessner, C., Gellert, M. & Bonner, W. (2000). A critical role for histone H2AX in recruitment of repair factors to nuclear foci after DNA damage. *Current Biology*, 10(15), pp.886-895.

Pawlik, T. M., & Keyomarsi, K. (2004). Role of cell cycle in mediating sensitivity to radiotherapy. *International journal of radiation oncology, biology, physics*, *59*(4), 928–942. https://doi.org/10.1016/j.ijrobp.2004.03.005

Pearson, B. J., & Sánchez Alvarado, A. (2008). Regeneration, stem cells, and the evolution of tumor suppression. *Cold Spring Harbor symposia on quantitative biology*, *73*, 565–572. https://doi.org/10.1101/sqb.2008.73.045

Pearson, B. J., & Sánchez Alvarado, A. (2010). A planarian p53 homolog regulates proliferation and self-renewal in adult stem cell lineages. *Development (Cambridge, England)*, *137*(2), 213–221. https://doi.org/10.1242/dev.044297

Peiris, T. H., García-Ojeda, M. E., & Oviedo, N. J. (2016a). Alternative flow cytometry strategies to analyze stem cells and cell death in planarians. *Regeneration (Oxford, England)*, *3*(2), 123–135. https://doi.org/10.1002/reg2.53

Peiris, T. H., Ramirez, D., Barghouth, P. G., & Oviedo, N. J. (2016b). The Akt signaling pathway is required for tissue maintenance and regeneration in planarians. *BMC developmental biology*, *16*, 7. https://doi.org/10.1186/s12861-016-0107-z

Peiris, T. H., Ramirez, D., Barghouth, P. G., Ofoha, U., Davidian, D., Weckerle, F., & Oviedo, N. J. (2016c). Regional signals in the planarian body guide stem cell fate in the presence of genomic instability. *Development (Cambridge, England)*, *143*(10), 1697–1709. https://doi.org/10.1242/dev.131318

Pellettieri, J., & Sánchez Alvarado, A. (2007). Cell turnover and adult tissue homeostasis: from humans to planarians. *Annual review of genetics*, *41*, 83–105. https://doi.org/10.1146/annurev.genet.41.110306

Pellettieri, J., Fitzgerald, P., Watanabe, S., Mancuso, J., Green, D. R., & Sánchez Alvarado, A. (2010). Cell death and tissue remodeling in planarian regeneration. *Developmental biology*, *338*(1), 76–85. https://doi.org/10.1016/j.ydbio.2009.09.015

Pellin, D., Loperfido, M., Baricordi, C., Wolock, S. L., Montepeloso, A., Weinberg, O. K., Biffi, A., Klein, A. M., & Biasco, L. (2019). A comprehensive single cell transcriptional landscape of human hematopoietic progenitors. *Nature communications*, *10*(1), 2395. https://doi.org/10.1038/s41467-019-10291-0

Peng, Y., Zhang, M., Zheng, L., Liang, Q., Li, H., Chen, J. T., Guo, H., Yoshina, S., Chen, Y. Z., Zhao, X., Wu, X., Liu, B., Mitani, S., Yu, J. S., & Xue, D. (2017). Cysteine protease cathepsin B mediates radiation-induced bystander effects. *Nature*, *547*(7664), 458–462. https://doi.org/10.1038/nature23284

Petes, T. (2001). Meiotic recombination hot spots and cold spots. *Nature Reviews Genetics*, 2(5), pp.360-369. https://doi.org/10.1038/35072078

Pfister, D., De Mulder, K., Philipp, I., Kuales, G., Hrouda, M., Eichberger, P., Borgonie, G., Hartenstein, V., & Ladurner, P. (2007). The exceptional stem cell system of Macrostomum lignano: screening for gene expression and studying cell proliferation by hydroxyurea treatment and irradiation. *Frontiers in zoology*, 4, 9. https://doi.org/10.1186/1742-9994-4-9

Pietras, C. O., Vendelin, J., Anedda, F., Bruce, S., Adner, M., Sundman, L., Pulkkinen, V., Alenius, H., D'Amato, M., Söderhäll, C., & Kere, J. (2011). The asthma candidate gene NPSR1 mediates isoform specific downstream signalling. *BMC pulmonary medicine*, *11*, 39. https://doi.org/10.1186/1471-2466-11-39

Pizzino, G., Irrera, N., Cucinotta, M., Pallio, G., Mannino, F., Arcoraci, V., Squadrito, F., Altavilla, D., & Bitto, A. (2017). Oxidative Stress: Harms and Benefits for Human Health. *Oxidative medicine and cellular longevity*, *2017*, 8416763. https://doi.org/10.1155/2017/8416763

Plass, M., Solana, J., Wolf, F. A., Ayoub, S., Misios, A., Glažar, P., Obermayer, B., Theis, F. J., Kocks, C., & Rajewsky, N. (2018). Cell type atlas and lineage tree of a whole complex animal by single-cell transcriptomics. *Science (New York, N.Y.)*, *360*(6391), eaaq1723. https://doi.org/10.1126/science.aaq1723

Polo, S. E., & Jackson, S. P. (2011). Dynamics of DNA damage response proteins at DNA breaks: a focus on protein modifications. *Genes & development*, 25(5), 409–433. https://doi.org/10.1101/gad.2021311

Poprawa, I., Hyra, M., & Rost-Roszkowska, M. M. (2015). Germ cell cluster organization and oogenesis in the tardigrade Dactylobiotus parthenogeneticus Bertolani, 1982 (Eutardigrada, Murrayidae). *Protoplasma*, *252*(4), 1019–1029. https://doi.org/10.1007/s00709-014-0737-6

Potten, C., Gandara, R., Mahida, Y., Loeffler, M. & Wright, N. (2009). The stem cells of small intestinal crypts: where are they?. *Cell Proliferation*, 42(6), pp.731-750. https://doi.org/10.1111/j.1365-2184.2009.00642.x

Preston, B. D., Albertson, T. M., & Herr, A. J. (2010). DNA replication fidelity and cancer. *Seminars in cancer biology*, 20(5), 281–293. https://doi.org/10.1016/j.semcancer.2010.10.009

Putnam, N. H., Butts, T., Ferrier, D. E., Furlong, R. F., Hellsten, U., Kawashima, T., Robinson-Rechavi, M., Shoguchi, E., Terry, A., Yu, J. K., Benito-Gutiérrez, E. L., Dubchak, I., Garcia-Fernàndez, J., Gibson-Brown, J. J., Grigoriev, I. V., Horton, A. C., de Jong, P. J., Jurka, J., Kapitonov, V. V., Kohara, Y., … Rokhsar, D. S. (2008). The amphioxus genome and the evolution of the chordate karyotype. *Nature*, 453(7198), 1064–1071. https://doi.org/10.1038/nature06967

Qin, H., Wang, J., Liang, Y., Taniguchi, Y., Tanigaki, K., & Han, H. (2004). RING1 inhibits transactivation of RBP-J by Notch through interaction with LIM protein KyoT2. *Nucleic acids research*, *32*(4), 1492–1501. https://doi.org/10.1093/nar/gkh295

Qin, H., Yu, T., Qing, T., Liu, Y., Zhao, Y., Cai, J., Li, J., Song, Z., Qu, X., Zhou, P., Wu, J., Ding, M. & Deng, H. (2007). Regulation of Apoptosis and Differentiation by p53 in Human Embryonic Stem Cells. *Journal of Biological Chemistry*, 282(8), pp.5842-5852.

R Core Team. (2021). R: A language an environment for statistical computing. R Foundation for Statistical Computing, Vienna, Austria. http://www.R-project.org/.

Ramsden, D. (2011). Polymerases in Nonhomologous End Joining: Building a Bridge over Broken Chromosomes. *Antioxidants & Redox Signaling*, 14(12), pp.2509-2519. https://doi.org/10.1089/ars.2010.3429

Rastogi, R., Richa, Kumar, A., Tyagi, M. & Sinha, R. (2010). Molecular Mechanisms of Ultraviolet Radiation-Induced DNA Damage and Repair. *Journal of Nucleic Acids*, 2010, pp.1-32. https://doi.org/10.4061/2010/592980

Rayess, H., Wang, M. & Srivatsan, E. (2011). Cellular senescence and tumor suppressor gene p16. *International Journal of Cancer*, 130(8), pp.1715-1725. https://doi.org/10.1002/ijc.27316

Raz, A. A., Wurtzel, O., & Reddien, P. W. (2021). Planarian stem cells specify fate yet retain potency during the cell cycle. *Cell stem cell*, 28(7), 1307–1322.e5. https://doi.org/10.1016/j.stem.2021.03.021

Reddien P. W. (2022). Positional Information and Stem Cells Combine to Result in Planarian Regeneration. *Cold Spring Harbor perspectives in biology*, 14(4), a040717. https://doi.org/10.1101/cshperspect.a040717

Reddien, P. W. (2018). The Cellular and Molecular Basis for Planarian Regeneration. *Cell*, *175*(2), 327–345. https://doi.org/10.1016/j.cell.2018.09.021

Reddien, P. W. & Sánchez Alvarado, A. (2004). Fundamentals of Planarian Regeneration. *Annual Review of Cell and Developmental Biology,* 20(1), 725-757. doi:10.1146/annurev.cellbio.20.010403.095114

Reddien, P. W., Bermange, A. L., Murfitt, K. J., Jennings, J. R., & Sánchez Alvarado, A. (2005a). Identification of genes needed for regeneration, stem cell function, and tissue homeostasis by systematic gene perturbation in planaria. *Developmental cell*, *8*(5), 635–649. https://doi.org/10.1016/j.devcel.2005.02.014

Reddien, P. W., Oviedo, N. J., Jennings, J. R., Jenkin, J. C., & Sánchez Alvarado, A. (2005b). SMEDWI-2 is a PIWI-like protein that regulates planarian stem cells. *Science (New York, N.Y.)*, *310*(5752), 1327–1330. https://doi.org/10.1126/science.1116110

Rees, G. (1962). Effects of Gamma Radiation on Two Decapod Crustaceans, Palaemonetes pugio and Uca pugnax. *Chesapeake Science*, 3(1), p.29. https://doi.org/10.2307/1350410

Regev, A., Teichmann, S. A., Lander, E. S., Amit, I., Benoist, C., Birney, E., Bodenmiller, B., Campbell, P., Carninci, P., Clatworthy, M., Clevers, H., Deplancke, B., Dunham, I., Eberwine, J., Eils, R., Enard, W., Farmer, A., Fugger, L., Göttgens, B., Hacohen, N., … Human Cell Atlas Meeting Participants (2017). The Human Cell Atlas. *eLife*, *6*, e27041. https://doi.org/10.7554/eLife.27041

Reichle, D., Witherspoon, J., Mitchell, M., Styron, C. (1972). Effects of beta-gamma radiation of earthworms under simulated fallout conditions. In: *Proceedings of Survival of Food Crops and Livestock in the Event of Nuclear War. AEC Symposium Series 24*. Brookhaven National Laboratory, 1970. CONF - 700909 US Atomic Engergy Commission, Washington, DC, pp. 527–534.

Reisz, J., Bansal, N., Qian, J., Zhao, W. & Furdui, C. (2014). Effects of Ionizing Radiation on Biological Molecules—Mechanisms of Damage and Emerging Methods of Detection. *Antioxidants & Redox Signaling*, 21(2), pp.260-292. https://doi.org/10.1089/ars.2013.5489

Ren, J., Wen, L., Gao, X., Jin, C., Xue, Y., & Yao, X. (2009). DOG 1.0: illustrator of protein domain structures. *Cell research*, *19*(2), 271–273. https://doi.org/10.1038/cr.2009.6

Reya, T., Morrison, S., Clarke, M. & Weissman, I. (2001). Stem cells, cancer, and cancer stem cells. *Nature*, 414(6859), pp.105-111. https://doi.org/10.1038/35102167

Rink, J. C. (2013). Stem cell systems and regeneration in planaria. *Development genes and evolution*, *223*(1-2), 67–84. https://doi.org/10.1007/s00427-012-0426-4

Rippe, V., Drieschner, N., Meiboom, M., Murua Escobar, H., Bonk, U., Belge, G., & Bullerdiek, J. (2003). Identification of a gene rearranged by 2p21 aberrations in thyroid adenomas. *Oncogene*, *22*(38), 6111–6114. https://doi.org/10.1038/sj.onc.1206867

Robb, S. M., Ross, E., & Sánchez Alvarado, A. (2008). SmedGD: the Schmidtea mediterranea genome database. *Nucleic acids research*, *36*(Database issue), D599–D606. https://doi.org/10.1093/nar/gkm684

Roberts-Galbraith, R. H., Brubacher, J. L., & Newmark, P. A. (2016). A functional genomics screen in planarians reveals regulators of whole-brain regeneration. *eLife*, *5*, e17002. https://doi.org/10.7554/eLife.17002

Rodier, F., Coppé, J. P., Patil, C. K., Hoeijmakers, W. A., Muñoz, D. P., Raza, S. R., Freund, A., Campeau, E., Davalos, A. R., & Campisi, J. (2009). Persistent DNA damage signalling triggers senescence-associated inflammatory cytokine secretion. *Nature cell biology*, *11*(8), 973–979. https://doi.org/10.1038/ncb1909

Roots, R., Kraft, G., & Gosschalk, E. (1985). The formation of radiation-induced DNA breaks: the ratio of double-strand breaks to single-strand breaks. *International journal of radiation oncology, biology, physics*, *11*(2), 259–265. https://doi.org/10.1016/0360-3016(85)90147-6

Rosenbaum, D. M., Rasmussen, S. G., & Kobilka, B. K. (2009). The structure and function of G-protein-coupled receptors. *Nature*, *459*(7245), 356–363. https://doi.org/10.1038/nature08144

Rossi, A., Ross, E. J., Jack, A., & Sánchez Alvarado, A. (2014). Molecular cloning and characterization of SL3: a stem cell-specific SL RNA from the planarian Schmidtea mediterranea. *Gene*, *533*(1), 156–167. https://doi.org/10.1016/j.gene.2013.09.101

Rossi, L., Salvetti, A., Marincola, F. M., Lena, A., Deri, P., Mannini, L., Batistoni, R., Wang, E., & Gremigni, V. (2007). Deciphering the molecular machinery of stem cells: a look at the neoblast gene expression profile. *Genome biology*, *8*(4), R62. https://doi.org/10.1186/gb-2007-8-4-r62

Rozanski, A., Moon, H., Brandl, H., Martín-Durán, J. M., Grohme, M. A., Hüttner, K., Bartscherer, K., Henry, I., & Rink, J. C. (2019). PlanMine 3.0-improvements to a mineable resource of flatworm biology and biodiversity. *Nucleic acids research*, *47*(D1), D812–D820. https://doi.org/10.1093/nar/gky1070

Ruggero, D., Grisendi, S., Piazza, F., Rego, E., Mari, F., Rao, P. H., Cordon-Cardo, C., & Pandolfi, P. P. (2003). Dyskeratosis congenita and cancer in mice deficient in ribosomal RNA modification. *Science (New York, N.Y.)*, *299*(5604), 259–262. https://doi.org/10.1126/science.1079447

Ryoo, H. D., & Baehrecke, E. H. (2010). Distinct death mechanisms in Drosophila development. *Current opinion in cell biology, 22(6)*, 889–895. https://doi.org/10.1016/j.ceb.2010.08.022

Sahu, S., Dattani, A. & Aboobaker, A. (2017). Secrets from immortal worms: What can we learn about biological ageing from the planarian model system?. *Seminars in Cell & Developmental Biology*, 70, pp.108-121. https://doi.org/10.1016/j.semcdb.2017.08.028

Sahu, S., Sridhar, D., Abnave, P., Kosaka, N., Dattani, A., Thompson, J. M., Hill, M. A., & Aboobaker, A. (2021). Ongoing repair of migration-coupled DNA damage allows planarian adult stem cells to reach wound sites. *eLife*, *10*, e63779. https://doi.org/10.7554/eLife.63779

Saito, S., Goodarzi, A. A., Higashimoto, Y., Noda, Y., Lees-Miller, S. P., Appella, E., & Anderson, C. W. (2002). ATM mediates phosphorylation at multiple p53 sites, including Ser(46), in response to ionizing radiation. *The Journal of biological chemistry*, *277*(15), 12491–12494. https://doi.org/10.1074/jbc.C200093200

Sakashita, T., Takanami, T., Yanase, S., Hamada, N., Suzuki, M., Kimura, T., Kobayashi, Y., Ishii, N., & Higashitani, A. (2010). Radiation biology of Caenorhabditis elegans: germ cell response, aging and behavior. *Journal of radiation research*, *51*(2), 107–121. https://doi.org/10.1269/jrr.09100

Salo, E. (2006). The power of regeneration and the stem-cell kingdom: freshwater planarians (Platyhelminthes). *BioEssays : news and reviews in molecular, cellular and developmental biology*, *28*(5), 546–559. https://doi.org/10.1002/bies.20416

Salvetti, A., Rossi, L., Bonuccelli, L., Lena, A., Pugliesi, C., Rainaldi, G., Evangelista, M., & Gremigni, V. (2009). Adult stem cell plasticity: neoblast repopulation in non-lethally irradiated planarians. *Developmental biology*, *328*(2), 305–314. https://doi.org/10.1016/j.ydbio.2009.01.029

San Filippo, J., Sung, P. & Klein, H. (2008). Mechanism of Eukaryotic Homologous Recombination. *Annual Review of Biochemistry*, 77(1), pp.229-257. https://doi.org/10.1146/annurev.biochem.77.061306.125255

Sánchez Alvarado, A., & Newmark, P. A. (1999). Double-stranded RNA specifically disrupts gene expression during planarian regeneration. *Proceedings of the National Academy of Sciences of the United States of America*, 96(9), 5049–5054. https://doi.org/10.1073/pnas.96.9.5049

Sano, R., & Reed, J. C. (2013). ER stress-induced cell death mechanisms. *Biochimica et biophysica acta*, *1833*(12), 3460–3470. https://doi.org/10.1016/j.bbamcr.2013.06.028

Saunders, A., Macosko, E. Z., Wysoker, A., Goldman, M., Krienen, F. M., de Rivera, H., Bien, E., Baum, M., Bortolin, L., Wang, S., Goeva, A., Nemesh, J., Kamitaki, N., Brumbaugh, S., Kulp, D., & McCarroll, S. A. (2018). Molecular Diversity and Specializations among the Cells of the Adult Mouse Brain. *Cell*, *174*(4), 1015–1030.e16. https://doi.org/10.1016/j.cell.2018.07.028

Schimmer, A. D. (2004). Inhibitor of apoptosis proteins: translating basic knowledge into clinical practice. *Cancer research*, *64*(20), 7183–7190. https://doi.org/10.1158/0008-5472.CAN-04-1918

Schindelin, J., Arganda-Carreras, I., Frise, E., Kaynig, V., Longair, M., Pietzsch, T., Preibisch, S., Rueden, C., Saalfeld, S., Schmid, B., Tinevez, J. Y., White, D. J., Hartenstein, V., Eliceiri, K., Tomancak, P., & Cardona, A. (2012). Fiji: an open-source platform for biological-image analysis. *Nature methods*, *9*(7), 676–682. https://doi.org/10.1038/nmeth.2019

Schneider, L., Pellegatta, S., Favaro, R., Pisati, F., Roncaglia, P., Testa, G., Nicolis, S. K., Finocchiaro, G., & d'Adda di Fagagna, F. (2013). DNA damage in mammalian neural stem cells leads to astrocytic differentiation mediated by BMP2 signaling through JAK-STAT. *Stem cell reports*, *1*(2), 123–138. https://doi.org/10.1016/j.stemcr.2013.06.004

Schulz, A., Meyer, F., Dubrovska, A., & Borgmann, K. (2019). Cancer Stem Cells and Radioresistance: DNA Repair and Beyond. *Cancers*, *11*(6), 862. https://doi.org/10.3390/cancers11060862

Scimone, M. L., Cote, L. E., & Reddien, P. W. (2017). Orthogonal muscle fibres have different instructive roles in planarian regeneration. *Nature*, *551*(7682), 623–628. https://doi.org/10.1038/nature24660

Scimone, M. L., Kravarik, K. M., Lapan, S. W., & Reddien, P. W. (2014). Neoblast specialization in regeneration of the planarian Schmidtea mediterranea. *Stem cell reports*, *3*(2), 339–352. https://doi.org/10.1016/j.stemcr.2014.06.001

Scimone, M. L., Srivastava, M., Bell, G. W., & Reddien, P. W. (2011). A regulatory program for excretory system regeneration in planarians. *Development (Cambridge, England)*, *138*(20), 4387–4398. https://doi.org/10.1242/dev.068098

Scimone, M. L., Wurtzel, O., Malecek, K., Fincher, C. T., Oderberg, I. M., Kravarik, K. M., & Reddien, P. W. (2018). foxF-1 Controls Specification of Non-body Wall Muscle and Phagocytic Cells in Planarians. *Current biology : CB*, *28*(23), 3787–3801.e6. https://doi.org/10.1016/j.cub.2018.10.030

Serrano, M., Hannon, G. & Beach, D. (1993). A new regulatory motif in cell-cycle control causing specific inhibition of cyclin D/CDK4. *Nature*, 366(6456), pp.704-707. https://doi.org/10.1038/366704a0

Sethi, N., Yan, Y., Quek, D., Schupbach, T., & Kang, Y. (2010). Rabconnectin-3 is a functional regulator of mammalian Notch signaling. *The Journal of biological chemistry*, *285*(45), 34757–34764. https://doi.org/10.1074/jbc.M110.158634

Shangary, S., Brown, K. D., Adamson, A. W., Edmonson, S., Ng, B., Pandita, T. K., Yalowich, J., Taccioli, G. E., & Baskaran, R. (2000). Regulation of DNA-dependent protein kinase activity by ionizing radiation-activated abl kinase is an ATM-dependent process. *The Journal of biological chemistry*, *275*(39), 30163–30168. https://doi.org/10.1074/jbc.M004302200

Shao, L., Luo, Y., & Zhou, D. (2014). Hematopoietic stem cell injury induced by ionizing radiation. *Antioxidants & redox signaling*, *20*(9), 1447–1462. https://doi.org/10.1089/ars.2013.5635

Shathasivam, T., Kislinger, T., & Gramolini, A. O. (2010). Genes, proteins and complexes: the multifaceted nature of FHL family proteins in diverse tissues. *Journal of cellular and molecular medicine*, *14*(12), 2702–2720. https://doi.org/10.1111/j.1582-4934.2010.01176.x

Shaul, Y., & Ben-Yehoyada, M. (2005). Role of c-Abl in the DNA damage stress response. *Cell research*, *15*(1), 33–35. https://doi.org/10.1038/sj.cr.7290261

She, M., Zhang, J., Jiang, T., Zhang, Y., Liu, Y., Tang, M., & Zeng, Q. (2022). The function of Lmpt in Drosophila heart tissue. *Biochemical and biophysical research communications*, *612*, 15–21. https://doi.org/10.1016/j.bbrc.2022.04.098

Sheard, M. (2001). Ionizing radiation as a response-enhancing agent for CD95-mediated apoptosis. *International Journal of Cancer*, 96(4), pp.213-220. https://doi.org/10.1002/ijc.1020

Shekhar, K., Lapan, S. W., Whitney, I. E., Tran, N. M., Macosko, E. Z., Kowalczyk, M., Adiconis, X., Levin, J. Z., Nemesh, J., Goldman, M., McCarroll, S. A., Cepko, C. L., Regev, A., & Sanes, J. R. (2016). Comprehensive Classification of Retinal Bipolar Neurons by Single-Cell Transcriptomics. *Cell*, *166*(5), 1308–1323.e30. https://doi.org/10.1016/j.cell.2016.07.054

Shen, Y. H., Godlewski, J., Zhu, J., Sathyanarayana, P., Leaner, V., Birrer, M. J., Rana, A., & Tzivion, G. (2003). Cross-talk between JNK/SAPK and ERK/MAPK pathways: sustained activation of JNK blocks ERK activation by mitogenic factors. *The Journal of biological chemistry*, *278*(29), 26715–26721. https://doi.org/10.1074/jbc.M303264200

Shen, Y., Chen, H., Zhang, J., Chen, Y., Wang, M., Ma, J., Hong, L., Liu, N., Fan, Q., Lu, X., Tian, Y., Wang, A., Dong, J., Lan, Q., & Huang, Q. (2015). Increased Notch Signaling Enhances Radioresistance of Malignant Stromal Cells Induced by Glioma Stem/ Progenitor Cells. *PloS one*, *10*(11), e0142594. https://doi.org/10.1371/journal.pone.0142594

Shibata, N., Umesono, Y., Orii, H., Sakurai, T., Watanabe, K., & Agata, K. (1999). Expression of vasa(vas)-related genes in germline cells and totipotent somatic stem cells of planarians. *Developmental biology*, *206*(1), 73–87. https://doi.org/10.1006/dbio.1998.9130

Shiroor, D. A., Bohr, T. E., & Adler, C. E. (2020). Injury Delays Stem Cell Apoptosis after Radiation in Planarians. *Current biology*: CB, 30(11), 2166–2174.e3. https://doi.org/10.1016/j.cub.2020.03.054

Shiroor, D. A., Wang, K. T., Sanketi, B. D., Tapper, J. K., & Adler, C. E. (2023). Inhibition of ATM kinase rescues planarian regeneration after lethal radiation. *EMBO reports*, 24(5), e56112. https://doi.org/10.15252/embr.202256112

Shivji, M., Davies, O., Savill, J., Bates, D., Pellegrini, L. & Venkitaraman, A. (2006). A region of human BRCA2 containing multiple BRC repeats promotes RAD51-mediated strand exchange. *Nucleic Acids Research*, 34(14), pp.4000-4011. https://doi.org/10.1093/nar/gkl505

Sibbritt, T., Ip, C. K., Khoo, P. L., Wilkie, E., Jones, V., Sun, J. Q. J., Shen, J. X., Peng, G., Han, J. J., Jing, N., Osteil, P., Ramialison, M., Tam, P. P. L., & Fossat, N. (2018). A gene regulatory network anchored by LIM homeobox 1 for embryonic head development. *Genesis (New York, N.Y. : 2000)*, *56*(9), e23246. https://doi.org/10.1002/dvg.23246

Simakov, O., Bredeson, J., Berkoff, K., Marletaz, F., Mitros, T., Schultz, D. T., O'Connell, B. L., Dear, P., Martinez, D. E., Steele, R. E., Green, R. E., David, C. N., & Rokhsar, D. S. (2022). Deeply conserved synteny and the evolution of metazoan chromosomes. *Science advances*, 8(5), eabi5884. https://doi.org/10.1126/sciadv.abi5884

Singh, A. & Singh, H. (1982). Time-scale and nature of radiation-biological damage: Approaches to radiation protection and post-irradiation therapy. *Progress in Biophysics and Molecular Biology*, 39, pp.69-107. https://doi.org/10.1016/0079-6107(83)90014-7

Skvortsov, S., Debbage, P. & Skvortsova, I. (2014). Proteomics of cancer stem cells. *International Journal of Radiation Biology*, 90(8), pp.653-658. https://doi.org/10.3109/09553002.2013.873559

Skvortsov, S., Debbage, P., Lukas, P. & Skvortsova, I. (2015). Crosstalk between DNA repair and cancer stem cell (CSC) associated intracellular pathways. *Seminars in Cancer Biology*, 31, pp.36-42. https://doi.org/10.1016/j.semcancer.2014.06.002

Skvortsov, S., Jimenez, C., Knol, J., Eichberger, P., Schiestl, B., Debbage, P., Skvortsova, I. & Lukas, P. (2011). Radioresistant head and neck squamous cell carcinoma cells: Intracellular signaling, putative biomarkers for tumor recurrences and possible therapeutic targets. *Radiotherapy and Oncology*, 101(1), pp.177-182. https://doi.org/10.1016/j.radonc.2011.05.067

Smith, D. & DeCosse, J. (1986). Radiation damage to the small intestine. *World journal of surgery*, *10*(2), 189–194. https://doi.org/10.1007/BF01658135

Smith, M. & Schnellmann, R. G. (2012). Calpains, mitochondria, and apoptosis. *Cardiovascular research*, *96*(1), 32–37. https://doi.org/10.1093/cvr/cvs163

Smits, V., Klompmaker, R., Vallenius, T., Rijksen, G., Mäkelä, T. & Medema, R. (2000). p21 Inhibits Thr161 Phosphorylation of Cdc2 to Enforce the G2 DNA Damage Checkpoint. *Journal of Biological Chemistry*, 275(39), pp.30638-30643. https://doi.org/10.1074/jbc.M005437200

Sokolov, M. & Neumann, R. (2010). Radiation-Induced Bystander Effects in Cultured Human Stem Cells. *PLoS ONE*, 5(12), p.e14195. https://doi.org/10.1371/journal.pone.0014195

Sokolov, M. & Neumann, R. (2012). Human Embryonic Stem Cell Responses to Ionizing Radiation Exposures: Current State of Knowledge and Future Challenges. *Stem Cells International*, 2012, pp.1-11. https://doi.org/10.1155/2012/579104

Sokolov, M., Panyutin, I. & Neumann, R. (2011). Dynamics of the transcriptome response of cultured human embryonic stem cells to ionizing radiation exposure. *Mutation Research/Fundamental and Molecular Mechanisms of Mutagenesis*, 709-710, pp.40-48. https://doi.org/10.1016/j.mrfmmm.2011.02.008

Solana, J., Irimia, M., Ayoub, S., Orejuela, M. R., Zywitza, V., Jens, M., Tapial, J., Ray, D., Morris, Q., Hughes, T. R., Blencowe, B. J., & Rajewsky, N. (2016). Conserved functional antagonism of CELF and MBNL proteins controls stem cell-specific alternative splicing in planarians. *eLife*, *5*, e16797. https://doi.org/10.7554/eLife.16797

Solana, J., Kao, D., Mihaylova, Y., Jaber-Hijazi, F., Malla, S., Wilson, R., & Aboobaker, A. (2012). Defining the molecular profile of planarian pluripotent stem cells using a combinatorial RNAseq, RNA interference and irradiation approach. *Genome biology*, *13*(3), R19. https://doi.org/10.1186/gb-2012-13-3-r19

Spano, S., & Galán, J. E. (2012). A Rab32-dependent pathway contributes to Salmonella typhi host restriction. *Science (New York, N.Y.)*, *338*(6109), 960–963. https://doi.org/10.1126/science.1229224

Squair, J. W., Gautier, M., Kathe, C., Anderson, M. A., James, N. D., Hutson, T. H., Hudelle, R., Qaiser, T., Matson, K. J. E., Barraud, Q., Levine, A. J., La Manno, G., Skinnider, M. A., & Courtine, G. (2021). Confronting false discoveries in single-cell differential expression. *Nature communications*, *12*(1), 5692. https://doi.org/10.1038/s41467-021-25960-2

Srivastava, M., Larroux, C., Lu, D. R., Mohanty, K., Chapman, J., Degnan, B. M., & Rokhsar, D. S. (2010). Early evolution of the LIM homeobox gene family. *BMC biology*, *8*, 4. https://doi.org/10.1186/1741-7007-8-4

Station, E. (2013). Pairfq: Sync paired-end FASTA/Q files and keep singleton reads. Retrieved from http://github.com/sestation/Pairfq.

Stearner, S. & Christian, E. (1972). Late Effects of Ionizing Radiations in the Chicken: Survival, Body Weight, and Pathology. *Radiation Research*, 52(1), p.179. https://doi.org/10.2307/3573598

Stenmark, H. (2009). Rab GTPases as coordinators of vesicle traffic. *Nature reviews. Molecular cell biology*, *10*(8), 513–525. https://doi.org/10.1038/nrm2728

Stevens, A. S., Wouters, A., Ploem, J. P., Pirotte, N., Van Roten, A., Willems, M., Hellings, N., Franken, C., Koppen, G., Artois, T., Plusquin, M., & Smeets, K. (2018). Planarians Customize Their Stem Cell Responses Following Genotoxic Stress as a Function of Exposure Time and Regenerative State. *Toxicological sciences : an official journal of the Society of Toxicology*, *162*(1), 251–263. https://doi.org/10.1093/toxsci/kfx247

Storer, J. (1966). Chapter 22, Acute responses to ionizing radiation. In: Green EL, editor. *Biology of the Laboratory Mouse*. 2nd ed. New York: Dover Publications Inc.

Street, K., Risso, D., Fletcher, R. B., Das, D., Ngai, J., Yosef, N., Purdom, E., & Dudoit, S. (2018). Slingshot: cell lineage and pseudotime inference for single-cell transcriptomics. *BMC genomics*, *19*(1), 477. https://doi.org/10.1186/s12864-018-4772-0

Stuart, T., Butler, A., Hoffman, P., Hafemeister, C., Papalexi, E., Mauck, W. M., 3rd, Hao, Y., Stoeckius, M., Smibert, P., & Satija, R. (2019). Comprehensive Integration of Single-Cell Data. *Cell*, *177*(7), 1888–1902.e21. https://doi.org/10.1016/j.cell.2019.05.031

Su, B., Zhong, M., Zhang, Y., Wu, K., Huang, Q., Zhu, C., & Zeng, T. (2022). Deficiency of kin17 Facilitates Apoptosis of Cervical Cancer Cells by Modulating Caspase 3, PARP, and Bcl-2 Family Proteins. *Journal of oncology*, 2022, 3156968. https://doi.org/10.1155/2022/3156968

Su, T. (2019). What Drosophila Can Teach Us About Radiation Biology of Human Cancers. *Advances in experimental medicine and biology*, *1167*, 225–236. https://doi.org/10.1007/978-3-030-23629-8_13

Suzuki, J., & Egami, N. (1983). Mortality of the earthworms, Eisenia foetida, after gamma-irradiation at different stages of their life history. *Journal of radiation research*, *24*(3), 209–220. https://doi.org/10.1269/jrr.24.209

Svensson, V., & Pachter, L. (2018). RNA Velocity: Molecular Kinetics from Single-Cell RNA-Seq. *Molecular cell*, *72*(1), 7–9. https://doi.org/10.1016/j.molcel.2018.09.026

Swapna, L. S., Molinaro, A. M., Lindsay-Mosher, N., Pearson, B. J., & Parkinson, J. (2018). Comparative transcriptomic analyses and single-cell RNA sequencing of the freshwater planarian Schmidtea mediterranea identify major cell types and pathway conservation. *Genome biology*, 19(1), 124. https://doi.org/10.1186/s13059-018-1498-x

Takeda, H., Nishimura, K., & Agata, K. (2009). Planarians maintain a constant ratio of different cell types during changes in body size by using the stem cell system. *Zoological science*, *26*(12), 805–813. https://doi.org/10.2108/zsj.26.805

Tali, G., Payne, A. E., Hudson, T. J., da Silva, S. D., Pusztaszeri, M., Tamilia, M., & Forest, V. I. (2023). The Difference in Clinical Behavior of Gene Fusions Involving *RET/PTC* Fusions and *THADA/IGF2BP3* Fusions in Thyroid Nodules. *Cancers*, *15*(13), 3394. https://doi.org/10.3390/cancers15133394

Tam, S. Y., Wu, V. W., & Law, H. K. (2017). Influence of autophagy on the efficacy of radiotherapy. *Radiation oncology (London, England)*, *12*(1), 57. https://doi.org/10.1186/s13014-017-0795-y

Tamaddondoust, R. N., Wong, A., Chandrashekhar, M., Azzam, E. I., Alain, T., & Wang, Y. (2022). Identification of Novel Regulators of Radiosensitivity Using High-Throughput Genetic Screening. *International journal of molecular sciences*, *23*(15), 8774. https://doi.org/10.3390/ijms23158774

Tamura, K., Stecher, G., & Kumar, S. (2021). MEGA11: Molecular Evolutionary Genetics Analysis Version 11. *Molecular biology and evolution*, *38*(7), 3022–3027. https://doi.org/10.1093/molbev/msab120

Tan, T. C., Rahman, R., Jaber-Hijazi, F., Felix, D. A., Chen, C., Louis, E. J., & Aboobaker, A. (2012). Telomere maintenance and telomerase activity are differentially regulated in asexual and sexual worms. *Proceedings of the National Academy of Sciences of the United States of America*, *109*(11), 4209–4214. https://doi.org/10.1073/pnas.1118885109

Tang, J., Wang, J. Y., & Parker, L. L. (2012). Detection of early Abl kinase activation after ionizing radiation by using a peptide biosensor. *Chembiochem : a European journal of chemical biology*, *13*(5), 665–673. https://doi.org/10.1002/cbic.201100763

Tasaki, J., Shibata, N., Sakurai, T., Agata, K., & Umesono, Y. (2011). Role of c-Jun N-terminal kinase activation in blastema formation during planarian regeneration. *Development, growth & differentiation*, *53*(3), 389–400. https://doi.org/10.1111/j.1440-169X.2011.01254.x

Tejada-Romero, B., Carter, J. M., Mihaylova, Y., Neumann, B., & Aboobaker, A. A. (2015). JNK signalling is necessary for a Wnt- and stem cell-dependent regeneration programme. *Development*, 142(14), 2413–2424. https://doi.org/10.1242/dev.115139

Theys, J., Yahyanejad, S., Habets, R., Span, P., Dubois, L., Paesmans, K., Kattenbeld, B., Cleutjens, J., Groot, A. J., Schuurbiers, O. C. J., Lambin, P., Bussink, J., & Vooijs, M. (2013). High NOTCH activity induces radiation resistance in non-small cell lung cancer. *Radiotherapy and oncology : journal of the European Society for Therapeutic Radiology and Oncology*, *108*(3), 440–445. https://doi.org/10.1016/j.radonc.2013.06.020

Thiruvalluvan, M., Barghouth, P. G., Tsur, A., Broday, L., & Oviedo, N. J. (2018). SUMOylation controls stem cell proliferation and regional cell death through Hedgehog signaling in planarians. *Cellular and molecular life sciences : CMLS*, *75*(7), 1285–1301. https://doi.org/10.1007/s00018-017-2697-4

Tissier, A., Kannouche, P., Biard, D. S., Timchenko, T., Mazin, A., Araneda, S., Allemand, I., Mauffrey, P., Frelat, G., & Angulo, J. F. (1995). The mouse Kin-17 gene codes for a new protein involved in DNA transactions and is akin to the bacterial RecA protein. *Biochimie*, *77*(11), 854–860. https://doi.org/10.1016/0300-9084(95)90003-9

Tomoyasu, Y., Miller, S. C., Tomita, S., Schoppmeier, M., Grossmann, D., & Bucher, G. (2008). Exploring systemic RNA interference in insects: a genome-wide survey for RNAi genes in Tribolium. *Genome biology*, *9*(1), R10. https://doi.org/10.1186/gb-2008-9-1-r10

Trapani, J. A., & Smyth, M. J. (2002). Functional significance of the perforin/granzyme cell death pathway. *Nature reviews. Immunology*, *2*(10), 735–747. https://doi.org/10.1038/nri911

Trapnell, C., Cacchiarelli, D., Grimsby, J., Pokharel, P., Li, S., Morse, M., Lennon, N. J., Livak, K. J., Mikkelsen, T. S., & Rinn, J. L. (2014). The dynamics and regulators of cell fate decisions are revealed by pseudotemporal ordering of single cells. *Nature biotechnology*, *32*(4), 381–386. https://doi.org/10.1038/nbt.2859

Traver, D., Winzeler, A., Stern, H. M., Mayhall, E. A., Langenau, D. M., Kutok, J. L., Look, A. T., & Zon, L. I. (2004). Effects of lethal irradiation in zebrafish and rescue by hematopoietic cell transplantation. *Blood*, 104(5), 1298–1305. https://doi.org/10.1182/blood-2004-01-0100.

Trost, T., Haines, J., Dillon, A., Mersman, B., Robbins, M., Thomas, P., & Hubert, A. (2018). Characterizing the role of SWI/SNF-related chromatin remodeling complexes in planarian regeneration and stem cell function. *Stem cell research*, *32*, 91–103. https://doi.org/10.1016/j.scr.2018.09.004

Trueba, S. S., Augé, J., Mattei, G., Etchevers, H., Martinovic, J., Czernichow, P., Vekemans, M., Polak, M., & Attié-Bitach, T. (2005). PAX8, TITF1, and FOXE1 gene expression patterns during human development: new insights into human thyroid development and thyroid dysgenesis-associated malformations. *The Journal of clinical endocrinology and metabolism*, *90*(1), 455–462. https://doi.org/10.1210/jc.2004-1358

Tu, K. C., Cheng, L. C., T K Vu, H., Lange, J. J., McKinney, S. A., Seidel, C. W., & Sánchez Alvarado, A. (2015). Egr-5 is a post-mitotic regulator of planarian epidermal differentiation. *eLife*, *4*, e10501. https://doi.org/10.7554/eLife.10501

Tugendreich, S., Tomkiel, J., Earnshaw, W., Hieter, P. (1995). CDC27Hs colocalizes with CDC16Hs to the centrosome and mitotic spindle and is essential for the metaphase to anaphase transition. *Cell. 81(2):261-8*. doi: 10.1016/0092-8674(95)90336-4.

Tumbar, T., Guasch, G., Greco, V., Blanpain, C., Lowry, W., Rendl, M. & Fuchs, E. (2004). Defining the Epithelial Stem Cell Niche in Skin. *Science*, 303(5656), pp.359-363. https://doi.org/10.1126/science.1092436

Tuttle, A. M., Hoffman, T. L., & Schilling, T. F. (2014). Rabconnectin-3a regulates vesicle endocytosis and canonical Wnt signaling in zebrafish neural crest migration. *PLoS biology*, *12*(5), e1001852. https://doi.org/10.1371/journal.pbio.1001852

Ungar, L., Yosef, N., Sela, Y., Sharan, R., Ruppin, E., & Kupiec, M. (2009). A genome-wide screen for essential yeast genes that affect telomere length maintenance. *Nucleic acids research*, *37*(12), 3840–3849. https://doi.org/10.1093/nar/gkp259

Untergasser, A., Cutcutache, I., Koressaar, T., Ye, J., Faircloth, B. C., Remm, M., & Rozen, S. G. (2012). Primer3--new capabilities and interfaces. *Nucleic acids research*, *40*(15), e115. https://doi.org/10.1093/nar/gks596

Upadhyay, R., Robay, A., Fakhro, K., Abi Khalil, C., Zirie, M., Jayyousi, A., El-Shafei, M., Kiss, S., D'Amico, D. J., Salit, J., Staudt, M. R., O'Beirne, S. L., Chen, X., Tuana, B., Crystal, R. G., & Ding, H. (2015). Role of SLMAP genetic variants in susceptibility of diabetes and diabetic retinopathy in Qatari population. *Journal of translational medicine*, *13*, 61. https://doi.org/10.1186/s12967-015-0411-6

Uprichard, S. L. (2005). The therapeutic potential of RNA interference. *FEBS letters*, *579*(26), 5996–6007. https://doi.org/10.1016/j.febslet.2005.08.004

Vaisnav, M., Xing, C., Ku, H. C., Hwang, D., Stojadinovic, S., Pertsemlidis, A., & Abrams, J. M. (2014). Genome-wide association analysis of radiation resistance in Drosophila melanogaster. *PloS one*, *9*(8), e104858. https://doi.org/10.1371/journal.pone.0104858

Vakifahmetoglu, H., Olsson, M., & Zhivotovsky, B. (2008). Death through a tragedy: mitotic catastrophe. *Cell death and differentiation*, *15*(7), 1153–1162. https://doi.org/10.1038/cdd.2008.47

van Dam, T. J., Bos, J. L., & Snel, B. (2011). Evolution of the Ras-like small GTPases and their regulators. *Small GTPases*, *2*(1), 4–16. https://doi.org/10.4161/sgtp.2.1.15113

van Haaften, G., Romeijn, R., Pothof, J., Koole, W., Mullenders, L. H., Pastink, A., Plasterk, R. H., & Tijsterman, M. (2006). Identification of conserved pathways of DNA-damage response and radiation protection by genome-wide RNAi. *Current biology : CB*, *16*(13), 1344–1350. https://doi.org/10.1016/j.cub.2006.05.047

van Haaften, G., Vastenhouw, N. L., Nollen, E. A., Plasterk, R. H., & Tijsterman, M. (2004). Gene interactions in the DNA damage-response pathway identified by genome-wide RNA-interference analysis of synthetic lethality. *Proceedings of the National Academy of Sciences of the United States of America*, *101*(35), 12992–12996. https://doi.org/10.1073/pnas.0403131101

van Wolfswinkel, J. C., Wagner, D. E., & Reddien, P. W. (2014). Single-cell analysis reveals functionally distinct classes within the planarian stem cell compartment. *Cell stem cell*, *15*(3), 326–339. https://doi.org/10.1016/j.stem.2014.06.007

Vellanki, S. H., Grabrucker, A., Liebau, S., Proepper, C., Eramo, A., Braun, V., Boeckers, T., Debatin, K. M., & Fulda, S. (2009). Small-molecule XIAP inhibitors enhance gamma-irradiation-induced apoptosis in glioblastoma. *Neoplasia (New York, N.Y.)*, *11*(8), 743–752. https://doi.org/10.1593/neo.09436

Vicidomini, R., Petrizzo, A., di Giovanni, A., Cassese, L., Lombardi, A. A., Pragliola, C., & Furia, M. (2017). Drosophila dyskerin is required for somatic stem cell homeostasis. *Scientific reports*, *7*(1), 347. https://doi.org/10.1038/s41598-017-00446-8

Vigneswara, V., & Ahmed, Z. (2020). The Role of Caspase-2 in Regulating Cell Fate. *Cells*, *9*(5), 1259. https://doi.org/10.3390/cells9051259

Villani, A. C., Satija, R., Reynolds, G., Sarkizova, S., Shekhar, K., Fletcher, J., Griesbeck, M., Butler, A., Zheng, S., Lazo, S., Jardine, L., Dixon, D., Stephenson, E., Nilsson, E., Grundberg, I., McDonald, D., Filby, A., Li, W., De Jager, P. L., Rozenblatt-Rosen, O., … Hacohen, N. (2017). Single-cell RNA-seq reveals new types of human blood dendritic cells, monocytes, and progenitors. *Science (New York, N.Y.)*, *356*(6335). https://doi.org/10.1126/science.aah4573

Viret, C., Rozières, A., & Faure, M. (2018). Novel Insights into NDP52 Autophagy Receptor Functioning. *Trends in cell biology*, *28*(4), 255–257. https://doi.org/10.1016/j.tcb.2018.01.003

Vitale, I., Manic, G., De Maria, R., Kroemer, G. & Galluzzi, L. (2017). DNA Damage in Stem Cells. *Molecular Cell*, 66(3), pp.306-319. https://doi.org/10.1016/j.molcel.2017.04.006

Völkening, L., Vatselia, A., Asgedom, G., Bastians, H., Lavin, M., Schindler, D., Schambach, A., Bousset, K., & Dörk, T. (2020). RAD50 regulates mitotic progression independent of DNA repair functions. *FASEB journal : official publication of the Federation of American Societies for Experimental Biology*, *34*(2), 2812–2820. https://doi.org/10.1096/fj.201902318R

Vu, H., Rink, J. C., McKinney, S. A., McClain, M., Lakshmanaperumal, N., Alexander, R., & Sánchez Alvarado, A. (2015). Stem cells and fluid flow drive cyst formation in an invertebrate excretory organ. *eLife,* 4, e07405. https://doi.org/10.7554/eLife.07405

Wagle, R. & Song, Y. (2020). Ionizing radiation reduces larval brain size by inducing premature differentiation of Drosophila neural stem cells. *Biochemical and Biophysical Research Communications*, 523(3), pp.555-560. https://doi.org/10.1016/j.bbrc.2019.12.047

Wagner, D. E., Ho, J. J., & Reddien, P. W. (2012). Genetic regulators of a pluripotent adult stem cell system in planarians identified by RNAi and clonal analysis. *Cell stem cell*, *10*(3), 299–311. https://doi.org/10.1016/j.stem.2012.01.016

Wagner, D. E., Wang, I. E., & Reddien, P. W. (2011). Clonogenic neoblasts are pluripotent adult stem cells that underlie planarian regeneration. *Science (New York, N.Y.)*, *332*(6031), 811–816. https://doi.org/10.1126/science.1203983

Wang, C., Han, X. S., Li, F. F., Huang, S., Qin, Y. W., Zhao, X. X., & Jing, Q. (2016). Forkhead containing transcription factor Albino controls tetrapyrrole-based body pigmentation in planarian. *Cell discovery*, *2*, 16029. https://doi.org/10.1038/celldisc.2016.29

Wang, C., Liu, Z., & Huang, X. (2012). Rab32 is important for autophagy and lipid storage in Drosophila. *PloS one*, *7*(2), e32086. https://doi.org/10.1371/journal.pone.0032086

Wang, C., Lv, X., He, C., Davis, J. S., Wang, C., & Hua, G. (2020). Four and a Half LIM Domains 2 (FHL2) Contribute to the Epithelial Ovarian Cancer Carcinogenesis. *International journal of molecular sciences*, *21*(20), 7751. https://doi.org/10.3390/ijms21207751

Wang, G. F., Niu, X., Liu, H., Dong, Q., Yao, Y., Wang, D., Liu, X., & Cao, C. (2021). c-Abl kinase regulates cell proliferation and ionizing radiation-induced G2/M arrest via phosphorylation of FHL2. *FEBS open bio*, *11*(6), 1731–1738. https://doi.org/10.1002/2211-5463.13177

Wang, I. E., Wagner, D. E., & Reddien, P. W. (2018). Clonal Analysis of Planarian Stem Cells by Subtotal Irradiation and Single-Cell Transplantation. *Methods in molecular biology (Clifton, N.J.)*, *1774*, 479–495. https://doi.org/10.1007/978-1-4939-7802-1_20

Wang, J., Wakeman, T. P., Lathia, J. D., Hjelmeland, A. B., Wang, X. F., White, R. R., Rich, J. N., & Sullenger, B. A. (2010). Notch promotes radioresistance of glioma stem cells. *Stem cells (Dayton, Ohio)*, *28*(1), 17–28. https://doi.org/10.1002/stem.261

Wang, M. C., Bohmann, D., & Jasper, H. (2003). JNK signaling confers tolerance to oxidative stress and extends lifespan in Drosophila. *Developmental cell*, *5*(5), 811–816. https://doi.org/10.1016/s1534-5807(03)00323-x

Wang, X. C., Yue, X., Zhang, R. X., Liu, T. Y., Pan, Z. Z., Yang, M. J., Lu, Z. H., Wang, Z. Y., Peng, J. H., Le, L. Y., Wang, G. Y., Peng, Q. H., Meng, Y., Huang, W., & Liu, R. Y. (2019). Genome-wide RNAi Screening Identifies RFC4 as a Factor That Mediates Radioresistance in Colorectal Cancer by Facilitating Nonhomologous End Joining Repair. *Clinical cancer research : an official journal of the American Association for Cancer Research*, *25*(14), 4567–4579. https://doi.org/10.1158/1078-0432.CCR-18-3735

Wang, X., Zeng, L., Wang, J., Chau, J. F., Lai, K. P., Jia, D., Poonepalli, A., Hande, M. P., Liu, H., He, G., He, L., & Li, B. (2011). A positive role for c-Abl in Atm and Atr activation in DNA damage response. *Cell death and differentiation*, *18*(1), 5–15. https://doi.org/10.1038/cdd.2010.106

Waselenko, J. K., MacVittie, T. J., Blakely, W. F., Pesik, N., Wiley, A. L., Dickerson, W. E., Tsu, H., Confer, D. L., Coleman, C. N., Seed, T., Lowry, P., Armitage, J. O., Dainiak, N., & Strategic National Stockpile Radiation Working Group (2004). Medical management of the acute radiation syndrome: recommendations of the Strategic National Stockpile Radiation Working Group. *Annals of internal medicine*, *140*(12), 1037–1051. https://doi.org/10.7326/0003-4819-140-12-200406150-00015

Watanabe, R., Rahmanian, S., & Nikjoo, H. (2015). Spectrum of Radiation-Induced Clustered Non-DSB Damage - A Monte Carlo Track Structure Modeling and Calculations. *Radiation research*, *183*(5), 525–540. https://doi.org/10.1667/RR13902.1

Wei, J., Meng, L., Hou, X., Qu, C., Wang, B., Xin, Y., & Jiang, X. (2018). Radiation-induced skin reactions: mechanism and treatment. *Cancer management and research*, 11, 167–177. https://doi.org/10.2147/CMAR.S188655

Wei, X., & Zhang, H. (2020). Four and a half LIM domains protein 1 can be as a double-edged sword in cancer progression. *Cancer biology & medicine*, *17*(2), 270–281. https://doi.org/10.20892/j.issn.2095-3941.2019.0420

Weinberg, W. C., & Denning, M. F. (2002). P21Waf1 control of epithelial cell cycle and cell fate. *Critical reviews in oral biology and medicine : an official publication of the American Association of Oral Biologists*, *13*(6), 453–464. https://doi.org/10.1177/154411130201300603

Weissman I. L. (2000). Stem cells: units of development, units of regeneration, and units in evolution. *Cell*, *100*(1), 157–168. https://doi.org/10.1016/s0092-8674(00)81692-x

Welch, J. D., Hartemink, A. J., & Prins, J. F. (2016). SLICER: inferring branched, nonlinear cellular trajectories from single cell RNA-seq data. *Genome biology*, *17*(1), 106. https://doi.org/10.1186/s13059-016-0975-3

Whelan, S., & Goldman, N. (2001). A general empirical model of protein evolution derived from multiple protein families using a maximum-likelihood approach. *Molecular biology and evolution*, *18*(5), 691–699. https://doi.org/10.1093/oxfordjournals.molbev.a003851

White, E. (2015). The role for autophagy in cancer. *The Journal of clinical investigation*, *125*(1), 42–46. https://doi.org/10.1172/JCI73941

White, J. & Angelovic, J. (1966). Tolerances of Several Marine Species to Co-60 Irradiation. *Chesapeake Science*, 7(1), p.36. https://doi.org/10.2307/1350987

Wielowieyski, P. A., Sevinc, S., Guzzo, R., Salih, M., Wigle, J. T., & Tuana, B. S. (2000). Alternative splicing, expression, and genomic structure of the 3' region of the gene encoding the sarcolemmal-associated proteins (SLAPs) defines a novel class of coiled-coil tail-anchored membrane proteins. *The Journal of biological chemistry*, *275*(49), 38474–38481. https://doi.org/10.1074/jbc.M007682200

Wiggans, M., Zhu, S. J., Molinaro, A. M., & Pearson, B. J. (2023). The BAF chromatin remodeling complex licenses planarian stem cells access to ectodermal and mesodermal cell fates. *BMC biology*, *21*(1), 227. https://doi.org/10.1186/s12915-023-01730-y

Wilson, K., Sun, N., Huang, M., Zhang, W., Lee, A., Li, Z., Wang, S. & Wu, J. (2010). Effects of Ionizing Radiation on Self-Renewal and Pluripotency of Human Embryonic Stem Cells. *Cancer Research*, 70(13), pp.5539-5548. https://doi.org/10.1158/0008-5472.CAN-09-4238

Winchell, C. J., & Jacobs, D. K. (2013). Expression of the Lhx genes apterous and lim1 in an errant polychaete: implications for bilaterian appendage evolution, neural development, and muscle diversification. *EvoDevo*, *4*(1), 4. https://doi.org/10.1186/2041-9139-4-4

Won, E. J., Han, J., Hagiwara, A., Oda, S., Mitani, H., & Lee, J. S. (2016). Acute Toxicity of Gamma Radiation to the Monogonont Rotifer Brachionus koreanus. *Bulletin of environmental contamination and toxicology*, 97(3), 387–391. https://doi.org/10.1007/s00128-016-1843-2

Wong, J., Filippi, A., Dabaja, B., Yahalom, J. & Specht, L. (2018). Total Body Irradiation: Guidelines from the International Lymphoma Radiation Oncology Group (ILROG). *International Journal of Radiation Oncology*Biology*Physics*, 101(3), pp.521-529. https://doi.org/10.1016/j.ijrobp.2018.04.071

Wu, G., Niu, M., Qin, J., Wang, Y., & Tian, J. (2019). Inactivation of Rab27B-dependent signaling pathway by calycosin inhibits migration and invasion of ER-negative breast cancer cells. *Gene*, *709*, 48–55. https://doi.org/10.1016/j.gene.2019.04.005

Wu, Q., Wu, W., Fu, B., Shi, L., Wang, X., & Kuca, K. (2019). JNK signaling in cancer cell survival. *Medicinal research reviews*, *39*(6), 2082–2104. https://doi.org/10.1002/med.21574

Wu, S., Al-Eryani, G., Roden, D. L., Junankar, S., Harvey, K., Andersson, A., Thennavan, A., Wang, C., Torpy, J. R., Bartonicek, N., Wang, T., Larsson, L., Kaczorowski, D., Weisenfeld, N. I., Uytingco, C. R., Chew, J. G., Bent, Z. W., Chan, C. L., Gnanasambandapillai, V., Dutertre, C. A., … Swarbrick, A. (2021). A single-cell and spatially resolved atlas of human breast cancers. *Nature genetics*, *53*(9), 1334–1347. https://doi.org/10.1038/s41588-021-00911-1

Wu, X., Liu, Y., Jin, S., Wang, M., Jiao, Y., Yang, B., Lu, X., Ji, X., Fei, Y., Yang, H., Zhao, L., Chen, H., Zhang, Y., Li, H., Lipsky, P. E., Tsokos, G. C., Bai, F., & Zhang, X. (2021). Single-cell sequencing of immune cells from anticitrullinated peptide antibody positive and negative rheumatoid arthritis. *Nature communications*, *12*(1), 4977. https://doi.org/10.1038/s41467-021-25246-7

Wurtzel, O., Cote, L. E., Poirier, A., Satija, R., Regev, A., & Reddien, P. W. (2015). A Generic and Cell-Type-Specific Wound Response Precedes Regeneration in Planarians. *Developmental cell*, *35*(5), 632–645. https://doi.org/10.1016/j.devcel.2015.11.004

Xing, L., Shi, G., Mostovoy, Y., Gentry, N. W., Fan, Z., McMahon, T. B., Kwok, P. Y., Jones, C. R., Ptáček, L. J., & Fu, Y. H. (2019). Mutant neuropeptide S receptor reduces sleep duration with preserved memory consolidation. *Science translational medicine*, *11*(514), eaax2014. https://doi.org/10.1126/scitranslmed.aax2014

Xing, X., Yang, F., Huang, Q., Guo, H., Li, J., Qiu, M., Bai, F., & Wang, J. (2021). Decoding the multicellular ecosystem of lung adenocarcinoma manifested as pulmonary subsolid nodules by single-cell RNA sequencing. *Science advances*, *7*(5). https://doi.org/10.1126/sciadv.abd9738

Xiong, G., Qadota, H., Mercer, K. B., McGaha, L. A., Oberhauser, A. F., & Benian, G. M. (2009). A LIM-9 (FHL)/SCPL-1 (SCP) complex interacts with the C-terminal protein kinase regions of UNC-89 (obscurin) in Caenorhabditis elegans muscle. *Journal of molecular biology*, *386*(4), 976–988. https://doi.org/10.1016/j.jmb.2009.01.016

Xu, H., & Jia, J. (2021). Single-Cell RNA Sequencing of Peripheral Blood Reveals Immune Cell Signatures in Alzheimer's Disease. *Frontiers in immunology*, *12*, 645666. https://doi.org/10.3389/fimmu.2021.645666

Xu, Y., Chen, L., Liu, M., Lu, Y., Yue, Y., Liu, Y., Chen, H., Xie, F. and Zhang, C. (2019). High-throughput transcriptome sequencing reveals extremely high doses of ionizing radiation-response genes in Caenorhabditis elegans. *Toxicology Research*, 8(5), pp.754-766. https://doi.org/10.1039/c9tx00101h

Xue, Y., Gao, X., Lindsell, C. E., Norton, C. R., Chang, B., Hicks, C., Gendron-Maguire, M., Rand, E. B., Weinmaster, G., & Gridley, T. (1999). Embryonic lethality and vascular defects in mice lacking the Notch ligand Jagged1. *Human molecular genetics*, *8*(5), 723–730. https://doi.org/10.1093/hmg/8.5.723

Yahyanejad, S., Theys, J., & Vooijs, M. (2016). Targeting Notch to overcome radiation resistance. *Oncotarget*, *7*(7), 7610–7628. https://doi.org/10.18632/oncotarget.6714

Yan, J., Zhu, J., Zhong, H., Lu, Q., Huang, C., & Ye, Q. (2003). BRCA1 interacts with FHL2 and enhances FHL2 transactivation function. *FEBS letters*, *553*(1-2), 183–189. https://doi.org/10.1016/s0014-5793(03)00978-5

Yan, Y., Denef, N., & Schüpbach, T. (2009). The vacuolar proton pump, V-ATPase, is required for notch signaling and endosomal trafficking in Drosophila. *Developmental cell*, *17*(3), 387–402. https://doi.org/10.1016/j.devcel.2009.07.001

Yang, Z. (1994). Maximum likelihood phylogenetic estimation from DNA sequences with variable rates over sites: approximate methods. *Journal of molecular evolution*, *39*(3), 306–314. https://doi.org/10.1007/BF00160154

Yang, M., Chang, S., Chiou, S., Liu, C., Chi, C., Chen, P., Teng, S. & Wu, K. (2007). Overexpression of NBS1 induces epithelial–mesenchymal transition and co-expression of NBS1 and Snail predicts metastasis of head and neck cancer. *Oncogene*, 26(10), pp.1459-1467. https://doi.org/10.1038/sj.onc.1209929

Yang, M., Chiang, W., Chou, T., Chang, S., Chen, P., Teng, S. & Wu, K. (2006). Increased NBS1 Expression Is a Marker of Aggressive Head and Neck Cancer and Overexpression of NBS1 Contributes to Transformation. *Clinical Cancer Research*, 12(2), pp.507-515. https://doi.org/10.1158/1078-0432.CCR-05-1231

Yang, Q., Zhang, H., Wei, T., Lin, A., Sun, Y., Luo, P., & Zhang, J. (2021). Single-Cell RNA Sequencing Reveals the Heterogeneity of Tumor-Associated Macrophage in Non-Small Cell Lung Cancer and Differences Between Sexes. *Frontiers in immunology*, *12*, 756722. https://doi.org/10.3389/fimmu.2021.756722

Yang, S. A., & Deng, W. M. (2018). Serrate/Notch Signaling Regulates the Size of the Progenitor Cell Pool in *Drosophila* Imaginal Rings. *Genetics*, *209*(3), 829–843. https://doi.org/10.1534/genetics.118.300963

Yang, Z. J., Chee, C. E., Huang, S., & Sinicrope, F. A. (2011). The role of autophagy in cancer: therapeutic implications. *Molecular cancer therapeutics*, *10*(9), 1533–1541. https://doi.org/10.1158/1535-7163.MCT-11-0047

Yin, E., Nelson, D., Coleman, M., Peterson, L. & Wyrobek, A. (2003). Gene expression changes in mouse brain after exposure to low-dose ionizing radiation. *International Journal of Radiation Biology*, 79(10), pp.759-775. https://doi.org/10.1080/09553000310001610961

Yin, S., Huang, Y., Zhangfang, Y., Zhong, X., Li, P., Huang, J., Liu, D., & Songyang, Z. (2016). SmedOB1 is Required for Planarian Homeostasis and Regeneration. *Scientific reports*, *6*, 34013. https://doi.org/10.1038/srep34013

Yoo, S., Nair, S., Kim, H. J., Kim, Y., Lee, C., Lee, G., & Park, J. H. (2020). Knock-in mutations of scarecrow, a Drosophila homolog of mammalian Nkx2.1, reveal a novel function required for development of the optic lobe in Drosophila melanogaster. *Developmental biology*, *461*(2), 145–159. https://doi.org/10.1016/j.ydbio.2020.02.008

Yoshida, Y., Horikawa, D., Sakashita, T., Yokota, Y., Kobayashi, Y., Tomita, M., & Arakawa, K. (2021). RNA sequencing data for gamma radiation response in the extremotolerant tardigrade *Ramazzottius varieornatus*. *Data in brief*, *36*, 107111. https://doi.org/10.1016/j.dib.2021.107111

Yu, S., Li, L., Fan, K., Li, Y., & Gao, Y. (2021). A Genome-Scale CRISPR Knock-Out Screen Identifies MicroRNA-5197-5p as a Promising Radiosensitive Biomarker in Colorectal Cancer. *Frontiers in oncology*, *11*, 696713. https://doi.org/10.3389/fonc.2021.696713

Yuan, S. S., Chang, H. L., & Lee, E. Y. (2003). Ionizing radiation-induced Rad51 nuclear focus formation is cell cycle-regulated and defective in both ATM(-/-) and c-Abl(-/-) cells. *Mutation research*, *525*(1-2), 85–92. https://doi.org/10.1016/s0027-5107(03)00009-5

Yuan, Z. M., Huang, Y., Ishiko, T., Nakada, S., Utsugisawa, T., Kharbanda, S., Wang, R., Sung, P., Shinohara, A., Weichselbaum, R., & Kufe, D. (1998). Regulation of Rad51 function by c-Abl in response to DNA damage. *The Journal of biological chemistry*, *273*(7), 3799–3802. https://doi.org/10.1074/jbc.273.7.3799

Zdobnov, E. M., Kuznetsov, D., Tegenfeldt, F., Manni, M., Berkeley, M., & Kriventseva, E. V. (2021). OrthoDB in 2020: evolutionary and functional annotations of orthologs. *Nucleic acids research*, *49*(D1), D389–D393. https://doi.org/10.1093/nar/gkaa1009

Zebarjadian, Y., King, T., Fournier, M. J., Clarke, L., & Carbon, J. (1999). Point mutations in yeast CBF5 can abolish in vivo pseudouridylation of rRNA. *Molecular and cellular biology*, *19*(11), 7461–7472. https://doi.org/10.1128/MCB.19.11.7461

Zeng, A., Li, H., Guo, L., Gao, X., McKinney, S., Wang, Y., Yu, Z., Park, J., Semerad, C., Ross, E., Cheng, L. C., Davies, E., Lei, K., Wang, W., Perera, A., Hall, K., Peak, A., Box, A., & Sánchez Alvarado, A. (2018). Prospectively Isolated Tetraspanin^{+} Neoblasts Are Adult Pluripotent Stem Cells Underlying Planaria Regeneration. *Cell*, *173*(7), 1593–1608.e20. https://doi.org/10.1016/j.cell.2018.05.006

Zeng, A., Li, Y. Q., Wang, C., Han, X. S., Li, G., Wang, J. Y., Li, D. S., Qin, Y. W., Shi, Y., Brewer, G., & Jing, Q. (2013). Heterochromatin protein 1 promotes self-renewal and triggers regenerative proliferation in adult stem cells. *The Journal of cell biology*, *201*(3), 409–425. https://doi.org/10.1083/jcb.201207172

Zeng, T., Gao, H., Yu, P., He, H., Ouyang, X., Deng, L., & Zhang, Y. (2011). Up-regulation of kin17 is essential for proliferation of breast cancer. *PloS one*, *6*(9), e25343. https://doi.org/10.1371/journal.pone.0025343

Zhang, W., & Liu, H. T. (2002). MAPK signal pathways in the regulation of cell proliferation in mammalian cells. *Cell research*, *12*(1), 9–18. https://doi.org/10.1038/sj.cr.7290105

Zhang, X. P., Liu, F., & Wang, W. (2011). Two-phase dynamics of p53 in the DNA damage response. *Proceedings of the National Academy of Sciences of the United States of America*, *108*(22), 8990–8995. https://doi.org/10.1073/pnas.1100600108

Zhang, Y. (2020). Split-seq pipeline. Retrieved from https://github.com/yjzhang/split-seq-pipeline.

Zhang, Y. & Martin, S. (2014). Redox Proteins and Radiotherapy. *Clinical Oncology*, 26(5), pp.289-300. https://doi.org/10.1016/j.clon.2014.02.003

Zhang, Y., Huang, S., Gao, H., Wu, K., Ouyang, X., Zhu, Z., Yu, X., & Zeng, T. (2017). Upregulation of KIN17 is associated with non-small cell lung cancer invasiveness. *Oncology letters*, *13*(4), 2274–2280. https://doi.org/10.3892/ol.2017.5707

Zhao, H., Li, Z., Gao, Y., Li, J., Zhao, X., & Yue, W. (2021). Single-Cell RNA-Sequencing Portraying Functional Diversity and Clinical Implications of IFI6 in Ovarian Cancer. *Frontiers in cell and developmental biology*, *9*, 677697. https://doi.org/10.3389/fcell.2021.677697

Zhao, Y., Kwan, K. M., Mailloux, C. M., Lee, W. K., Grinberg, A., Wurst, W., Behringer, R. R., & Westphal, H. (2007). LIM-homeodomain proteins Lhx1 and Lhx5, and their cofactor Ldb1, control Purkinje cell differentiation in the developing cerebellum. *Proceedings of the National Academy of Sciences of the United States of America*, *104*(32), 13182–13186. https://doi.org/10.1073/pnas.0705464104

Zheng, L., Wu, X., Li, S., Liu, B., & Xue, D. (2019). Cathepsin B inhibitors block multiple radiation-induced side effects in C. elegans. *Cell research*, *29*(12), 1042–1045. https://doi.org/10.1038/s41422-019-0247-3

Zheng, Q., & Zhao, Y. (2007). The diverse biofunctions of LIM domain proteins: determined by subcellular localization and protein-protein interaction. *Biology of the cell*, *99*(9), 489–502. https://doi.org/10.1042/BC20060126

Zhou, Q., Li, H., & Xue, D. (2011). Elimination of paternal mitochondria through the lysosomal degradation pathway in C. elegans. *Cell research*, *21*(12), 1662–1669. https://doi.org/10.1038/cr.2011.182

Zhou, Z., Chen, G., Shen, M., Li, J., Liu, K., Liu, M., Shi, S., Yang, D., Chen, W., Chen, S., Yin, Y., Qin, Y., Su, X., Chen, W., & Kang, M. (2023). Genome-scale CRISPR-Cas9 knockout screening in nasopharyngeal carcinoma for radiosensitive and radioresistant genes. *Translational oncology*, *30*, 101625. https://doi.org/10.1016/j.tranon.2023.101625

Zhu, G. D., Yu, J., Sun, Z. Y., Chen, Y., Zheng, H. M., Lin, M. L., Ou-Yang, S., Liu, G. L., Zhang, J. W., & Shao, F. M. (2021). Genome-wide CRISPR/Cas9 screening identifies CARHSP1 responsible for radiation resistance in glioblastoma. *Cell death & disease*, *12*(8), 724. https://doi.org/10.1038/s41419-021-04000-3

Zhu, S. J., & Pearson, B. J. (2013). The Retinoblastoma pathway regulates stem cell proliferation in freshwater planarians. *Developmental biology*, *373*(2), 442–452. https://doi.org/10.1016/j.ydbio.2012.10.025

Zhu, S. J., Hallows, S. E., Currie, K. W., Xu, C., & Pearson, B. J. (2015). A mex3 homolog is required for differentiation during planarian stem cell lineage development. *eLife*, *4*, e07025. https://doi.org/10.7554/eLife.07025

Zywitza, V., Misios, A., Bunatyan, L., Willnow, T. E., & Rajewsky, N. (2018). Single-Cell Transcriptomics Characterizes Cell Types in the Subventricular Zone and Uncovers Molecular Defects Impairing Adult Neurogenesis. *Cell reports*, *25*(9), 2457–2469.e8. https://doi.org/10.1016/j.celrep.2018.11.003

Appendix

List of contents

Appendix Table 1. List of Neoblast cluster markers and associated statistics

Integrated Neoblast Cluster 1 Marker genes					
Gene Name	**Identifier**	**P_value**	**Average log_2 fold change**	**pct.1**	**pct.2**
H1.A	MSTRG.8605	1.09E-176	2.768	1	0.277
Smedwi-1	MSTRG.11390	1.52E-174	2.688	0.827	0.082
EF1a-1	MSTRG.18279	1.62E-174	2.642	0.656	0.043
RRM1	MSTRG.9822	1.09E-158	2.384	0.693	0.056
Smedwi-2	MSTRG.20672	5.69E-145	2.291	0.656	0.055
EF1a-2	MSTRG.18267	5.59E-131	2.248	0.626	0.058
Vasa-1	MSTRG.20195	5.50E-129	2.203	0.571	0.106
Tub3a	MSTRG.6262	2.89E-114	2.054	0.632	0.069
Hsp90a	MSTRG.20956	1.63E-112	2.126	0.638	0.072
H2A	MSTRG.5669	1.29E-67	1.903	0.632	0.069
SART-3	MSTRG.4084	1.74E-93	2.000	0.933	0.215
H1.B	MSTRG.6486	4.00E-93	2.192	0.442	0.04
H2B	MSTRG.20196	1.12E-79	1.890	0.687	0.122
EEF2	MSTRG.8811	7.56E-87	1.874	0.466	0.048
H.9.1h	MSTRG.8603	7.55E-81	1.718	0.252	0.012
HSPD1	MSTRG.19445	1.73E-76	1.693	0.288	0.018
Bruli	MSTRG.6703	1.49E-70	1.617	0.299	0.019
YBX-2	MSTRG.15848	5.24E-70	1.585	0.196	0.007
Hsp90b	MSTRG.20955	7.27E-70	1.730	0.724	0.152
CCAR-1	MSTRG.15974	2.79E-67	1.556	0.233	0.013
UMSBP	MSTRG.15777	3.06E-67	1.529	0.411	0.048
TUB4b	MSTRG.13335	3.99E-67	1.757	0.331	0.031
RPL4	MSTRG.2815	8.14E-67	1.472	0.19	0.007
RPL3	MSTRG.7334	3.61E-66	1.629	0.16	0.004
DDX43	MSTRG.3517	1.10E-65	1.694	0.982	0.402
TMEM145	MSTRG.21016	2.74E-65	1.807	0.601	0.113
PPP6R1	MSTRG.5338	4.55E-65	1.598	0.368	0.04
RPL7a	MSTRG.7157	8.83E-65	1.667	0.632	0.122
EIF4G	MSTRG.14077	1.77E-64	1.674	0.233	0.014
NUP210	MSTRG.14458	2.73E-64	1.547	0.742	0.17
Integrated Neoblast Cluster 2 Marker Genes					
Gene Name	**Identifier**	**P_value**	**Average log_2 fold change**	**pct.1**	**pct.2**
H1.A	MSTRG.8605	4.12E-149	2.811	0.991	0.264
Smedwi-1	MSTRG.11390	3.34E-78	2.383	0.631	0.113
RRM1	MSTRG.9822	3.05E-63	1.973	0.504	0.169
Tub3a	MSTRG.6262	1.24E-60	1.463	0.95	0.494
SART-3	MSTRG.4084	5.86E-60	2.286	0.39	0.067
Smedwi-2	MSTRG.20672	2.22E-53	1.772	0.661	0.222
Vasa-1	MSTRG.20195	5.76E-50	1.566	0.385	0.081
H1.B	MSTRG.6486	1.22E-49	2.184	0.389	0.058
Smedwi-3	MSTRG.22903	9.08E-46	2.150	0.619	0.169
EF1a-1	MSTRG.18279	7.93E-44	1.474	0.817	0.403
H2B	MSTRG.20196	2.91E-40	2.194	0.356	0.07
Bruli	MSTRG.6703	4.29E-38	2.161	0.299	0.058
Hsp90a	MSTRG.20956	5.42E-37	1.285	0.803	0.427
HSPD1	MSTRG.19445	6.40E-37	2.033	0.312	0.068
EF1a-2	MSTRG.18267	2.25E-36	2.063	0.275	0.054
H.9.1h	MSTRG.8603	3.35E-34	1.511	0.596	0.238
YBX-2	MSTRG.15848	3.40E-33	2.031	0.303	0.072

Appendix Table 1 (continued)

EF-2	MSTRG.8811	5.95E-31	1.619	0.454	0.162
Rad50	MSTRG.12624	7.12E-28	1.751	0.265	0.036
Hsp90b	MSTRG.20955	4.70E-27	2.028	0.298	0.084
H2A	MSTRG.5669	9.00E-27	1.596	0.385	0.132
Hsp70	MSTRG.13213	1.62E-23	1.745	0.362	0.133
RPL3	MSTRG.7334	5.98E-23	1.708	0.115	0.014
TOP2B	MSTRG.11752	2.03E-21	1.582	0.248	0.07
FMC1	MSTRG.15536	2.30E-21	1.281	0.495	0.231
CCAR-1	MSTRG.15974	3.37E-21	1.691	0.307	0.104
UMSBP	MSTRG.15777	1.73E-20	1.671	0.202	0.05
BRG-1	MSTRG.13350	2.48E-20	1.336	0.25	0.144
TMEM145	MSTRG.21016	4.20E-20	1.740	0.128	0.021
EIF4G	MSTRG.14077	6.47E-20	1.467	0.294	0.099
Integrated Neoblast Cluster 3 Marker genes					
Gene Name	**Identifier**	**P_value**	**Average log_2 fold change**	**pct.1**	**pct.2**
H1.A	MSTRG.8605	2.30E-125	1.606	0.688	0.368
Smedwi-1	MSTRG.11390	2.48E-69	1.503	0.262	0.134
SART-3	MSTRG.4084	3.59E-45	1.427	0.237	0.131
Vasa-1	MSTRG.20195	5.86E-32	1.304	0.256	0.122
Tub3a	MSTRG.6262	2.05E-31	1.390	0.896	0.477
H1.B	MSTRG.6486	2.43E-30	1.338	0.294	0.090
Smedwi-3	MSTRG.22903	2.59E-28	1.125	0.368	0.184
EF1a-1	MSTRG.18279	2.72E-27	1.282	0.810	0.472
C3H8.02L	MSTRG.22724	3.90E-25	1.315	0.390	0.148
slc38a-4	MSTRG.9785	1.75E-24	1.280	0.163	0.087
H2A	MSTRG.5669	1.79E-24	1.170	0.279	0.111
YBX-2	MSTRG.15846	1.89E-24	0.851	0.217	0.008
ACTB	MSTRG.3619	2.53E-23	0.783	0.148	0.114
RPL4	MSTRG.2815	2.86E-22	0.579	0.252	0.163
Tub4B	MSTRG.11531	3.78E-22	0.883	0.224	0.083
MRVI1	MSTRG.16792	5.49E-21	0.933	0.251	0.175
pmp5	MSTRG.4614	5.86E-20	0.819	0.135	0.094
Ros1	MSTRG.18995	6.44E-20	0.751	0.240	0.152
Tub4A	MSTRG.14813	7.23E-19	0.960	0.804	0.533
HNRPUL1	MSTRG.10587	7.24E-19	0.632	0.093	0.058
Hmcn-1	MSTRG.7905	7.25E-19	0.627	0.132	0.099
Hsp90	MSTRG.8165	7.84E-18	0.677	0.219	0.142
A2ML1	MSTRG.12008	8.05E-18	0.678	0.125	0.081
AMPKγ	MSTRG.8330	1.10E-18	0.591	0.152	0.106
N/A	MSTRG.3940	1.28E-16	0.532	0.116	0.091
Hsp70	MSTRG.13147	1.22E-16	0.546	0.228	0.164
Slc4a-1	MSTRG.8586	2.16E-15	0.520	0.11	0.078
VWA5A	MSTRG.16317	2.64E-14	0.529	0.144	0.099
SYNE-1	MSTRG.5145	4.10E-11	0.582	0.1	0.054
3HiB	MSTRG.4204	4.64E-09	0.534	0.217	0.163

Key – Pct.1 represents the percentage of cells within the target Neoblast cluster with detectable expression of the corresponding gene. Pct.2 represents the percentage of cells where the gene is detected in all other clusters except the target Neoblast cluster. Highlighted genes are referenced in text (Chapter 3).

Appendix Table 2. Differentially expressed genes (Log2FC > 1, P-value < 0.05) from pseudo-bulk analysis between wild-type Neoblasts 1 and wild-type Neoblasts 2.

Upregulated in wild-type Neoblasts 1 versus wild-type Neoblasts 2					
Gene Name	**Identifier**	**P_value**	**Average log_2 fold change**	**pct.1**	**pct.2**
MPCP	MSTRG.18502	3.10E-08	1.507	0.273	0.009
6PGD	MSTRG.1675	3.20E-07	1.412	0.359	0.037
SYLM	MSTRG.21087	2.70E-05	1.406	0.297	0.028
KCNH2	MSTRG.8535	4.10E-06	1.321	0.365	0.05
RLA2	MSTRG.15815	7.20E-06	1.294	0.34	0.041
RS21	MSTRG.2390	5.60E-05	1.286	0.26	0.014
RL11	MSTRG.4583	4.40E-07	1.278	0.377	0.046
DPOD1	MSTRG.10465	1.40E-05	1.265	0.273	0.014
BRD1	MSTRG.14727	4.10E-06	1.238	0.346	0.041
MTMRE	MSTRG.15314	7.70E-05	1.233	0.279	0.023
RS14	MSTRG.11423	1.70E-07	1.232	0.432	0.069
DPOG1	MSTRG.13338	7.50E-07	1.224	0.383	0.05
IF2P	MSTRG.3618	4.50E-06	1.216	0.365	0.05
CAF1A	MSTRG.18513	1.30E-04	1.215	0.31	0.041
BMR1B	MSTRG.19318	9.20E-05	1.193	0.267	0.018
CNNM4	MSTRG.14423	3.70E-04	1.193	0.254	0.018
UBE4B	MSTRG.17995	5.00E-05	1.184	0.273	0.018
LEUTX	MSTRG.17691	2.40E-06	1.178	0.414	0.073
SC6A2	MSTRG.15483	2.70E-04	1.171	0.303	0.041
STRC	MSTRG.15911	3.60E-04	1.158	0.254	0.018
LIMA1	MSTRG.568	4.80E-05	1.136	0.273	0.018
FBP12	MSTRG.9884	3.30E-04	1.136	0.334	0.06
SSH2	MSTRG.20860	1.10E-04	1.133	0.322	0.046
MADD	MSTRG.235	1.10E-04	1.132	0.254	0.014
GPDA	MSTRG.2616	9.60E-05	1.118	0.267	0.018
ADDA	MSTRG.611	2.90E-04	1.114	0.267	0.023
IF4A3	MSTRG.15619	2.40E-07	1.114	0.414	0.06
IGFN1	MSTRG.13018	1.30E-03	1.092	0.26	0.028
RACK1	MSTRG.22464	1.50E-07	1.084	0.604	0.156
CEP70	MSTRG.13267	1.60E-04	1.079	0.402	0.092
PLK1	MSTRG.7935	1.80E-04	1.073	0.26	0.018
AFG1L	MSTRG.20578	2.70E-04	1.065	0.285	0.032
GSH1	MSTRG.16208	2.80E-05	1.061	0.328	0.041
EPS15	MSTRG.12018	7.20E-05	1.061	0.31	0.037
FKBP4	MSTRG.77	1.10E-03	1.051	0.254	0.023
KC1G2	MSTRG.6966	1.70E-04	1.044	0.291	0.032
FBX38	MSTRG.10992	2.00E-05	1.037	0.359	0.055
MBTD1	MSTRG.8252	1.80E-05	1.035	0.395	0.073
GBB3	MSTRG.12399	1.60E-04	1.025	0.273	0.023
ESYT2	MSTRG.670	1.80E-04	1.025	0.291	0.032
IF5A1	MSTRG.22720	5.90E-05	1.021	0.26	0.014
FLOT1	MSTRG.2398	9.60E-05	1.019	0.297	0.032
OFUT2	MSTRG.9207	1.70E-03	1.012	0.267	0.032
MGT5A	MSTRG.5513	9.80E-04	1.01	0.273	0.032
CNOT4	MSTRG.13339	3.70E-03	1.009	0.297	0.055
RFFL	MSTRG.14105	2.00E-04	1.006	0.334	0.055
ATAD2	MSTRG.3476	2.60E-05	1.003	0.365	0.06

Appendix Table 2 (continued)

Downregulated in wild-type Neoblasts 1 versus wild-type Neoblasts 2					
Gene Name	**Identifier**	**P_value**	**Average log_2 fold change**	**pct.1**	**pct.2**
MAGP	MSTRG.12760	1.44E-03	-1.632	0.135	0.205
UBNX4	MSTRG.14610	2.91E-03	-1.395	0.117	0.278
PRP16	MSTRG.4439	1.22E-03	-1.291	0.11	0.278
FANCI	MSTRG.16231	2.15E-03	-1.285	0.104	0.256
P85B	MSTRG.21789	5.96E-03	-1.276	0.098	0.251
ENASE	MSTRG.15059	5.61E-03	-1.204	0.112	0.22
S61A1	MSTRG.834	9.33E-03	-1.177	0.086	0.256
PD1A4	MSTRG.4061	1.18E-02	-1.165	0.117	0.265
CSKI1	MSTRG.19455	5.86E-03	-1.149	0.129	0.256
ARMC8	MSTRG.18191	1.79E-03	-1.144	0.135	0.256
WDFY4	MSTRG.12481	5.07E-03	-1.135	0.135	0.26
ANR17	MSTRG.4664	4.37E-04	-1.132	0.194	0.306
SMC1	MSTRG.7817	3.57E-02	-1.193	0.196	0.352
KI21B	MSTRG.18180	4.38E-03	-1.128	0.129	0.246
RBM4B	MSTRG.17825	8.31E-03	-1.115	0.117	0.215
DTWD2	MSTRG.12145	3.11E-03	-1.113	0.11	0.251
CDC16	MSTRG.15497	8.40E-03	-1.113	0.178	0.278
HROB	MSTRG.19230	5.74E-03	-1.112	0.123	0.246
AB12B	MSTRG.5569	1.17E-02	-1.111	0.135	0.256
PDC6I	MSTRG.6082	5.89E-03	-1.104	0.104	0.237
SMC2	MSTRG.17822	1.57E-03	-1.103	0.117	0.251
XKR9	MSTRG.8669	7.57E-03	-1.102	0.166	0.21
DOC11	MSTRG.5909	9.87E-03	-1.089	0.104	0.233
ODO1	MSTRG.7184	8.86E-03	-1.063	0.153	0.269
TDRD7	MSTRG.147	8.86E-03	-1.062	0.103	0.196
CCNL2	MSTRG.22099	5.87E-03	-1.060	0.166	0.265
ATR	MSTRG.23227	1.21E-02	-1.050	0.11	0.228
P20L1	MSTRG.8883	3.35E-02	-1.033	0.123	0.265
APBA3	MSTRG.9223	4.10E-02	-1.015	0.11	0.237

Key: Pct.1 represents the percentage of Neoblast Cluster 1 cells with detectable expression of the corresponding gene. Pct.2 represents the percentage of Neoblast Cluster 2 cells with detectable expression of the corresponding gene. Highlighted genes are referenced in text (Chapter 3).

Appendix Table 3. Differentially expressed genes (Log2FC > 1, P-value < 0.05) from pseudo-bulk analyses between Neoblasts 1 at 3 hours post 10 Gy irradiation against wild-type Neoblasts 1

Upregulated in Neoblasts 1 at 3 hours post 10 Gy irradiation relative to wild-type					
Gene Name	**Identifier**	**P_value**	**Average log_2 fold change**	**pct.1**	**pct.2**
slc38a-4	MSTRG.9785	5.52E-05	2.011	0.318	0.092
C4orf51	MSTRG.17503	4.41E-04	1.770	0.398	0.172
ATXN2L	MSTRG.3214	6.24E-04	1.679	0.155	0.011
RBCK1	MSTRG.22714	5.90E-05	1.560	0.409	0.138
TBC1D20	MSTRG.8513	1.37E-03	1.405	0.164	0.023
Rad51C	MSTRG.11576	1.12E-04	1.305	0.273	0.057
LUC7L3	MSTRG.18867	3.31E-03	1.271	0.185	0.023
TLE1	MSTRG.21461	1.68E-03	1.267	0.176	0.011
MAPK10	MSTRG.2001	8.76E-03	1.220	0.185	0.034
NR1L3	MSTRG.19781	2.69E-03	1.169	0.167	0.011
H.108.10b	MSTRG.2824	3.06E-03	1.146	0.247	0.069
CYLD	MSTRG.2983	7.60E-03	1.121	0.167	0.023
ND-20	MSTRG.11477	5.99E-03	1.120	0.203	0.046
TRAF3	MSTRG.542	2.19E-03	1.088	0.167	0.011
NOVA2	MSTRG.19688	5.91E-03	1.062	0.203	0.046
ZCCHC14	MSTRG.23094	1.05E-02	1.059	0.16	0.011
EIF-2	MSTRG.7182	1.51E-02	1.048	0.185	0.046
LIMS1	MSTRG.3473	3.30E-02	1.022	0.182	0.08
AxinB	MSTRG.521	1.41E-02	1.017	0.136	0.034
SNRK	MSTRG.925	4.22E-03	1.015	0.128	0.011
Downregulated in Neoblasts 1 at 3 hours post 10 Gy irradiation relative to wild-type					
Gene Name	**Identifier**	**P_value**	**Average log_2 fold change**	**pct.1**	**pct.2**
NDUFS6	MSTRG.6193	2.60E-04	-2.071	0.018	0.161
Nop60B	MSTRG.9959	6.98E-03	-1.298	0.027	0.126
RMDN1	MSTRG.12061	3.77E-08	-1.182	0.7	0.854
GRIN1B	MSTRG.3810	2.86E-03	-1.160	0.027	0.138
CPT1A	MSTRG.12714	4.12E-02	-1.142	0.064	0.138
MPHOSPH8	MSTRG.14064	1.05E-04	-1.141	0.355	0.575
DYRK2	MSTRG.17475	6.09E-03	-1.132	0.027	0.126
AMMECR1	MSTRG.15737	1.68E-02	-1.112	0.055	0.149
AHNAK	MSTRG.7906	1.41E-02	-1.092	0.1	0.218
RPS25	MSTRG.15728	3.28E-03	-1.091	0.082	0.23
CCDC17	MSTRG.16105	1.14E-03	-1.085	0.318	0.475
ANKRD28	MSTRG.22364	1.90E-02	-1.076	0.136	0.253
H2A.j	MSTRG.1771	8.74E-03	-1.067	0.038	0.105
FAM155A	MSTRG.18397	2.70E-02	-1.034	0.036	0.115

Key – Pct.1 represents the percentage of Neoblasts 1 cells at 3 hours post 10 Gy irradiation with detectable expression of the corresponding gene. Pct.2 represents the percentage of wild-type Neoblasts 1 cells with detectable expression of the corresponding gene.

Appendix Table 4. Differentially expressed genes (Log2FC > 1, P-value < 0.05) from pseudo-bulk analyses between Neoblasts 1 at 3 hours post 5 Gy irradiation against wild-type Neoblasts 1

Upregulated in Neoblasts 1 at 3 hours post 5 Gy irradiation relative to wild-type					
Gene Name	**Identifier**	**P_value**	**Average log_2 fold change**	**pct.1**	**pct.2**
slc38a-4	MSTRG.9785	5.96E-04	2.182	0.318	0.142
UMSBP	MSTRG.15778	5.16E-07	1.693	0.264	0.019
UBXN6	MSTRG.919	1.19E-05	1.512	0.255	0.038
CNOT4	MSTRG.13339	1.96E-03	1.421	0.173	0.057
COASY	MSTRG.6514	8.69E-04	1.397	0.192	0
C4orf51	MSTRG.17503	2.02E-02	1.257	0.364	0.172
PNPL7	MSTRG.1246	2.44E-03	1.228	0.184	0.038
HTT	MSTRG.5095	1.92E-03	1.225	0.236	0.085
H.90.11a	MSTRG.7658	4.05E-03	1.202	0.185	0.038
PHTF2	MSTRG.15676	5.25E-03	1.157	0.192	0.038
RBCK2	MSTRG.22714	5.39E-06	1.116	0.409	0.113
H.34.6e	MSTRG.20883	3.86E-04	1.092	0.136	0.009
KARS	MSTRG.1419	3.62E-04	1.088	0.2	0.038
LRRC24	MSTRG.3408	2.76E-03	1.055	0.164	0.038
TDC7	MSTRG.2704	3.14E-04	1.052	0.188	0.038
PCNX1	MSTRG.17283	9.58E-04	1.032	0.164	0.028
LARS	MSTRG.10349	8.69E-04	1.030	0.174	0
ORAB-1	MSTRG.22316	4.75E-03	1.022	0.164	0.028
Downregulated in Neoblasts 1 at 3 hours post 5 Gy irradiation relative to wild-type					
Gene Name	**Identifier**	**P_value**	**Average log_2 fold change**	**pct.1**	**pct.2**
UPS34	MSTRG.10066	2.30E-02	-1.506	0.091	0.189
CG6282	MSTRG.2186	2.51E-03	-1.452	0.018	0.123
RIMS2	MSTRG.11775	3.64E-03	-1.341	0.236	0.368
SUPT20H	MSTRG.19964	1.06E-02	-1.269	0.082	0.198
NSA2	MSTRG.9135	8.73E-03	-1.142	0.082	0.198
CHRM3	MSTRG.10577	5.49E-07	-1.099	0.536	0.755
H.35.2a	MSTRG.4901	4.77E-02	-1.021	0.109	0.189
ITSN1	MSTRG.19591	4.64E-02	-1.012	0.145	0.226
SPRK3	MSTRG.19190	4.92E-02	-1.003	0.145	0.217

Key – Pct.1 represents the percentage of Neoblasts 1 cells at 3 hours post 5 Gy irradiation with detectable expression of the corresponding gene. Pct.2 represents the percentage of wild-type Neoblasts 1 cells with detectable expression of the corresponding gene.

Appendix Table 5. Differentially expressed genes (Log2FC > 1, P-value < 0.05) from pseudo-bulk analyses between Neoblasts 1 at 24 hours post 10 Gy irradiation against wild-type Neoblasts 1

Upregulated in Neoblasts 1 at 24 hours post 10 Gy irradiation relative to wild-type					
Gene Name	**Identifier**	**P_value**	**Average log_2 fold change**	**pct.1**	**pct.2**
Ubm2	MSTRG.17023	3.03E-09	1.931	0.39	0.055
RL37	MSTRG.23038	1.04E-06	1.678	0.31	0.123
GCR037	MSTRG.19362	2.68E-05	1.612	0.15	0
MAPKKK3	MSTRG.6508	8.36E-08	1.544	0.53	0.191
NSA2	MSTRG.9135	2.08E-04	1.466	0.27	0.082
Dkc	MSTRG.9959	1.08E-03	1.488	0.22	0.027
MAPKAPK2	MSTRG.6513	9.82E-06	1.310	0.39	0.127
MRTO4	MSTRG.7179	3.34E-04	1.295	0.24	0.064
XIAP	MSTRG.456	1.38E-04	1.263	0.35	0.136
ABCF1	MSTRG.9034	1.93E-06	1.256	0.26	0.073
SMT3	MSTRG.6033	4.25E-05	1.255	0.28	0.064
FAU	MSTRG.19511	8.00E-07	1.250	0.5	0.173
RhoGEF10	MSTRG.7881	2.91E-06	1.245	0.61	0.3
RPS-26	MSTRG.15549	2.93E-04	1.243	0.3	0.109
14-3-3T	MSTRG.16752	2.23E-07	1.241	0.26	0.073
Tincar-like	MSTRG.3292	3.55E-04	1.234	0.17	0.027
TUBB4b	MSTRG.7466	2.85E-04	1.215	0.64	0.291
WHSC1L1	MSTRG.12507	2.95E-08	1.211	0.71	0.327
ETFb	MSTRG.451	1.96E-04	1.206	0.22	0.045
BTF3	MSTRG.598	8.88E-05	1.199	0.25	0.055
RL18	MSTRG.5388	1.53E-07	1.187	0.63	0.282
HIG1	MSTRG.18733	4.31E-05	1.187	0.35	0.118
ATP5G1	MSTRG.17876	6.97E-06	1.182	0.36	0.091
Calm1	MSTRG.4051	3.19E-03	1.181	0.23	0.091
TNX9	MSTRG.5940	6.70E-05	1.176	0.36	0.118
RAN	MSTRG.21224	3.64E-08	1.163	0.68	0.3
YBX1	MSTRG.15848	3.12E-05	1.158	0.95	0.709
H.8.11d	MSTRG.16867	9.69E-06	1.147	0.31	0.064
TIF1a	MSTRG.21584	4.51E-05	1.142	0.42	0.173
DnaJ	MSTRG.5473	9.94E-05	1.137	0.28	0.109
MATE1	MSTRG.2562	2.62E-02	1.126	0.34	0.209
PPIB	MSTRG.12048	8.00E-05	1.125	0.22	0.036
UMSBP	MSTRG.15777	3.82E-11	1.124	0.91	0.618
TXN2	MSTRG.12229	5.22E-03	1.095	0.16	0.045
RS6	MSTRG.1199	8.41E-06	1.093	0.69	0.4
RPL19	MSTRG.17345	4.21E-06	1.080	0.67	0.391
H.43.11a	MSTRG.11928	4.60E-05	1.080	0.61	0.355
YBX2	MSTRG.15845	6.44E-08	1.080	0.75	0.436
H.45.1e	MSTRG.1950	2.82E-03	1.076	0.31	0.145
EEF1D	MSTRG.22674	7.05E-03	1.074	0.18	0.064
SRP20	MSTRG.12827	2.61E-02	1.064	0.19	0.055
RPS4	MSTRG.76	4.35E-05	1.063	0.56	0.245
RTP4-like	MSTRG.10424	3.02E-03	1.060	0.1	0.009
SARNP	MSTRG.20498	7.40E-03	1.044	0.18	0.064
Tex9	MSTRG.3070	4.98E-02	1.041	0.12	0.009
MOK	MSTRG.13512	7.12E-05	1.040	0.44	0.182
RPS13	MSTRG.8816	1.99E-02	1.030	0.27	0.109
CALM2	MSTRG.11180	5.93E-04	1.028	0.29	0.1
FTH1	MSTRG.12670	3.55E-02	1.021	0.12	0.018
ADF6	MSTRG.7931	2.80E-06	1.020	0.45	0.145
PDIA6	MSTRG.5061	4.11E-02	1.010	0.19	0.036

Appendix Table 5 (continued)

Downregulated in Neoblasts 1 at 24 hours post 10 Gy irradiation relative to wild-type					
Gene Name	**Identifier**	**P_value**	**Average log_2 fold change**	**pct.1**	**pct.2**
RBCK1	MSTRG.1905	3.38E-06	-2.335	0.09	0.357
LRRC24	MSTRG.3408	2.81E-03	-1.410	0.04	0.194
N/A	MSTRG.16517	1.22E-03	-1.346	0.18	0.385
SNRNP27	MSTRG.9276	6.20E-04	-1.337	0.07	0.266
MITD1	MSTRG.823	1.62E-03	-1.293	0.12	0.312
PNPLA7	MSTRG.1246	7.41E-03	-1.257	0.05	0.194
GRIK4	MSTRG.13500	1.21E-03	-1.221	0	0.13
DIP2A	MSTRG.16159	7.39E-04	-1.149	0.02	0.185
TTC39B	MSTRG.10321	2.12E-02	-1.116	0.03	0.139
FLO1	MSTRG.2398	1.79E-03	-1.114	0.02	0.166
NUDT17	MSTRG.13298	9.46E-03	-1.090	0.24	0.385
ATXN2L	MSTRG.3214	1.11E-02	-1.065	0.05	0.185
BLH8	MSTRG.20883	1.79E-03	-1.058	0.02	0.166
CPLX1	MSTRG.3538	8.54E-03	-1.057	0.24	0.394
COASY	MSTRG.6514	1.44E-02	-1.052	0.02	0.13
GTF2IRD2	MSTRG.20805	2.33E-02	-1.042	0.07	0.185
PGBD4	MSTRG.54	3.14E-02	-1.036	0.1	0.194
Hb.20.10d	MSTRG.8560	6.43E-03	-1.031	0.08	0.239
RPS6KA3	MSTRG.21623	4.91E-02	-1.025	0.02	0.148
SF3B3	MSTRG.1242	3.90E-02	-1.015	0.13	0.312
NPa1p	MSTRG.6657	4.18E-02	-1.013	0.03	0.166
PATS1	MSTRG.19698	4.94E-02	-1.011	0.07	0.166
MRP1	MSTRG.6056	9.97E-03	-1.004	0.16	0.321

Key – Pct.1 represents the percentage of Neoblasts 1 cells at 24 hours post 10 Gy irradiation with detectable expression of the corresponding gene. Pct.2 represents the percentage of wild-type Neoblasts 1 cells with detectable expression of the corresponding gene. Highlighted genes are referenced in text (Chapter 3).

Appendix Table 6. Differentially expressed genes (Log2FC > 1, P-value < 0.05) from pseudo-bulk analyses between Neoblasts 1 at 24 hours post 5 Gy irradiation against wild-type Neoblasts 1

Upregulated in Neoblasts 1 at 24 hours post 5 Gy irradiation relative to wild-type					
Gene Name	**Identifier**	**P_value**	**Average log_2 fold change**	**pct.1**	**pct.2**
MATE1	MSTRG.2562	6.34E-06	2.087	0.396	0.209
Ank1	MSTRG.13808	8.88E-05	1.448	0.297	0.091
RPS25	MSTRG.15728	3.90E-04	1.433	0.257	0.082
SMT3	MSTRG.17023	6.01E-03	1.410	0.168	0.055
RhoGEF10	MSTRG.7881	4.36E-05	1.354	0.515	0.3
RPL18	MSTRG.5388	7.70E-05	1.324	0.505	0.282
FAU	MSTRG.19511	4.61E-04	1.285	0.366	0.173
Dkc	MSTRG.9959	1.55E-02	1.268	0.179	0.027
14-3-3T	MSTRG.15606	2.02E-03	1.257	0.218	0.073
UGDH	MSTRG.12666	1.84E-02	1.243	0.149	0.055
ABCF1	MSTRG.9034	2.04E-02	1.217	0.188	0.073
RPLP0	MSTRG.23294	4.87E-05	1.187	0.614	0.391
NCAPH	MSTRG.11727	2.40E-02	1.179	0.129	0.045
DnaJ	MSTRG.5473	2.07E-02	1.176	0.218	0.109
ATP5G1	MSTRG.21785	5.89E-03	1.156	0.109	0.018
RPS5	MSTRG.22251	1.29E-04	1.148	0.505	0.282
NSA2	MSTRG.9135	8.04E-04	1.143	0.198	0.082
ACBD6	MSTRG.10208	8.25E-03	1.134	0.327	0.191
MSH6	MSTRG.21454	7.36E-03	1.118	0.228	0.1
CypA	MSTRG.2885	3.90E-05	1.090	0.624	0.427
UBB	MSTRG.17258	1.50E-02	1.088	0.248	0.127
CTNS	MSTRG.5239	4.02E-02	1.076	0.149	0.073
ARID2	MSTRG.18864	1.20E-02	1.071	0.158	0.055
RPS-26	MSTRG.15549	1.92E-02	1.068	0.218	0.109
MAPKAPK2	MSTRG.6513	2.47E-02	1.067	0.238	0.127
TIM17B	MSTRG.9432	2.32E-02	1.066	0.327	0.209
HEN1	MSTRG.11886	1.58E-02	1.062	0.109	0.027
MOK	MSTRG.13512	8.59E-04	1.053	0.376	0.182
RPS6	MSTRG.1199	1.66E-04	1.052	0.594	0.4
RPLP2	MSTRG.15815	1.71E-03	1.051	0.337	0.164
TM9SF3	MSTRG.5235	1.10E-02	1.042	0.129	0.036
slc3a-1	MSTRG.6120	4.18E-02	1.019	0.109	0.055
MX2	MSTRG.1546	3.07E-02	1.007	0.168	0.1
PES3	MSTRG.20107	6.66E-03	1.006	0.158	0.045
RPL10A	MSTRG.277	2.33E-02	1.004	0.327	0.218
Downregulated in Neoblasts 1 at 24 hours post 5 Gy irradiation relative to wild-type					
Gene Name	**Identifier**	**P_value**	**Average log_2 fold change**	**pct.1**	**pct.2**
Tub3A	MSTRG.3735	2.75E-06	-1.851	0.04	0.328
Slc38-a11	MSTRG.9785	4.63E-02	-1.490	0.238	0.358
Unc22	MSTRG.13018	8.17E-03	-1.489	0.04	0.185
TTC25	MSTRG.20562	1.15E-03	-1.443	0	0.14
BPTF	MSTRG.4811	5.49E-04	-1.434	0.089	0.313
SEMA-like	MSTRG.5812	1.05E-03	-1.360	0.02	0.185
N/A	MSTRG.17895	3.62E-04	-1.280	0.129	0.367
NARFL	MSTRG.9121	1.15E-03	-1.240	0	0.152
H.73.5c	MSTRG.3056	3.62E-04	-1.232	0.089	0.322
H.68.1g	MSTRG.13348	4.24E-02	-1.180	0.059	0.167
UBX-6	MSTRG.919	7.42E-04	-1.165	0.079	0.295

Appendix Table 6 (continued)

PLOD-1	MSTRG.20691	3.44E-03	-1.157	0.03	0.185
CEP135	MSTRG.23315	1.31E-03	-1.139	0.03	0.204
SF3B3	MSTRG.1242	1.62E-03	-1.120	0.109	0.322
H.20.12e(T3)	MSTRG.7529	1.90E-03	-1.101	0.05	0.231
PRKRIP1	MSTRG.21865	4.85E-03	-1.101	0.02	0.158
RNF34	MSTRG.14105	2.00E-04	-1.095	0.05	0.276
N/A	MSTRG.23323	2.19E-02	-1.087	0.129	0.285
ANKRD28	MSTRG.16982	5.15E-03	-1.053	0.03	0.176
ABCC1	MSTRG.6056	5.04E-03	-1.031	0.139	0.331
MED14	MSTRG.19471	7.75E-03	-1.010	0.04	0.167
INPP5A	MSTRG.20568	8.47E-03	-1.005	0.04	0.185
BTBD2	MSTRG.5766	2.25E-02	-1.003	0.03	0.167

Key – Pct.1 represents the percentage of Neoblasts 1 cells at 24 hours post 5 Gy irradiation with detectable expression of the corresponding gene. Pct.2 represents the percentage of wild-type Neoblasts 1 cells with detectable expression of the corresponding gene. Highlighted genes are referenced in text (Chapter 3).

Appendix Table 7. List of primer sequences for cloned genes

Gene	Identifier	Forward Primer	Reverse Primer
Ulk-2	dd_Smed_v6_1620_0_1	cgtggtgagaatgttcag	ctagtctgtcgtcgcgatc
HFM-1	dd_Smed_v6_24408_0_4	gaccacacaagtgttggc	ctgttgtcaaattgcggcc
DnaJ	dd_Smed_v6_5753_0_1	cagtcaaacaatcccgcg	ggattccgtaaagccaccg
Nucb1	dd_Smed_v6_6010_0_1	ggctcaaggtcgaacgaag	tcccaatgcccgtcttgatt
ZNFX-1	dd_Smed_v6_10633_0_1	tgggtggccagtgtaaagg	ccaacactttcgtgggcatg
RNF144-A	dd_Smed_v6_4845_0_1	acatttggtgttcatgcggc	ccacttttcgcgcctcttc
Shk2	dd_Smed_v6_2745_0_2	tccttgttcatgggaggcg	cgttgtgattgccgtcgatg
MMP1	dd_Smed_v6_274_0_1	gtgactgcacacgaaatgg	cttcagcagagacttgccg
Tspan5	dd_Smed_v6_1003_0_1	ctggtagacatgcttgccg	caccgatcaaaataccgag
TNFAIP8	dd_Smed_v6_2386_0_1	gctcgatgaagtgcaatcg	tgtgccgatcgatcattgc
Rab32	dd_Smed_v6_1037_0_1	tcactacgtcattcggagag	gagttttgcgctggcttatc
Mib-1	dd_Smed_v6_4880_0_1	gtcatcggattcgaaggaa	tttgttctgggaacctctgg
MMP19	dd_Smed_v6_321_0_1	tgggacacgctattggcttg	tctccgtcttgaagtgccc
MAPKKK4	dd_Smed_v6_4259_0_1	ggacgtctttgtcgaggttg	acgcgatgaatatcccaag
TBX-2	dd_Smed_v6_17143_0_1	agttcgatcgcttgaccatc	atggcacttggtttggactc
FHL-A	dd_Smed_v6_5037_0_1	tcggataggatcatcgcgc	gaaactcttggctccgatcg
FHL-2	dd_Smed_v6_10293_0_1	gtttgcagtacatgccagg	tcctgggcaaaagatttga
FHL-3	dd_Smed_v6_1251_0_1	cggacgacaaagtagtttg	ctcaaatcatgatgtttag
FHL-4	dd_Smed_v6_1244_0_1	aacatctgtgcgagtgttgg	accagccagagtttgtttgc
LHX-1	dd_Smed_v6_8252_0_1	ggatccgtgatcattcttgg	ctgggatcaatttcgctgac
Tspan6	dd_Smed_v6_9692_0_1	atcataccaccgctgcatc	ggcagagaatcaccacaac
Tspan18	dd_Smed_v6_5409_0_2	ctgggagggtgcatatttg	gatgcagatgcagataacg
Tspan11	dd_Smed_v6_8060_0_1	tggtcactgctattcgttcg	gcttgattgctcccattcac
Wnt11-1	dd_Smed_v6_14391_0_1	gtccacgagaaacttcttgg	acttcacggtacccccctacc
JSAP-1	dd_Smed_v6_3798_0_1	tctactgtaggccgctgtca	acgaagaggctggattctc
BIGH3	dd_Smed_v6_1088_0_1	catgtgacccttttgccttt	ttccgcttcgaggaactaa
wnt5b	dd_Smed_v6_15469_0_1	cggtgtcgttcatgctattgc	tccagtttgcactctcgacc
TLK	dd_Smed_v6_6431_0_1	gcggcttttctgaggttcac	ccagacatcgaccttgctg
Tspan-39D	dd_Smed_v6_440_0_1	gacagttatagctgctctgg	gcaaatgaccaccaaagc
PDLIM7	dd_Smed_v6_10318_0_1	ataacctgtgactcggtggc	tcctaggggaatttcgcac
LTBP1	dd_Smed_v6_7311_0_1	ttcccagagatttgcggacc	cgcataaattgtcgcctccg
RAB27B	dd_Smed_v6_10266_0_1	cattaggctgcttgcattagg	tccatggcctcttcaactcg
PAK2	dd_Smed_v6_3244_0_8	caatcaaagactccgaaacg	tggtttcactttccgagagg
JAG-1	dd_Smed_v6_6929_0_1	acctcaaaacgaccttgtgg	caagtgccttgacgattcc
Mth	dd_Smed_v6_16587_0_1	tctgcgtccaattcggtgat	caagcgcgagtggaatttg
PTPRS	dd_Smed_v6_16093_0_1	gacctagacacgccaaagct	ctaaagggccctgagttgc
LRRK2	dd_Smed_v6_7343_0_1	gtgcttcttcaacggatcgc	gcattcgattcgtgtctgcc
PTPN13	dd_Smed_v6_4490_0_1	tcccgagcagaaacacgaa	tccgttgatccaacccagg
TRAF2	dd_Smed_v6_13174_0_1	tcagtgaaatggaggcaaacc	tgtccaagcatctttccagc
EGF2	dd_Smed_v6_4666_0_1	tgccatccagattttgtgca	gaccaacaaagcgatgaa
CTSB	dd_Smed_v6_81_0_1	tgggcatttggagctgttga	atcctttgtcgccccatgtc
TTF-1	dd_Smed_v6_33456_0_1	aacatctttgccaggaatgc	ggaattgtggaggatgctg
Rab9B	dd_Smed_v6_6588_0_1	tgcaaaggtatgtcaccaaca	ccaagcttgaaaacccatg
Rasl-12	dd_Smed_v6_11635_0_1	gattcctcgatgcctatgga	gtcggaagttttctgccaat

Appendix Table 7 (continued)

Dlx6	dd_Smed_v6_9596_0_1	attgcctcctcatcctcctc	tgatttgttccctgttgcga
RFX-2	dd_Smed_v6_11406_0_1	aacgcgctcagttatacagc	atgttccgggcaagttttcc
POSTN	dd_Smed_v6_1505_0_1	gcatgggaagcagctaagtc	cagtggttttccgccattat
IGFBP7	dd_Smed_v6_4437_0_1	ggagtttgcaatgcaggttt	ttgccttcgtgtttcaactg
Ank2	dd_Smed_V6_10835_0_1	cggatttactccccttcaca	gcaattgtcttgcgacttga
BMP7	dd_Smed_v6_17402_0_1	aaacatggtcatccgttggt	ttctgaggggctatgatcca
NFX-1	dd_Smed_v6_4795_0_1	gttgcgatgatgtgtgtgg	tccgctcacagacattccc
FAM200B	dd_Smed_v6_15477_0_4	aagcgagaacgggagagtg	acgtgagccactgcaaatg
CBS	dd_smed_v6_1585_0_1	ctggagttgcgaggaaaatc	cagtcattggagcgttgaga
LTBP3	dd_Smed_v6_2649_0_1	cgtgtgcaatgatggatttc	tgcaatcgcatgtaaagctc
bHLHa30	dd_Smed_v6_6869_0_1	ccgcagataaaacatttttag	aacagaggaggtggcaatg
BEST2	dd_Smed_v6_8073_0_1	aattaatggtggcgacaagg	ggccagttattttgctttcg
ETS-1-like	dd_Smed_v6_9165_0_1	ctcaagaatgcttgcaatgg	gaaacgcacaaaccaaac
NDP52	dd_Smed_v6_2828_0_1	ggcctgtccactatgtttgg	gaaacaaaacgccatcag
GPCR154-like	dd_Smed_v6_13150_0_1	ttgcaaattctttggcactc	cgccaacattccaactatcc
C33E10.6-like	dd_Smed_v6_9974_1_2	gcgtgcaaatgcagttagtg	acccttagctcgcattgttg
DMXL-1	dd_Smed_v6_5944_0_1	gaatcaacaggtgggagcga	gtgaaggggcaaaggagg
RASGRP3	dd_Smed_v6_15742_0_1	cctccaaccgttgatgttct	ttccaaggtgctcatgtcag
ST13	dd_Smed_v6_668_0_1	aatccggattccgctcttgc	tcattggaccagcccctc
SH3GLB1	dd_Smed_v6_4055_0_1	ggagccgaatctagctttcc	tcaagtcgctcaagttctcg
Mapkkk2	dd_Smed_v6_2030_0_1	aattcctgcacggaaacaac	acacgaatgcaacctttcc
Mapkkk19	dd_Smed_v6_3989_0_1	acctgatcaaccgaccagac	catttggatacctgccttgg
Kin17	dd_Smed_v6_5219_0_1	cgtcaatttggtgggaaaag	tccgttcctgttccagtttc
ZFAND5	dd_Smed_v6_2038_0_1	cagctttgcaaaacaggatg	gcaatcaccgataaaaatg
BBS-2	dd_Smed_v6_10186_0_1	gttgtgattggtggcagttg	taacttgtgaggcgttgctg
BRCTCP-1	dd_Smed_v6_8247_0_1	tgcacctcagtcttgcaatc	ttgaaatacttgcgccattg
Rpz-1	dd_Smed_v6_688_0_1	cacgggacctttggattta	cacccccgtcatgtatctct
AMERL-1	dd_Smed_v6_1660_0_6	ggcatcttattgttttggtagc	ctgtacagccacagcaagg
NUB1L	dd_Smed_v6_3402_0_5	gtgttgcatatcagcgagga	gcaatgagattcccatcaa
SLMAP	dd_Smed_v6_3763_0_1	atcactgccaaccaacacaa	cgtagcttttggctttcctg
GTF2IRD1	dd_Smed_v6_3260_0_1	ggtgcaaattcttgggagtc	caattattttcaatgttagg
arhGAP15	dd_Smed_v6_3975_0_2	tcgtgcccattgtcaataaa	tggtcccgttaaaaccatgt
TMEM107	dd_Smed_v6_13204_0_5	caaaataggaactatggaag	caaataactaacgaaattg
FBXO-like-1	dd_Smed_v6_2369_0_1	gcaactggttttatttgttcac	acgcacataaggttttcc
CDPK1	dd_Smed_v6_299_0_1	ggtggaattatttggcatgg	ccactgcaatcacattttgg
ABL-1	dd_Smed_v6_5996_0_1	tcagggttaggcacttccag	tccgttaatccgaaatcagc
MAP3k1-like	dd_Smed_v6_3194_0_1	acagacgaggtcgaaattgg	acattctgtttgccggtgag
PTHrP	dd_Smed_v6_16180_0_1	tcgtatggctttgtcgactg	ttcggtcatttcgttgtctg
THADA	dd_Smed_v6_12316_0_1	tgcgagtatttgtgccactc	ttgatgatgccagcttgttc
Ubb-like-1	dd_Smed_v6_783_0_1	gatgttgaataaatttgaatg	cctctggttctcatcaatac
TADBPL	dd_Smed_v6_10863_0_2	gcaatttcctaaagtcagtgg	ctcgtggcgctgagaaatg
EB2	dd_Smed_v6_5879_0_5	aaaaagtgcgccatgaattt	cacatttgttacggcatcg
EGRPl-1	dd_Smed_v6_7038_0_1	caaatgtgccatgtgtaggg	tgtcgagaactggcatgg
TIGD-7	dd_Smed_v6_12091_0_1	cgcttccgaaaaagacacgg	ggatgcgcaggacaattatc
MAPKKK3	dd_Smed_v6_12176_0_1	aggtggcgaattgttctgtc	tgcaacccatggatgaac
NSD2	dd_Smed_v6_17850_0_1	ctgatgcaatgacagattcag	cattttcagaagacgattc

Appendix Table 7 (continued)

YBOX-3	dd_Smed_v6_52_0_1	tggtttcatcagtgttgacg	caaaaacgtaaagtcgtg
arhGEF10	dd_Smed_v6_11936_0_1	ccagatttgcaactgaatgg	ggcaccattgcgaataag
1433T	dd_Smed_v6_138_0_1	catcgccttggattgaagag	caatttgcaagcttctgcac
Dkc	dd_Smed_v6_4087_0_1	ccaaaccgggtattgatgtc	tttgcgtggactccgtaac
Larpl-1	dd_Smed_v6_1572_0_1	ggatccaattctgccaaatg	tgttgacttcttgcgcacac
UMSBP	dd_Smed_v6_62_0_1	gtttgtttgtatacgcattgg	caattaacaccgaaaacg
DRG-1	dd_Smed_v6_5779_0_1	attgagggtgcaaaagatgg	cgatcgatggagtttgttg
VRK2	dd_Smed_v6_11627_0_1	aatacgttcacgccgacatc	tacaagccggtttccagtc
CBX4	dd_Smed_v6_12608_0_1	gctttacccgaacgtcactg	cagaaccattgcatttgac
DDX50	dd_Smed_v6_673_0_1	tgtaagcagtgacgacgatg	gaacctccctcaatcgatc
Emx-2	dd_Smed_v6_56082_0_1	tgacaggattttctgttgcag	gattgagagatgccgcgag
Nudc1	dd_Smed_v6_3736_0_1	tagacacattgtgcccggac	tgtgcaaatgcgtccattgg
ALX4	dd_Smed_v6_16955_0_1	cagtgaatcccacccagtcc	tggaccttggaaactccgc
ST18	dd_Smed_v6_18107_0_1	agttccaccagtctcatcgg	gcacccagagagacttctg
FAX	dd_Smed_v6_1736_0_1	catgcatatcgccttttgcc	gaggataattgacgcttgg

Appendix Table 8. List of RNAi candidate genes and their selected features

Gene	Proportional expression in FACS categories			Log_2 Fold change (X1, 24 hpi)	Transcription factor function	DNA/RNA binding activity	Signalling activity	Mammalian orthologue
	X1	X2	Xins					
BRCTCP-1	0.859	0.106	0.036	+4.13	NO	YES	NO	ABSENT
Rpz-1	0.689	0.013	0.298	+3.52	NO	NO	YES	ABSENT
Kin17	0.672	0.216	0.113	+4.37	NO	YES	NO	PRESENT
HFM-1	0.627	0.124	0.249	+2.43	NO	YES	NO	PRESENT
Dkc	0.602	0.260	0.138	+3.03	NO	YES	NO	PRESENT
DDX50	0.565	0.314	0.121	+2.19	NO	YES	NO	PRESENT
Nudc1	0.402	0.411	0.188	+2.62	NO	NO	YES	PRESENT
VRK2	0.538	0.292	0.170	+3.00	NO	NO	YES	PRESENT
LRRK2	0.534	0.283	0.183	+3.88	NO	NO	YES	PRESENT
NUB1L	0.518	0.284	0.198	+2.66	NO	NO	NO	ABSENT
Emx-2	0.512	0.388	0.100	+2.90	YES	YES	NO	PRESENT
CBX4	0.485	0.439	0.076	+2.51	NO	NO	YES	PRESENT
UMSBP	0.472	0.297	0.231	+2.66	NO	YES	NO	PRESENT
YBOX-3	0.466	0.356	0.178	+3.05	YES	YES	NO	PRESENT
GTF2IRD1	0.437	0.070	0.493	+2.79	YES	YES	NO	PRESENT
Ubb-like-1	0.422	0.546	0.032	+2.15	NO	NO	NO	ABSENT
FBXO-l-1	0.418	0.342	0.240	+3.20	NO	NO	YES	ABSENT
THADA	0.414	0.411	0.175	+2.11	NO	NO	YES	PRESENT
MAPKKK3	0.410	0.265	0.325	+2.72	NO	NO	YES	PRESENT
NSD2	0.405	0.336	0.259	+2.40	NO	YES	NO	PRESENT
arhGEF10	0.401	0.351	0.247	+3.00	NO	NO	YES	PRESENT
DRG-1	0.394	0.266	0.340	+2.37	YES	YES	NO	PRESENT
TMEM107	0.390	0.217	0.393	+3.37	NO	NO	YES	PRESENT
NFX-1	0.383	0.460	0.156	+3.87	YES	YES	NO	PRESENT
ST13	0.373	0.390	0.237	+2.57	NO	NO	YES	PRESENT
NDP52	0.368	0.574	0.058	+2.75	NO	NO	YES	PRESENT
TADBPL	0.366	0.383	0.252	+3.15	YES	YES	NO	PRESENT
Larp-1-L	0.366	0.424	0.211	+2.76	NO	YES	NO	ABSENT
ZFAND5	0.341	0.306	0.353	+2.76	YES	YES	NO	PRESENT
FAM200B	0.340	0.593	0.067	+2.64	NO	NO	YES	PREENT
TLK	0.336	0.523	0.141	+3.78	NO	NO	YES	PRESENT
JSAP-1	0.336	0.413	0.252	+2.67	NO	NO	YES	PRESENT
Tspan5	0.317	0.082	0.602	+2.98	NO	NO	YES	PRESENT
SLMAP	0.309	0.452	0.239	+2.62	NO	NO	YES	PRESENT
C33E10.6l	0.302	0.620	0.078	+4.66	NO	YES	NO	ABSENT
AMERL-1	0.301	0.446	0.254	+3.44	NO	NO	NO	PRESENT
BBS-2	0.300	0.351	0.349	+2.40	NO	NO	YES	PRESENT
1433T	0.299	0.272	0.429	+2.78	NO	NO	YES	PRESENT
BEST2	0.274	0.336	0.390	+2.96	NO	NO	YES	PRESENT
TIGD-7	0.269	0.240	0.491	+2.18	NO	YES	NO	PRESENT
MMP1	0.262	0.141	0.597	+3.92	NO	NO	NO	PRESENT

Appendix table 8 (continued)

MMP19	0.260	0.094	0.647	+3.90	NO	NO	NO	PRESENT
JAG-1	0.251	0.639	0.111	+3.66	NO	NO	YES	PRESENT
TBX-2	0.247	0.290	0.463	+3.30	YES	YES	NO	PRESENT
FHL-2	0.226	0.447	0.327	+2.11	NO	NO	YES	ABSENT
DMXL-1	0.215	0.422	0.363	+5.22	NO	NO	YES	PRESENT
arhGAP15	0.198	0.462	0.340	+2.29	NO	NO	YES	PRESENT
ZNFX-1	0.187	0.262	0.551	+2.83	NO	YES	YES	PRESENT
CBS	0.115	0.189	0.696	+2.82	NO	NO	YES	PRESENT
PAK2	0.102	0.117	0.781	+3.75	NO	NO	YES	PRESENT
Mapkkk2	0.092	0.192	0.717	+2.99	NO	NO	YES	PRESENT
ST18	0.091	0.638	0.271	+4.55	YES	YES	NO	PRESENT
RFX-2	0.086	0.240	0.674	+2.56	YES	YES	NO	PRESENT
MAPKKK4	0.081	0.319	0.600	+2.48	NO	NO	YES	PRESENT
Shk2	0.069	0.598	0.333	+2.72	NO	NO	YES	PRESENT
Mapkkk19	0.067	0.361	0.572	+2.03	NO	NO	YES	PRESENT
EB2	0.067	0.328	0.605	+3.76	NO	NO	YES	PRESENT
ALX4	0.065	0.346	0.589	+2.87	YES	YES	NO	PRESENT
Ulk-2	0.062	0.414	0.525	+4.20	NO	NO	YES	PRESENT
Dlx6	0.052	0.356	0.592	+2.79	YES	YES	NO	PRESENT
RNF144-A	0.048	0.160	0.792	+2.86	NO	NO	NO	PRESENT
PTHrP	0.044	0.084	0.872	+3.39	NO	NO	YES	PRESENT
TTF-1	0.042	0.375	0.583	+2.67	YES	YES	NO	PRESENT
LHX-1	0.041	0.238	0.720	+3.12	YES	YES	YES	PRESENT
RASGRP3	0.037	0.203	0.760	+3.05	NO	NO	YES	PRESENT
Mib-1	0.037	0.145	0.818	+3.55	NO	NO	YES	PRESENT
EGRPl-1	0.036	0.131	0.833	+3.17	YES	YES	NO	ABSENT
ETS1l	0.036	0.196	0.769	+3.44	YES	YES	NO	ABSENT
FAX	0.036	0.191	0.773	+2.80	NO	NO	NO	PRESENT
PTPRS	0.032	0.144	0.823	+4.88	NO	NO	YES	PRESENT
MAP3k1-L	0.031	0.196	0.773	+3.14	NO	NO	YES	ABSENT
LTBP3	0.029	0.283	0.687	+2.72	NO	NO	YES	PRESENT
RAB27B	0.029	0.318	0.653	+3.52	NO	NO	YES	PRESENT
Tspan18	0.029	0.651	0.321	+3.42	NO	NO	YES	PRESENT
EGF2	0.026	0.099	0.875	+2.51	NO	NO	YES	PRESENT
Rab9B	0.025	0.180	0.795	+2.58	NO	NO	YES	PRESENT
LTBP1	0.024	0.198	0.778	+2.54	NO	NO	YES	PRESENT
CTSB	0.022	0.148	0.830	+3.17	NO	NO	YES	PRESENT
Tspan-39d	0.021	0.146	0.832	+2.45	NO	NO	NO	PRESENT
Rab32	0.021	0.134	0.845	+3.78	NO	NO	YES	PRESENT
TRAF2	0.020	0.474	0.506	+3.75	NO	NO	YES	PRESENT
Ank2	0.020	0.129	0.851	+2.46	NO	NO	YES	PRESENT
FHL-3	0.019	0.084	0.897	+2.40	NO	NO	YES	ABSENT
Nucb1	0.017	0.378	0.604	+3.15	NO	YES	YES	PRESENT
ABL-1	0.017	0.315	0.667	+2.54	NO	NO	YES	PRESENT
POSTN	0.016	0.061	0.923	+2.83	NO	NO	YES	PRESENT
TNFAIP8	0.016	0.225	0.759	+2.56	NO	NO	YES	PRESENT

Appendix Table 8 (continued)

SH3GLB1	0.014	0.188	0.799	+3.09	NO	NO	YES	PRESENT
bHLHa30	0.013	0.754	0.234	+3.22	YES	YES	NO	PRESENT
BIGH3	0.011	0.051	0.937	+3.57	NO	NO	YES	PRESENT
PTPN13	0.010	0.144	0.846	+3.87	NO	NO	YES	PRESENT
DnaJ	0.010	0.059	0.931	+2.47	NO	NO	YES	PRESENT
IGFBP7	0.009	0.069	0.922	+2.38	NO	NO	YES	PRESENT
PDLIM7	0.007	0.048	0.944	+2.40	NO	NO	YES	PRESENT
CDPK1	0.007	0.098	0.895	+3.65	NO	NO	YES	PRESENT
FHL-4	0.007	0.035	0.958	+2.59	NO	NO	YES	ABSENT
GPCR154-l	0.006	0.125	0.869	+3.15	NO	NO	YES	ABSENT
BMP7	0.006	0.085	0.908	+2.03	NO	NO	YES	PRESENT
FHL-A	0.005	0.073	0.922	+2.09	NO	NO	YES	PRESENT
Tspan6	0.005	0.039	0.956	+3.53	NO	NO	YES	PRESENT
Rasl-12	0.004	0.084	0.912	+4.02	NO	NO	YES	ABSENT
wnt11-1	0.002	0.040	0.959	+3.94	NO	NO	YES	PRESENT
Tspan11	0.002	0.064	0.935	+3.15	NO	NO	YES	PRESENT
wnt5b	0.002	0.066	0.932	+2.69	NO	NO	YES	PRESENT
Mth	0.000	0.019	0.980	+4.05	NO	NO	YES	PRESENT

Appendix Table 9. List of genes excluded from RNAi screen

Epidermal-progeny associated genes			
Gene	Identifier	Log_2 Fold Change – X1, 24 hpi	Reference(s)
Prog-1	dd_Smed_v6_332_0_1	+1.72	Eisenhoffer et al., 2008
Agat-1	dd_Smed_v6_920_0_1	+3.49	Eisenhoffer et al., 2008
Mcp-1	dd_Smed_v6_10436_0_1	+3.14	Eisenhoffer et al., 2008
Odc-1	dd_Smed_v6_4916_0_1	+3.61	Eisenhoffer et al., 2008
Cp1A1	dd_Smed_v6_2162_0_1	+3.74	Eisenhoffer et al., 2008
Pmp-4	dd_Smed_v6_2147_0_1	+4.36	Zhu et al., 2015
Pmp-5	dd_Smed_v6_5958_0_1	+3.63	Zhu et al., 2015
Pmp-6	dd_Smed_v6_263_0_1	+3.80	Zhu et al., 2015
Pmp-8	dd_Smed_v6_3226_0_1	+4.21	Zhu et al., 2015
Pmp-9	dd_Smed_v6_468_0_1	+3.92	Zhu et al., 2015
Pmp-11	dd_Smed_v6_771_0_1	+3.74	Zhu et al., 2015
Rcn-1	dd_Smed_v6_5307_0_1	+3.93	Fincher et al., 2018; Plass et al., 2018
H.93.2a	dd_Smed_v6_3680_0_1	+4.19	Fincher et al., 2018; Plass et al., 2018
Hb.18.1f	dd_Smed_v6_5905_0_1	+2.47	Fincher et al., 2018; Plass et al., 2018
Pfn-1	dd_Smed_v6_3725_0_1	+2.63	Fincher et al., 2018; Plass et al., 2018
Apoptosis-associated genes			
Gene	Identifier	Log_2 Fold Change – X1, 24 hpi	Reference(s)
Slo-1	dd_Smed_v6_17366_0_1	+2.73	McFerrin et al., 2012
CalpA	dd_Smed_v6_1752_0_3	+3.85	Smith and Schnellmann, 2012
Calp9	dd_Smed_v6_1971_0_1	+3.74	Smith and Schnellmann, 2012
DTHD1	dd_Smed_v6_15379_0_1	+2.34	Park et al., 2007
Casp3	dd_Smed_v6_4986_0_1	+2.50	Brentnall et al., 2013
Casp2	dd_Smed_v6_7164_0_1	+2.98	Vigneswara and Ahmed, 2020
SMPD1	dd_Smed_v6_5377_0_1	+3.04	Andrieu-Abadie and Levade, 2002
DNM1L	dd_Smed_v6_388_0_1	+3.38	Frank et al., 2001
GzmA	dd_Smed_v6_66_0_1	+4.34	Trapani and Smyth, 2002

Appendix Table 10. Complete list of genes screened and their knockdown phenotypes

Gene	% animal mortality		% stem cell count relative to GFP	
	15 Gy	0 Gy	15 Gy, 7 dpi	0 Gy
Ulk-2	10	0	39.15	98.45
HFM-1	0	0	93.32	100.28
DnaJ	0	0	86.86	99.11
Nucb1	0	0	97.01	100.52
ZNFX-1	0	0	89.60	99.37
RNF144-A	0	0	103.32	97.63
Shk2	0	0	99.45	99.45
MMP1	0	0	101.19	98.41
Tspan5	0	0	85.22	97.54
TNFAIP8	0	0	105.24	100.95
Rab32	100	0	5.81	97.24
Mib-1	10	0	42.12	98.03
MMP19	0	0	99.53	99.06
MAPKKK4	0	0	67.16	97.74
TBX-2	0	0	86.57	98.39
FHL-A	0	0	13.61	98.95
FHL-2	0	0	22.55	99.53
FHL-3	0	0	14.04	101.08
FHL-4	0	0	18.30	100.21
LHX-1	0	0	21.70	98.01
Tspan6	0	0	99.66	99.81
Tspan18	0	0	103.08	99.08
Tspan11	0	0	91.77	100.69
wnt11-1	0	0	96.21	101.46
JSAP-1	0	0	45.96	99.94
BIGH3	0	0	99.35	100.04
wnt5b	0	0	94.18	97.07
TLK	0	0	89.05	98.64
Tspan-39D	0	0	83.84	101.10
PDLIM7	0	0	85.19	99.80
LTBP1	0	0	94.63	98.16
RAB27B	0	0	38.30	98.81
PAK2	0	0	100.45	100.93
JAG-1	10	0	34.47	100.26
Mth	0	0	97.95	101.87
PTPRS	0	0	89.15	100.84
LRRK2	0	0	101.75	99.32
PTPN13	0	0	100.03	100.15
TRAF2	0	0	80.00	98.68
EGF2	0	0	94.18	100.23
CTSB	10	0	22.98	98.34
TTF-1	0	0	33.61	100.03

Appendix Table 10 (continued)

Rab9B	0	0	40.43	99.48
Rasl-12	100	0	7.36	97.21
Dlx6	0	0	74.61	101.94
RFX-2	0	0	83.90	100.89
POSTN	0	0	98.30	99.79
IGFBP7	0	0	101.19	101.00
Ank2	0	0	94.56	99.47
BMP7	0	0	89.04	98.34
NFX-1	0	0	91.95	98.76
FAM200B	0	0	103.28	100.98
CBS	0	0	104.95	100.72
LTBP3	0	0	87.71	98.52
bHLHa30	0	0	90.14	99.54
BEST2	0	0	84.21	97.91
ETS1l	0	0	99.30	99.55
NDP52	0	0	27.23	100.84
GPCR154-like	10	0	17.87	98.98
C33E10.6-like	0	0	101.42	100.91
DMXL-1	80	0	11.06	99.03
RASGRP3	0	0	94.47	98.44
ST13	0	0	98.08	100.40
SH3GLB1	0	0	70.50	97.56
Mapkkk2	0	0	75.63	100.97
Mapkkk19	0	0	41.70	99.82
Kin17	100	0	3.47	94.16
ZFAND5	0	0	95.02	101.13
BBS-2	0	0	91.25	99.17
BRCTCP-1	0	0	98.58	99.36
Rpz-1	0	0	47.23	98.57
AMERL-1	0	0	113.01	99.04
NUB1L	0	0	104.52	97.31
SLMAP	100	0	2.13	78.32
GTF2IRD1	0	0	104.89	99.19
arhGAP15	0	0	94.46	98.87
TMEM107	0	0	87.71	101.93
FBXO-like-1	0	0	93.63	97.45
CDKPK1	0	0	102.33	100.32
ABL-1	0	0	25.95	99.60
MAP3k1-like	0	0	90.73	100.71
PTHrP	0	0	93.29	101.11
THADA	0	0	48.51	99.26
Ubb-like-1	0	0	88.88	97.09
TADBPL	0	0	85.45	99.12
EB2	0	0	90.16	97.34
EGRPl-1	0	0	102.24	100.05
TIGD-7	0	0	95.90	98.82

Appendix Table 10 (continued)

MAPKKK3	0	0	86.44	99.17
NSD2	0	0	60.15	100.62
YBOX-3	0	0	75.54	97.31
arhGEF10	0	0	91.32	99.52
1433T	0	0	55.86	100.70
Dkc	100	0	5.96	95.45
Larpl-1	0	0	49.78	100.42
UMSBP	0	0	97.05	97.72
DRG-1	0	0	93.64	100.41
VRK2	0	0	94.60	100.61
CBX4	0	0	87.71	99.04
DDX50	0	0	99.86	100.43
Emx-2	0	0	84.49	98.62
Nudc1	0	0	103.22	97.25
ALX4	0	0	100.06	101.08
ST18	0	0	92.97	98.88
FAX	0	0	99.43	97.37

Appendix Table 11: List of key reagents

Reagent	Manufacturer and catalogue number
TRIzol	Invitrogen – 15595026
Oligo(dT)$_{18}$	Invitrogen – SO131
Superscript Reverse Transcriptase III	Invitrogen – 18080093
RNAse H	NEB – M0297S
OneTaq 2X Master mix	NEB – M0482L
SmaI	NEB – R0141S
NEBuffer r2.1	NEB – B6002S
T4 DNA Polymerase	NEB – M0203S
T7 RNA Polymerase	NEB – M0251S
TURBO DNAse	Invitrogen – AM2238
10X DIG RNA labelling mix	Roche – 11277073910
10X FITC RNA labelling mix	Roche – 11685619910
20X EvaGreen	Biotium – 31000
Proteinase K (RNA Grade)	Invitrogen – 25530049
Anti-DIG-POD	Roche – 11207733910
Anti-FITC-POD	Roche – 11426346910
Alexa-Fluor-488	Invitrogen – A20000
5-TAMRA	Invitrogen – C1171
DAPI	Invitrogen – D1306
Anti-H3P (Ser 10), Rabbit polyclonal	Sigma-Aldrich – 06-570
Goat anti-Rabbit IgG (Heavy chain)-AF-488	Invitrogen – A27034
Horse Serum	Gibco – 26050070
Western Blocking Reagent	Roche – WESTBL-RO
Draq5	Invitrogen – 65-0880-92
Concanavalin-A-AF-488 conjugate	Invitrogen – C21401
Bovine Serum Albumin	Sigma-Aldrich – A9418
SUPERase-In RNAse Inhibitor	Invitrogen – AM2694
Maxima H Minus Reverse Transcriptase	ThermoFisher – EP0753
KAPA Pure Beads	Roche – KK8000
Nextera XT DNA Library Preparation Kit	Illumina – FC-131-1024
T4 DNA Ligase	NEB – M0202L
Dynabeads MyOne Streptavidin C1	Invitrogen – 65001
RiboLock RNAse Inhibitor	ThermoFisher – EO0381
TRIzol LS	Invitrogen – 10296028
Glycogen, RNA-grade	ThermoFisher – R0551
DH5-alpha competent cells	ThermoFisher – EC0111